AN INTEGRATED LASER CLADDING AND STRESS IMPROVEMENT PROCESS FOR ENHANCING SURFACE PROPERTIES

A thesis submitted to

The University of Manchester

For the degree of

Doctor of Philosophy (PhD)

In the Faculty of Engineering and Physical Sciences

2016

Alonso Martinez Hurtado

School of Mechanical, Aerospace and Civil Engineering

Table of contents

List of figures

List of tables

Abstract

The University of Manchester
Alonso Martinez Hurtado
Doctor of Philosophy
An Integrated Laser Cladding and Stress Improvement for Enhancing Surface Properties
March 2016

Laser cladding is a process that is used to improve the properties of a metal surface. The properties in question may include hardness, wear-, corrosion- and/or fatigue-resistance. The process involves fusing a thin layer of additional metal to the original surface, using a laser as the heat source. Unfortunately, residual stresses are generated due to the rapid and highly localised thermal expansion and contraction that occur during the heating-melting-solidification-cooling cycle. These residual stresses can have a detrimental effect on the final performance of the clad component, especially with respect to corrosion resistance. Detrimental tensile residual stresses can be mitigated through the use of post-processing techniques such as laser shock peening (LSP). LSP is a process that uses a pulsed laser to generate intense spots of recoil pressure on a surface, thereby introducing compressive residual stresses. Post weld heat treatment (PWHT) is another process that could be also used in laser cladding in order to relieve tensile residual stresses. In this work, laser cladding was carried out by depositing a clad layer of AISI grade 316L stainless steel on to either a S275 steel substrate or an AISI grade 316L stainless steel substrate, using different process parameters. The hardness and residual stresses in the overlay and substrate were assessed for each laser clad sample before and after being treated with LSP and PWHT. The corrosion rate and microstructure were also assessed in each case. The novelty of this work is two-fold. Firstly, to the author's knowledge, it is the first study that attempts to link process parameters to both the residual stresses and the corrosion performance of austenitic stainless steel overlays deposited by laser cladding. The second novel aspect is based on the application of both LSP and PWHT to the deposited overlay in order to investigate whether an improvement in the mechanical properties and the corrosion resistance can be realised. In this study, tensile residual stresses were generated in the clad layers. However, the magnitude of the residual stresses did not appear to be particularly sensitive to the deposition parameters. Indeed, it was found that the number of layers that is deposited is more important than the choice of process parameters. LSP was effective in reducing the tensile residual stresses and in fact it introduced compressive stresses to all the samples that were treated. In contrast, PWHT only led to satisfactory stress relief when the AISI grade 316L stainless steel was deposited on to a matching substrate material. This was related to the fact that a difference between the thermal expansion coefficients of the overlay and substrate led to the development of significant tensile residual stresses on cooling down after PWHT. The corrosion tests on the clad coupons led to the development of pits and cracks. However, after LSP only pits were found, without any sign of cracking, for the test durations that were investigated owing to the fact that compressive stresses were generated. Similar results were found after PWHT for the clad samples in which the overlay material matched the substrate material. However, signs of cracking were observed after PWHT in samples where AISI grade 316L stainless steel was deposited on to an S275 steel substrate due to tensile residual stresses remaining within the overlay. This result suggests that there may be little benefit in carrying out PWHT for components in which grade 316L stainless steel is deposited on to a steel substrate. In contrast, there appear to be clear benefits associated with carrying out LSP in order to mitigate the residual stresses and retard the onset of cracking.

Declaration

I hereby declare that no portion of the work referred to in the thesis has been submitted in support of an application for another degree or qualification of this or any other university or other institute of learning.

Alonso Martinez Hurtado

2016

Copyright statement

i. The author of this thesis (including any appendices and/or schedules to this thesis) owns certain copyright or related rights in it (the "Copyright") and s/he has given The University of Manchester certain rights to use such Copyright, including for administrative purposes.

ii. Copies of this thesis, either in full or in extracts and whether in hard or electronic copy, may be made only in accordance with the Copyright, Designs and Patents Act 1988 (as amended) and regulations issued under it or, where appropriate, in accordance with licensing agreements which the University has from time to time. This page must form part of any such copies made.

iii. The ownership of certain Copyright, patents, designs, trade marks and other intellectual property (the "Intellectual Property") and any reproductions of copyright works in the thesis, for example graphs and tables ("Reproductions"), which may be described in this thesis, may not be owned by the author and may be owned by third parties. Such Intellectual Property and Reproductions cannot and must not be made available for use without the prior written permission of the owner(s) of the relevant Intellectual Property and/or Reproductions.

iv. Further information on the conditions under which disclosure, publication and commercialisation of this thesis, the Copyright and any Intellectual Property and/or Reproductions described in it may take place is available in the University IP Policy (see http://documents.manchester.ac.uk/DocuInfo.aspx?DocID=487), in any relevant Thesis restriction declarations deposited in the University Library, The University Library's regulations (see http://www.manchester.ac.uk/library/aboutus/regulations) and in The University's policy on Presentation of Theses.

List of publications

Journal Articles

Martinez-Hurtado A., Francis J.A., Stevens N. *An assessment of residual stress mitigation strategies for laser clad deposits*, Materials Science and Technology, Submitted to journal, March 2016.

Conference publications

Martinez-Hurtado A., Pinkerton A.J., Stevens N. *Improvements of surface properties via laser cladding and shock peening,* 26th International Conference on Surface Modification Technologies (SMT 26), June 2012. Lyon, France.

Acknowledgements

Firstly I would like to thank to God, because he gave me the opportunity to be here. He has been generous providing me with health and courage to sort out any difficulties that I could find in my life.

I want to give a special thank to my family because they have been supporting me with their love, comprehension and patience, especially in those difficult moments we have been through.

I want to acknowledge the CONACYT (National Council for Science and Technology in Mexico) for providing the funding for my studies. My sincere gratitude to the people of my country, that works very hard every day. Furthermore, I want to thank The University of Guanajuato for the support provided in the beginning of this beautiful adventure. Special thanks to Professor Teresa Alonso Rasgado for creating this program that allows many students to come to this country.

My greatest thank goes to my supervisor, Dr John Francis, for all his support, patience, guidance and dedication. In the same way, I want to thank my Co-Supervisor, Dr Nicholas Stevens who has been an important support in this research. I also want to thank all the people who helped me in my research, Dr David Whitehead, Dr Matt Roy, Dr Joana Walsh, Dr Philipp Frankel, Dr Wei Guo, Daniel Wilson, Gary, Ian and all my colleagues.

I would also like to thank Metal Improvement, part of Curtiss-Wright Surface Technologies, for carrying out the laser shock peening work in this study. In particular, I would like to thank Mr. Ben Hayes for coordinating and overseeing the laser shock peening operations. Furthermore, I want to thank the Science and Technology Facilities Council (ISIS).

Finally, thanks to all my friends that have been with me during this incredible time.

Nomenclature

i_{corr}	Corrosion current density ($A.cm^{-2}$)
A	Absorption coefficient for surface coating (0.01)
B	Stern-Geary constant (mV)
d	average grain size
D	laser spot size diameter (mm)
D_{ov}	overlay dilution under steady state conditions
F	Faraday constant ($Coulom.Mol^{-1}$)
H_{ss}	steady state average height (mm^2)
I	laser power density ($GWcm^{-2}$)
K_y	(constant) strengthening coefficient
m	powder feed rate ($gmin^{-1}$)
n	valence
P	laser power (W)
P_{ss}	steady state average penetration (mm^2)
RMM	atomic weight ($g.Mol^{-1}$)
R_p	polarisation resistance ($ohm.cm^2$)
V	traverse speed ($mm.min^{-1}$)
Z	Shock impedance ($g.cm^{-2}.s^{-1}$)

Greek letters

α	Ratio of thermal to internal energy

σ_y Yield stress of the material

σ_o Material constant corresponding to initial stress that is required for dislocation movement

ρ density of the material ($g.cm^{-1}$)

Acronyms

3D	Three dimensional
ASTM	American Society for Testing and Materials
CAD	Computer Aided Design
CNC	Computer Numeric Control
DMD	Direct Metal Deposition
DMLS	Direct Metal Laser Sintering
EDM	Electric Discharge Machine
EDS	Energy Dispersive Spectroscopy
FEM	Finite Element Method
HPDL	High Power Diode Laser
LASER	Light Amplification by Stimulated Emission of Radiation
LENS	Laser Engineering Net Shaping
LPR	Linear Polarisation Resistance
LRM	Laser Rapid Manufacturing
LSP	Laser Shock Peening
Nd:YAG	Neodymium doped yttrium aluminium garnet
PWHT	Post Weld Heat Treatment
SCE	Saturated Calmonel Electrode
SDM	Shape Deposition Manufacturing
SLC	Selective Laser Cladding
SLPR	Selective Laser Powder Re-melting

SRT	Short Rise Time
Yb:YAG	Ytterbium doped yttrium aluminium garnet

Dedications

I dedicate this work to my family and especially to my beloved brother Ivan de Jesus, God bless you.

Chapter 1

Introduction

1.1 Research and motivation

The implementation of lasers in industry has widely increased over the years because of their capability to perform different tasks. Lasers can be used in different applications such as the measurement of length, holography, analytical techniques, communications, printing, medical applications and as a heat source [1]. However, the high operational cost of some lasers has limited their application in some areas. In materials processing areas, the laser is used as heat source and due to fact that the laser beam can be easily focused on small areas, the power intensity achieved is high enough to ensure that any kind of material capable of absorbing the laser energy can be evaporated. Therefore, industries have implemented the use of lasers in their production processes in order to perform different applications such as welding, bending, surface treatments, alloying, cutting, machining, cleaning, heat treatments, stereolithography and cladding.

Owing to the necessity for producing materials with better mechanical properties and reducing the production costs, surfacing processes such as laser cladding have been under investigation for decades. It has been found that laser cladding is capable of satisfy the new requirements of the automobile, aerospace and nuclear industries. However, the process involves several variables that in turn make laser cladding a complex process.

Laser cladding is a surface process treatment that has been used by industries in order to improve the mechanical properties of metals such as hardness, wear-, corrosion- and also fatigue-resistance. This process requires the use of a laser as a heat source in order to melt and deposit a protective coating over a metal surface [2]. It can be used to restore worn components or to develop coatings with better mechanical properties than the base material. The use of inert gases (commonly argon) is necessary in order to reduce or avoid oxidation during the melting process. Typical lasers used for laser

cladding are carbon dioxide (CO_2), gas lasers, neodymium lasers (Nd: glass or Nd: YAG), solid state lasers, high-power diode lasers (HPDL), semiconductor lasers and sometimes fibre lasers [3-5]. Some physical aspects of the laser define the interaction between the laser beam and the material. Owing to the benefits achieved, laser cladding has been used to repair turbine blades in the aerospace industry [6-8], to repair moulds used in the plastic industry [9], in rapid prototyping [10], to repair die-casting dies [11], in the repair of heavy mining equipment, and for the reclamation of pump components in the oil recovery and refining industry. In some production processes, the corrosion resistance of the material is fundamental; therefore, an exhaustive study of cladding materials that provides good mechanical properties and excellent corrosion resistance has been performed. Ceramics, metal matrix composites (cermets), and Ni alloys are some of the materials used as coatings [12].

Since laser cladding is a melting process; the process parameters play an important role in avoiding the generation of some flaws during solidification such as porosity and cracks or to produce a coating with desired characteristics. Furthermore, the use of a dissimilar material as a coating is an aspect to consider because the differences in thermal properties between the coating and base material could also affect the final performance. For instance, differences in the thermal expansion coefficient can lead to the generation of a highly tensile residual stresses in the overlay during cooling, which could later contribute to cracking. Several studies have shown that residual stresses generated in laser cladding, resulting from the constrained contraction of the metal after solidification, could produce high tensile residual stresses capable of generating cracks in the cladding [13] affecting the fatigue resistance. Furthermore, the state of the residual stresses could also affect the performance of the metals in corrosive environments, promoting a failure related to corrosion mechanisms such as stress corrosion cracking. Even though, the nature of the process has some drawbacks, there are some post-processing operations that could be used in order to enhance the performance of the metals.

Laser shock peening is a surface treatment process used by various industries in order to improve the fatigue life and corrosion resistance of metals, by introducing compressive residual stresses in order to mitigate the tensile residual stresses generated by manufacturing processes such as welding, cutting and forming [5, 14-17]. This process requires the use of a laser capable of providing high intensity energy pulses. Laser

shock peening could, therefore, be used in order to mitigate the state of residual stresses developed in laser cladding.

Another post-process used frequently in welding applications in order to mitigate the effects of residual stresses is Post Weld Heat Treatment. PWHT is usually applied in order to restore toughness. However, it usually achieves stress relief, and it could be used for this purpose after laser cladding in order to improve the fatigue and corrosion resistance of the metals.

1.2 Aim and objectives

The aim of this work is to study the laser cladding process and understand the effects of the process parameters on the development of the microstructure, hardness, residual stresses and corrosion resistance, using both similar and dissimilar materials for the cladding and base material. Furthermore, laser shock peening and post weld heat treatment processes will be applied after laser cladding in order to investigate how these processes interact, and to assess whether they can be used effectively in combination in order to improve the hardness, corrosion resistance and the mitigation of residual stresses. This thesis focuses on overlays based on AISI grade 316L stainless steel. This is an austenitic stainless steel that is widely utilised in marine applications, pharmaceuticals, food processing equipment, oil and refinery components and medical applications such as orthopaedic implants.

Based on this over-arching aim, specific objectives have been established as follows:

- To determine the appropriate laser cladding parameters that produce a cladding without discontinuities such as porosity and cracks, and avoid lack of fusion between overlapping tracks and the base material, using similar and dissimilar coatings and base materials;
- To examine the microstructure and hardness developed with different process parameters;
- To examine the corrosion resistance and the state of residual stresses in the laser clad samples;

- To apply laser shock peening to the laser clad samples and to examine its effects on the microstructure, hardness, residual stresses and corrosion resistance;
- To apply post weld heat treatment to the laser clad samples and to examine its effects on the residual stress and corrosion resistance.

This work will be the first detailed study that links laser deposition parameters, dilution, hardness and residual stresses to the corrosion performance of laser deposited overlays in AISI grade 316L stainless steels. In doing so, the potential benefits of residual stress mitigation processes such as laser shock peening and post-weld heat treatment will also be investigated.

1.3 Thesis outline

Chapter 2 is a literature review covering the main types of laser used in material processing, discussing some characteristics that are relevant at present to select the appropriate laser. Furthermore, a literature review of laser cladding is also included where the different ways of feeding material are explained. Also, the effects of laser processing parameters such as laser power, powder feed rate and traverse speed on the development of the clad layer are explained in detail. The different forces acting on the molten pool and the associated temperature distributions are also explained. A review of laser shock peening is also included, providing an explanation of the main process parameters. In addition, a brief discussion on the microstructure and hardness developed by laser cladding is also included. Finally, a review of the residual stresses developed in laser cladding and laser shock peening and their measurement is covered, together with the different mechanisms of corrosion.

Chapter 3 describes the laser cladding experiments. The set up of for the experimental work is also described. In addition, a detailed explanation concerning the issues involved in the generation of cladding without discontinuities is presented.

Chapter 4 provides a description of the procedure utilised in order to reveal the microstructures developed in the clad samples. Furthermore, the effects of the processing parameters on the microstructure have been investigated. In addition, the hardness developed in the clad samples is also assessed.

Chapter 5 presents the assessment of the residual stresses generated in the cladding samples, as measured by the shallow hole drilling technique and the contour method.

Chapter 6 describes the effects produced by laser shock peening and post weld heat treatment on the residual stresses in the clad layer. Furthermore, an assessment of the hardness of the material after laser shock peening is also provided.

Chapter 7 provides information relating to the exposure of the clad samples to corrosive environments, in order to assess the stress corrosion cracking mechanism. Furthermore, the results are related to the residual stresses in the samples, with and without the application of laser shock peening and post weld heat treatment.

Chapter 8 presents a summary of the conclusions obtained from this study. Furthermore, suggestions for future work are provided.

Chapter 2

Literature Review

2.1 Introduction

The use of lasers in industry has promoted the development of different manufacturing techniques such as laser rapid manufacturing (LRM), laser engineering net shaping (LENS), selective laser powder re-melting (SLPR), direct metal deposition (DMD), selective laser cladding (SLC), shape deposition manufacturing (SDM) and direct metal laser sintering (DMLS). These techniques have been continuously incorporated into various industries because they have offered reductions in production time and production costs. The principle of these techniques is based on a fabrication approach which involves the deposition of material layer by layer. Although these techniques are similar in concept, since they all involve laser deposition, they are used for different applications [18-21].

Even though lasers have contributed significantly to the evolution of manufacturing techniques based on laser deposition, different applications which do not involve the deposition of material can be also performed. Their application is based on the laser power density and interaction time, which affects whether the laser heats, melts or shocks the surface of the base material [22]. Figure 2.1 shows a classification of some laser surface treatments performed by lasers. The rapid manufacturing techniques can be classified as melting laser surface treatments. In this work, the emphasis is placed on laser cladding and laser shock peening processes.

This chapter describes the principles of the laser cladding deposition process and highlights some factors that could affect its performance. A brief description of some categories of laser that are frequently used in laser cladding and their general characteristics are also discussed. The mass transfer produced by a powder stream and the relationship between process parameters such as laser power, traverse speed and powder feed rate in the generation of a single cladding track is described. The different

forces acting in the melt pool are also discussed. An examination of the microstructures developed after rapid solidification, and the residual stresses generated by the steep temperature gradients in the vicinity of the cladding, and their measurements, are discussed in detail. Attention is also given to the different mechanisms of corrosion that can affect the performance of clad surfaces. Finally, the effects of different processing operations that could be used post cladding in order to improve mechanical properties such as hardness, and the corrosion resistance, are described.

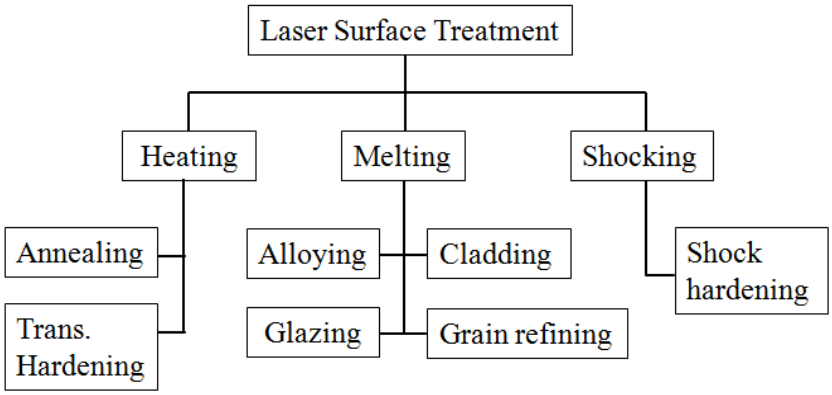

Figure 2.1 Methods of some laser treatments. Adapted from [22]

2.2 Types of lasers

The word “laser” derives from the acronym “light amplification by stimulated emission of radiation”. A laser consists of a chamber in which light is oscillating; the chamber contains an active medium which amplifies the light oscillations. The active medium is excited by an external source of power [1]. There are different types of lasers; these are normally classified by the active medium used to amplify the light. The principal categories are as follows [5]:

1. Fibre lasers
2. Solid-state lasers
3. Gas lasers
4. Semiconductor (diode) lasers

Although lasers are used for different applications, the most commonly used in industrial processes are the gas lasers, solid-state lasers and semiconductors lasers.

Fibre lasers:

Fibre lasers constitute another class of laser used in industrial processes such as welding and cladding. They have a good beam quality and are capable of achieving small spot sizes in the order of micrometres. The output powers have been typically in the hundreds of watts although more recently fibre lasers with beam powers of several kilowatts have become prevalent. They can be operated in pulse mode or in continuous wave mode and they use an optical fibre where the core is doped with either erbium (Er), neodymium (Nd) or ytterbium (Yb) rare earth elements as the active medium. Care is needed at high powers because the potential exists to damage the fibre [5].

Solid-state lasers:

Solid-state lasers used in industrial processes include Nd:YAG or Nd:glass. These lasers are more efficient than CO_2 lasers and they have an immense power laser (i.e. Nd:YAG in continuous mode up to kW and in pulsed mode up to MW). Nd:YAG laser uses a non-destructive solid of crystal as an active medium and Nd:glass lasers use a glass composition instead. The laser light output can be continuous wave or Q-switched (or pulsed) mode [3, 14]. This laser has been successfully used in order to shock peen material surfaces.

Gas lasers:

Carbon dioxide (CO_2) and Excimer lasers are different gas lasers used in industrial processes such as cutting or cleaning. They are suited to different applications according to the maximum laser power which varies in the range of kilowatts to milliwatts. The wavelengths emitted by the carbon dioxide and excimer lasers are approximately 10.6 μm and 249 nm respectively. In each case, the laser beam can be easily focused to a circular spot. Furthermore, CO_2 laser can be operated in continuous wave or pulsed mode while an excimer laser can only be used in pulsed mode. [3]

Semiconductor (diode) laser

High power diode lasers (HPDL) were introduced to the industry such as aerospace and, automotive in order to perform applications that involved welding, cladding or surface treatment. One advantage of this laser corresponds to the short wave-length emitted, which is in the range between of 0.65 and 0.94 μm. This leads to a higher level of absorption (and therefore more efficient use) of the laser light on material surfaces. The effect of short wave-lengths can be observed in Figure 2.2 where a CO_2 laser exhibited high reflectivity on steel material. Furthermore, with a HPDL laser, the output beam has a rectangular or square shape; although this can be changed to circular shapes with the use of special optics [5, 23-24]. This laser has been used in laser cladding processes because of its high energy efficiency and high power outputs. However, HPDL lasers have a poor beam quality, which means that a small spot size, in the order of micrometres, cannot be achieved. However, this does not present a problem in laser cladding operations since wider areas of a surface need to be covered. Furthermore, the laser beam profile is considered to more uniform in intensity as opposed to a Gaussian distribution.

A summary of the most common parameters used in laser cladding operations with different types of laser is presented in Table 2.1.

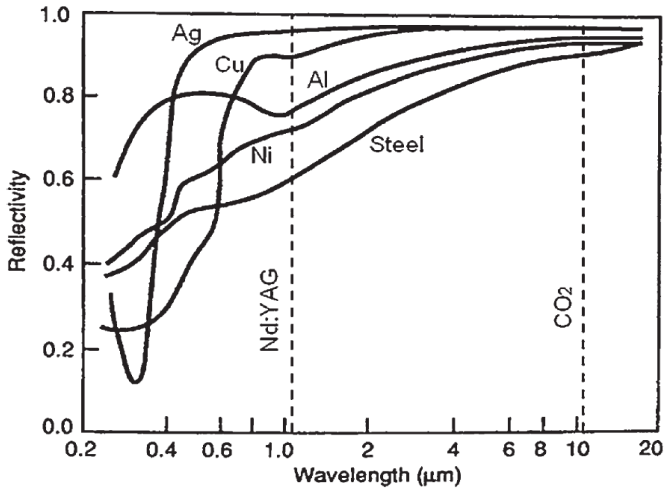

Figure 2.2 Reflectivity vs. Wavelengths for various metals [14].

Table 2.1 Typical laser parameters for lasers frequently used in laser cladding [3].

Characteristics	**CO_2**	**Nd:YAG Lamp-pumped**	**Nd:YAG Diode-pumped**	**HPDL**	**Fibre**
Wavelength (μm)	10.64	1.06	1.06	0.65-0.94	1.03-1.6
Efficiency (%)	5-10	1-4	10-12	30-50	20
Maximum power used in cladding operations (kW)	45	4	5	6	2
Average power density (W/cm^2)	10^6 to 10^8	10^5 to 10^7	10^6 to 10^9	10^3 to 10^5	10^7
Service period (hours)	1000-2000	200	5000-10000	5000-10000	100000
Beam parameter product (BBP) (mm × mradian)	12	20-45	12	100-1000	-
Fibre coupling	No	Yes	Yes	Yes	Yes

2.3 Laser cladding process

The laser cladding process involves producing a new coating layer on a base material. The new layer of material is fed on to the base material surface and melted by a heat of source in the form of high power laser. A CNC stage is used in order to move the base material to any position and produce different configurations of coating layers. In some circumstances the laser is moved by robotic arms and the base material remains static. The laser cladding process can be classified according the way the material is fed. There are four methods by which the new material can be delivered in order to produce the coating layer. These methods will now be discussed:

2.3.1 Pre-placed powder

The powder is mixed with a binder to produce cohesion between the powder and the substrate. The mixture is placed on the surface to be clad before the laser beam irradiates the substrate (Figure 2.3) [25]. There are some drawbacks with this method. For example, it should only be used on flat surfaces, the evaporation of the binder in the pre-placed powder can produce porosity, and it is difficult to maintain control of the molten zone. However, this process is straightforward and economical [1, 5, 26].

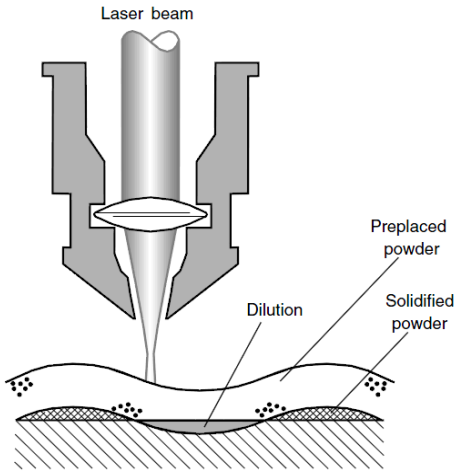

Figure 2.3 Pre-placed powder methods [5].

2.3.2 Paste

In this method, the powder is mixed with a binder in order to produce the paste and this mixture is deposited over the substrate. The difference between the paste and pre-placed method is that the paste is deposited almost at the same time as the laser beam irradiates the base material [3, 27]. Specific equipment is required in order to feed the paste; and this can be a drawback. Additionally, in order to have a strong coating, it is critical to control the substrate and paste feeding speeds. Figure 2.4 provides a schematic representation of the paste method.

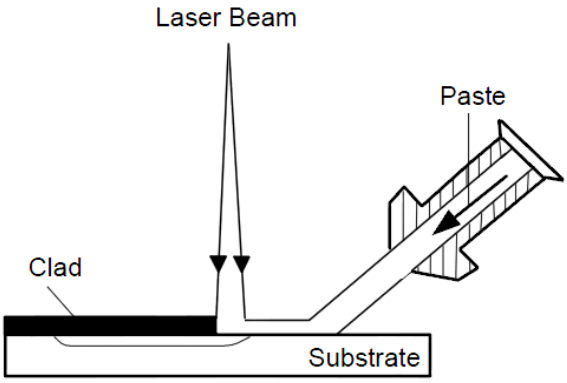

Figure 2.4 Paste methods [3].

2.3.3 Wire feeding

The cladding material is fed in the form of a wire toward the base material in order to produce a coating layer. This approach can be used to produce coatings in complex geometries. However this method tends to produce porosity, cracks, and sometimes poor bonding between the cladding and substrate, because only a small proportion of the laser energy is absorbed by the wire [3, 28-29]. On the other hand, the equipment used to feed the wire is straightforward and inexpensive. Figure 2.5 provides a schematic illustration of the wire feeding method.

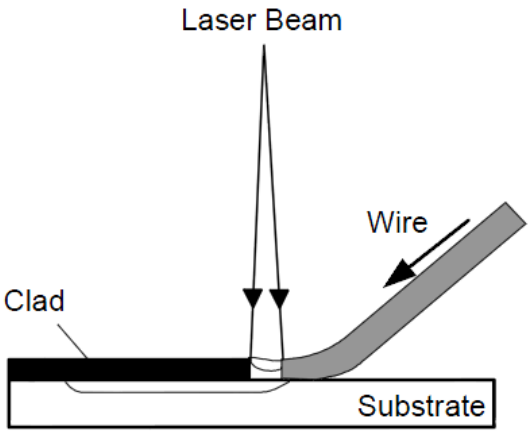

Figure 2.5 Wire feeding methods [3].

2.3.4 Powder feeding

The powder is delivered to the molten pool by a lateral or coaxial nozzle with the help of gases: typically argon or helium (these will be discussed later) [3, 11]. An illustration of this method is given in Figure 2.6. The powder feeding method has some advantages over the other methods. For instance, a lower power density is required to produce the melt pool, the use of a binder is not necessary, it can produce cladding with more stable geometry, and various powder combinations can be used in order to produce better wear and corrosion resistant coatings.

Owing to the benefits of powder feeding, this method has become prominent and is widely used in laser cladding applications. Therefore, the majority information and research presented in this work is focused on this method.

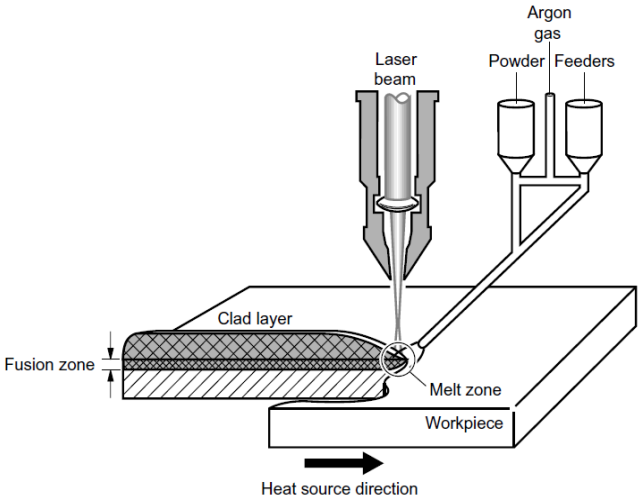

Figure 2.6 Powder feeding methods [5].

2.4 Mass transfer by powder stream

2.4.1 Feeding system

Two different options have been considered in laser cladding to deliver the powder over the substrate surface in order to produce the coating; these are using either a lateral or coaxial nozzle (Figure 2.6 and Figure 2.7 respectively).

The lateral nozzle was the first method used in laser cladding as a means of feeding. With this method, the powder is delivered by the lateral nozzle towards the substrate with the help of a gas (argon) and the laser beam is also shrouded by a gas (argon) in order to avoid oxidation. An advantage of using a lateral nozzle is that a sufficient volume of powder can be rapidly deposited over the substrate [30]. However, the movement of the cladding head is limited to one direction.

On the other hand, the use of a coaxial nozzle enhanced the use of laser cladding as a laser surface treatment. A coaxial nozzle improves the powder delivery efficiency because the powder, the carrier gas and the protective gas are delivered by the same nozzle [3, 31-32]. The coaxial nozzle can be used in robotic arms [33] and this led to laser cladding being used in processes such as additive manufacturing. Furthermore, 3D metal components can be manufactured using a CAD drawing, which offers a significant decrease in the production time for the manufacturing process [34-35].

As can be seen, three locations are highlighted in Figure 2.7: (1) the main hollow the laser beam passes through within the nozzle prior to reaching the substrate, (2) a flow of gas (argon or sometimes CO_2) is injected to protect the focussing lens from spatter and avoid powder oxidation, and (3) the powder is injected through the special cavities with the help of gas (argon) and it is fed toward the substrate. At the outlet of the nozzle, the powder becomes molten due to heating by the laser beam.

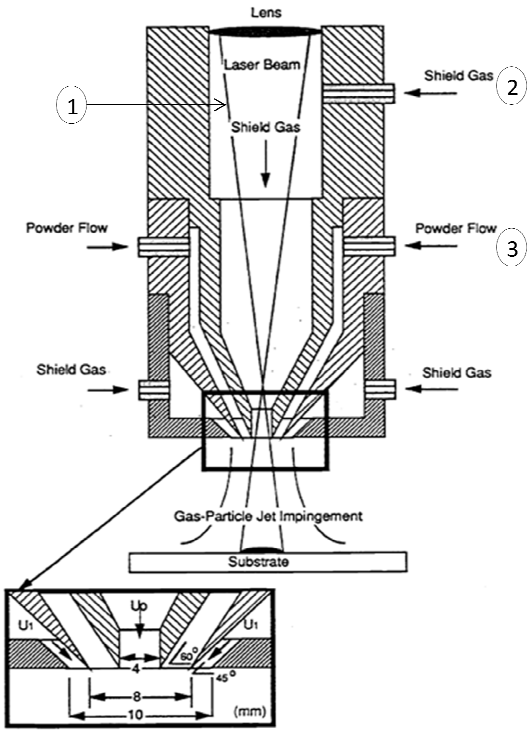

Figure 2.7 Coaxial nozzle [36].

2.4.2 Powder stream process

Laser cladding by powder feeding can use a lateral or coaxial nozzle so as to transport the powder to the molten pool. Here, the focus will be on the powder stream produced by the coaxial nozzle. The condition in which the powder stream arrives at the molten pool is critical; this means the powder should be homogenous in order to get a proper cladding. Toyserkany [3] suggested that if the powder stream maintains a laminar flow while it is transported then a homogenous powder stream will be achieved. Sometimes, it is difficult to get this condition because the flow of the powder stream also depends of factors such as powder feed rate, the powder itself and the nozzle profile.

Owing to the importance of the powder stream flow, many investigations have been carried out in order to understand the behaviour of powder stream flow under different conditions. Lin [34] and Lin and Steen[37] found that by using a coaxial nozzle, the density of the powder stream flow follows a Gaussian distribution, with maximum flow occurring at the centre of the nozzle. This mode of powder stream concentration has been further verified by Pinkerton and Li [38-39]. This kind of information can be useful for the design of coaxial nozzles.

On the other hand, apart from the design of the coaxial nozzle, other factors that could affect the powder stream flow include the velocities of the shielding and the carrier gas. As mentioned in section 2.4.1, the coaxial nozzle is built with special compartments for the shielding and carrier gases. The velocities of these gases are related to the velocity of the powder stream flow. If the velocity of the carrier gas is too high, most of the powder will not be melted because the powder will ricochet after hitting the base metal surface. Furthermore, if the velocity of the shielding gas is considerably higher than that of the carrier gas, some powder particles will be thrown out of the molten pool [40]. This means, there is a relationship between the velocity of the carrier and shielding gases. Figure 2.8 shows an example where the velocity of the shielding gas has been increased considerably and, as a result, some powder particles have been thrown out of the molten pool.

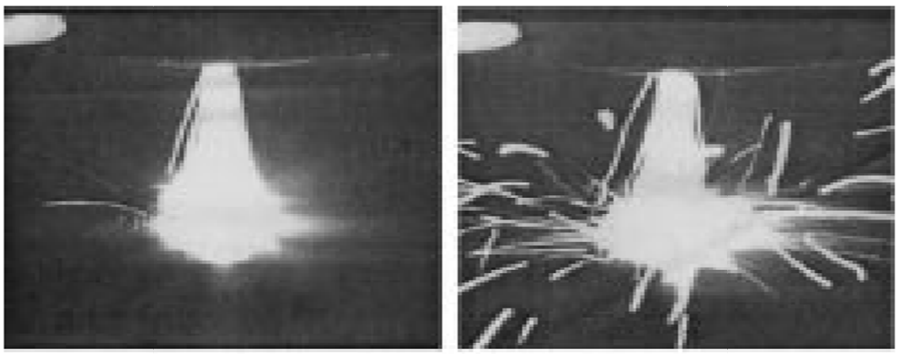

Figure 2.8 Hot powder streams. (a) Shielding velocity gas of 2 $m.s^{-1}$; (b) Shielding velocity gas of 8 $m.s^{-1}$ [40].

2.4.3 Laser cladding single track dimensions

The dimensions of laser cladding single tracks can be related to different process parameters such as the laser power, the powder feed rate and the traverse speed, and to some laser configuration parameters such as the laser beam diameter. The combination of these parameters can lead to the generation of various cladding configurations, for instance, they can lead to different values for the height and width of tracks (Figure 2.9); even though single track widths are strictly related to the beam spot size because the melt pool width is limited by the spot size [41]. This means, no further melting can

occur beyond the spot size. Several studies have focussed on this topic due to the importance of understanding the effects of process parameters on cladding configurations [41-46].

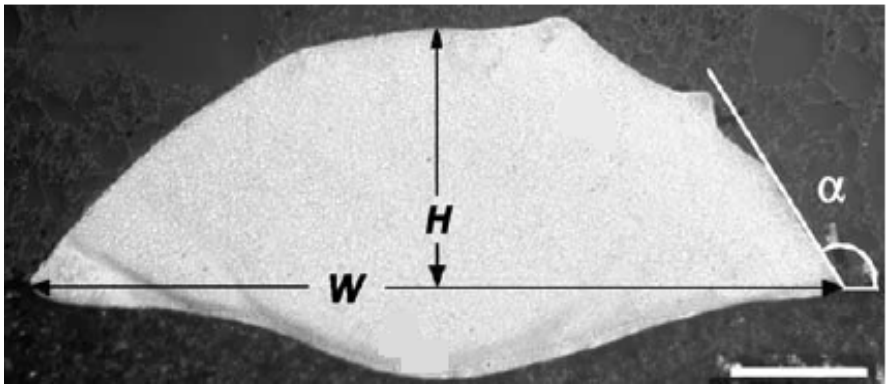

Figure 2.9 Cross-sectional area of single laser cladding track. Width W, height H and cladding angle α [44].

Figure 2.10 shows the change in single track height as a function of powder feed rate and traverse speed at constant laser power. It can be seen that the height increases as the powder feed rate increases. This is because higher amounts of powder have been deposited. However, low heights were also produced using a high traverse speed. In this case, because the traverse speed has been increased, less powder was deposited per unit length. Figure 2.11 shows the effects of laser power and traverse speed on track width at constant powder feed rate. Here, the single track width increases at high values of laser power. In this case, it is possible to melt most of the powder that is deposited. However, the widths are lower at high traverse speeds. Again, this is because less powder was fed into the melt pool.

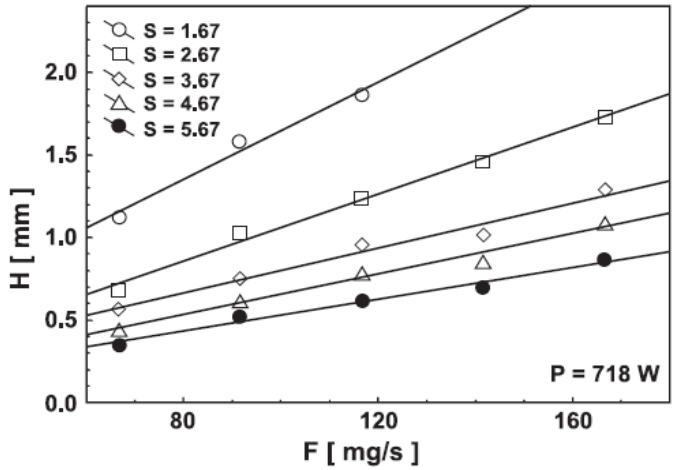

Figure 2.10 Single track heights, H, at different powder feed rates, F, and traverse speeds, S ($mm.s^{-1}$), at constant laser power, P [44].

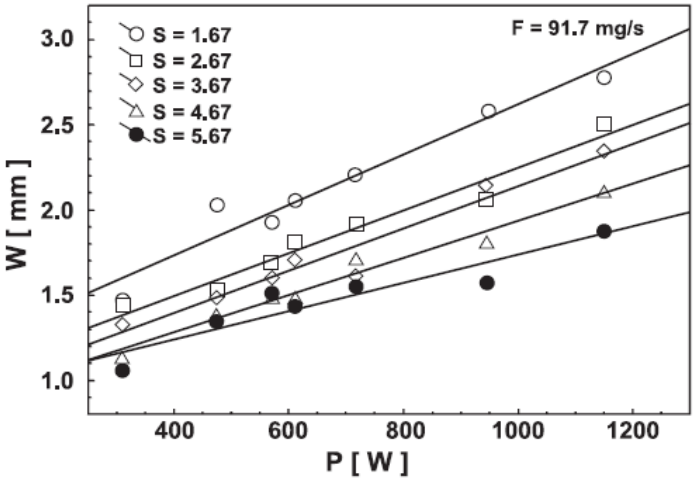

Figure 2.11 Single track widths, W, at different laser powers, P, and different traverse speeds, S ($mm.s^{-1}$), at constant powder feed rates, F [44].

Two parameters can be used in order to assess the likely changes in cladding geometry when considering the effects of process parameters on the height and width of a single laser cladding track. These are the specific energy and the powder density. The specific energy is defined as the energy per unit of irradiated area on the sample surface that is used to melt the materials [45], while the powder density is defined as the mass of powder that is deposited per unit of irradiated area [3].

$$Specific\ energy = \frac{P}{DV} \tag{2.1}$$

$$Powder\ density = \frac{m}{DV} \tag{2.2}$$

where P is the laser power, m is the powder feed rate, D is the spot size diameter and V is the traverse speed.

According to Equations 2.1 and 2.2, changes in traverse speed directly affect the specific energy and the powder density. Although, there are other functions that can help to describe the laser cladding profiles such as laser specific energy input [47]. However, most researchers refer to specific energy and powder density. Figure 2.12 shows how the thickness of the clad layer (or the layer thickness) is influenced by the specific energy and the powder feed rate. It appears that there may be a linear behaviour between the layer thickness and both the specific energy and the powder feed rate.

The cladding angle, α, (Figure 2.9) is an important parameter when several single tracks are overlapped in order to cover a larger area [48]. This angle must be approximately 120°; otherwise lack of fusion between single tracks will be expected. This means, angles lower than 90^{o} will produce an irregular track shape, where an unfused area can be generated between the base material surface and the deposited material. The gap that is produced with low angle cladding will prevent the incident beam from reaching the base material when a subsequent track is deposited. The specific energy and the powder density also have an influence on the dilution, which will be discussed in the next section.

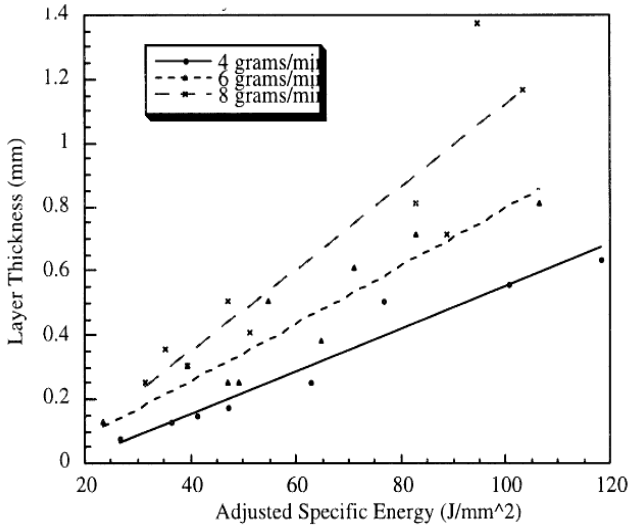

Figure 2.12 Effect of specific energy and powder feed rate on layer thickness [49].

2.4.4 Dilution

Dilution refers to the extent to which the deposited material is diluted by the substrate. When examining a cross-section of a single track, dilution can be defined as the ratio of the substrate area that is melted to the total melted area [5]. Figure 2.13 illustrates the measurement of dilution for a single laser cladding track. Single track dilution can be expressed as:

$$Dilution = \frac{Substrate\ area\ melted(2)}{Clad\ region\ area(1) + Substrate\ area\ melted(2)} \tag{2.3}$$

Several studies have been carried out in order to understand how dilution is affected by laser power, traverse speed and powder feed rate. Basically, it has been found that each parameter affects dilution in different ways [5, 46, 50-53]. Dilution increases if an increment in laser power is produced. In this case, an increment in laser power represents an increase in the amount of energy used in order to melt the powder and the base material. Figure 2.14 show the changes in dilution with changing laser power, where a linear relationship between laser power and dilution can be observed.

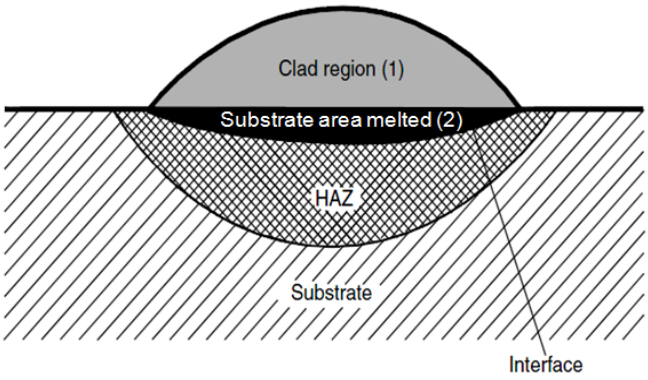

Figure 2.13 Dilution in single track laser cladding [5].

Powder feed rates also affect dilution. It has been seen that an increase in powder feed rate leads to a reduction in dilution. This is because with an increment in powder feed rate, a higher percentage of the laser energy is used for melting the powder and a smaller percentage of the energy is used to melt the base material [54]. The changes in dilution originating from an increment in powder feed rate are depicted in Figure 2.15 where it is possible to observe that higher powder feed rates produced low values of dilution. Although a low dilution is generally expected in laser cladding, very low values can lead to lack of fusion between overlapping tracks.

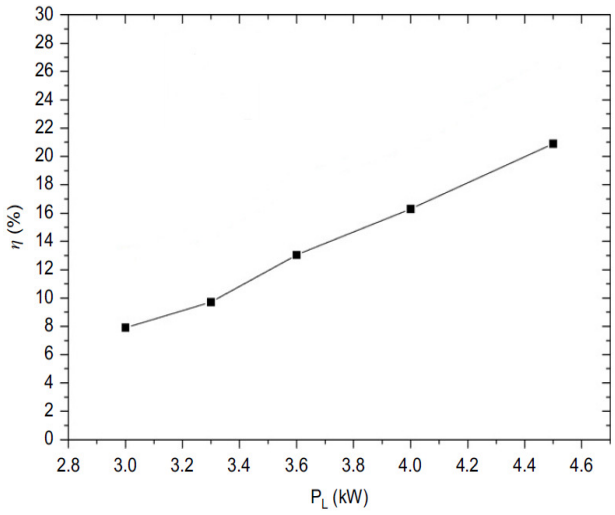

Figure 2.14 Dilution developed in Ni-based alloy deposited on carbon steel substrate at different laser powers with traverse speed of 11mms^{-1} and powder mass flow rate of 11.3gmin^{-1} [51].

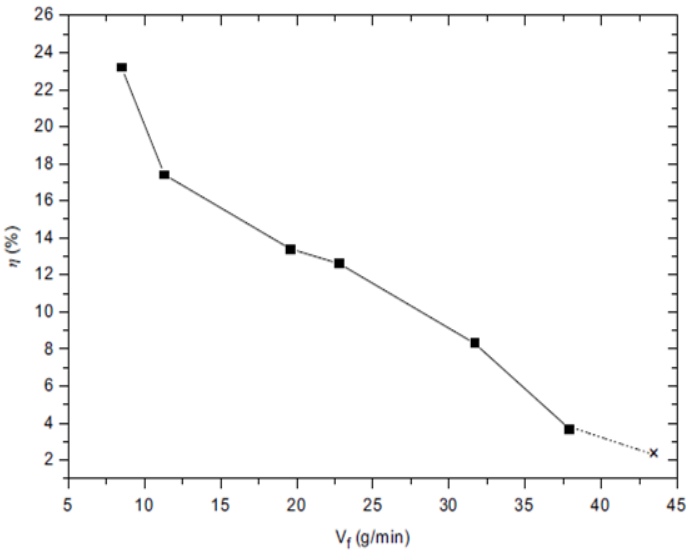

Figure 2.15 Relationship between powder feed rate ,V_f , and dilution, η. Laser power = 4kW, Traverse speed = 15mm.s^{-1} [51].

Dilution shows different behaviours when the travel speed is changed. At low travel speeds a reduction in dilution is observed when the travel speed starts rising. However, with further increases in speed, an increase in dilution starts to manifest. In this case, the quantity of powder material that is deposited per unit length is reduced to the point where more laser energy is reaching the base material surface. This effect can be observed in Figure 2.16.

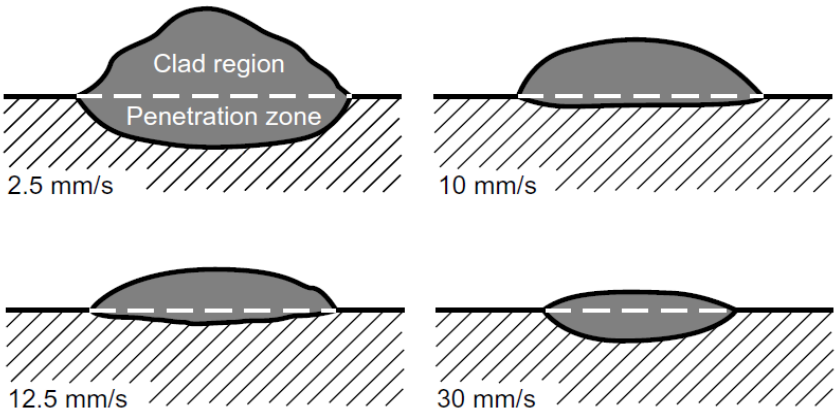

Figure 2.16 Effects of traverse speed on clad configuration. Cross-sectional view of the clad track [5].

Dilution can also be related to the specific energy and the powder density (Equations 2.1 and 2.2). It is often easier to understand the effects of specific operating parameters on dilution when they are interpreted in the form of combined parameters such as specific energy and powder density. A number of studies have been carried out in order to model the track formation and dilution [52, 55-57], given the importance of dilution in laser cladding and other process.

Laser cladding is generally used to either produce a coating with superior mechanical properties to those of the substrate, or to repair worn component surfaces by the overlapping of several single tracks. In this case equation 2.3 should be redefined when more than two tracks are deposited. For such cases, the dilution equation can be defined as (Figure 2.17): [55, 57-58]

$$D_{ov} = \frac{P_{ss}}{P_{ss} + H_{ss}} \tag{2.4}$$

where D_{ov} is the overlay dilution under steady state conditions, P_{ss} is the steady state average penetration and H_{ss} is the steady state average height. This equation should only be applied under steady state conditions. Steady state conditions are reached when the penetration is similar for each track, and the overlay height has stabilised. In laser cladding this seems to occur after approximately five tracks have been deposited. In order to get an accurate estimate for dilution, several tracks should be measured and the average can be considered as the dilution.

In laser cladding, it is desirable to achieve low dilution especially when dissimilar materials are used, due to a high dilution resulting in more base material being melted and mixed with the powder material, thereby changing considerably the chemical composition and properties of the newly deposited layer. If a high dilution results, it will usually be necessary to deposit more than one clad layer in order to reduce the effects of dilution. However, if similar materials are used, dilution will not produce considerable changes in the newly deposited layer.

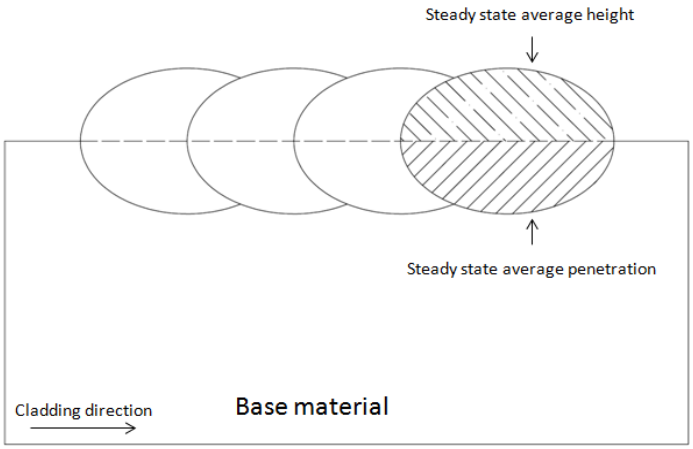

Figure 2.17 Dilution under steady state conditions.

2.5 Melt pool dynamics

2.5.1 Heat transport in the melt pool

It is important to understand the temperature histories experienced during laser processing because this defines the development of the microstructure. The peak temperature and the cooling rate are especially important [5]. Laser process parameters such as laser power, traverse speed and powder mass flow rate directly affect the temperature distribution and the size of the molten pool [59-61]. However, the thermal properties of the materials involved and some physical characteristics also have considerable effects on the temperature distribution. Several studies have been carried out in order to model the temperature distributions in laser processes. Good approximations have been found using the Rosenthal equations [5]. Figure 2.18 shows the temperature distribution represented by a family of isotherms developed in materials of different thermal conductivity in a single pass. The form of the isotherms indicate that the temperature travel faster through the material with higher thermal conductivity.

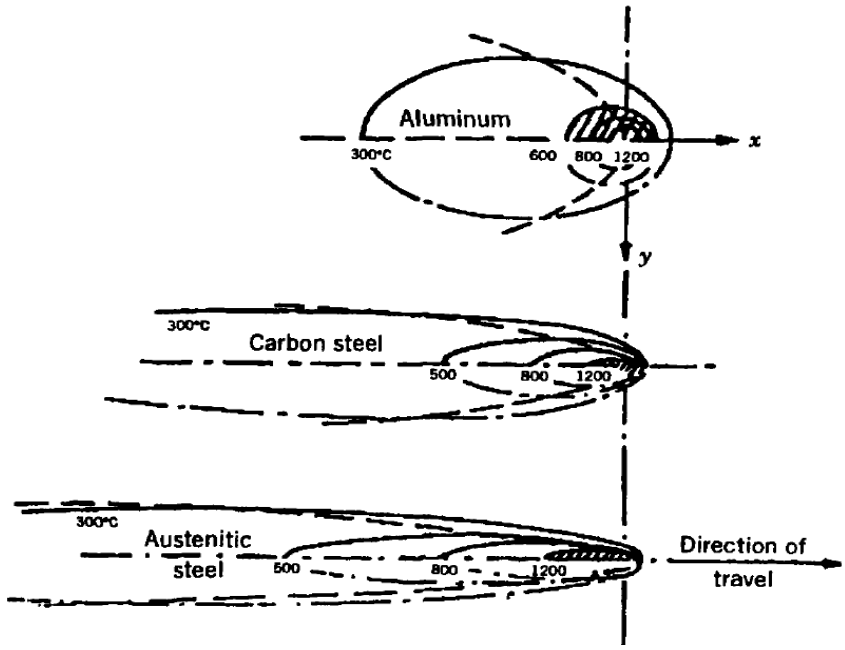

Figure 2.18 Effect of the thermal conductivity in different base materials. Heat input (q) = 3.1 kJ.s^{-1}; traverse speed (v) = 480 mm.min^{-1}; Plate thickness (d) = 60 mm. [62]

Higher temperatures are reached when several single tracks are deposited one on top of another in order to produce vertical walls. Peyre [63] showed the different melt pool sizes that result in the deposition of single tracks, where the melt pool size increases according to the number of single tracks deposited. The increase in the molten pool size and in the overlay temperature for subsequent tracks can be explained by the lower heat dissipation that results as the tracks move further away from the base material. The same effect is produced when a single layer of overlapping tracks is deposited in order to generate a clad surface. In this case, the substrate temperature starts increasing as the deposition of the overlapping tracks proceeds [64]. Figure 2.19 shows the temperature distribution in overlapped tracks.

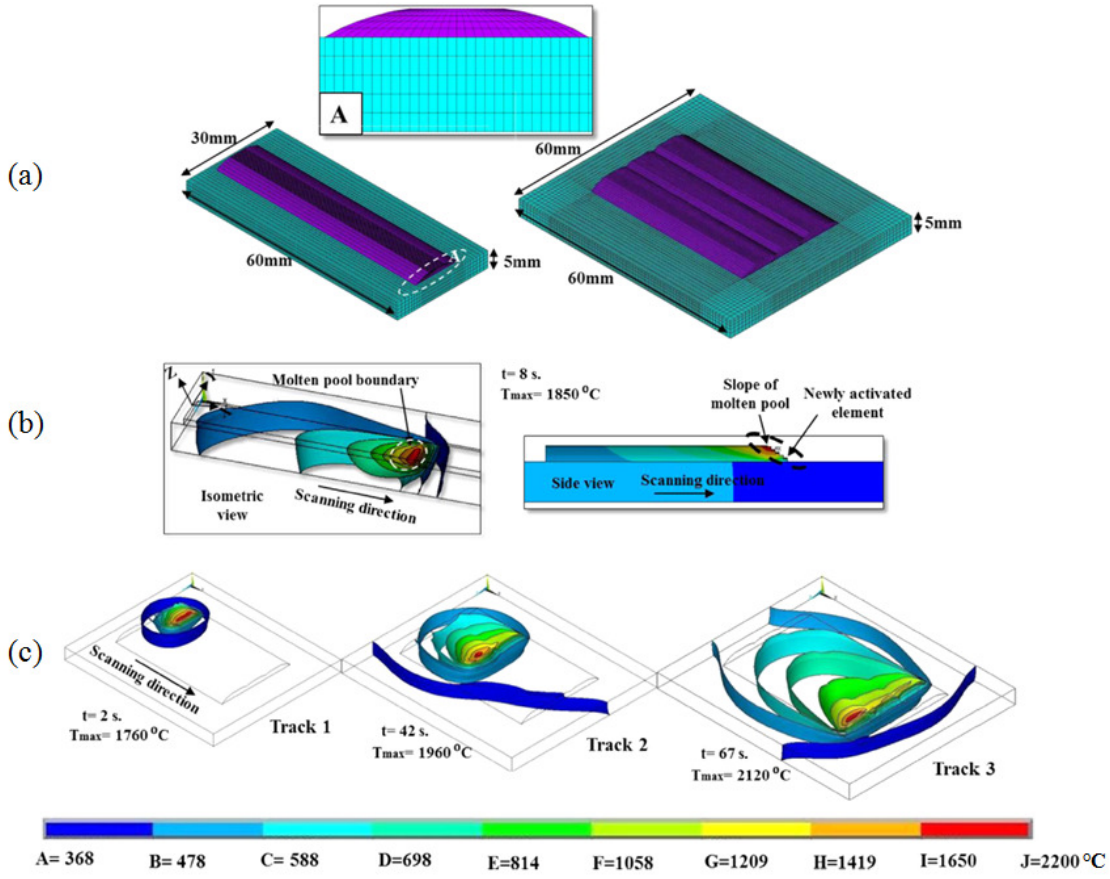

Figure 2.19 Temperature distributions in laser cladding process produced with a laser power of 3800 W, traverse speed of 300 mm.s^{-1}, and a powder feed rate of 18 g.min^{-1}. (a) Geometry of the FEM model for single and multi-track clad deposition. (b) Temperature distribution in single track. (c) Temperature distribution in overlapped tracks. High temperatures are generated along the base material with overlapped tracks compared with the temperature produced for a single track [64].

2.5.2 Flow in the melt pool

The flow of material in the molten pool in processes such as laser cladding or laser welding directly affects the penetration and bead width, the solidification structure, and the likelihood of porosity and lack of fusion. Two of the most important driving forces for flow in the molten pool are surface tension and buoyancy. The surface tension force produces thermocapillary flow due to changes in the temperature. The flow of material driven by surface tension is also known as Marangoni convection [5, 65-66]. The buoyancy force is also considered as a gravitational force, and it manifests due to differences in density owing to the temperature gradients within the weld pool.

Surface tension gradients are present in the molten pool surface owing to differences in temperature. A flow of material is induced in which material travels from locations with lower surface tension to locations with higher surface tension. Surface tension gradients are usually dependent on the presence of temperature gradients, and the surface tension gradient can either be negative (i.e. decrease with increasing temperature) or positive (increase with increasing temperature). Figure 2.20 illustrates the effects of negative and positive surface tension gradients on the shape of the deposited bead.

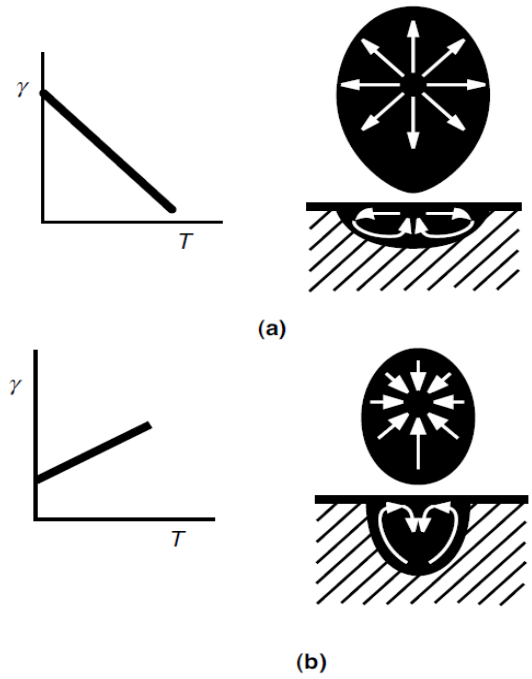

Figure 2.20 Flow of material in molten pool with (a) negative gradient; the bead shape is wider and penetration is small and (b) positive gradient; the bead penetration is high [5].

If a negative gradient is developed (Figure 2.20a), a wider melt pool with low penetration is produced because the flow of molten metal tends to go outward from the centre of the pool. This leads to the hottest material at the centre of the pool being transported outward to the periphery and then turning downward before returning to the centre of the pool [5, 60, 62, 67-68]. In pure metals, a negative gradient would be most likely. However, the sign of the surface tension gradient is affected by the presence of active elements such as sulphur and oxygen in the base material. If these elements are present a positive gradient can develop (Figure 2.20b). In such cases, the flow of the

molten material moves from the periphery to the centre of the pool owing to the surface tension forces. Then the hottest material in the centre is then driven downward, producing deeper penetration [5, 67].

2.6 Discontinuities

Laser cladding can introduce discontinuities in to the clad layer such as porosity and cracks, and there are several factors that must be avoided in order to produce a sound overlay. If cracks or porosity are present in the overlay, the mechanical properties of the final coating or the corrosion resistance can be affected.

Three different types of porosity can be found in laser cladding: inter-track porosity, inter-layer porosity and intra-layer porosity [69]. Inter-track porosity arises when several parallel tracks with irregular shapes (inappropriate laser cladding angle) are deposited. In this case, lack of fusion occurs between overlapping tracks near the base material. Inter-layer porosity is found in the deposition of several vertical layers. Lack of fusion is produced either due to the presence of oxide films between layers which prevents bonding, or due to variability in the specific energy or misplaced tracks [70]. Intra-layer porosity is produced by the presence of gas pores trapped into the molten pool during solidification. The primary reason for the presence of pores is surface contamination (e. g. due to oils, moisture or paint). The gases produced due to the evaporation of these sources of contamination lead to porosity [5]. Furthermore, oxygen, nitrogen and hydrogen are the principal gases that produce porosity. Therefore, techniques that help to clean the surface of the work piece are always recommended.

According to Refs. [70-71], inter-layer and intra-layer porosity can be controlled by increasing the traverse speed and the laser power. However Wang [72] has showed that lack of fusion between the base material and the coating is produced by a high traverse speed. If the traverse speed is increased an increment in laser power should be considered if lack of fusion occurs.

Other factors that can promote porosity are related to the process parameters. For instance, if a low laser power and a high traverse speed are used, some proportion of the powder particles will not be melted [73]. Figure 2.21 shows an example in which a poor

selection of process parameters has led to gas being trapped in the cladding. Furthermore if moisture is present in the powder, this can also promote porosity. Therefore, sometimes it is recommended to bake the powder prior to deposition.

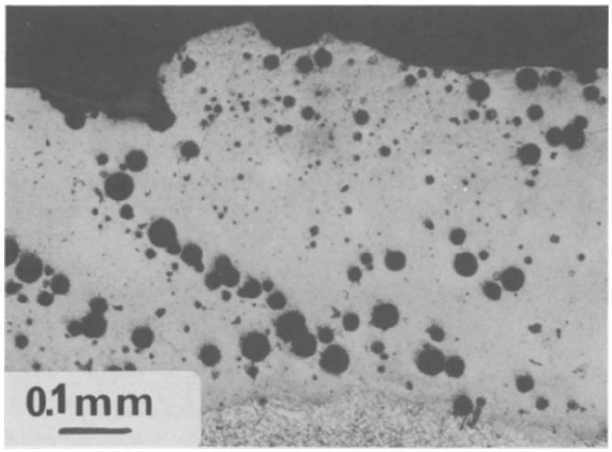

Figure 2.21 Presence of porosity due to gas being trapped in the cladding after solidification with a laser power of 1.9 kW and a scanning velocity of 1.5 cm.s^{-1} [73].

Cracks can be introduced by the laser cladding process and there are various contributing factors: residual stresses developed after solidification, high cooling rates, low–melting at the fusion zone, and the use of brittle materials. Cracking can occur in the fusion zone, in the heat affected zone, and sometimes in both, and can manifest during solidification, a short time after solidification or even days after the cladding operation.

Cracking can be classified as either hot cracking (solidification) or cold cracking (hydrogen cracking). Hot cracking refers to cracks that appear immediately after solidification, most likely in the fusion zone. It is related to the formation of liquid films along the grain boundaries due to low-melting constituents that develop localized weaknesses once segregation takes place. Therefore, the material is susceptible to fail in the presence of tensile residual stresses. Cold cracking, however, refers to cracking that occurs after solidification, closer to room temperature, and commonly appears in the fusion zone or in the heat affected zone. The occurrence of cold cracking is related to processes such as material hardening (martensite formation) and embrittlement by

hydrogen. Cracking is often transgranular, however sometimes it can be intergranular [5].

Even though the causes of cracking are often related to the solidification process, it has been established that the presence of some contaminants at the work piece surface can also cause cracking [5, 74-75].

Substrate preheating can mitigate the generation of cracks in the laser cladding process [76-80]. Due to the localised melting, steep thermal gradients are generated. After solidification, high thermal strains are generated because of the contraction of material. The thermal strains lead to the development of residual stresses, which normally are tensile stresses [81-82]. The magnitude of these tensile stresses is sometimes high enough to produce cracks in the cladding. Therefore substrate preheating is used to reduce the temperature gradients. Figure 2.22 depicts the preheating effects in different materials. It can be observed that cracks tend to disappear with increasing the preheating temperatures. Furthermore, the magnitudes of the tensile stresses are also affected.

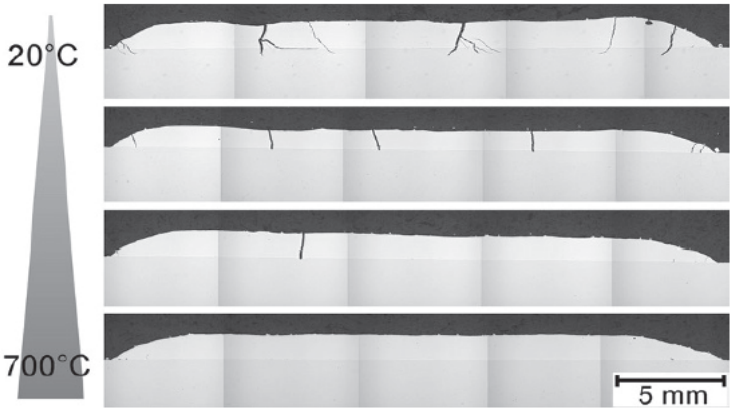

Figure 2.22 Decrease in frequency of cracking with increase in substrate preheating temperature for Stellite 20 coatings deposited on AISI 1045 base material [2].

2.7 Laser shock peening

The laser shock peening process involves irradiating a surface with sufficient laser energy (in the order of Joules), and power density (in the order of $GW.cm^{-2}$), in a short

period of time (nanoseconds), so that plasma is developed. The plasma generates shock waves that hit the metal surface and consequently compressive residual stresses are developed. Shock peening can be carried out in different modes: confined ablation and direct ablation [14]. Figure 2.23 provides a schematic representation for each of these modes

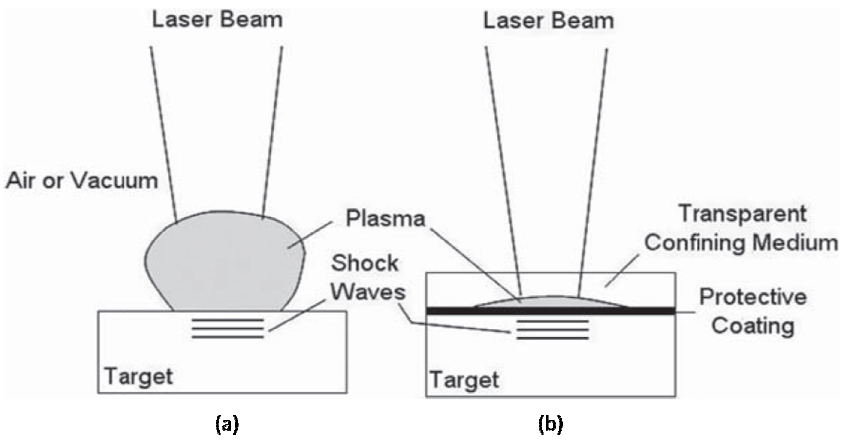

Figure 2.23 The laser shock peening process: (a) direct ablation, (b) confined ablation [14].

In confined ablation, an absorbing layer is placed over the surface of the work piece (normally a black layer), and this is covered by a dielectric layer that must be transparent to the laser beam (normally water or glass). The laser beam vaporizes the black layer; the vapour is ionized with the remaining laser energy leading to the generation of plasma (Figure 2.23b). This immediately expands and creates high pressures at the work piece surface. The dielectric layer maintains the high pressure over the work piece surface; the high pressure is converted to shock waves that are transmitted toward the work piece and then compressive stresses are produced.

In direct ablation, in order to produce a plasma, a few microns of the metal surface are vaporized and ionized (Figure 2.23a). The plasma expands freely and the peak pressure that is developed is smaller than for confined ablation. Although the peak pressure is smaller, it is still in the order of GigaPascals, which is sufficient for some applications. According to Ref. [83], it is necessary to use double the laser energy that would be needed to get the same effect with confined ablation.

The use of a thermo-protective or absorbing layer avoids melting the surface of metals with the radiation. If the absorbing layer is thick, the shock waves may be stronger whereas if the absorbing layer is thin, thermal effects are produced over the surface due to some material surface can be melted by the laser irradiation; and thermal damage may occur [15].

Most of the literature that is reviewed in the current work relates to laser shock peening in confined ablation owing to this mode being more common than direct ablation. However, as is explained above, confined and direct ablation follow the same principles. The primary difference is that higher pressures are developed by confined ablation [5, 15].

2.7.1 Advantages

Laser shock peening is a relatively new process that is used in industrial applications involving metallic surfaces in order to generate compressive residual stresses. It has some advantages when compared with conventional stress-mitigating processes such as shot peening, and these include [5]:

- It can introduce high levels of compressive residual stress to a greater depth below the surface than is possible with shot peening.
- At the moment compressive stresses are generated, the work piece suffers less cold work
- Shot peening always leaves dimples over the metal surface, and this can be a drawback for some applications that require a satisfactory aesthetical appeal. This problem is not present with laser shock peening.
- Laser shock peening can be used for pieces that have complex shapes.
- Laser shock peening can create micro dents over the work piece surface that can be used as reservoirs of lubricant in order to improve wear resistance. [84]

Furthermore, laser shock peening offers good control of the precise locations of the impacts and there is no need to replace the shot constantly, which would be the case in conventional shot peening. In general, laser shock peening can also be used to reduce or eliminate tensile residual stresses, without necessarily introducing compressive stresses.

However, it is considered a process that is still under development and it is also an expensive process. The expense can be considered a disadvantage.

2.7.2 Requirements for laser shock peening

As mentioned previously, laser shock peening requires a powerful laser in order to achieve the best results. Hence the selection of the appropriate laser system is crucial. The principal parameters to consider in laser shock peening are the laser power, the pulse power density, the pulse energy and the pulse duration. However, laser wavelength is another parameter that also has an influence on the peak plasma pressure that is generated. Table 2.2 shows typical ranges for these parameters. A brief explanation of these parameters is given in the next section [5].

Table 2.2 Typical parameters used in Laser Shock Peening [5].

Parameters	Values	Units
Power (average)	1	kW
Pulse power density	1-50	$GW.cm^{-2}$
Pulse energy	100	J
Pulse duration	1-50	ns

The selection of the laser system is a critical point for consideration because of its bearings on the cost and efficiency of the process. The cost of maintenance and the replacement of parts must also be considered due to their direct relationship with the cost of the process.

Laser shock peening processes use the laser beam in pulsed form and laser systems such as neodymium-doped glass or yttrium aluminium garnet (YAG) crystal lasing rod. Table 2.3 provides a summary of the common lasers used in laser shock peening, and it also gives typical values for the common parameters of the laser system.

Some researchers [85-87] have used a femto second pulse laser to perform laser shock peening. Although these lasers are not so powerful, the energy generated by the short pulse (in the order of femto seconds) is enough to achieve an acceptable peak pressure in the ablation zone and hence to introduce compressive residual stresses.

Recent investigations have revealed a different way to carry out shock peening. The process can be performed under water without an ablative layer, whereby the laser energy that is used is in the order of mili-Joules and a high frequency is employed. Despite the significant differences between this approach and the conventional confined ablation process, the results achieved are satisfactory [88-89].

Table 2.3 Typical laser systems used in laser shock peening processes [15].

Treated materials	Laser type	Laser power (J)	Power density (GW/cm^2)	Pulse duration (ns)	Laser spot size (mm)	Absorbent coating	Transparent overlay	Peak pressure (GPa)	References
Rock	Nd: glass	5–100	1–15	20	2–6.6	–	Water	1.4	Bolger *et al.*, 1999
Al foil	Nd: glass	40	0–25	25–30	3–5	–	Water (glass)	5.5	Berthe *et al.*, 1997
Thin Al	Nd: YAG	6	0.05–1	150	3	–	–	0.8	Griffin *et al.*, 1986
Al 2024-T351 and T851, 7075-T631 and T73	Nd: glass	–	–	20–30	0.6–3	Black paint	Water (quartz)	10	Clauer and Fairand, 1979
2024-T3 Al	Nd: glass	–	5	18	10	Black paint	Water	–	Yang *et al.*, 2001
2024-T62 Al	Nd: glass	–	1.57–7.32	18–23	6–8	Black paint	K7 glass	–	Zhang and Yu, 1998
Al-12Si, A356 Al, 7075Al	Nd: glass	80	1–8	15–30	5–12	Black paint	Water	2.5	Peyre *et al.*, 1996
Ti-6Al-4V	Nd: glass	–	5.5–9	–	5.6	Black paint	Water	–	Smith *et al.*, 2000
SUS304 s.	Nd: YAG	0.1	4.5	5	0.75	–	Water	0.5	Sano *et al.*, 1997
316L s.s.	Nd: glass	40–100	8–20	3–10	–	Black paint	Water	10	Peyre *et al.*, 2000b
Al, 55C1 s., 316L s.s.	Nd: glass	40	8–10	8–10	3–4	Al paint	Water	6	Peyre *et al.*, 1998a
316L s.s., X12CrNi12-2-2 s.	Nd: glass	40–100	1–100	0.6–30	0.5–1	Al foil, Al adhesive	Water	6	Peyre *et al.*, 1998b
Hypoeutectoid s.	Nd: glass	80	5–10	25	5	Black paint	Water (BK7 glass)	5	Masse and Barreau, 1995a, b
Fe-30%Ni Al	KDP	4000	10^2–10^4	1	4.3–25	–	–	0.6	Grevey *et al.*, 1992
304 s.s.	Nd: glass	80	300	0.6	7.2	Black paint	Water	18	Gerland *et al.*, 1992
Hadfield manganese	Nd: glass	100	2400	0.6	3–3.5	Black paint	Quartz	39.5	Chu *et al.*, 1995
18Ni(250) s.	Nd: YAG	0.03	1000	0.15	0.1	Black paint	Water	–	Banas *et al.*, 1990b

s. = steel, s.s. = stainless steel.
KDP = potassium dihydrogen phosphate.

2.7.3 Laser power density

Pulse power density is a fundamental parameter to consider in laser shock peening because it affect the generation of plasma and it also defines the maximum pressure generated at the target surface. This means that with increases in power density, the pressure generated owing to the plasma also increases. There are other parameters that also have an influence on the process such as the wavelength of the laser and the laser pulse duration. These will be discussed in the next sections.

In order to generate a plasma, the target surface should be exposed to a power density higher than 10^9 W.cm^{-2} [14]. However, for some metals this value can be different. Fabbro [83] showed that cooper requires a power density of above 0.6 GW.cm^{-2} in direct ablation and above 0.5 GW.cm^{-2} in confined ablation in order to generate a plasma.

It is worth noting that, the pressure generated in the process does not always increase with increasing power density. This means, that at a certain power density, pressure saturation occurs. In confined ablation, this is due to the confined layer exceeding its dielectric breakdown threshold [14-15, 90]. This effect is depicted in Figure 2.24 where dielectric breakdown in water confinement occurs at a power density of 10 GW.cm^{-2}. In Figure 2.25, dielectric breakdown in glass confinement occurs at a power density of 9-10 GW.cm^{-2}.

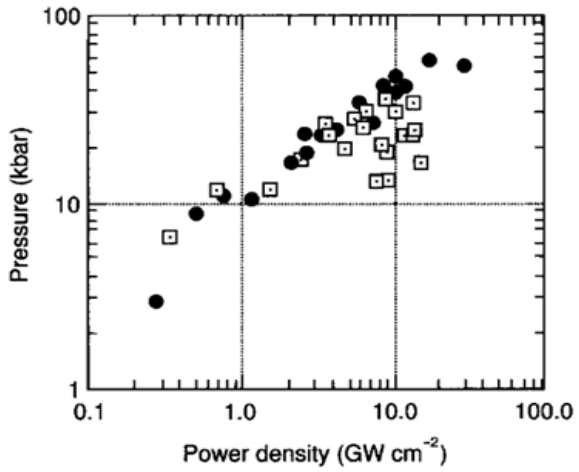

Figure 2.24 Maximum pressure as a function of power density in water confinement: Gaussian pulse (□) 30ns duration, short rise time (SRT) pulse (•) 25 ns pulse duration [90].

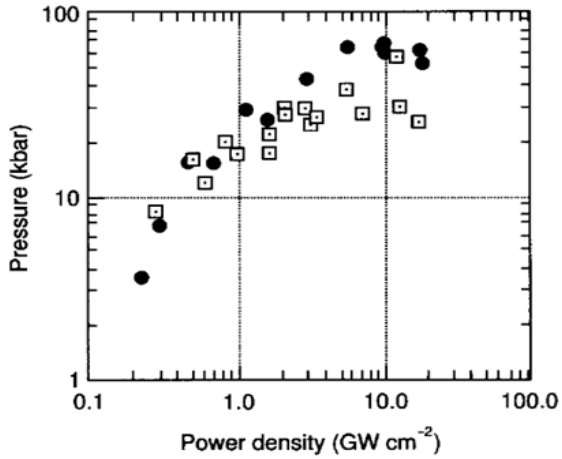

Figure 2.25 Maximum pressure as a function of power density in glass confinement: Gaussian pulse (□) 30ns duration, SRT pulse (•) 25ns duration [90].

Another significant effect of the power density is related to the rate at which pressure decays in the process. The "pressure duration" decreases considerably when high power densities are used due to a saturation of pressure. An example in which the pressure duration reduces with increases in power density is depicted in Figure 2.26. [91]

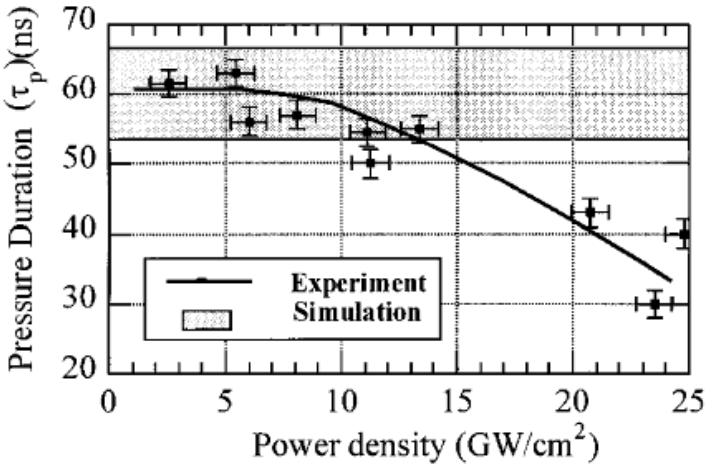

Figure 2.26 Duration of pressure as a function of power density [91].

2.7.4 Laser pulse duration

As mentioned in the previous section, pulse duration also has an influence on the generation of pressure in the laser shock peening process. The pulse duration can be described in two ways: the duration of the laser pulse or the time in which the laser beam irradiates the target surface. Normally a short pulse laser is used in shock peening, and the duration is in the order of nanoseconds [5].

Pulse duration is related to the pressure duration in the shock peening process. In direct ablation, the pressure duration is approximately equal to the pulse duration. In confined ablation, the pressure duration is 3-4 times larger [14]. Some researchers have reported that with a short laser pulse it is possible to generate larger peak pressures [14, 90]. This can be appreciated in Figure 2.24 and in Figure 2.25 where short laser pulses (SRT 25 ns pulse duration) generated higher pressures.

2.7.5 Laser wavelength

Thus far the effects of pulse duration and power density on the generation of plasma and consequently the plasma pressure that is generated in the laser shock peening process have been described, but laser wavelength is another critical parameter in the process. The different effects of short and long wavelengths will be explained.

Using short wavelengths at a certain power density increases the photon interaction between the laser and the work piece and this improves the shock wave generation. However, the peak plasma pressure decreases with short wavelengths. This is because, at shorter wavelengths, the confinement breakdown threshold appears at lower power densities. This phenomenon is depicted in Figure 2.27. Here, three different wavelengths have been plotted. The shorter wavelength (355 nm) developed a maximum pressure of 3.5 GPa at 6 $GW.cm^{-2}$; while the larger wavelength (1064 nm) developed a maximum pressure of 5 GPa at 10 $GW.cm^{-2}$. [14-15, 92-94]

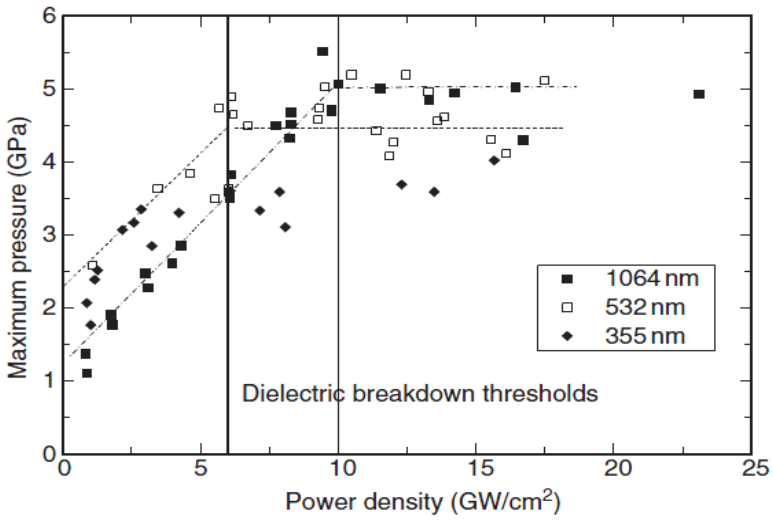

Figure 2.27 Peak pressure in water confined medium as a function of power density at different wavelengths [15].

2.7.6 Pressure generated

A mathematical model developed to calculate the pressure generated in laser shock peening has been proposed in Refs. [83, 90-91] and it is described in three steps.

1) In the moment the laser beam irradiates the interface between the surface material and the confined layer, the pressure developed by the plasma generates two shock waves with velocities D_1 and D_2, which propagate into the treated material and in to the confined layer (Figure 2.28). Owing to the shock waves, a distance, *L*, between the surface being treated and the confined layer is generated and this distance increases due to the pressure.
2) When the laser beam is stopped, the pressure generated is maintained for a short period of time (nanoseconds) and then it starts to decrease due to adiabatic cooling. At this stage, the treated material acquires a mechanical momentum due to the shock waves.
3) After some time, the hot gas trapped at the interface impacts the material surface as a projectile, adding more mechanical momentum to the material surface.

The distance, *L*, can be considered to be the thickness of the interface and its value is governed by the following equation: [83]

$$\frac{dL(t)}{dt} = \frac{2}{Z} P(t) \tag{2.5}$$

where t is time, $P(t)$ is the plasma pressure and Z is the shock impedance. Regarding the heating phase, the absorbed laser energy increases the energy of the plasma at the interface and is also used to generate the gap between the confined layer and the base materials, L. This can be represented by:[83]

$$I(t) = P(t)\frac{dL}{dt} + \frac{d[E(t)L]}{dt} \tag{2.6}$$

where $I(t)$ is the energy per unit area deposited by the laser, $P(t)$ is the plasma pressure, and $E(t)$ is the thermal energy for the plasma. The first term of equation 2.6 refers to the work done by the plasma and the second term refers to its internal energy.

Finally, if the plasma is considered to be a perfect gas, and if we introduce a factor (α), to represent the ratio of the internal to thermal energy, equations 2.5 and 2.6 can be used to calculate the pressure generated by a plasma as follows: [90]

$$Pressure = A\left(\frac{\alpha}{2\alpha + 3}\right)^{1/2} Z^{1/2} I^{1/2} \tag{2.7}$$

where A is the absorption coefficient for surface coating, α is the ratio of thermal to internal energy, Z is the shock impedance ($g.cm^{-2}.s^{-1}$) and I is the laser intensity ($GW.cm^{-2}$). However, if a water or a glass confined layer is used the pressure can be reduced according to: [90]

$$Pressure(Kbar) = BI^{1/2} \tag{2.8}$$

where B is 21 for a glass confined layer and 10.1 for a water confined layer, and I is the laser intensity in $GWcm^{-2}$. A satisfactory approximation for the pressure generated can

be obtained using these equations. As mentioned before, the pressure generated in confined ablation is 3-4 times higher than in direct ablation.

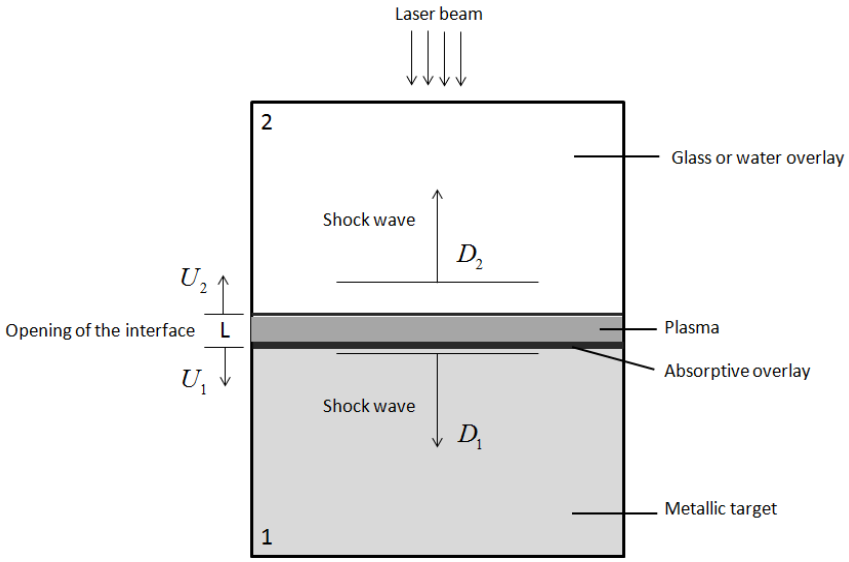

Figure 2.28 Effects of the shock waves generated by laser shock peening.

2.8 Microstructure

When stainless steels are used as the overlay material, the microstructures developed after solidification in laser cladding can be described as either planar, cellular, columnar dendritic or equiaxed dendritic microstructures. The generation of a finer microstructure is attributed to the rapid solidification and the high cooling rates [5, 25, 79, 95-97]. Also, the temperature gradients developed in the process have an important effect on the microstructure. The cooling rates that arise in laser cladding can be described by [5]:

$$\frac{dT}{dt} = \frac{\partial T}{\partial x}\frac{\partial x}{\partial t} \tag{2.9}$$

where dT/dt represent the cooling rate, $\partial T/\partial x$ is the thermal gradient and $\partial x/\partial t$ represent the solid-liquid interface velocity. Figure 2.29 shows an example of the different microstructural morphologies that can develop in laser cladding.

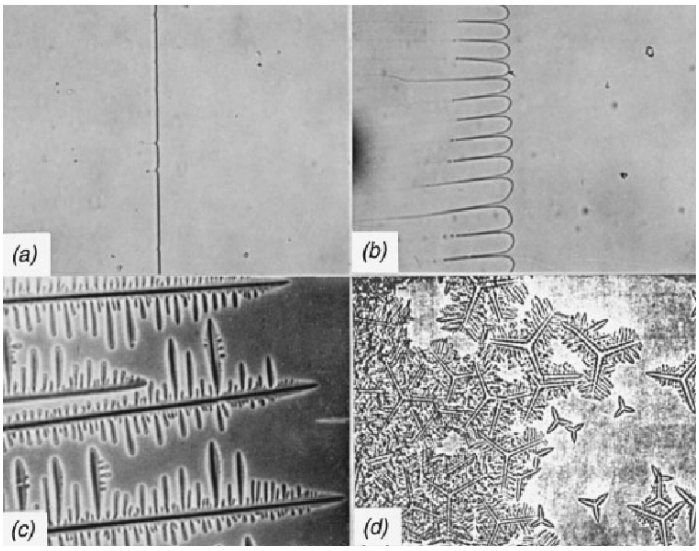

Figure 2.29 Microstructures developed after of solidification: a) planar microstructure of carbon tetrabromide, b) cellular microstructure of carbon tetrabromide, c) columnar dendritic microstructure of carbon tetrabromide, d) equiaxed dendritic of cyclohexanol [96].

According to Refs. [5, 96] the main parameters that define the final microstructure in the process are the solidification rate and the temperature gradient in the melt pool close to the solid-liquid interface. However, these parameters are directly related to process parameters such as laser power, interaction time, traverse speed, and powder mass flow rate. The relationship between the temperature gradient and rapid solidification is presented in Figure 2.30.

It is possible to observe that if the solidification rate increases and the temperature gradient decreases, and the result is a finer microstructure. Furthermore, if the solidification rate decreases and the temperature gradient increases, coarse microstructures are developed. Therefore, it is necessary to remark that rapid solidification produces finer microstructures. Traverse speeds in laser cladding are usually high. Hence this characteristic also leads to the process generating finer microstructures or in other words, equiaxed dendritic microstructures, and this usually occurs in the last stage of solidification [5].

The grains normally grow in the direction of the maximum temperature gradient, and when solidification occurs the growth is normal to the molten pool boundary. The benefits of obtaining a finer microstructure are that the space between the dendritic arms

and the dendrites is small and this generally leads to better ductility, toughness and strength [5].

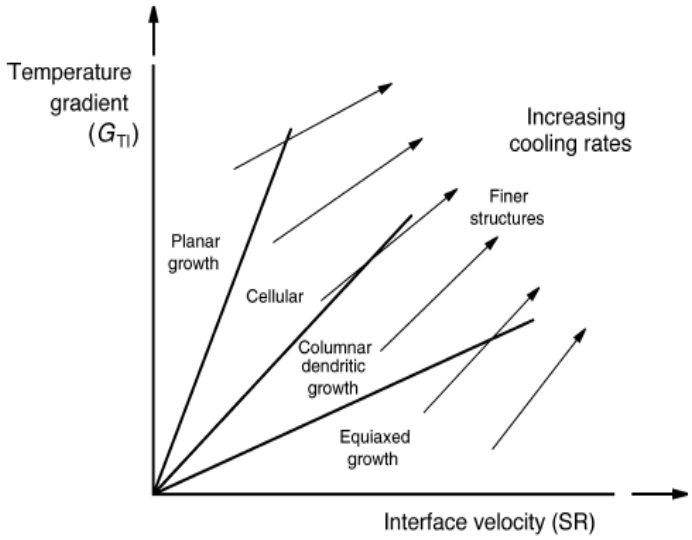

Figure 2.30 Relationship between solidification rate and temperature gradient in solidification process [5].

Several investigations have been carried out in order to understand the development of microstructures in laser cladding. Hemmati [95] has observed that a transition from planar to cellular and columnar dendrites can occur in the deposition of one single layer of AISI 431 martensitic stainless steel. However, when five layers where deposited, it was possible to observe equiaxed transition at the top surface. This was attributed to the heat accumulation in the five layers, which may have reduced the temperature gradients.

On the other hand, different solidification modes can be developed in austenitic stainless steels. The solidification mode is related to two aspects, (1) the concentrations of ferrite promoting elements (chromium, molybdenum, silicon, titanium, aluminium, vanadium and tungsten) and austenite promoting elements (nickel, manganese, carbon, nitrogen, copper and cobalt) and (2) the cooling rates. [98]

In general, considering the aspects mentioned above, four solidification modes can arise in austenitic stainless steels: austenitic, austenitic-ferritic, ferritic-austenitic and ferritic. These solidification modes are explained below in Figure 2.31 which shows the four solidification modes in a Fe-Cr-Ni system. The effects of the nickel content (austenitic promoter) and the chromium content (ferritic promoter) on the development of different solidification modes at different temperatures can be observed.

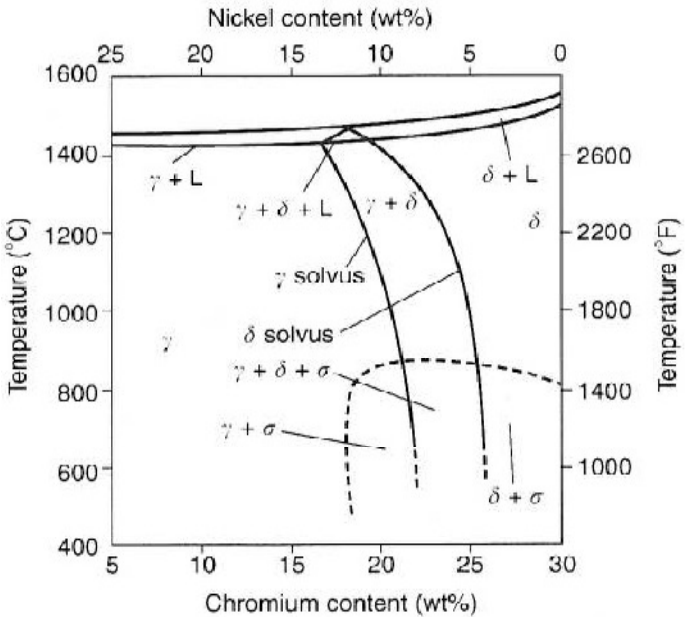

Figure 2.31 Pseudobinary section of the Fe-Cr-Ni system at 70% iron [98].

Figure 2.32 shows the solidification modes considering the ratio of chromium equivalent and nickel equivalent. The chromium and nickel equivalent are the sum of different components of the material used in order to estimate the phases morphologies developed after a melting process such as welding or cladding. The chromium and nickel equivalent are defined as:[98]

$$Cr_{eq} = Cr + 2.5\,Si + 1.8\,Mo + 2\,Cb \quad (2.10)$$

$$Ni_{eq} = Ni + 0.5\,Mn + 30\,C \quad (2.11)$$

Fully Austenitic Solidification (A)

In this solidification mode austenite is the primary phase, and once the material starts to solidify, austenite remains until room temperature is reached. This means, the cooling rate does not affect the development of austenite. Figure 2.33 shows a microstructure developed via fully austenitic solidification.

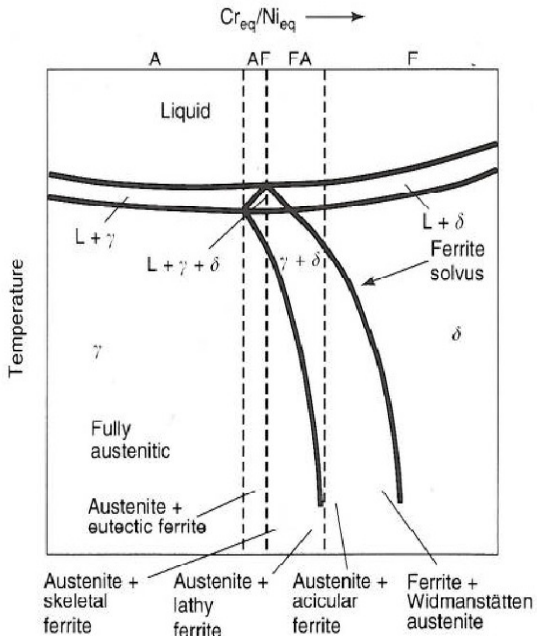

Figure 2.32 Solidification modes for different ratios of chromium equivalent and nickel equivalent [98].

Figure 2.33 Stainless steel microstructures developed by fully austenitic solidification [98].

Austenitic-Ferritic Solidification (AF)

In this mode, ferrite-promoting elements (primarily chromium and molybdenum) are present in sufficient quantities to develop ferrite during solidification. Austenite remains as the primary phase, but ferrite will appear along the grain boundaries and it remains stable to room temperature. Figure 2.34 shows an example of a stainless steel microstructure resulting from the AF solidification mode.

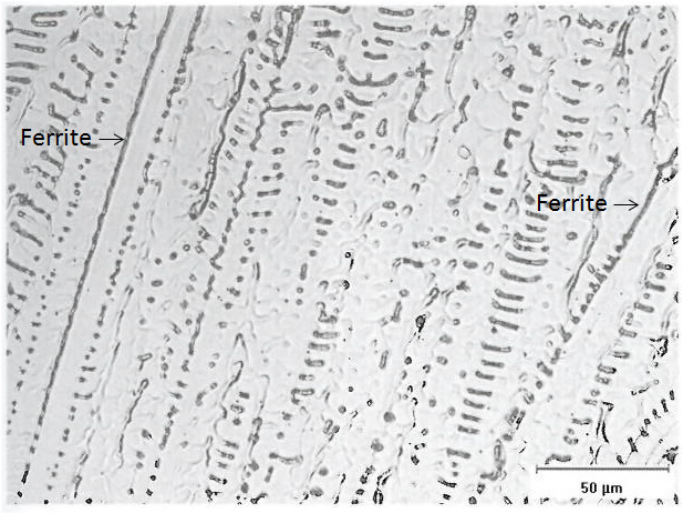

Figure 2.34 Stainless steel microstructures developed via Austenitic-Ferritic solidification mode [98].

Ferritic-Austenitic Solidification (FA)

In this zone ferrite is the primary phase and some austenite can develop during solidification. Different ferritic-austenitic morphologies can be developed in this zone (Figure 2.32) such as skeletal and lathy ferrite. The development of these morphologies is related to the cooling rate and the ratio of the chromium equivalent and the nickel equivalent. Figure 2.35 shows an example of a stainless steel microstructure produced via the ferritic-austenitic solidification mode.

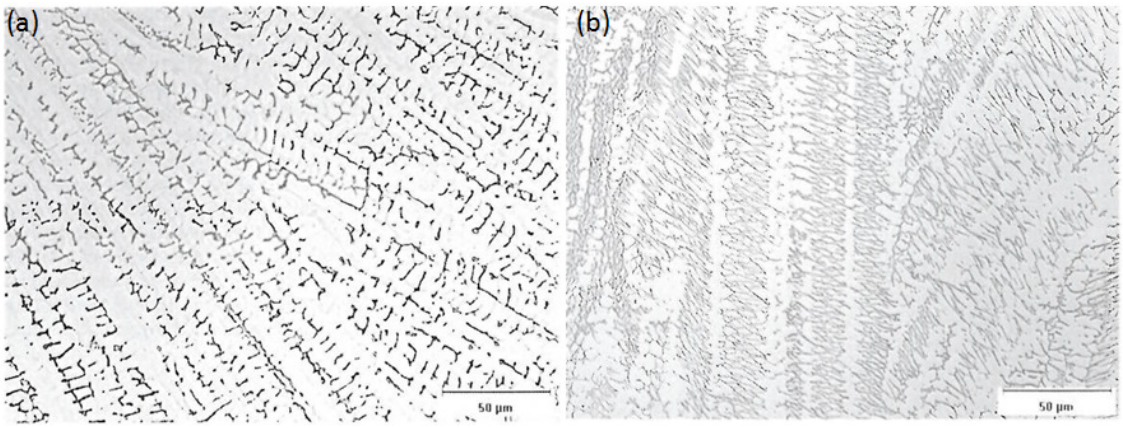

Figure 2.35 Stainless steel microstructures developed by Ferritic-Austenitic solidification: (a) skeletal ferrite morphology; and (b) lathy ferrite morphology [98].

Ferritic solidification (F)

Ferrite is the primary phase in this mode and the microstructure developed during solidification is fully ferritic. However, some austenite could form after solidification according to Figure 2.32. The development of austenite is related to the cooling rate and the ratio of the chromium and nickel equivalents. Figure 2.36 shows an example of a stainless steel microstructure resulting from ferritic solidification.

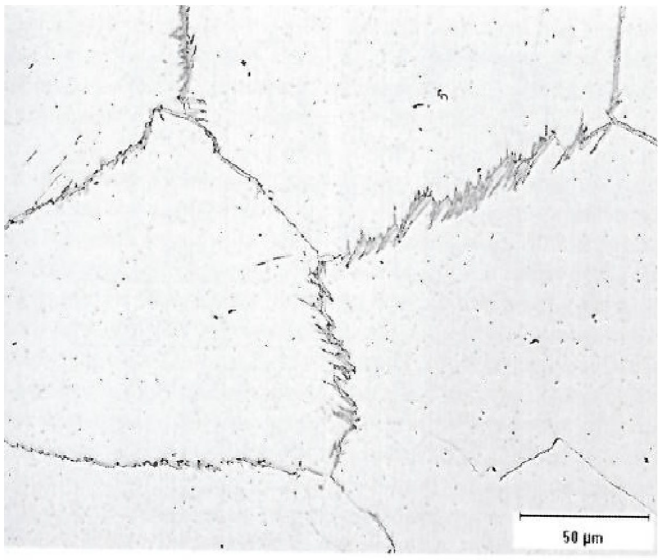

Figure 2.36 Stainless steel microstructures developed via ferritic solidification: Widmanstätten austenite nucleates from ferrite along ferrite grain boundaries [98].

Other constitution diagrams that are useful in order to know the final microstructure after the solidification process are the Shaeffler, DeLong and the Welding Research Council 1992 (WRC 1992) diagrams [98-99]. The purpose of these diagrams is to predict the microstructure that will develop according to the chemical composition of the metals. The chromium equivalence and the nickel equivalence are also required in order to predict the phase microstructure.

Some corrections have been made to these diagrams since they were first published in order to improve the accuracy of predictions for the final microstructure. These diagrams are used to predict microstructures for processes such as arc welding, laser welding and laser cladding. It is possible to predict the microstructure of stainless steel after accounting for the dilution associated with the process.

2.8.1 Shaeffler Diagram

The Shaeffler diagram is the basis for other diagrams such as the DeLong and the WRC-1992 diagrams and it was the first used to predict the final microstructure of stainless steels after the welding of dissimilar materials, by considering the chromium equivalent and the nickel equivalent of the stainless steels. Figure 2.37 shows a version of the Shaeffler diagram.

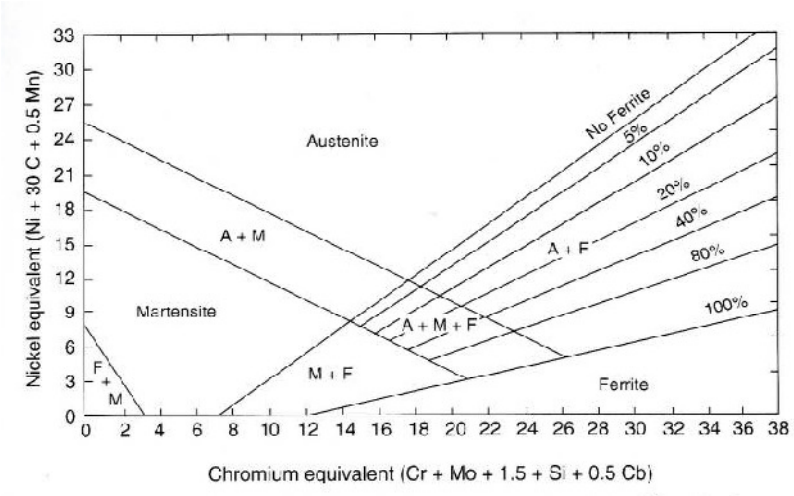

Figure 2.37 Shaeffler diagrams as of 1949 [98].

2.8.2 DeLong Diagram

This diagram incorporated some improvements to the Sheaffler diagram in order to predict the microstructure with improved accuracy. One of the improvements was the inclusion of nitrogen to the equation for the nickel equivalent (austenite promoting element). On the other hand, the range of compositions that were considered is smaller than for the Shaeffler diagram. Figure 2.38 shows a version of the DeLong diagram.

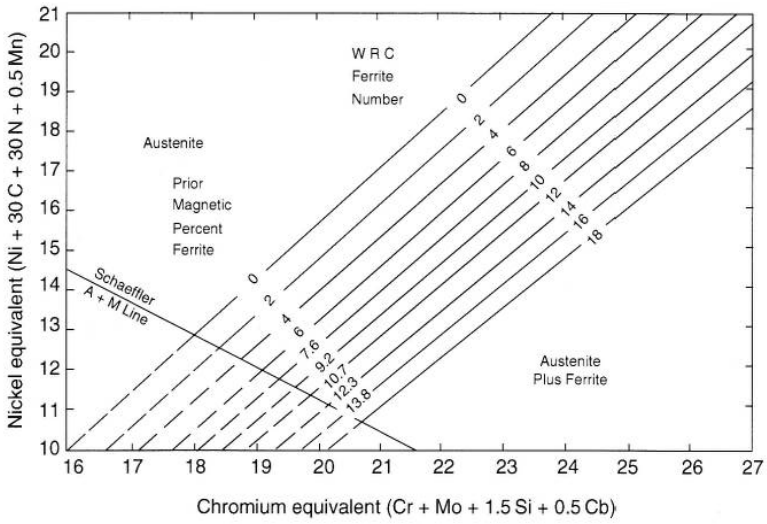

Figure 2.38 DeLong diagrams as of 1973 [98].

2.8.3 Welding Research Council-1992 diagram (WRC-1992)

The WRC-1992 diagram was introduced to address the limitations of the Shaeffler and DeLong diagrams. The four solidification modes have been included in this diagram and it has a ferrite number (FN) scale. It is possible to predict the microstructure developed by welding using dissimilar materials after considering dilution. In order to know the final microstructure, the chromium and nickel equivalent values are calculated for the two materials, i.e. the base material and filler or coating material; and then the two points are plotted on the diagram and a tie line is constructed. Finally the lever rule is used in order to predict the position of the weld metal on the diagram after considering the dilution. Figure 2.39 shows an example of the WRC-1992 diagram.

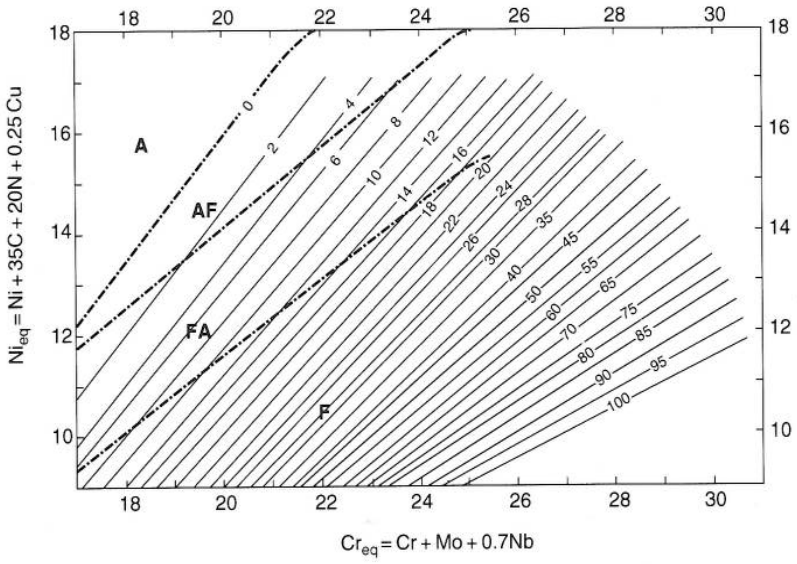

Figure 2.39 Welding Research Council-1992 (WRC-1992) diagrams [98].

2.8.4 Effects of laser shock peening on microstructure

Laser shock peening of metallic materials leads to changes in their microstructure owing to the high dislocation densities that are developed. This change is associated with a decrease in the size grains [100-106]. Figure 2.40 shows an example of the microstructure developed after laser shock peening of AZ31B Mg alloy where it is possible to observe a change in the grain size.

As mentioned before, finer microstructures generally lead to an improvement in corrosion resistance, fatigue life and hardness, and this corresponds to a material with better mechanical properties.

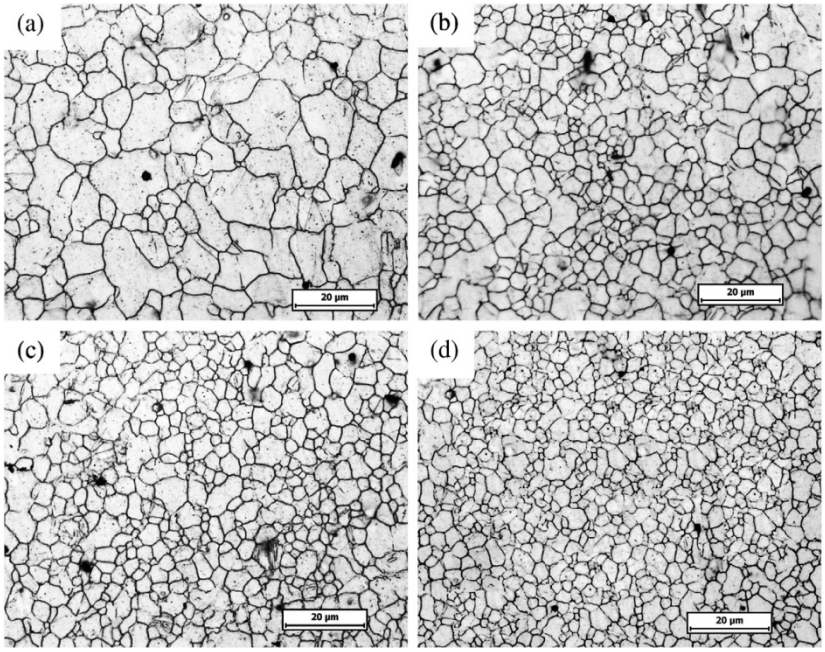

Figure 2.40 Microstructure developed of AZ31B Mg alloy (a) before laser shock peening, (b) after one impact, (c) after two impacts, and (d) after four impacts. It can be observed that finer microstructure is developed after various impacts [101].

2.9 Hardness

Hardness is considered to be the resistance of materials to indentation or being scratched by other materials. Once a material has been deformed plastically by external forces, a change in hardness is produced. Therefore hardness tests cannot be repeated in the same position. The hardness of a material is also related to the microstructure, whereby fine grained materials are harder and stronger than corresponding coarse grained materials. The yield strength of a material is related to the grain size and this relationship is described by the empirical Hall-Petch equation: [107]

$$\sigma_y = \sigma_o + K_y d^{-1/2} \tag{2.12}$$

where σ_y is the yield stress of the material, σ_o is a material constant corresponding to initial stress that is required for dislocation movement, K_y is a (constant) strengthening coefficient, and d is the average grain size. Since the yield strength is directly related to

the hardness [108], the Hall-Petch empirical equation can be rewritten to express the hardness as a function of grain size: [109]

$$H = H_o + Kd^{-1/2} \tag{2.13}$$

where H is the hardness and H_o and K are constants independent of the grain size.

Laser cladding is a surfacing process that develops finer microstructures after solidification owing to high associated cooling rates, and since different materials can be used as coatings, different chemical compositions and phase microstructures can be produced which lead to increases or reductions in hardness. It should also be mentioned that decreases in hardness can result after laser cladding under some circumstances. Mazumder et al [49] investigated the effects on hardness of a H13 steel tool coating. They found a reduction in hardness in subsequent deposited layers and this was attributed to annealing effect. The same effect can be found in other materials. Baufeld et al [110] used a Ti-6Al-4V wire as a coating material and noticed that no changes in hardness were produced using different process parameters. Furthermore, hardness was similar along the length of the clad surface. In contrast, changes in hardness were produced with different laser powers according to Ref. [111].

Dutta [112] built a vertical wall depositing several tracks of 316L stainless steel on to mild steel. An assessment of the hardness revealed a greater hardness close to the interface and this was attributed to the effect of quenching rate. The chemical composition of the metals also has an effect in hardness [113]. Syed et al [114] investigated the effects of chemical composition on hardness in the combined deposition of copper powder and nickel wire on to a H13 tool steel base material. They found that an increase in nickel content produced a higher hardness. On the contrary, when the copper concentration was increased a decrease in hardness was observed.

The hardness can change if hard phases are introduced in laser cladding. Alemohammad et al [115] produced a cladding using pre-placed Co-Ti alloy over a mild steel base material. An assessment of microstructure and phase composition revealed the presence of $TiCo_3$ elements in the cladding, which were considered the cause of greater hardness. The same effect was found in Ref. [116] when NiCrBSi alloy powder was deposited on

titanium base material. An increase in hardness occur and it was attributed to the generation of hard phases such as Cr_2Ni_3, $[Fe, Ni]_3 C_{26}$.

The hardness can also be enhanced by mechanical surface treatments such as laser shock peening (LSP). This novel process irradiates the surface of the sample using high power densities in order to produce a work hardened layer [117-118]. The effect of LSP as a function of depth depends on the process parameters. It has been found that LSP can increase the hardness of the samples to depths of up to several millimetres. Nalla et al [119] investigated the effect of LSP on Ti-6Al-4V material. The results showed an increase in hardness. Owing to the advantages of LSP, it is considered to be a practical surface treatment for increasing the hardness of metals.

2.10 Residual stresses

2.10.1 Introduction

Residual stresses are present in most metals. They can be generated by mechanical or thermal processes such as welding, cutting, and forming. The main reason is generally an unbalanced strain or misfit strain that has been generated between different regions within a material, or between phases or parts within the same body [120-121]. Residual stresses normally have a negative influence on the performance of metals because they reduce the fatigue life or wear resistance. Therefore, it is necessary to have knowledge of residual stresses and some control over them.

Laser process treatments, where heating is involved, may generate residual stresses in the fusion zone after solidification, as well as in the heat affected zone, and in the far field order to balance stresses generated in the vicinity of the treated zone. In laser cladding, the fusion zone is exposed to high thermal gradients, which generate thermal strains that lead to the generation of residual stresses; usually harmful tensile residual stresses. Sometimes non-uniform or localised plastic deformation also has an influence in the initiation of residual stresses. These effects can also lead to a change in the strength of the materials and produce distortion [5, 13, 64, 76, 122-123].

2.10.2 Thermal stresses

Thermal stresses are generated when the processes has been exposed to highly transient thermal gradients. These stresses can be associated with the following situations [62].

- A localised volumetric change, either shrinkage or expansion, such as may be associated with a change of phase,
- A difference in the coefficient of thermal expansion between the base and the coating material, i.e. a coefficient of thermal expansion mismatch,
- Temperature gradients can produce differential rates of contraction (on cooling) or expansion (on heating).

Whether or not the thermal stresses produce distortion in the material (macroscopically), they can produce internal cracks in the material (microscopically) or simply reside within the material. This is the reason they are called residual stresses. However, if a metal is heated uniformly without any restriction, this will expand uniformly and no thermal residual stresses will develop. This situation is not normally applicable to laser cladding. In general, thermal stresses are always present in laser clad surfaces and several detrimental effects such as the generation of cracks and low performance in corrosion environments can result.

2.10.3 Measurement techniques

Owing to the importance of the residual stress distributions that are generated in metals after manufacturing or surface treatment processes, different measurement techniques have been developed in order to quantify residual stresses. These techniques can be classified as non-destructive, semi-destructive and destructive [124]. The contour method, X-ray and Neutron diffraction, and hole drilling techniques have commonly been applied to measure residual stresses in welded joints, and in many cases to laser clad surfaces. However, some limitations have been observed among these techniques, depending on the condition of the specimen to be measured. The main characteristics of these techniques are presented in Table 2.4. In order to select an appropriate technique, three factors could be considered, the condition of the specimen, the area to be

measured and the orientation of the stresses. If the specimen surface has been work hardened, for instance, X-ray diffraction might not be a good option because x-rays may not penetrate far below the material surface [5]. Indeed, laboratory x-rays are capable of penetrating to depths of up to 50µm below the surface; which means only residual stresses close to the surface will be measured. However, neutron diffraction can measure the residual stresses up to a depth of 4 mm in titanium, to a depth of approximately 25 mm in iron based alloys and to depths of up to 200 mm in aluminium specimens, in three different directions. Even though neutron diffraction has several advantages over X-ray diffraction, access to neutron diffraction facilities is generally limited.

Since shallow hole drilling techniques have been used satisfactorily for processes such as welding and laser cladding and, more recently the contour method, these techniques are now discussed.

Table 2.4 Residual stress measurement technique [124].

Technique	**Restrictions on materials**	**Penetration depth**	**Spatial resolution**	**Accuracy**	**Comments**
X-ray diffraction	Crystalline	5µm (Ti) 50µm (Al)	20µm depth, 1mm Lateral	±20MPa	Combined often with layer removal for greater depth.
Neutron diffraction	Crystalline	4mm (Ti) 25mm (Fe) 200mm (Al)	500µm	±50 x 10^{-6} strain	Triaxial, low data acquisition rates, access difficulties.
Surface contour	Conductive				Expensive, requires the use of FEM*, well suited well to welds, destructive.
Hole drilling		~1.2 × hole diameter	50µm depth	±50MPa	Flat surface required, semi-destructive

*FEM Finite Element Method

2.10.4Shallow hole drilling method

Shallow hole drilling is a semi-destructive method that is used in order to measure residual stresses. It is also considered to be a stress relaxation technique. It consists of drilling a hole in the region of the sample surface that is of interest. Once the hole is drilled, the material surrounding it undergoes stress relaxation. The strains produced due to this stress relaxation can be measured using either a rosette of strain gauges; laser interferometry; or moire interferometry [5, 121]. The residual stresses, which were associated with the strains that were measured, can then be calculated using Hooke's Law. Figure 2.41 provides a schematic illustration of the shallow hole drilling technique.

It is possible to measure residual stresses to depths up to the diameter of the hole. Several studies have revealed some inconsistencies in the results when the residual stresses exceed approximately 50% of the yield stress. This has been attributed to localised yielding, since the method assumes that relaxation of stress is purely elastic. Furthermore, it has also been found that some problems arise when this technique is used to assess the residual stresses in coatings within thin layers, less than approximately 100 μm in thickness [121].

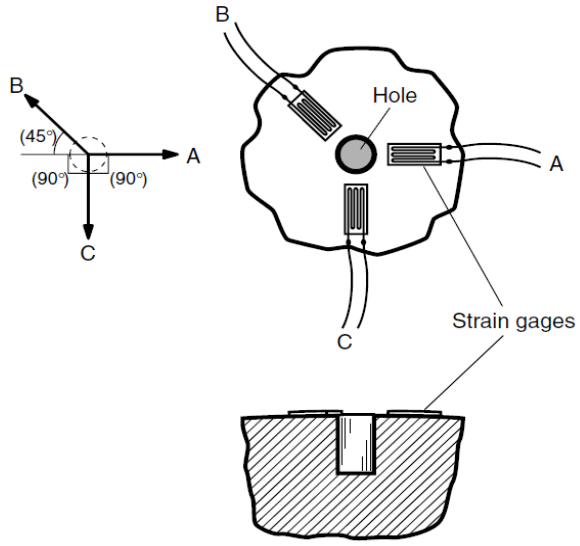

Figure 2.41 Schematic representation of the shallow hole drilling method [5].

2.10.5 Contour method

This method is considered to be destructive because the sample under consideration will be cut along a straight line in two separate pieces. A planar cut is performed on the plane that is normal to the component of stress under investigation. This method is also based on the principle of stress relaxation, whereby the deformation that occurs when a material is cut can be subsequently used to estimate the stress that was acting in the direction normal to the plane of the cut, prior to the cut being made. The contour method is based on Bueckner's superposition principle [125-127]. Figure 2.42 provides a schematic illustration of the superposition principle.

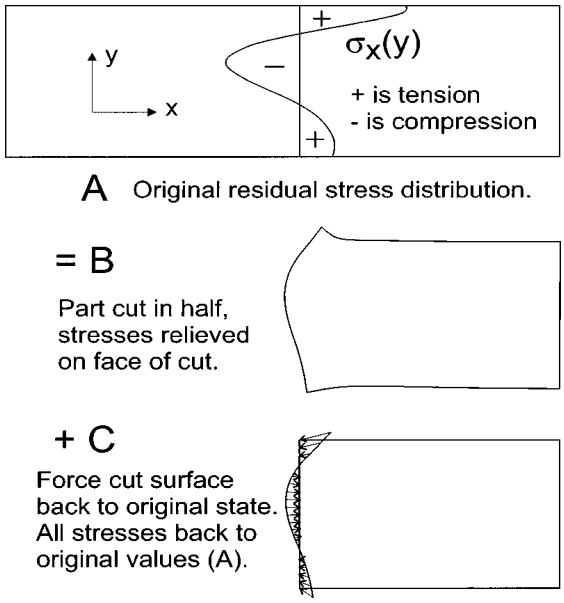

Figure 2.42 Application of superposition principle to calculate residual stresses using the contour method [125].

The cutting process is carried out using an EDM (electric discharge machining) process because this process does not introduce significant cold work or plastic strain to the cut surface. Once the deformations have been measured on both cut surfaces, the data is pre-processed so that it can be used in a finite element model in order to obtain the stresses that were originally present in the test piece.

One of the limitations of this method is that just one single stress component can be examined. The method also assumes that all deformation is due to the elastic relaxation

of stress. Errors associated with plasticity during cutting could appear. Since this method is based on the deformations produced after cutting, the sample should be well restrained on both sides of the cutting plane in order to not to introduce further deformation at the moment the sample is being cut.

2.10.6 Residual stresses in laser cladding

Residual stresses develop during laser cladding because the material tends to expand or contract non-uniformly due to the localised heating that takes place. The process involves heating and cooling every time a track is deposited. Figure 2.43 provides a schematic illustration of the development of residual stresses in a fusion welding process. However, it can also used to represent the development of residual stresses in laser cladding operations owing to both processes being similar in principle.

A region ahead of the molten pool is represented section A-A, and across this section the temperature is uniform and the stresses are zero. Section B-B corresponds to a section through the molten pool. In the vicinity of the molten pool, the temperature increases considerably, so the material tries to expand, but it is constrained by the surrounding cold material. Low levels of compressive stress are produced in the vicinity of the molten pool in section B-B and further afield tensile stresses are developed to balance the compressive stresses near the pool. There are no stresses in the molten pool itself since molten metal cannot sustain significant stresses.

In section C-C, the weld bead temperature is decreasing, so the hot material tries to shrink but it is constrained by the surrounding material. Tensile residual stresses are developed, and compressive stresses are developed further from the weld pool to balance the tensile stresses. Finally in section D-D, the temperature is lower and the tensile stresses are higher. This sequence of events can be taken as an example of the generation of residual stresses in a laser cladding process.

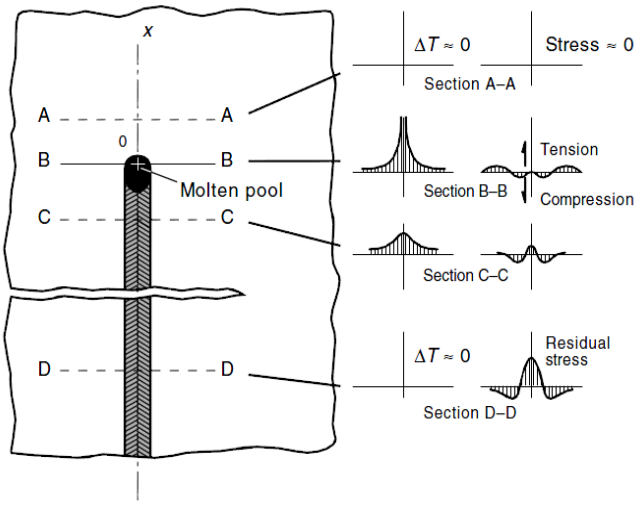

Figure 2.43 Development of residual stresses in a fusion welding process [5].

Since laser cladding can be applied to the repair of aircraft, automobile or nuclear components, different deposition configurations can be used. This means the way in which laser cladding will be performed will depend heavily on the application. Single tracks can be deposited on top of one another in order to build up walls, single overlapping tracks can be deposited in order to cover larger areas of a surface, or various layers can be deposited in order to produce different mechanical properties. For every laser cladding configuration, different residual stresses and orientations will be developed. Therefore, several investigations have been carried out in order to understand the development of residual stresses under certain conditions.

De Olivera [13] investigated the distribution of residual stresses that are developed during the deposition of Stellite 20 powder on to a flat material and then compared these results with those for the deposition of Eutroloy 16012 on a round steel substrate. The deposition of overlapping tracks of Stellite 20 indicated that the largest tensile residual stresses were produced in a direction at an angle of 40^{o} to the cladding direction. This was expected because the solidification front changes direction when part of the previous track is remelted. A crack was developed in the deposition of Eutroloy 16012 on a round steel substrate parallel to the solidification front. Owing to the importance of residual stresses to laser cladding, different investigations involving FEM and analytical modelling have been performed [76, 128].

Given that residual stresses are difficult to predict, different residual stress measurement techniques (such as those described above) have been explored. Table 2.5 provides a summary of different laser cladding configurations and the associated residual stress investigations. The residual stresses developed in the experiments presented in Table 2.5 reveals the generation of tensile stresses in most of the cases with some compressive stresses further from the deposited layer, which balance the tensile stresses. The magnitude of the stresses was in the order of 300-400 MP with the tensile stresses being higher than the compressive stresses.

Table 2.5 Summary of laser cladding residual stress measurements.

Base material	**Powder**	**Measurement Technique**	**Configuration**	**Reference**
AISI P20 tool steel	P20 tool steel	Neutron diffraction	Three layers were deposited	[122]
C45 low-alloyed	Eutrolloy 16012, Stellite 20	X-ray diffraction	Single track and 9 overlapped tracks	[13]
AISI 304 SS	Stellite 6B	Synchrotron	Single tracks and overlapping tracks (34%)	[128]
X10Cr13 steel	Stellite SF6	Not mentioned	Double layers coating	[78]
C45 carbon steel	Eutrolloy 16012	x-ray diffraction	Two overlapped tracks	[129]
AISI 304 SS	Stellite 6	Blind Hole	One, two and five layer; 30 % overlap	[130]
Inconel 718	Waspaloy	Neutron diffraction, contour method	20 layers of 6 overlapped tracks	[131]
A3 mild steel	Fe90 self-fluxing alloy	nanoidentation	Single track with 30 % overlap	[132]

2.10.7 Residual stresses generated by laser shock peening process

As was described in Section 2.7, the plasma generated by the incident laser energy generates pressure at the interface (refers to Figure 2.28). The pressure produces uniaxial compression over the irradiated surface in the direction of the shock waves. However, tensile stresses are also generated owing to material dilation. At the moment the laser stops, the surrounding material prevents the expansion of the irradiated area and compressive stresses are developed (Figure 2.44). Once compressive stresses are generated corrosion resistance and mechanical properties of materials such as the fatigue life, and hardness considerably improve [14-15].

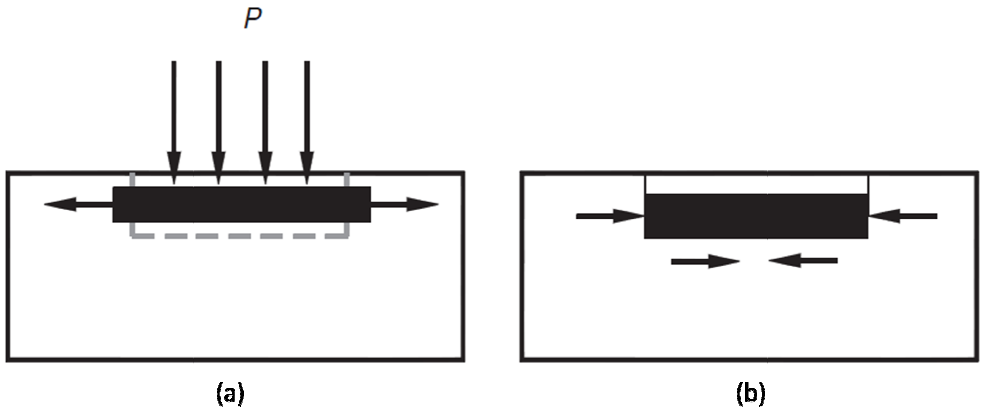

Figure 2.44 Compressive residual stresses generated by LSP during laser interaction (a) Stretching of the irradiated area, (b) surrounding material is recovered after the laser is switched off [15].

The optimization of the laser parameters is crucial in order to generate enough pressure at the interface zone. If the pressure generated is small, it is not possible to achieve plastic deformation or compressive residual stresses over the material surface.

There are other process parameters such as the pulse density, which can increase the magnitude of the compressive residual stresses. Figure 2.45 and Figure 2.46 show the effect of pulse density in the development of stresses in different aluminium alloys. It is possible to observe that deeper compressive stresses are achieved with higher pulse densities.

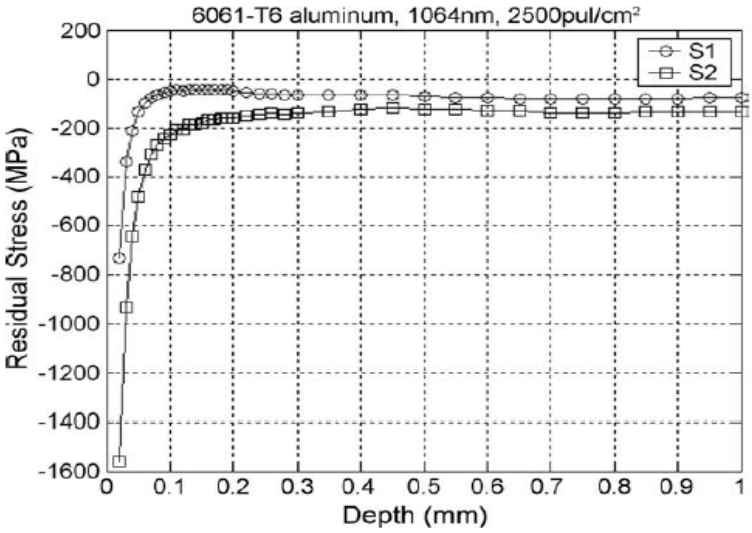

Figure 2.45 Compressive residual stresses generated with pulse density of 2500 pulse/cm^2. S1 and S2 are the main principal stresses [133].

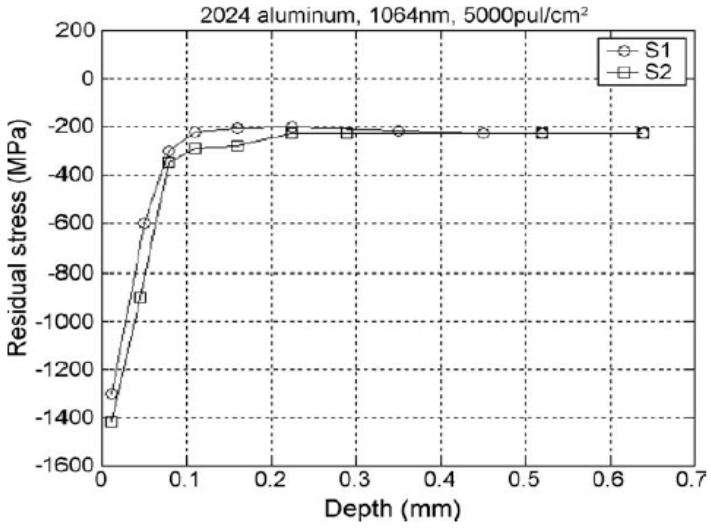

Figure 2.46 Compressive residual stresses generated with pulse density of 5000 pulse/cm^2. S1 and S2 are the main principal stresses [133].

In order to investigate the ability of laser shock peening to generate compressive residual stresses in different materials, several investigations have been carried out. Table 2.6 provides a summary of the assessment of residual stresses generated in different materials after treatment with laser shock peening. In general, compressive stresses were generated after laser shock peening although different process parameters were used due to the properties of each base material.

Table 2.6 Summary of laser shock peening residual stress measurements.

Base Material	Sample Dimensions (mm)	Measurement technique	Reference
SUS 304 SS	20 x 20	x-ray diffraction	[134]
T1-6Al-4V	45 x 45 x 7.7	Neutron and synchrotron diffraction	[135]
6061-T6 and 2024 aluminium alloy	15 x 15	Hole drilling	[133]
2205 duplex SS	20 x 20	Contour method	[136]
2024-T351 aluminium alloy	50.8 x 76.2	x-ray diffraction	[137]
T1-6Al-4V	50 x 30 x 15	Synchrotron diffraction	[138]
T1-2.5Cu	20 x 20 x 5	x-ray diffraction	[117]
00Cr12 alloy	6.5 diameter	x-ray diffraction	[139]

2.11 Post weld heat treatment

Post weld heat treatment is another process that can be used in order to improve the mechanical properties of metals such as hardness and ductility, and in some cases the corrosion resistance, wear resistance and fatigue life.

This process has been used on laser cladding samples in order to improve the properties of the new coating layer. The changes produced by heat treatments on metals are related to phase transformation in microstructure; in some cases the ductility of the metal is enhanced [140-145]. However, the hardness of some materials cannot be altered by post weld heat treatment such as, for example austenitic stainless steels. This is because no important changes in phases or microstructure are expected.

Figure 2.47 shows the changes in micro hardness produced by heat treatments on a Ni-alloy layer. The increase of micro hardness can be attributed to the metal borides precipitating from the austenite phase [145].

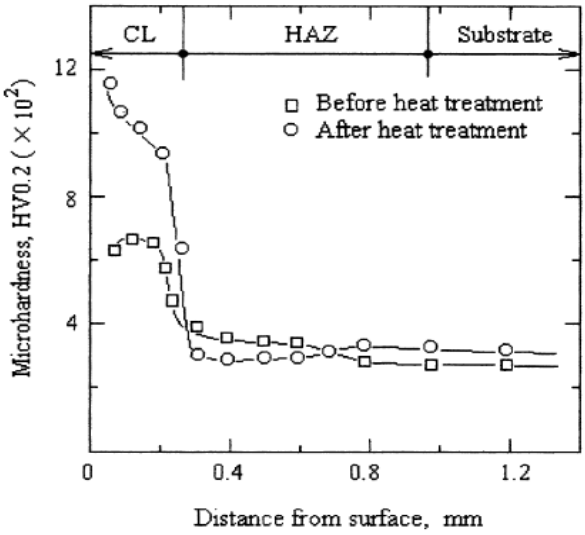

Figure 2.47 Micro hardness distributions through the depth for cross-sections though a laser-clad Ni alloy layer before and after heat treatment (550 °C, 1.5h) [145].

Post weld heat treatment is also used in order to relieve residual stresses produced by manufacturing processes. As mentioned before, the laser cladding process develops residual stresses, generally tensile stresses, due to the shrinkage of the metal after solidification begins. Although heat treatments can be beneficial to the performance of metals, detrimental effects can be also produced when inappropriate parameters are selected, specifically with respect to temperature and exposure time, because some materials can undergo sensitization after exposure to high temperatures for significant periods of time. Stress corrosion cracking can occur if sensitization or carbide precipitation is generated after heat treatment [99].

2.12 Corrosion performance

2.12.1 Introduction

Corrosion is defined as the normal process of metals returning to their most stable thermodynamic state. It can also be defined as the behaviour of metals with their environments. It is caused by reactive gases, solids or liquids that directly affect the material structures [146].

Physically, corrosion is indicated by a loss of mass of the material or by the development of a thin non-metallic layer on the surface of metals by process such as oxidation. In corrosion resistant metals such as stainless steel, it is common that an oxide layer is formed when the metal is exposed to corrosive environments. The oxide layer, often called the passive film, acts as a barrier in order to prevent oxidation.

Once the passive film has vanished, corrosion takes place on the surface of metals. The onset of corrosion is mainly focused at surface discontinuities such as cracks or porous regions. Discontinuities may be generated during the alloy casting process, although residual stresses and mechanical fatigue, deformation or damage also have influence on the surface behaviour.

The laser cladding process has been used to produce corrosion resistant clad layers on to material surfaces [147] owing to the generation of surfaces with finer microstructures and that are free from discontinuities. It has been demonstrated that finer microstructure shows better corrosion resistance [148-149].

Corrosion can be initiated by different mechanisms such as intergranular corrosion, pitting corrosion, crevice corrosion, galvanic corrosion and stress corrosion cracking. However, the surfaces developed by laser cladding are mainly affected by intergranular corrosion, pitting corrosion and stress corrosion cracking mechanisms. Therefore, a brief description of these mechanisms will be discussed in the next section.

2.12.2 Mechanisms of corrosion

2.12.2.1 Pitting corrosion

It can be considered either as corrosion mechanism or form of corrosion. Pitting is associated with the development of pits on the surface of metals exposed to corrosive environments. It occurs with the breakdown of the passive layer on the metal surface. The development of pits can produce weakness in some localized areas of the metals and this can produce failures in equipments [146].

The development of pits can be considered as sites of stress concentration on the surface of the metals; hence it can promote failures in equipment components because of fatigue

or stress corrosion cracking. Figure 2.48 shows different shapes of pits that can be developed by this mechanism.

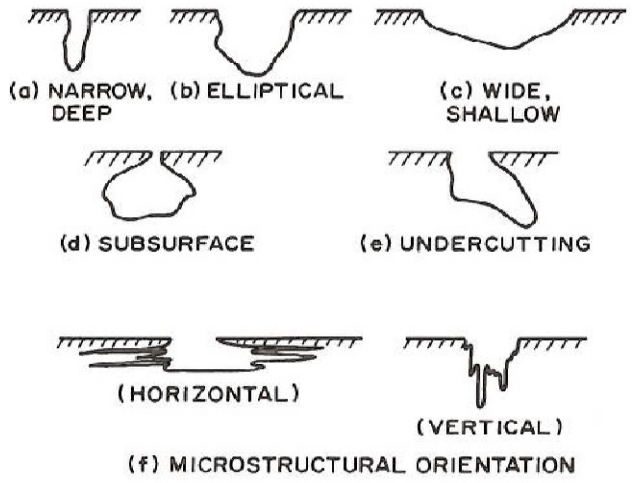

Figure 2.48 Different cross-sectional shape of pits: ASTM Practice G-46 [150].

2.12.2.2 Intergranular corrosion

Intergranular corrosion is associated with the presence of corrosion in the grain boundaries of the metals. The main factors that promote intergranular corrosion are the segregation, enrichment or depletion of some alloying elements or compounds and these are due to thermal exposure of metals [146].

In stainless steel, intergranular corrosion is developed because of sensitization. This means that chromium carbides are precipitated at the grain boundaries because of the metals has been exposed to a certain temperatures for high periods of time [150]. This can be a problem in nuclear components. An example of intergranular corrosion is presented in Figure 2.49.

Figure 2.49 Cracks on the grain boundaries caused by sensitization in austenitic alloy generated by the exposure of boiling sulphuric acid-ferritic solution [150].

2.12.2.3 Stress corrosion cracking

Stress corrosion cracking is produced when cracks propagate in metals that contain tensile residual stresses and are exposed to certain corrosive environments. The magnitude of the tensile residual stresses required for cracking is often much less than the ultimate tensile strength, and in some systems, the magnitude is just ten percent of the yield tensile strength.

Cracks can propagate through the metal in different ways, either across the grains or following the grain boundaries. Cracks crossing the grains are called “transgranular” and those that manifest through the grain boundaries are called “intergranular”. Figure 2.50 shows an example of transgranular and intergranular cracks.

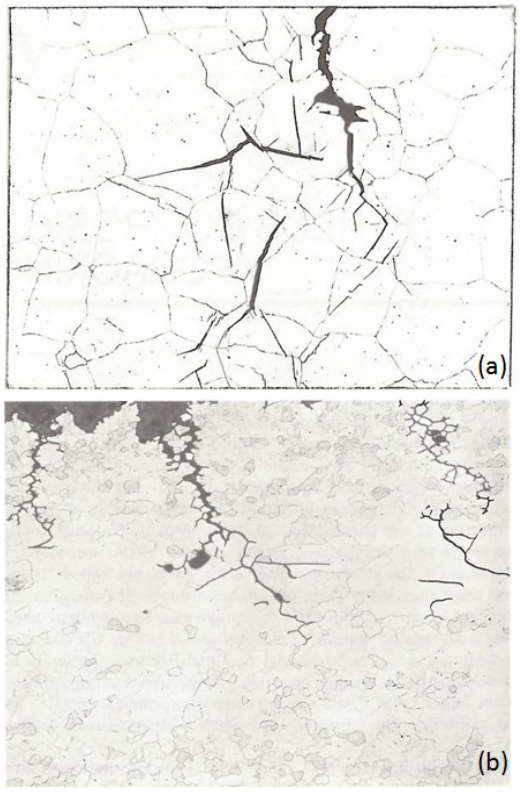

Figure 2.50(a) Transgranular cracks generated in austenitic stainless steel exposed to chloride environments (100x); (b) intergranular cracks in a ferritic stainless steel exposed to a high-temperature caustic environment (50x) [150].

2.12.3 Alloying elements

Stainless steels contain different alloying elements in order to improve their mechanical properties and corrosion resistance. The main alloying elements in stainless steel are chromium and nickel. However, some alloying additions could improve certain mechanical properties but affect others.

Chromium is added to stainless steels in order to improve the corrosion resistance; this is because chromium itself develops higher passive potential range [150]. An example of alloying chromium with iron is depicted in Figure 2.51, where it is shown that increasing the chromium percentage the current density required to reach the active-passive transition is less. However, chromium also promotes the development of ferrite. Furthermore, nickel tends to promote an austenitic phase and a decrease in stress corrosion cracking resistance is also developed. Another element added to stainless steel is molybdenum and its function is to improve corrosion resistance, specifically pitting

and crevice corrosion. In general, all the alloying elements play an important role in the performance of stainless steel.

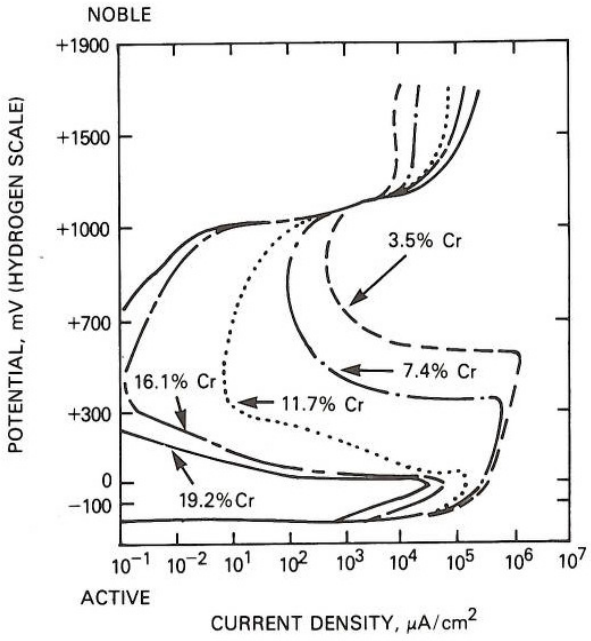

Figure 2.51 Polarization behaviour of Fe-Ni-Cr alloys with different chromium contents exposed to 2N H_2SO_4 solution at 90°C [150].

2.12.4 Corrosion resistance developed by laser cladding

Laser cladding process has been widely used in order to generate higher corrosion resistance coatings on different base materials. Owing to low dilution is generated with this process; the new coating material can preserve their corrosion resistance properties.

Numerous corrosion resistance coating materials have been used in order to protect the base metals under different environments and different mechanism of corrosion. However, special care should be considered selecting the coating material since some of these can be crack-sensitive materials and this can affect the corrosion resistance. Furthermore, thermo-mechanical properties such as the thermal conductivity, the coefficient of thermal expansion and even the melting point should be similar between the base and the coating material in order to avoid the generation of discontinuities after solidification. Discontinuities affect directly the corrosion performance of the metals [112, 151-156].

The stresses produced by fatigue, and the residual stresses (normally tensile residual stresses) developed by the heat generated in laser processes produce sometimes the generation of cracks. This is another factor that influences the initiation of corrosion. Therefore, it is necessary to have control of residual stresses in order to avoid problems such as stress corrosion cracking.

Table 2.7 shows a summary of different investigations about the corrosion resistance developed by laser cladding using different base and coating materials under different mechanisms of corrosion. In all the cases, the corrosion resistance developed after laser cladding was improved.

Table 2.7 Summary of corrosion investigation into materials developed by laser cladding.

Substrate	**Coating material**	**Mechanism of corrosion**	**Industry**	**Reference**
316L SS	Ni-Cr METCO 443	Pitting	Not mentioned	[151]
Mild steel	UNS S4470 super ferritic SS	Pitting	Not mentioned	[152]
Mild steel	UNS S31254 super austenitic SS	Pitting	Marine	[153]
Mild steel	Inconel 617 machining swarf	Pitting	Not mentioned	[154]
316L SS	Inconel 690	SCC	Nuclear	
Inconel 600	Inconel 690	SCC	Nuclear	[155]
Mild steel	316L SS	Pitting	Oil and gas	[112]
MRI 153M Mg alloy	Al and Al_2O_3	Galvanic	Automobile	[156]

2.12.5 Corrosion resistance developed by laser shock peening

Compressive residual stresses and changes in microstructure generated after laser shock peening over metallic materials are found to generate improvements in corrosion resistance. If compressive residual stresses are developed on the metal surfaces, the

onset of discontinuities such as cracks will be avoided or retarded. This means an enhancement in resistance to stress corrosion cracking or even in pitting corrosion. This is also related to the finer microstructure developed after shock peening.

Laser peening has been applied on different materials in order to investigate the effect generated in corrosion resistance [157-160]. Satisfactory results have been reported [134, 157-159, 161-162]. According to Ref. [160], corrosion cracking has been avoided after laser peening in materials such as SUS 304, alloy 600 and alloy 182. The process was carried out using confined medium (water layer) but without ablative layer. Table 2.8 shows a summary of different investigations of the corrosion resistance developed by laser shock peening for different mechanisms of corrosion. In all the cases, corrosion resistance developed after laser shock peening was improved.

Table 2.8 Summary of corrosion investigation developed by LSP.

Substrate	Mechanism of corrosion	Industry	Reference
Stainless Steel	Pitting	Desalination Plants	[161]
316L SS	Pitting	Power plants	[158]
SUS 304 SS	SCC	Nuclear	[134]
AZ31B Mg Alloy	SCC	Automobile	[162]
316L SS	Pitting	Not mentioned	[157]
2050-T8 Al alloy	Galvanic	Not mentioned	[159]

2.13 Motivation for current work

Laser cladding is considered to be a practical process for improving the mechanical properties, the corrosion resistance and the fatigue life of metals. It can be used to repair or restore different components for the aircraft, automotive, mining, food processing and oil and gas industries. Although laser cladding has advantages over other laser

surfacing processes, some aspects of the process could restrict its use on specific applications.

Owing to the relevance of the process, laser cladding has been under investigation for many years. Some aspects have been studied and understood. However; laser cladding is a complex process due to all the variables involved.

As mentioned in the previous sections, laser cladding generates residual stresses after solidification and this can have a detrimental effect on the performance of metals. The principal issue due to residual stresses is a reduction in the corrosion resistance and the fatigue life. This means laser cladding might not be an option where a highly corrosion resistant surface is required. However, there are some processes capable of mitigate the detrimental residual stresses that may develop in different laser surfacing processes.

To date, different studies have been carried out that explore the option of applying a residual stress mitigation technique to laser clad samples in order to enhance the fatigue performance of the cladding. Laser shock peening and heat treatment have been used for the most part. According to Refs. [163-166], the fatigue resistance and hardness were improved on clad surfaces treated with laser shock peening. Furthermore, fatigue resistance was also improved on laser-clad surfaces treated with post weld heat treatment [140-145]. There are also other studies that investigate the corrosion performance of laser-clad deposits [112, 154]. However, none of these studies examine the effects of residual stress on corrosion performance, nor do they investigate the potential benefits associated with residual stress mitigation.

The primary aim of this work is to investigate the effects of laser shock peening and post weld heat treatment on the corrosion performance of 316L laser clad samples. In doing so, this study will be the first to systematically investigate the role that residual stresses play in affecting the corrosion performance of laser-clad deposits. Through adopting a holistic approach, which simultaneously considers both residual stress and corrosion, it is expected that this work will provide new insights to the factors that govern the corrosion performance of laser-clad deposits, and how the corrosion performance of such alloys can be enhanced most effectively.

Chapter 3

Laser Cladding Trials

3.1 Introduction

This chapter describes the properties of the materials selected for the experimental work, applications, advantages and drawbacks. It is also described the equipment employed in the laser cladding process and the relevance in the generation of different cladding profiles. Furthermore, the methodology that was employed in order to choose the appropriate sample dimensions and the laser cladding process parameters which develop an acceptable overlay is also discussed.

In addition, some of the main issues involved in a melting process such as porosity, cracks and lack of fusion are also described. Finally, the effects of the process parameters in dilution and cladding heights were assessed.

3.2 Materials

Laser cladding can be used to repair or restore worn components, which means the cladding material can be similar or dissimilar to the base material. Two different base materials were used in this work; AISI 316L stainless steel and S275 steel. Their chemical composition is presented in Table 3.1.

AISI 316L stainless steel is classified as austenitic stainless steel [99]. This material is resistant to intergranular corrosion because of the low carbon concentration (0.03 wt. %). It also exhibits good corrosion resistance in oxidising environments because of its high chromium content, which is usually between 16 and 18 wt. %. Nickel is also present in concentrations between 10 and 14 wt. % and it serves as an austenite stabiliser. The melting point ranges between 1375 to 1400^{o}C and its density is 8.0 gcm^{-3}

[99]. Austenitic stainless steels have good ductility, formability and toughness and weldability. These materials are often used in construction, and food processing and oil applications. [99, 167]

Table 3.1 Elemental composition of AISI grade 316L stainless steel and S275 steel. [99]

Material	Composition (wt. %)							
	C	Mn	Si	P	S	Cr	Ni	Mo
Grade 316L	0.03	2.0	1.0	0.045	0.03	16-18	10-14	2-3
S275 steel	0.25	1.6	0.05	0.04	0.05	-		

All compositions are balance with Fe

BS EN 10025 S275 (British Standard) mild steel, or in abbreviated form S275 steel, is considered to be a structural material. It is used in many engineering and structural applications. Its advantages include that it can be easily machined and welded. Typical yield strengths for this material are in the vicinity of 275 MPa [168-169]. However a limitation of this material is its poor corrosion resistance.

The powder material used in the cladding process was AISI 316L stainless steel. Its properties have been already described above and its chemical composition described in Table 3.1. The particle size ranges between 53 and 150 μm and the shape is almost spherical.

3.3 Experimental Equipment

3.3.1 Diode laser: Laserline LDL 160-1500

The laser system used in this work is a class four, 1500W LDL 160-1500 diode laser. According to the European standard EN60825-1:2001 and the American standard ANSI Z 163.12000, lasers are classified considering their hazard [1]. The output wavelength is in the range between 808 to 940 nm. It can be operated in continuous wave and pulse mode. The beam parameter product (BBP) is 120 mm mradian.

High power diode lasers (HPDL) typically have poor a beam quality; this means that small laser beam size, in the order of micrometres, cannot be achieved. However, small beam sizes are normally used in process such as laser cutting typically using CO_2 and Fibre laser. HPDL has a non-Gaussian beam profile; it is of a uniform energy intensity distribution and is known as a flat top energy distribution. Therefore, stable cladding can be developed due to a uniform surface heating [3, 5].

The laser system consists of a control unit, a laser head and a fibre delivery system. The laser spot is converted from a rectangular cross-section to a circular shape by the arrays of optics located above the coaxial nozzle. In this work, the laser was always used in continuous mode. The distance between the nozzle exit and the base material was set to 7mm; and this resulted in a laser spot size on the surface of the base material of 1.7mm.

Some proportion of laser power is always lost due to the delivery system, due to losses between the diode bars and some inefficiency of lenses located in the laser head. Therefore, in order to know the real laser power delivered to the work piece, the laser power has to be measured. This was achieved by using a Gentec UP55N-300F-H9 power meter at the exit of the coaxial nozzle. This was done for different laser power settings, as set by the control unit. The laser power that was measured at the location of the work piece is plotted against the nominal laser power setting on the control unit in Figure 3.1. Some of the values in Figure 3.1, represented by a straight line, are extrapolated owing to limitations on the maximum power that could be received by the power meter. It can be observed that the laser power delivered on the work piece represents approximately seventy percent of the nominal laser power set on the unit control.

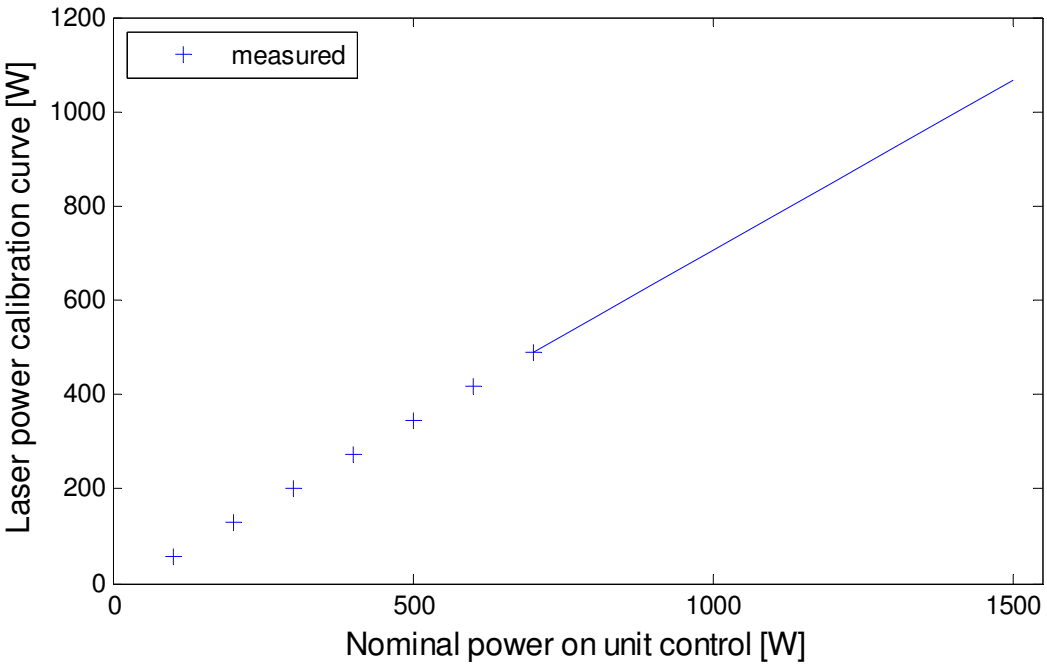

Figure 3.1 Measured versus nominal laser power for the 1500 W LDL 160-1500 diode laser used in the current work. Straight line represents a linear relationship between nominal and measured power.

3.3.2 Coaxial nozzle

An illustration of the coaxial nozzle used in this work is given in Figure 3.2. The nozzle comprised an upper housing, two oblique nozzles and a cooling compartment. On the upper housing, the fibre delivery system was connected to the optics that change the shape of the laser spot. The powder was fed in to one of the oblique nozzles and, finally, cooling water was delivered through the cooling compartment. The coaxial nozzle material was aluminium and the material for the tips was copper.

The powder mass stream produced by the coaxial nozzle was measured in order to find the location of the highest powder concentration. This experiment was done using a high intensity lamp, a high speed camera and a ruler. Different powder mass flows were assessed and no significant changes were found in the zone of highest powder concentration which was found to be approximately 5 to 8 mm below the nozzle exit. The zone of the highest powder concentration is illustrated in Figure 3.3.

As mentioned in the previous section, the focal position was set to be 7 mm from the end of the nozzle; hence the focal position coincided with the zone of the highest powder concentration. This was intended to ensure that powder wastage was minimised.

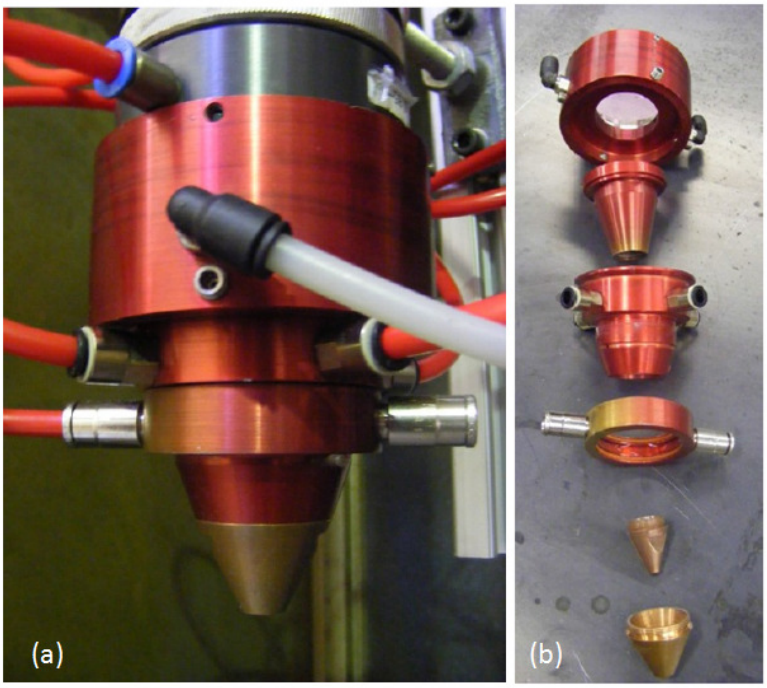

Figure 3.2 Coaxial nozzle: (a) assembled. (b) Individual components [170].

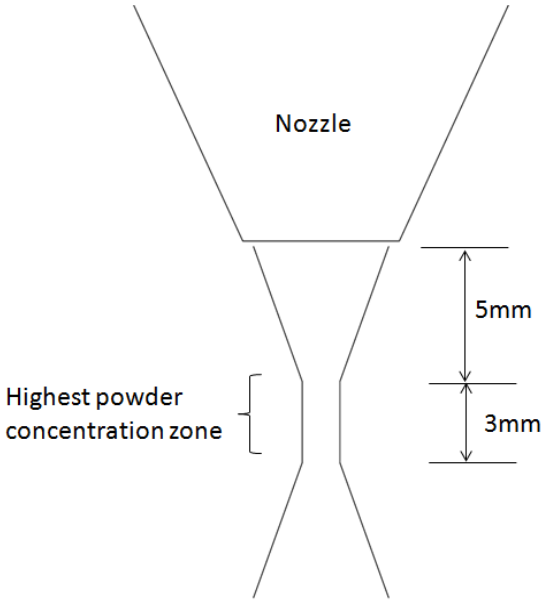

Figure 3.3 Illustration of the location of highest powder concentration with respect to the coaxial nozzle.

3.3.3 Powder feeder

The powder material was conveyed towards the coaxial nozzle using a powder feeder SIMATIC OP3 FST-PF manufactured by Flame Spray Technologies. The powder feeder consisted of two hoppers each with a capacity of 1.5 litres which store the powder. Each hopper had a grooved wheel that rotated at a specific rotational speed (rpm) in order to control the mass flow rate. The powder was conveyed from the grooved wheel to the coaxial nozzle by a flow of argon gas through a plastic tube. The argon gas flow rate was controlled by a flow meter.

The powder mass flow rate was measured with the feed wheel at different rotational speeds in order to determine the grams per minute of powder delivered at the exit of the coaxial nozzle. The experiments consisted of collecting the powder at the nozzle exit in a special container for an established period of time and then weighing it. The results are depicted in Figure 3.4. It can be observed that a liner relationship could be established.

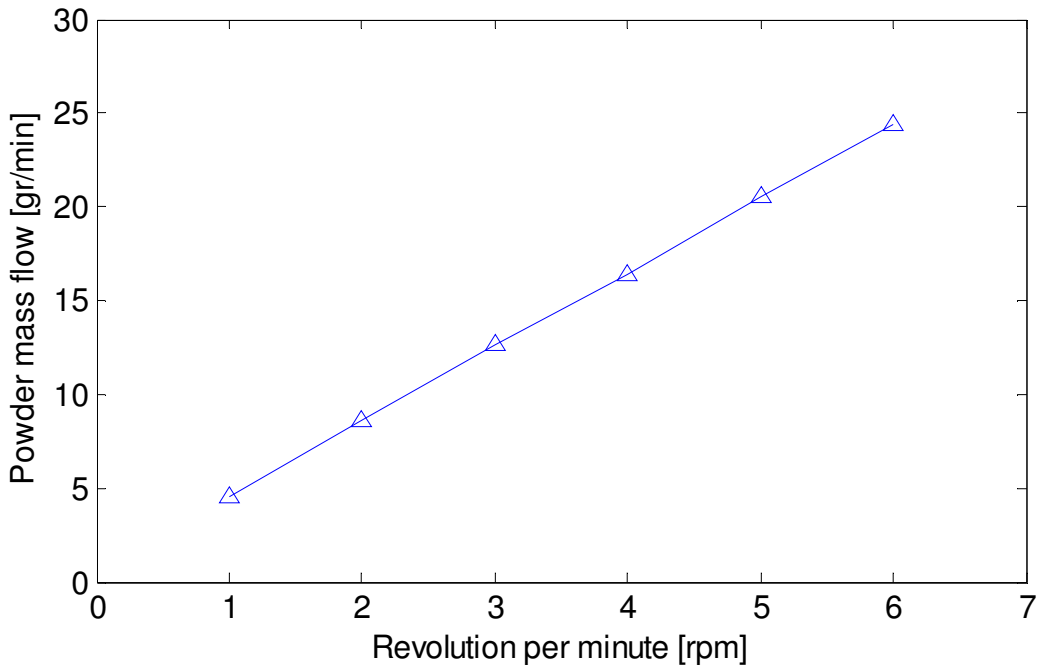

Figure 3.4 AISI 316L powder mass flow rate as function of the rotational speed of the grooved wheel in the hopper for a powder size ranging from 53 to 150 μm.

3.3.4 Auxiliary equipment

Various items of auxiliary equipment were used in preparation for and in the assessment of the laser cladding experiments. A sandblaster Guyson machine was used to sandblast the sample surfaces before laser deposition. A Struers Accutom-5 machine was used in order to make transverse cuts through the laser cladding samples. This machine is operated with a cooling system that avoids overheating the samples during the cutting operation. A presi Mecatec-334 machine was used to grind and polish the sectioned samples. This machine is also operated with a cooling system in order to avoid any damage due to the grinding process. A digital Keyence VHX-500 microscope was used in order to assess the cladding dimensions, microstructure and dilution.

3.4 Design of specimens

In order to select appropriate dimensions for the base material, several laser cladding experiments were performed. Firstly, it was necessary to know the quasi-stationary state conditions for laser cladding. This refers to the state of the process when it has stabilised or is independent of time. In the laser cladding process these conditions can be considered to arise when the cladding height, width and dilution do not change after a period of time or from one pass to the next. In these experiments, the single track height and overlapped single tracks were assessed.

Base material coupons with dimensions of 50 x 50 x 9.5 mm were proposed. The original dimensions of the coupons were 50 x 50 x 10 mm, however one face was machined in order to get a completely flat surface. Single tracks 45 mm in length were deposited using different settings for laser power, powder mass flow and traverse speed. After different single tracks were deposited, the bead heights were assessed and the results showed height stabilization 10-15 mm from the start of the weld bead. Single tracks were deposited in both S275 steel and grade 316L stainless steel and the results were similar. Figure 3.5 shows the variation in bead height as a function of distance from the start of the bead for a typical single track, where several measurements were taken from several cladding samples. The height measurements in all the samples were carried out following the same procedure at similar distances along the single bead

track. The results were consistent in all the samples. Quasi-stationary conditions were found in the centre of the samples due to small variations of the height. The height stabilization can be attributed to the temperature distribution within the base material.

In addition, a total of ten single parallel tracks, each 45 mm in length, with a bead overlap of 40 percent, were deposited on to base material coupons of the same size. These experiments were considered to be important since clad surfaces usually comprise many overlapping tracks. Figure 3.6 shows the results for a typical overlapped sample. These values were also obtained by measuring samples several times using the same procedure. Consistence in all the measurements was found. The height starts to increase after the second track; this is because part of the new track is deposited on to the previous track. However, this effect diminishes after the fifth track, and the height stabilises. Therefore, it can be considered that quasi-stationary state conditions are developed after the fifth overlapped track deposit. This effect also contributes to determining the temperature distribution within the base material. The precursors to achieving quasi-stationary state conditions were found to be similar to those in other investigations [48, 79, 171].

Given that it was feasible to achieve quasi-stationary state conditions using the base material dimensions proposed above, a decision was taken to use 50 x 50 x 9.5 mm coupons for all of the experimental work. It was also decided to use a total of 20 single tracks with a length of 40 mm and with a bead overlap of 40 percent in order to build the clad layers.

As mentioned above, conditions approaching quasi-stationary state conditions were achieved toward the centre of the base material coupons. It is in this location that the temperature distribution could be considered to be stable. However, if the cladding is placed close to an edge of the base material the temperature distribution will change because the edge of the specimen will not provide the same heat sink. This means the temperature distribution will be different close to the edges of the coupons. Therefore it is necessary to place the cladding away from the edges of the base material in order to avoid any undesired changes in temperature [46].

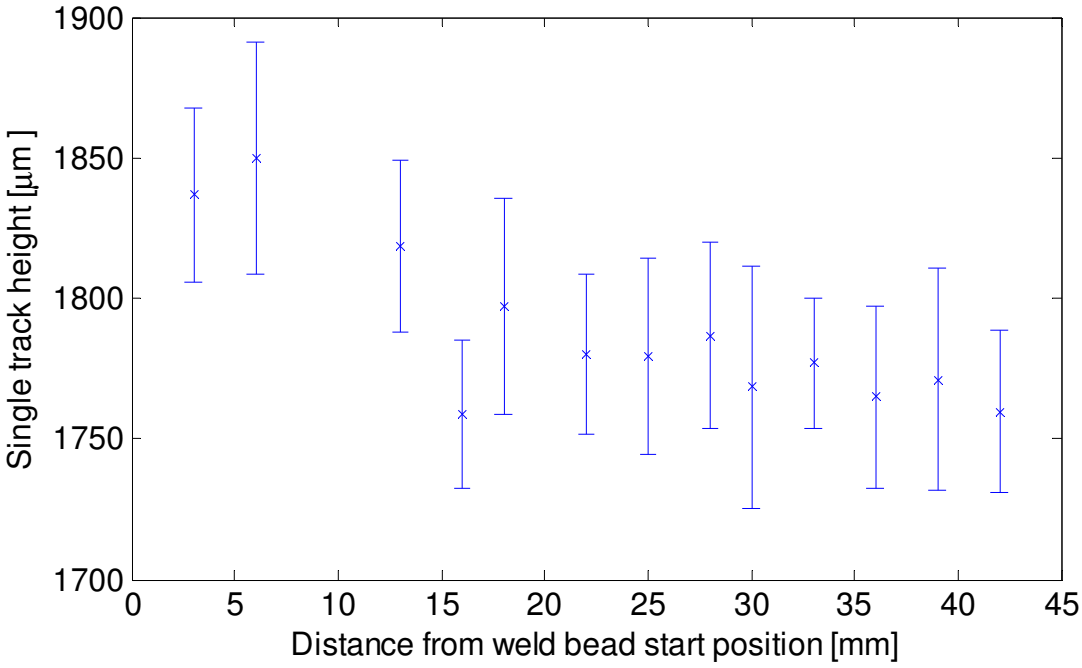

Figure 3.5 Variations in single track height with distance from the weld bead start position

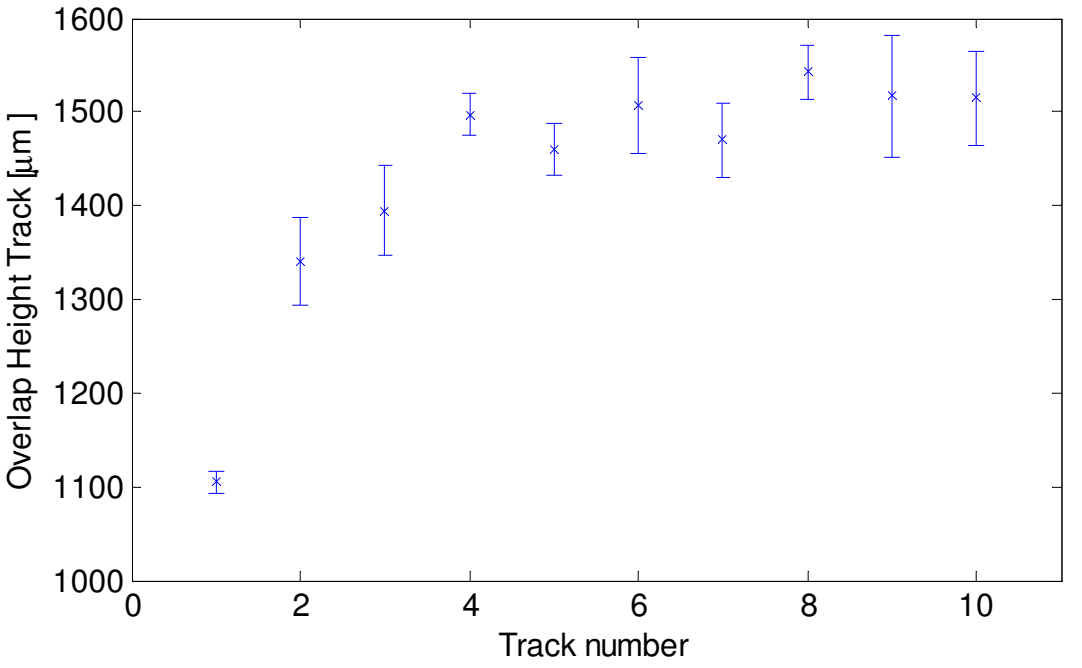

Figure 3.6 Height variations between successive weld beads when employing a bead overlap of 40%.

3.5 Parameters trials

The main parameters that need to be selected in order to carry out laser cladding are the laser power, the traverse speed and powder mass flow rate. Therefore, a parametric study was proposed, which covered different combinations of these parameters, in order to understand the effects of these process parameters on properties such as corrosion resistance and hardness. Furthermore, if samples were manufactured with different combinations of parameters, the effects of process parameters on microstructure and residual stress could also be assessed. The general approach of generating combinations of parameters for investigation is illustrated in Figure 3.7.

Once the parameters of interest had been identified, initial values for laser power, traverse speed and powder feed rate (also described as powder mass flow rate) were proposed. The optimum process parameter values were taken to be those that produced a clad layer with acceptable quality, meaning a clad layer free of discontinuities such as cracks, lack of fusion or porosity.

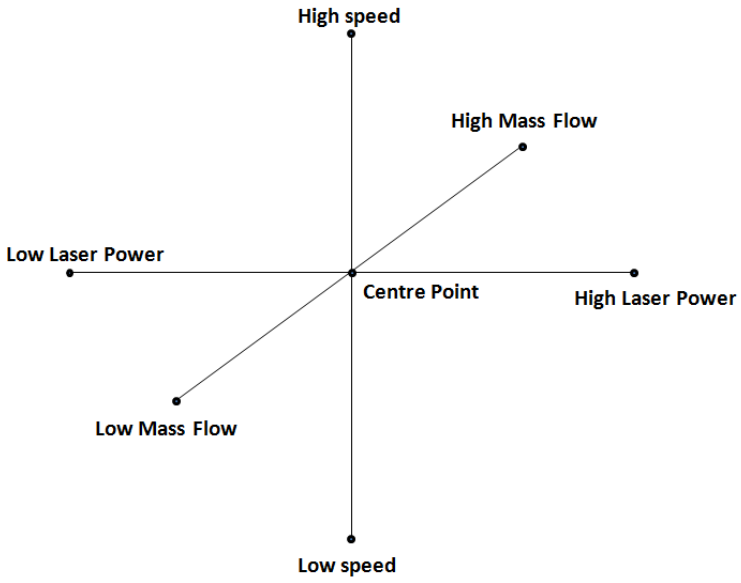

Figure 3.7 Schematic illustration of the approach used to generate combinations of parameters for the laser cladding experiments.

3.5.1 Sample preparation

As mentioned in Section 3.4, the dimensions of the base material coupons were 50 x 50 x 9.5 mm. The first trials were carried out using S275 steel as the base material. This decision was taken based on the assumption that, if problems were to arise, it was most likely that they would occur when S275 steel was clad with grade 316L stainless steel powder material, due to the differences in thermo-mechanical properties such as thermal conductivity and the coefficient of thermal expansion. Before deposition, the machined surface of each coupon was sandblasted in order to increase the roughness, and to increase the catchment of laser energy, and then the surface was cleaned with methanol. The surface needed to be free of any contamination in order to avoid the generation of porosity.

In order to get a uniform powder size and eliminate any impurities, the powder was strained with a 150 μm mesh sieve. Finally, the pressures for the shielding gas and the carrier gas were set at 5 bars, with gas flow rates of 4 and 5 l/min respectively.

3.5.2 Beads profiles

In the early trials involving the deposition of single tracks, the first point to consider was to identify values for each process parameter that would generate a single track bead profile where the cladding angle α (see Section 2.4.3) was close to 120°. If this condition was achieved, the possibility of lack of fusion between overlapping tracks was deemed to be low. However, this condition did not assure good bonding with the base material. The first attempts were made using laser powers of 700, 850 and 1000 W; traverse speeds of 420, 540 and 660 $mm.min^{-1}$, and powder feed rates of 8.6, 12.6, 16.4 $g.min^{-1}$. Similar process parameters have been used in previous cladding experiments with different powder materials [131, 154, 171-172]; therefore, it was generally expected that acceptable bead profiles could be generated.

The single tracks were sectioned in a direction that was transverse to the welding direction in order to measure the cladding angle and the height and width of the deposited bead. The results showed that a cladding angle of less than 90° occurred when

using a high mass flow rate and a low traverse speed. Furthermore, the presence of cracks was observed in some single tracks. Given that the results were not satisfactory, these parameters were discarded. Further experiments were performed, changing only the traverse speed and then the powder feed rate. A relationship between specific energy (Equation 2.1), the powder density and single track profiles was established in order to understand the effects of the process parameters. The single track profiles were consistent with those showed in Figure 2.10 and Figure 2.11.

The experiments with different powder feed rates and traverse speeds achieved acceptable single track profiles; so samples with overlapping single tracks were then manufactured. These samples were cut on a plane that was transverse to the welding direction in order to assess the suitability of the cladding conditions and to check for the presence of porosity and cracks. In the initial trials, porosity and cracks were found to be present.

As mentioned in Section 2.6, porosity can result from any kind of contamination; however contamination was prevented before deposition. Sources could include any contamination in the powder such as, for instance, humidity. If moisture were present, oxygen and hydrogen could be released in the melting process and porosity could be generated. For these reason, the powder was baked at 100^{o}C for 30 minutes prior to being used in laser cladding experiments. After this action, new experiments were carried out and the results showed no porosity, but cracks remained in the cladding.

Further changes in process parameters were considered in order to mitigate the cracks. Regarding the combination of parameters established in Figure 3.7, further sets of parameters that showed good single track profiles were found at laser power 700, 850, 1000W; traverse speed 240, 360, 480mm.min^{-1} and with powder feed rates of 4.56, 8.58 and 12.6g.min^{-1}. Figure 3.8 shows the cladding profiles for the centre point, high speed and high feed rate operating conditions.

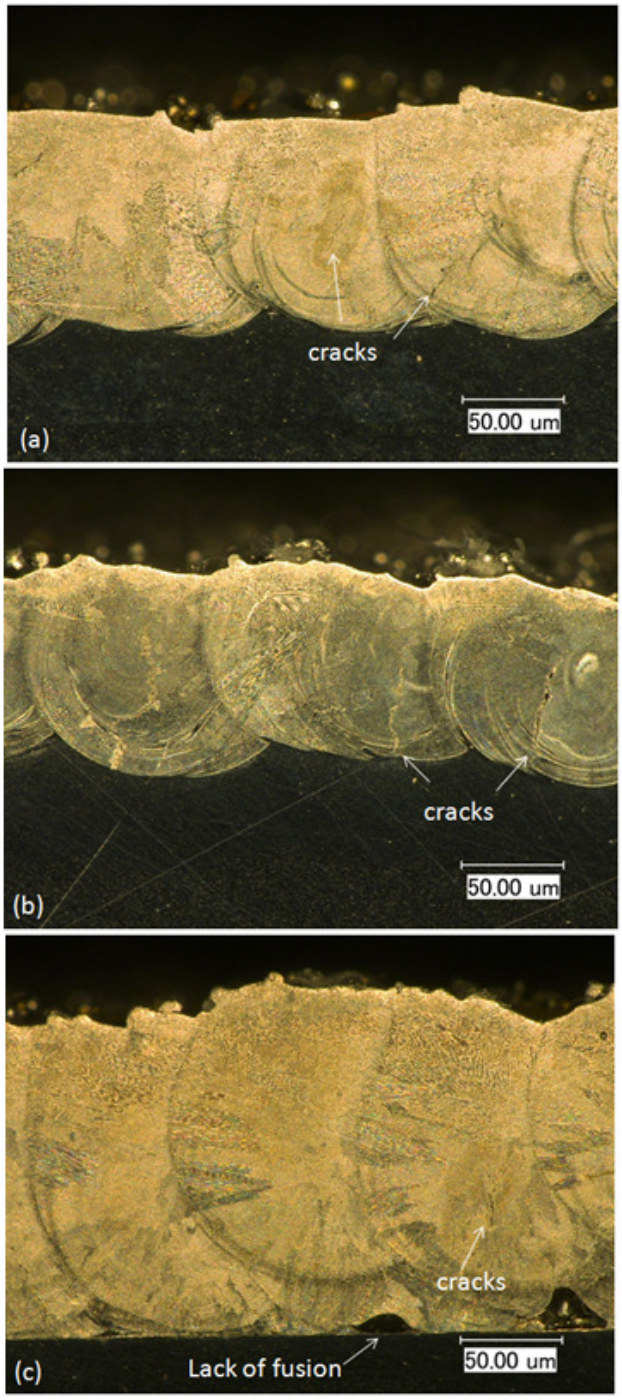

Figure 3.8 Optical micrographs showing the cross-sections of clad layers made with different process parameters: (a) Centre point (LP 850W, TS 360mm.min^{-1}, PFR 8.58g.min^{-1}), (b) High speed (LP 850W, TS 480mm.min^{-1}, PFR 8.58g.min^{-1}), (c) High feed rate (LP 850W, TS 360mm.min^{-1}, PFR 12.6g.min^{-1}). Cracks were developed in all the operating conditions and lack of fusion was also developed in the high feed rate condition.

The presence of cracks can clearly be observed in all the combinations of parameters represented in Figure 3.8. In addition, the high feed rate set of parameters (Figure 3.8c) shows lack of fusion between the cladding and base material.

Further experiments using different traverse speeds and powder feed rate values were performed in order to eliminate the cracks and the lack of fusion. However, cracks were still present in the new experiments. An investigation in to the causes of cracking in laser cladding was carried out and it was concluded that cracks can be generated by the high cooling rates developed in the cladding process. Consequently, preheating of the base material was explored in order reduce the cooling rates and to eliminate the cracks. [79-80]

New single track profile experiments were performed using different sets of process parameters. The base material was preheated to 200°C. This was the maximum temperature that could be achieved for the heater plate. Care was taken in these experiments in order to maintain the preheat/interpass temperature at all times. These experiments were carried out with laser powers of 700, 850, 1000 W; traverse speeds of 240, 360 and 480 mm.min^{-1}; and powder feed rates of 2.28, 6.3 and 10.32 g.min^{-1}. Figure 3.9 shows transverse cross-sections of the specimens made with different parameters.

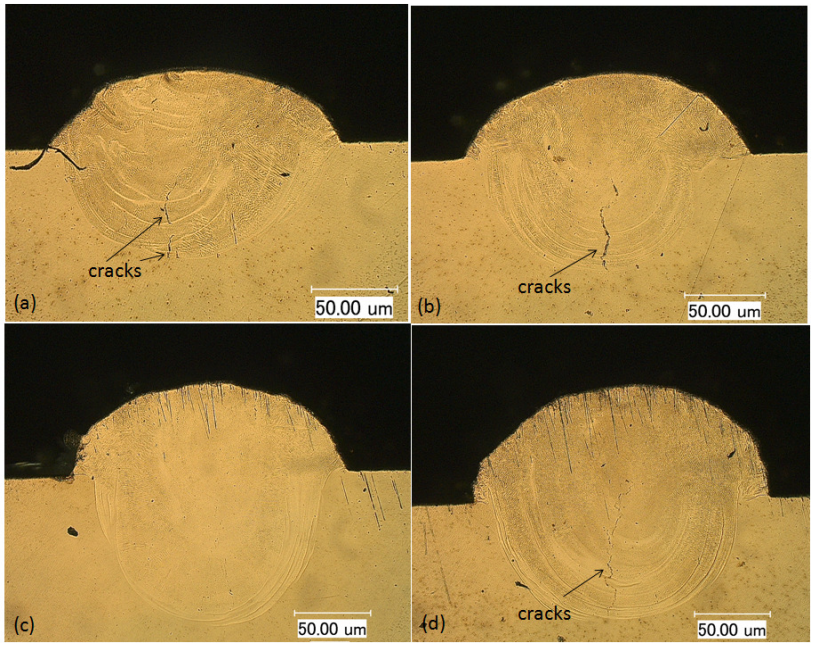

Figure 3.9 Optical micrographs showing the cross-sections of single tracks made with different process parameters: (a) Low laser power (LP 700W, TS 360mm.min^{-1}, PFR 6.3g.min^{-1}). (b) Centre point (LP 850, TS 360mm.min^{-1}, PFR 6.3g.min^{-1}). (c) High laser power (LP 1000W, TS 360mm.min^{-1}, PFR 6.3g.min^{-1}). (d) Low speed (LP 850W, TS 240mm.min^{-1}, PFR 6.3g.min^{-1}). The base material was preheated at 200°C in order to reduce the cooling rates, however the presence of cracks was still found except in the high laser power sample.

The presence of cracks in some of the specimen can be appreciated. In this case, substrate preheating did not make any difference. It is possible that a higher substrate preheat temperature was necessary. Further single track experiments with different process parameters were carried out but it was not possible to eliminate the cracks. Therefore, the option of changing the powder was considered.

A new set of experiments was defined where a new powder from a Höganäs Belgium supplier was used and no preheating or baking of the powder was employed. The revised process parameters included laser powers of 700, 850 and 1000W; traverse speeds of 240, 360 and 480mm.min^{-1}; and powder feed rates of 4.56, 6.3 and 8.58g.min^{-1}. Satisfactory results were obtained with the new conditions. The results showed clad layers free discontinuities with the different parameters; i.e. no cracking and no porosity. Furthermore, no lack of fusion occurred between overlapping single tracks and the base material.

Figure 3.10 shows the cross sections of the single track and clad layer manufactured with the process parameters of 850 and 1000W, traverse speed of 240 and 360 mm.min^{-1} and powder feed rate of 6.3 g.min^{-1}. It can be observed that good bonding between the overlap tracks and the base material was achieved while avoiding the lack of fusion. Furthermore, no cracks or porosity was found. The cladding angle developed by the single tracks corresponding to these parameters was higher than 90° which indicate that good bonding between overlap tracks and base material can be achieved.

These process parameters can be used in industrial cladding processes due to clad layers being produced without discontinuities. Furthermore, different clad heights with different dilution were also developed. This means, one or more layers can be produced as required in order to satisfy the industrial application. However, if a change of the values of the laser power, traverse speed and powder feed rate is considered, a new analysis should be carried out due the chance that a lack of fusion can be produced.

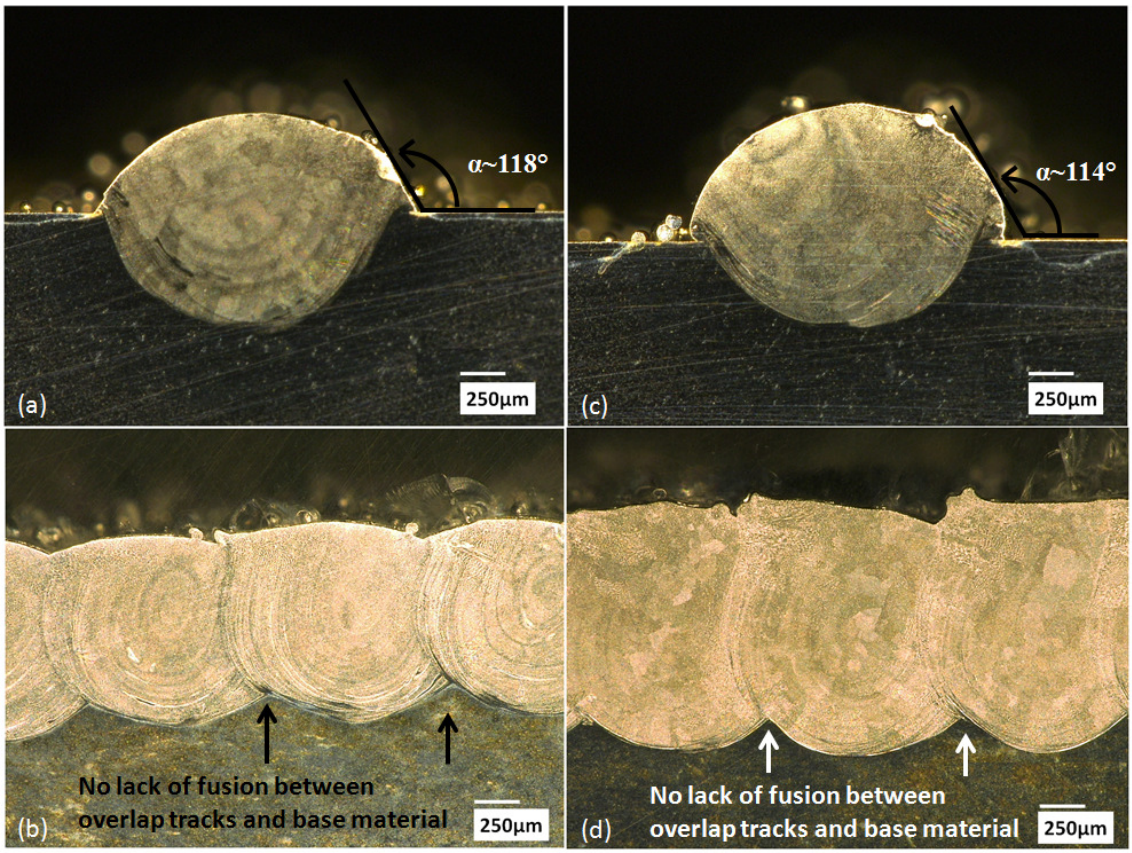

Figure 3.10 Optical micrographs showing the cross-section of the single track and clad layer manufactured with S275 steel as base material and cladding parameters of: (a) and (b) laser power of 1000W, traverse speed of 360mm.min^{-1} and powder feed rate of 6.3g.min^{-1}; (c) and (d) laser power of 850W, traverse speed of 240mm.min^{-1} and powder feed rate of 6.3g.min^{-1}. No cracks, porosity and lack of fusion were found on the clad layers. Furthermore, cladding angles higher than 90° were developed in the corresponding single tracks which promoted the good bonding between the overlap tracks and the base material.

Given that good results were achieved with S275 steel as the base material with grade 316L powder, a new set of experiments was carried out with the same parameters using grade 316L stainless steel as the base material. Figure 3.11 shows the cross sections of the single track and clad layer manufactured with the process parameters of 850 and 1000 W, traverse speed of 240 and 360 mm.min^{-1} and powder feed rate of 6.3 g.min^{-1}. It can be observed that clad layers without discontinuities were also achieved. This means, the values of the process parameters selected on the samples where S275 steel was used as base material also generated clad layers without lack of fusion, cracks and porosity.

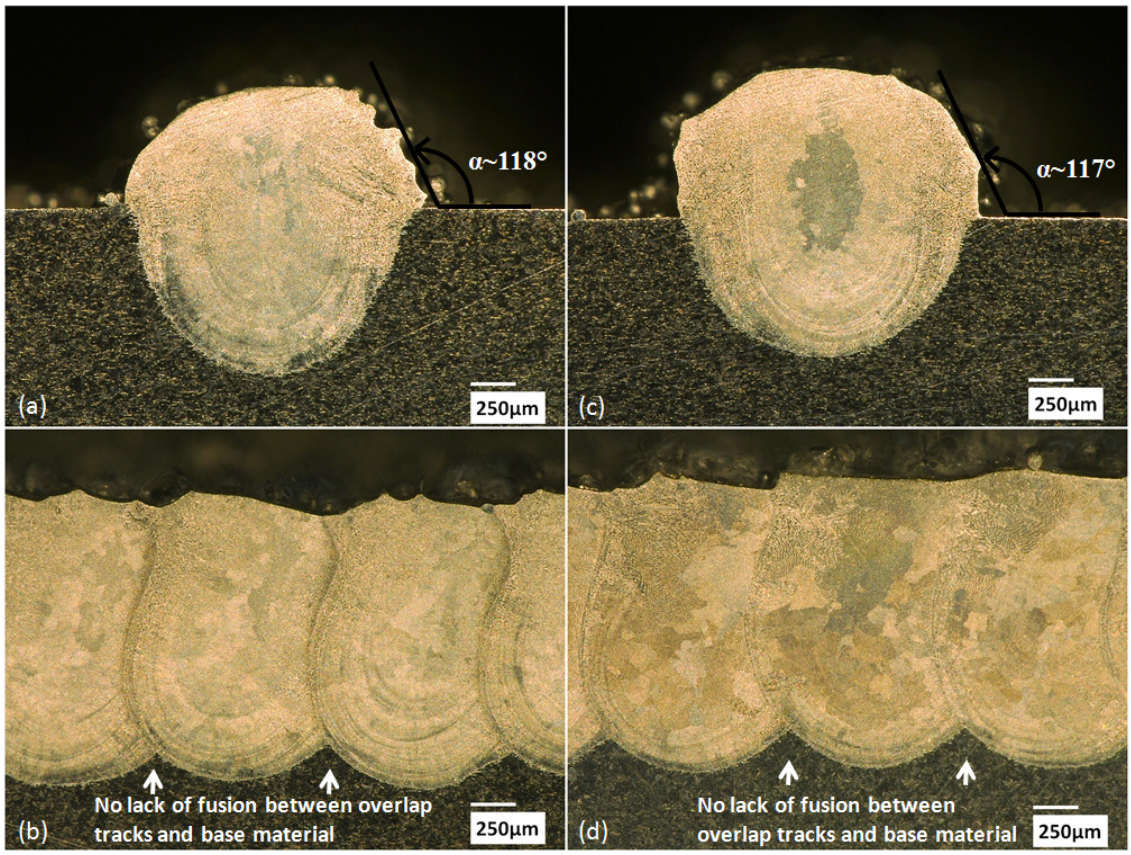

Figure 3.11 Optical micrographs showing the cross-section of the single track and clad layer manufactured with AISI grade 316L stainless steel as base material and cladding parameters of: (a) and (b) laser power of 1000W, traverse speed of 360mm.min^{-1} and powder feed rate of 6.3g.min^{-1}; (c) and (d) laser power of 850W, traverse speed of 240mm.min^{-1} and powder feed rate of 6.3g.min^{-1}. No cracks, porosity and lack of fusion were found on the clad layers. Furthermore, cladding angles higher than 90° were developed in the corresponding single tracks which promoted the good bonding between the overlap tracks and the base material.

In order to understand the effect of the powders, their chemical composition was examined using energy disperse x-ray fluorescence spectrometry. The results are showed in Table 3.2.

Table 3.2 Chemical composition of AISI grade 316L powders used in the laser cladding trials.

Powder	**wt. % of alloying element**				
	Cr	**Fe**	**Ni**	**Mo**	**Nb**
LPW Technology	12.6	45.7	8.3	1.3	0.17
Höganäs Belgium	18.2	66.9	11.7	2.99	-

The LPW Technology powder refers to the powder that was used in the first experiments where cracks were evident. The LPW Technology powder does not satisfy the standard chemical composition for AISI grade 316L stainless steel. This can explain the problems associated with the experimental work in which cracking was the main problem. With reference to the Shaeffler constitution diagram for stainless steels, the lower concentrations of chromium and nickel in the LPW Technology powder would have promoted the generation of martensite in the microstructure, thereby generating a brittle material upon cooling after solidification. Therefore, it is plausible that the cracking that occurred with the old powder was cold cracking (or hydrogen cracking).

Finally, the optimum values for the process parameters have been identified. These parameters were used throughout the laser cladding experimental work in which microstructure, corrosion resistance, hardness and residual stresses will be assessed. The final optimised parameters are summarised in Table 3.3. These parameters represent the multidimensional parametric study showed in Figure 3.7.

Table 3.3 Laser cladding process parameters.

Parameter	**Laser Power (W)**	**Traverse Speed ($mm.min^{-1}$)**	**Powder feed rate ($g.min^{-1}$)**
Low laser power	700	360	6.3
Centre point	850	360	6.3
High laser power	1000	360	6.3
Low speed	850	240	6.3
High speed	850	480	6.3
Low mass flow	850	360	4.56
High mass flow	850	360	8.58

It was essential for all of the work to be carried out in order to find the conditions that produced cladding without discontinuities such as porosity, cracks or lack of fusion, as these can have a detrimental effect on the performance of the clad layers. This mean, the

corrosion resistance or the fatigue life of the clad layer can be considerably affected if cracks are present. Therefore, an extensive study was carried out in order to eliminate discontinuities between clad layers.

3.6 Discussion

Laser cladding is a complicated process because several variables are involved. Two aspects should be considered in the selection of the process parameters.

1. The process parameters should provide good fusion between the overlapping single tracks and the base material
2. Discontinuities in the cladding such as porosity and cracks should be avoided

The lack of fusion between overlapping tracks and base material can be attributed to the process parameters. This means laser power, traverse speed and powder feed rate play an important role in the generation of good bonding between the base material and the overlapping single tracks deposited. Furthermore, the selection of the appropriate process parameters depends of the material to be treated and the final conditions required such as the cladding height or dilution.

The parameters chosen for the remainder of the cladding experiments resulted in a cladding angle (α) of approximately of 120°, therefore no lack of fusion between overlapping tracks and the base material was generated. The cladding angle is an important factor to consider in the selection of the process parameters, especially if overlapping tracks are used in order to cover larger areas. However, if laser cladding is used in order to build up walls, for instance as in 3D printing, the cladding angle can vary due to others issues which can become of greater concern than lack of fusion.

While process parameters may also have an effect on the likelihood of forming other discontinuities in the cladding, such as porosity and cracks, there are other potential contributing factors to the formation of these defects. For instance, if the cladding process is not performed in an isolated environment, contamination with air can produce flaws in the overlay. Furthermore, if there is contamination on the sample surface or if the powder is contaminated, discontinuities can also be generated after solidification.

In this work, it was found that the likelihood of cracking correlated with the chemical composition of the powder material that was used in the deposition of the single tracks. With the LPW Technology powder, which had lower levels of chromium and nickel, the formation of martensite would be expected according to the Schaeffler diagram. The formation of a brittle microstructure would make the overlay more susceptible to cracking through mechanisms such as, for example, cold cracking. This observation highlights the importance of the chemical composition of the materials involved in the generation of discontinuities.

Chapter 4

Metallurgical assessment of laser cladding deposits

4.1 Introduction

This chapter describes the experimental procedures used to reveal the microstructures developed in the laser cladding experiments. Furthermore, the changes in microstructure due to changes in process parameters and different base materials are examined. In addition, the phase microstructure is estimated in some samples with the help of the WRC-1992 diagram and the dilution. Owing to the importance of the material hardness, this is also examined and related to the changes in process parameters. A relationship between the hardness and dilution can be established in order to understand the effect of process parameters.

4.2 Experimental procedures

4.2.1 Sample preparation

Two sets of laser cladding samples were produced using the process parameters described in Table 3.3. The first set used grade 316L austenitic stainless steel as the powder material and S275 steel as the base material. The second set used grade 316L austenitic stainless steel as both the powder and the base material. In addition another sample, with centre point parameters was prepared depositing two layers of cladding for each combination of materials.

A total of 16 samples were examined and each sample was sectioned on the plane that was oriented transversely to the cladding direction at the mid-length position because at this location quasi-stationary state conditions will have been achieved. The samples were prepared using metallographic standard procedures [173]. Grinding was carried

out using 320 grit paper, followed by 600 grit paper, and finally with 1200 grit grinding paper. After grinding, the samples were manually polished using 6 μm, 3 μm and 1 μm slurry solutions.

4.2.2 Sample analysis

In order to reveal the microstructures, the samples were electrolytically etched in 10% oxalic acid. The samples were exposed to the solution for a period of 2 minutes, using a voltage of 7 V, and were then rinsed with plenty of water in order to stop the chemical reaction. The microstructures were examined using a Keyence VHX-500P optical microscope at different positions in order to visualize the microstructure along the length of the cladding.

The hardness of the samples was measured using a Buehler Micromet Vickers Hardness Tester following the Standard Test Method for Vickers Hardness of Metallic Materials (ASTM E 92-82). The hardness was measured in three different positions in the clad layer, corresponding to the positions of the 6^{th}, 10^{th} and 15^{th} cladding tracks to be deposited. These tracks represent an area where the dilution stabilised and it can be considered that quasi-stationary conditions were developed. The first indentation was applied close to the top of the ground clad surface and consecutive measurements were taken along the cladding until the base material was reached. The distance between indentations was three times the length of the diagonal for the indentations. An average of all measurements was taken to be as the hardness.

4.3 Results

4.3.1 Microstructures developed with Grade 316L austenitic stainless steel powder and S275 steel base material

Figure 4.1 and Figure 4.2 contain micrographs corresponding to the low laser power and low mass flow samples, respectively (Table 3.3). In general, the overall features of the

microstructures developed with laser cladding were similar for all of the combinations of process parameters that were tested.

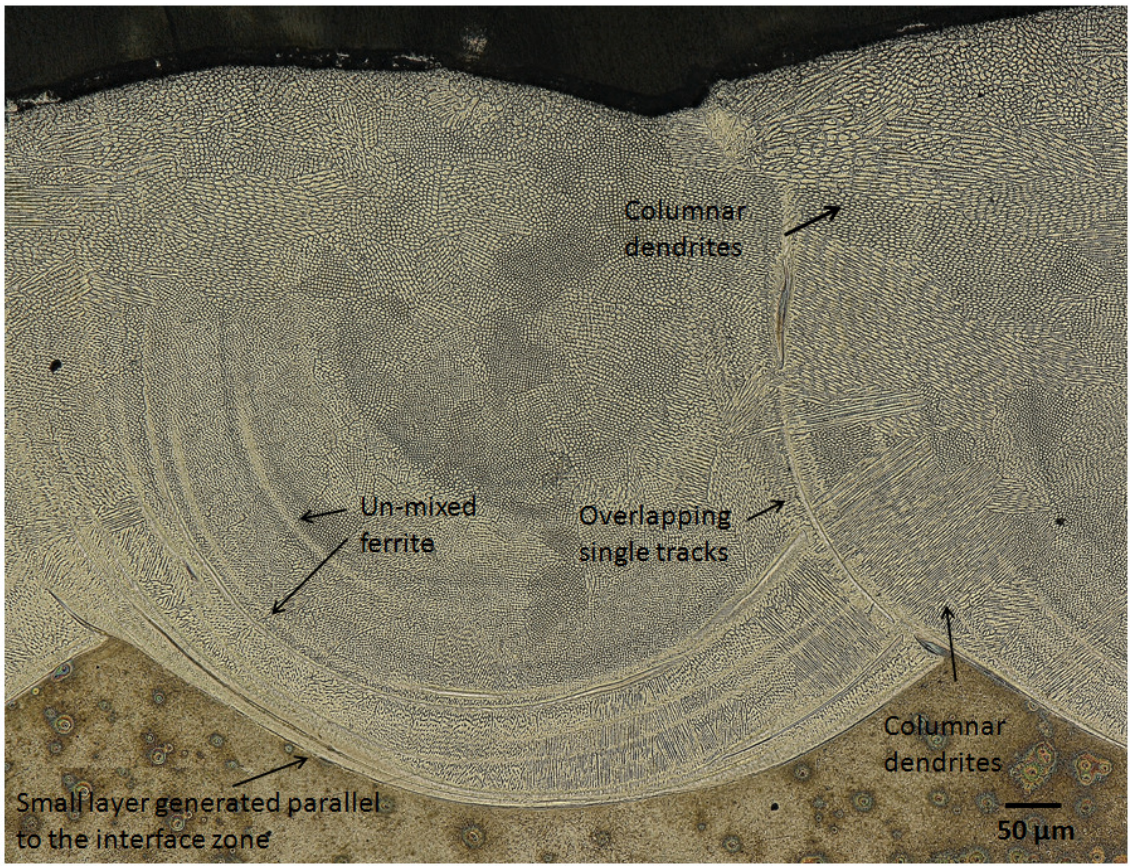

Figure 4.1 Optical micrographs showing the clad layer microstructure generated with a laser power of 700W, a powder feed rate of 6.3g.min^{-1}, and a traverse speed of 360 mm.min^{-1}. In some locations, evidence of columnar microstructures can be observed. A narrow layer was developed parallel to the interface zone and some un-mixed ferrite is also observed.

Coarser columnar microstructures were observed near the fusion boundary for each clad pass, whereas in the centre of each clad bead and towards the top surface finer columnar dendrites were observed, with multiple grain orientations that were not necessarily aligned with the direction of heat flow. A transition from columnar dendritic to equiaxed dendritic microstructures was not produced, as is evident in the higher magnification images presented in Figure 4.3 and Figure 4.4. Equiaxed dendritic microstructures are developed with low thermal gradients and higher solidification rates, a combination which is not likely to arise for the deposition conditions in this study.

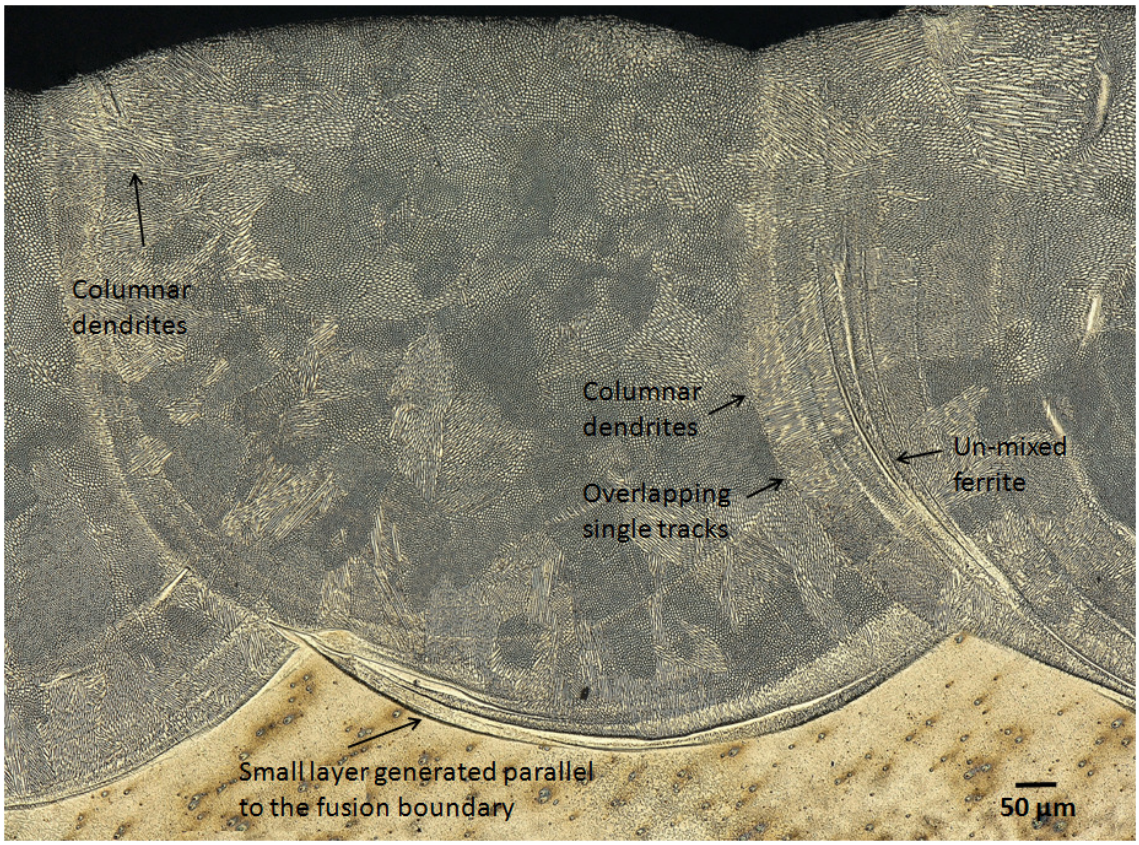

Figure 4.2 Optical micrographs showing the clad layer microstructure developed with a laser power of 850 W, a traverse speed of 360mm.min^{-1}, and a powder mass flow rate of 4.56 g.min^{-1}. Columnar morphology microstructures are observed. A narrow layer was developed parallel to the interface zone and some un-mixed ferrite is also observed.

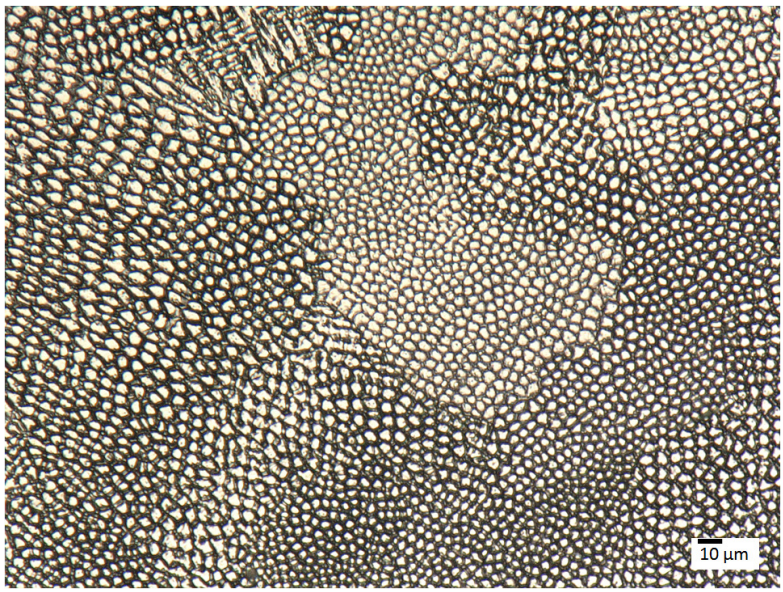

Figure 4.3 Optical micrographs showing the clad layer microstructure developed with a laser power of 850W, a traverse speed of 240 mm.min^{-1}, and a powder mass flow rate of 6.3 g.min^{-1}. Finer columnar microstructures are observed in the centre of the clad bead. No evidence of the generation of equiaxed microstructures.

New orientations of columnar dendrites were observed on the top of the cladding in some samples. This could be attributed to the effect of additional convective cooling [174]. The same effect was found in Ref. [175], where finer columnar dendrites were observed on the top of the cladding parallel to the scanning direction. Columnar dendritic microstructures were also observed in the zone of overlapping single tracks. The orientation of the new grains followed the grain orientation of the previous tracks.

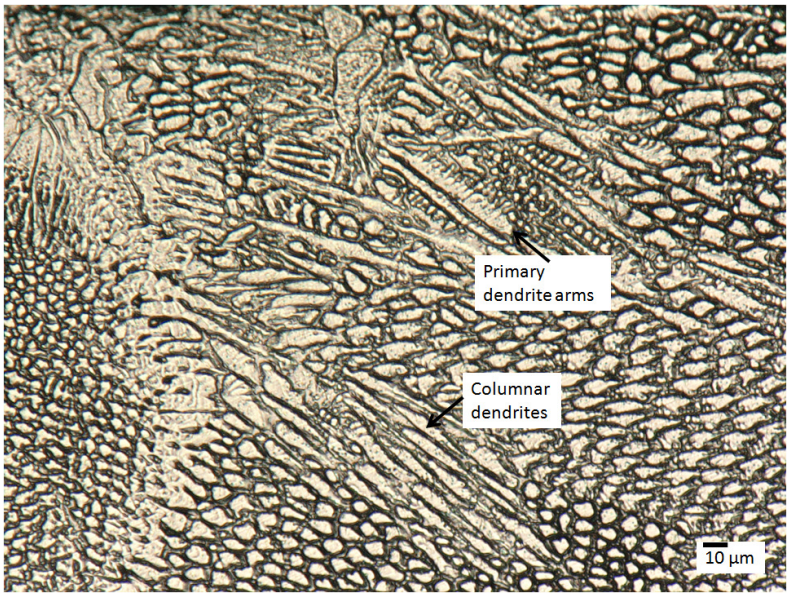

Figure 4.4 Optical micrographs showing the clad layer microstructure developed with a laser power of 850W, a traverse speed of 240 mm.min^{-1}, and a powder mass flow rate of 6.3 g.min^{-1}. Finer columnar microstructures are observed in the top surface of the clad bead. No evidence of the generation of equiaxed microstructures.

As mentioned in Section 2.8, the primary parameters for determining the microstructural morphologies are the thermal gradients and the solidification rates. If the temperature gradient is denoted by G and the solidification rate as R, the ratio G/R defines the solidification microstructure morphology and the product G.R defines the scale of the solidified microstructure [68, 95]. The product G.R is defined as the cooling rate (Equation 2.9). In general, fine microstructures are developed in laser process treatments; however the cooling rates define the exact scale of the solidification structure.

Owing to the high cooling rates developed by laser cladding, macrosegregation can occur. This means that non-uniform distribution phase can be produced during solidification [68, 176-178]. Macrosegregation can be caused by changes in growth

velocity during solidification, changes in convection patterns in the molten pool, or changes in the flow of solute enriched liquid, and it normally manifest as banding [68]. This effect was observed in most of the samples and can be related to un-mixed ferrite (Figure 4.1).

The deposition of two layers using the centre-point process parameters (Table 3.3) was also assessed where columnar microstructures were found. However, coarser dendrites could be promoted with the deposition of several overlapping tracks, owing to the accumulation of heat [175, 179]. This can reduce the thermal gradients, but the cooling rates will also change.

No epitaxially grown grains were developed perpendicular to the interface zone as would be expected. This was attributed to the generation of a narrow layer parallel to the fusion boundary (Figure 4.2). This layer formed parallel to the fusion boundary was observed in all the cladding samples. According to Refs. [180-182], when the base metal has a higher carbon content (ferritic steel) than the cladding material (austenite steel) some carbon from the heat affected zone will migrate to the fusion boundary generating a narrow martensitic layer parallel to the interface zone which will produce high hardness in that particular region. The generation of this layer can produce cracks due to hydrogen cracking at the fusion boundary and the performance of the material will be considerably affected.

In order to identify if a martensitic layer was formed parallel to the fusion boundary, hardness measurements were carried out on the high-laser-power and low-speed samples (Table 3.3). The dilution generated on the high-laser-power and low-speed samples was 30 and 10%, respectively. Figure 4.5 shows the hardness measurement on the high-laser-power sample where it can be seen that a considerable increment of hardness (approximately 60%) is found along the narrow layer parallel to the fusion boundary, and this starts to decrease towards to the centre of the cladding. Similarly, a considerable increment of hardness (approximately 50%) was also found along the narrow layer parallel to the fusion interface in the low-speed sample (Figure 4.6). Therefore, it would seem plausible that a martensitic layer was developed due to carbon migration from the heat affected zone to the fusion zone.

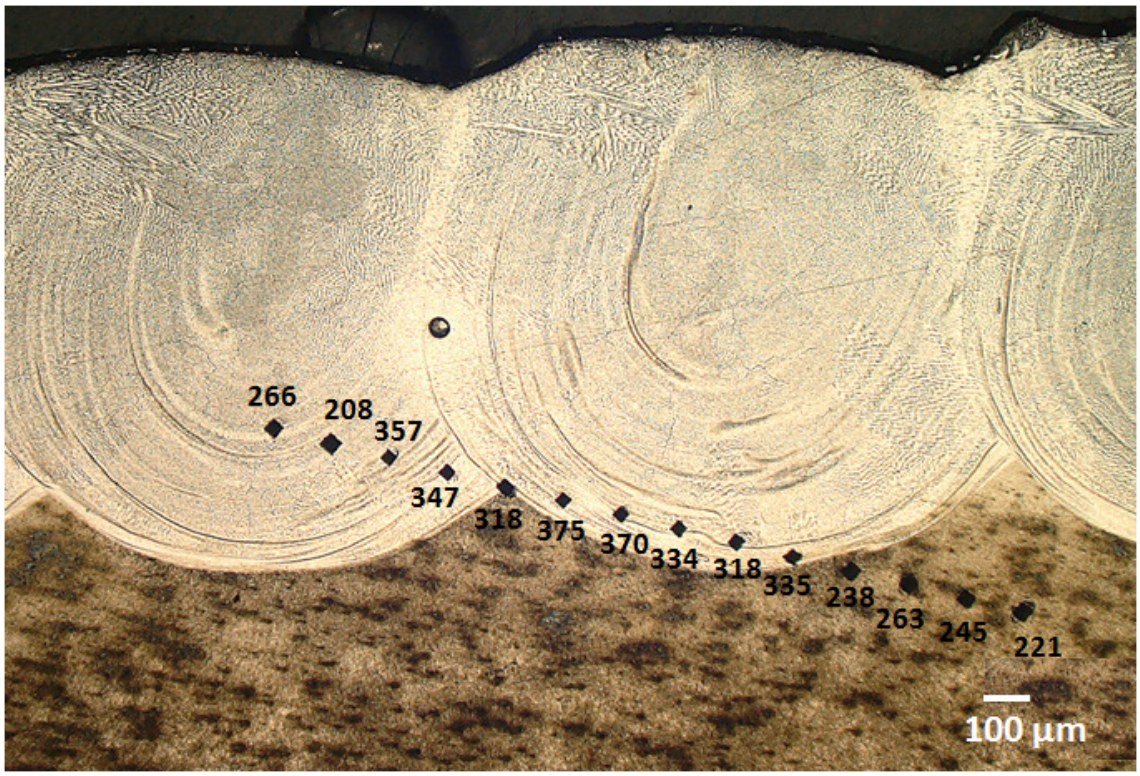

Figure 4.5 Optical micrographs showing the hardness measurements (HV0.3) on the high-laser power sample. An increment in hardness is developed near to the fusion boundary before the hardness starts to decrease towards the centre of the clad bead. (30% dilution)

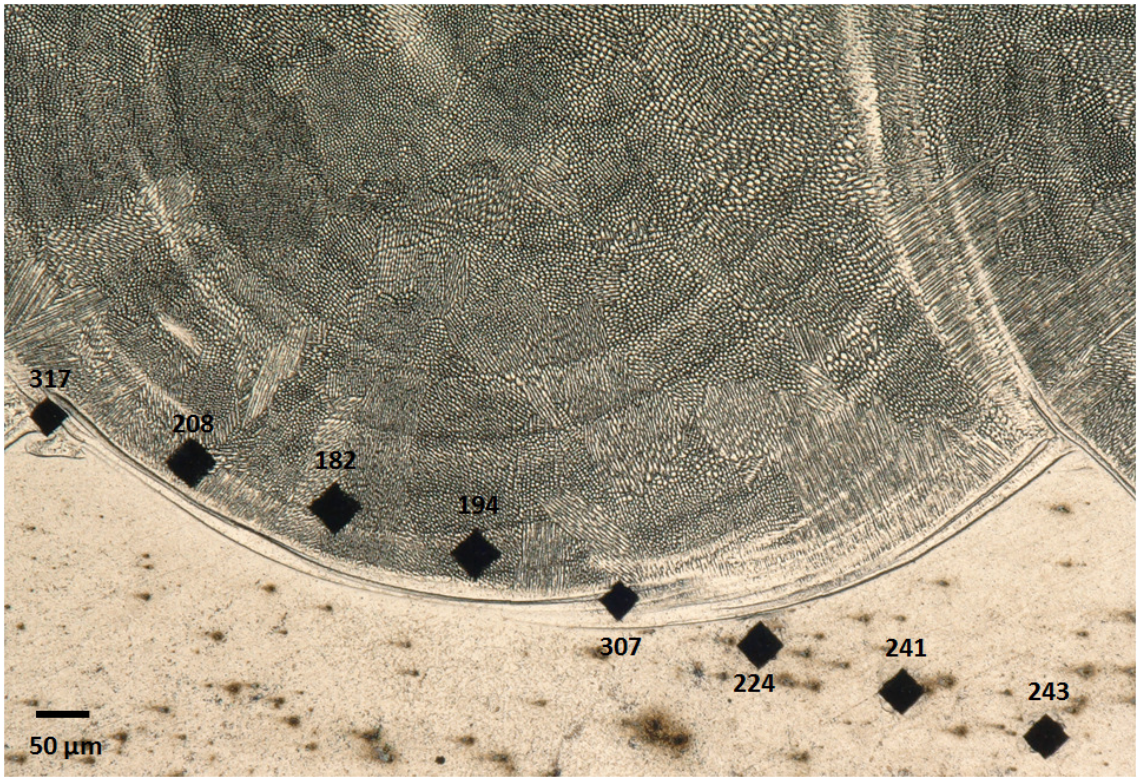

Figure 4.6 Optical micrographs showing the hardness measurements (HV0.3) on the low-speed sample. An increment in hardness is developed near to the fusion boundary. (10% dilution)

It is worth noting that dissimilar materials are normally used in laser cladding, which means that changes in phase or microstructure within the cladding material could be generated owing to dilution. In this case, since grade 316L stainless steel is deposited on to S275 steel, the generation of some ferrite [175] or martensite can occur during solidification. The Shaeffler diagram and the WRC-1992 diagram can be used to estimate the phases present in the microstructure of the clad metal. Therefore, the phase microstructure developed in some cladding samples were estimated using the WRC-1992 constitution diagram for stainless steel. The dilution was measured in all of the samples as was described in Section 2.4.4. Table 4.1 summarises the dilution that occurred with the different combinations of process parameters and Table 4.2 summarises the chemical composition for the low-speed, centre-point and low-mass-flow cladding parameters.

Based on the chemical compositions shown in Table 4.2, the microstructural phases developed for different values of dilution can be estimated using the WRC-1992 diagram (Figure 4.7).

Table 4.1 Dilution produced with different combinations of process parameters (%).

Parameter	**Laser Power (W)**	**Traverse Speed ($mm.min^{-1}$)**	**Powder feed rate ($g.min^{-1}$)**	**Dilution (%)**
Low laser power	700	360	6.3	17
Centre point	850	360	6.3	25
High laser power	1000	360	6.3	30
Low speed	850	240	6.3	10
High speed	850	480	6.3	35
Low mass flow	850	360	4.56	47
High mass flow	850	360	8.58	10

Table 4.2 Estimated chemical compositions for the low-speed (10%), centre-point (25%) and low-mass-flow (47%) cladding parameters (wt. %).

Material	S275 mild steel	AISI 316L SS	10% dilution	25 % dilution	47 % dilution
C	0.29	0.03	0.056	0.095	0.152
Mn	1	2	1.9	1.75	1.53
Si	0.2	1	0.92	0.8	0.624
P	0.04	0.045	0.045	0.0438	0.043
S	0.05	0.03	0.032	0.035	0.039
Cr	.....	17	15.3	12.75	9.01
Ni	.....	12	10.8	9	6.36
Mo	.....	2.5	2.25	1.88	1.33
Cu	0.2	.....	0.02	0.05	0.094
Cr_{eq}	0	19.5	17.55	14.63	10.34
Ni_{eq}	10.2	13.05	12.77	12.34	11.71

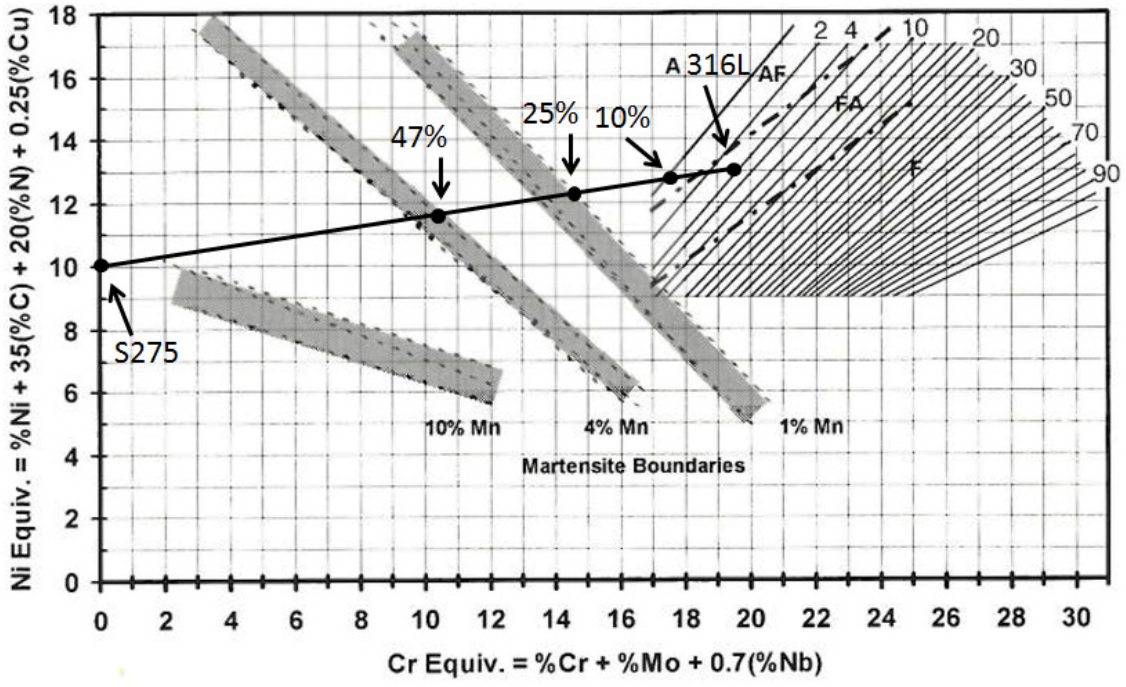

Figure 4.7 WRC-1992 diagram [183] overlayed with a mixing line between the compositions of the mild steel substrate (S275) and the stainless steel powder (316L). Estimated compositions for ~10% dilution, ~25% dilution and ~47% dilution are highlighted. Compositions on the left side of the 1% Mn boundary will tend to develop martensite.

It can be seen that γ-austenite with a small quantity of δ-ferrite would be expected to develop in the low speed sample (10% dilution). For the centre-point parameters (25% dilution), the phases in the microstructure would be expected to comprise γ-austenite with a small fraction of martensite. Finally, γ-austenite with some martensite would be expected to develop with the low-mass-flow parameters (47% dilution). Austenitic stainless steels do not normally develop martensite during cooling after solidification, unless severe cold work is applied or unless cryogenic temperatures are approached. Thus, the formation of martensite is normally unlikely, and it can be challenging to observe martensite based only on the morphologies that appear in the microstructure (Figure 4.8). However, as mentioned above, an increase in the hardness can indicate the presence of martensite within the overlay.

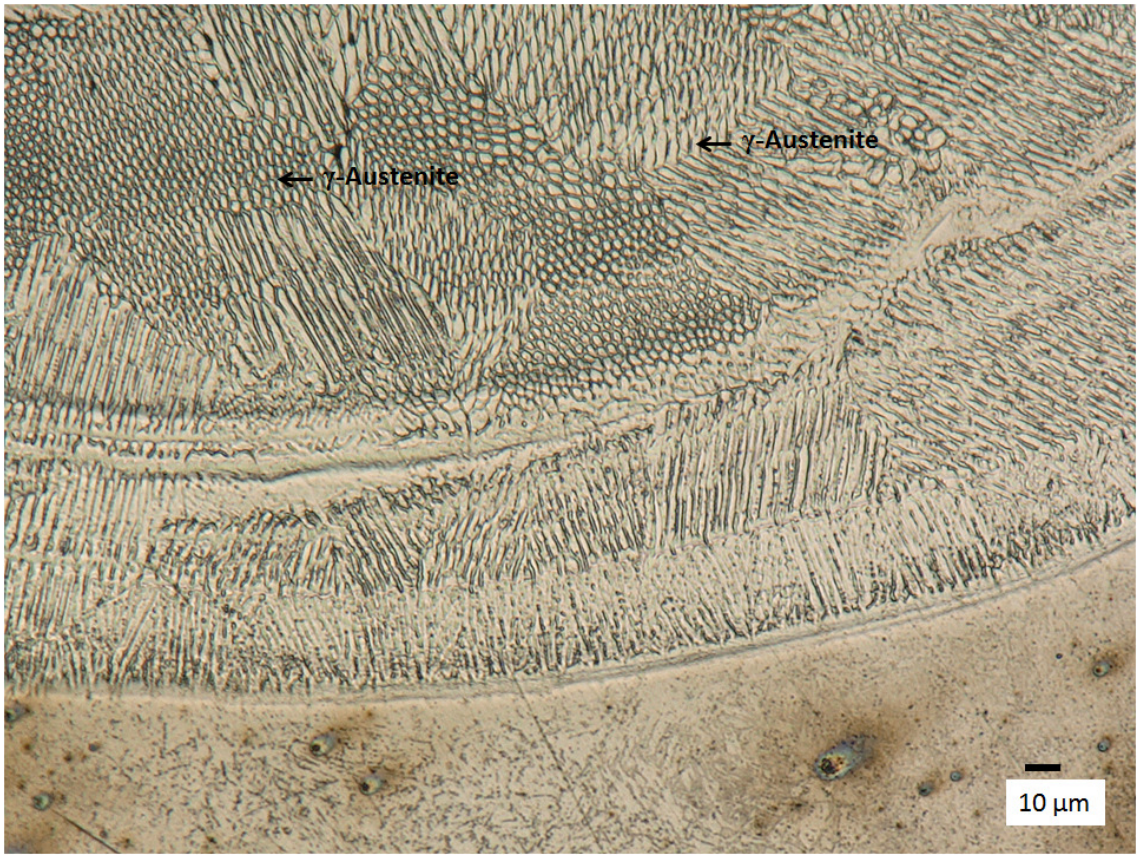

Figure 4.8 Optical micrographs showing the clad layer microstructure developed with a laser power of 850W, a traverse speed of 360 mm.min^{-1}, and a powder mass flow rate of 4.56 g.min^{-1}. The appearance of γ-austenite phase microstructure is observed in clad bead with no evidence of martensite.

There are other factors that can have an influence on the phases that are present in the microstructure at room temperature. As explained by Kou [96], if higher cooling rates

are present in the process (i.e. at welding speeds in the order of 120000 mm.min^{-1}), a change in phase can be generated. For instance, a material that normally solidifies as primary ferrite with a low cooling rate could solidify as primary austenite solidification under higher cooling rates. In this work, low traverse speeds were used (between 240 to 360 mm.min^{-1}); therefore a phase transformation due to higher cooling rates is not expected.

It can be observed that dilution plays an important role in the development of phases in the microstructure. Therefore, it can be appreciated that dilution will also influence the residual stresses that develop in the overlay through affecting the coefficients of thermal expansion, and through the effects that transformation strains have on the development of residual stress [184]. For example, the dilatational strain associated with a transformation from austenite to martensite is known to reduce the tensile nature of residual stresses, since the decrease in density that occurs during the transformation counteracts the development of thermal contraction strains upon cooling to room temperature [184].

4.3.1.1 Hardness

As was mentioned in Section 2.9, material hardness is an important mechanical property for metals, because it provides crucial information that is considered in the selection of materials. Hardness is directly related to the grain size, the chemical composition and the phase composition of the metal, and also to some external work hardening processes. Therefore, laser surfacing processes in which finer microstructures are developed could manifest high values of hardness. Furthermore, changes in the phases present in a microstructure can also lead to changes in hardness.

Figure 4.9 shows the hardnesses that were produced with different laser powers at a constant traverse speed and at a constant powder feed rate. The lowest hardness was produced with a laser power of 700 W and the highest with a power of 1000 W. According to the above discussion on microstructure, similar microstructures were developed in all of the samples; this suggests that variation in microstructure was not the cause of a significant variation in hardness. However, a high dilution was observed with the sample manufactured using a high laser power sample (Table 4.1), and the

cladding thickness was also higher. The first of these facts can explain the high hardness produced at high laser power, since the inclusion of some elements from the base material in the cladding may have promoted a change of phase in the microstructure.

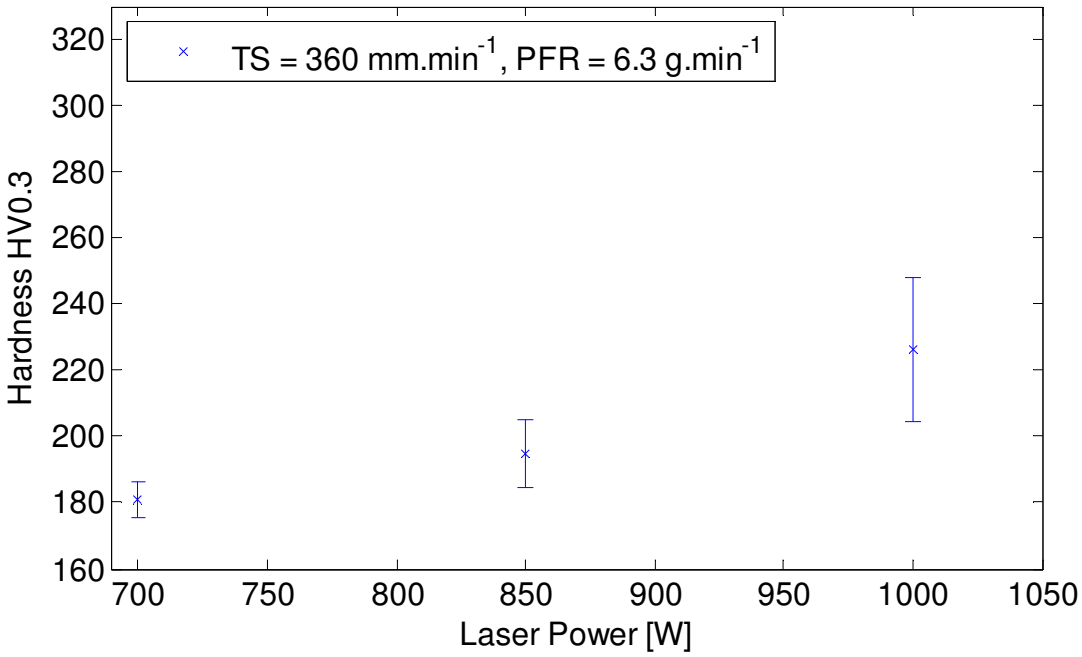

Figure 4.9 Hardnesses developed in laser cladding samples with grade 316L stainless steel as the powder, and S275 steel as the base material, at different laser powers, and with a constant traverse speed of 360 mm.min^{-1} and a constant powder feed rate of 6.3 g.min^{-1}.

Figure 4.10 depicts the hardness developed with different traverse speeds at a constant laser power and a constant powder feed rate. The highest value of hardness was produced with the highest traverse speed. In this case, the dilution with the high traverse speed was higher than for the condition with a high laser power. Therefore it can be assumed that a higher proportion of base material elements were distributed in the cladding and that this promoted high values of hardness, through the formation of martensite. Furthermore, the high speed led to a smaller cladding thickness than for the low speed because less powder was fed to the melt pool.

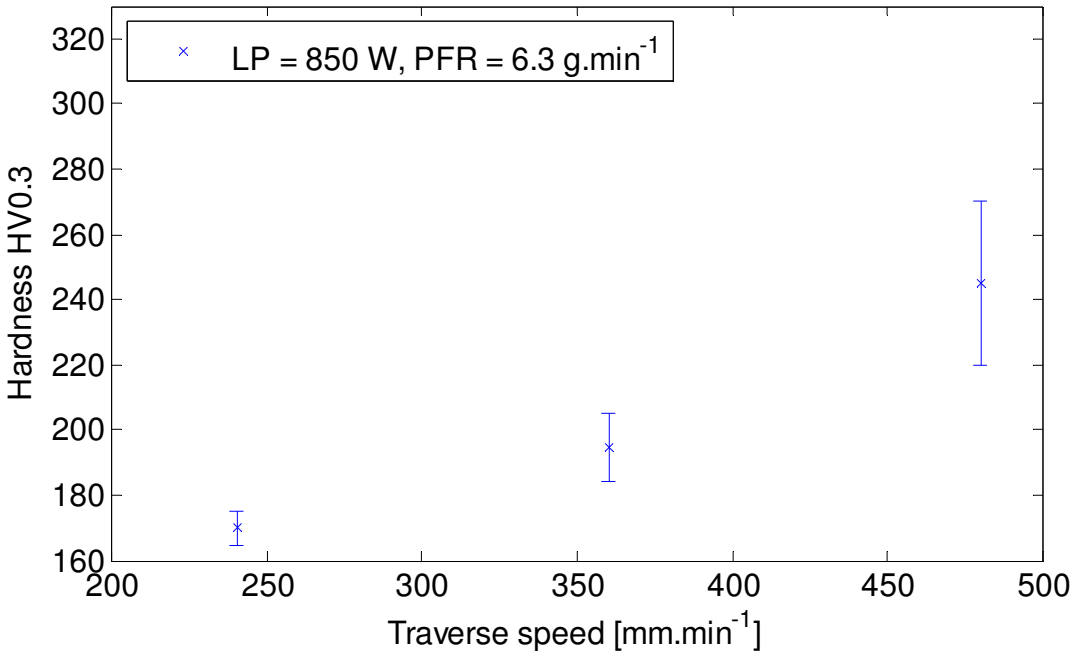

Figure 4.10 Hardnesses developed in laser cladding samples with grade 316L stainless steel as the powder and S275 steel as the base material, at different traverse speeds and with a constant laser power of 850 W and constant powder feed rate of 6.3 g.min^{-1}.

Figure 4.11 show the effect of powder feed rate on hardness. In this case the highest hardness was found with the lowest powder feed rate, in contrast to the results for the laser power and the traverse speed, where the highest values of each parameter developed the highest hardness. The results generated for the powder feed rate are in accordance with previous studies [111], because the low powder feed rate produced the highest dilution according to the information provided in Table 4.1.

The hardnesses obtained with different combinations of process parameters such as laser power, traverse speed and powder feed rate were in the range of 170 to 320 HV0.3. It can be observed that a high dilution promoted high hardness, with the low powder feed rate condition generating the highest value of hardness. As it was seen in Table 4.2, the chemical composition of the cladding can change considerably due to the inclusion of base material elements, thereby promoting the development of different phases in the microstructure. Therefore, it can be assumed that the phases estimated with the WRC-1992 diagram were consistent with the assertion that the parameters that produced higher dilution levels also showed higher values of hardness.

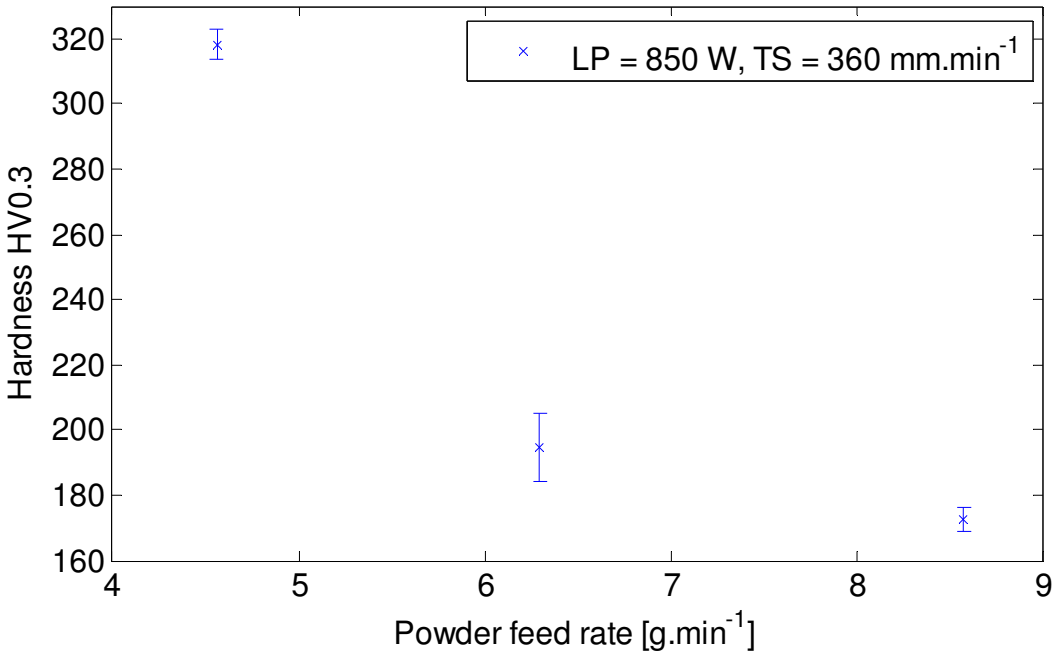

Figure 4.11 Hardnesses developed in laser cladding samples with grade 316L stainless steel as the powder and S275 steel as the base material at different powder feed rates, and at a constant laser power (850 W) and with a constant traverse speed (360 mm.min^{-1}).

4.3.2 Microstructures developed with Grade 316L austenitic stainless steel as both powder and base material

The microstructures developed using grade 316L stainless steel as both the powder and the base material were similar to those for the case described above. Figure 4.12 shows the microstructure developed with a laser power of 850 W, a traverse speed of 240 mm.min^{-1}, and a powder feed rate of 6.3 mm.min^{-1}. In general, epitaxial microstructures were found to develop in the direction perpendicular to the interface zone and in the opposite direction to the heat flow, with the presence of columnar dendritic morphologies. Equiaxed dendritic microstructures were also observed toward the top of the cladding due to the high cooling rates that would be expected to develop in this zone (Figure 4.13). Furthermore, primary and secondary dendrites arms were also present.

Macrosegregation manifested as banding was also found in all of the samples. As mentioned above, this is related to non-equilibrium solidification which is occurs in some rapid solidification processes.

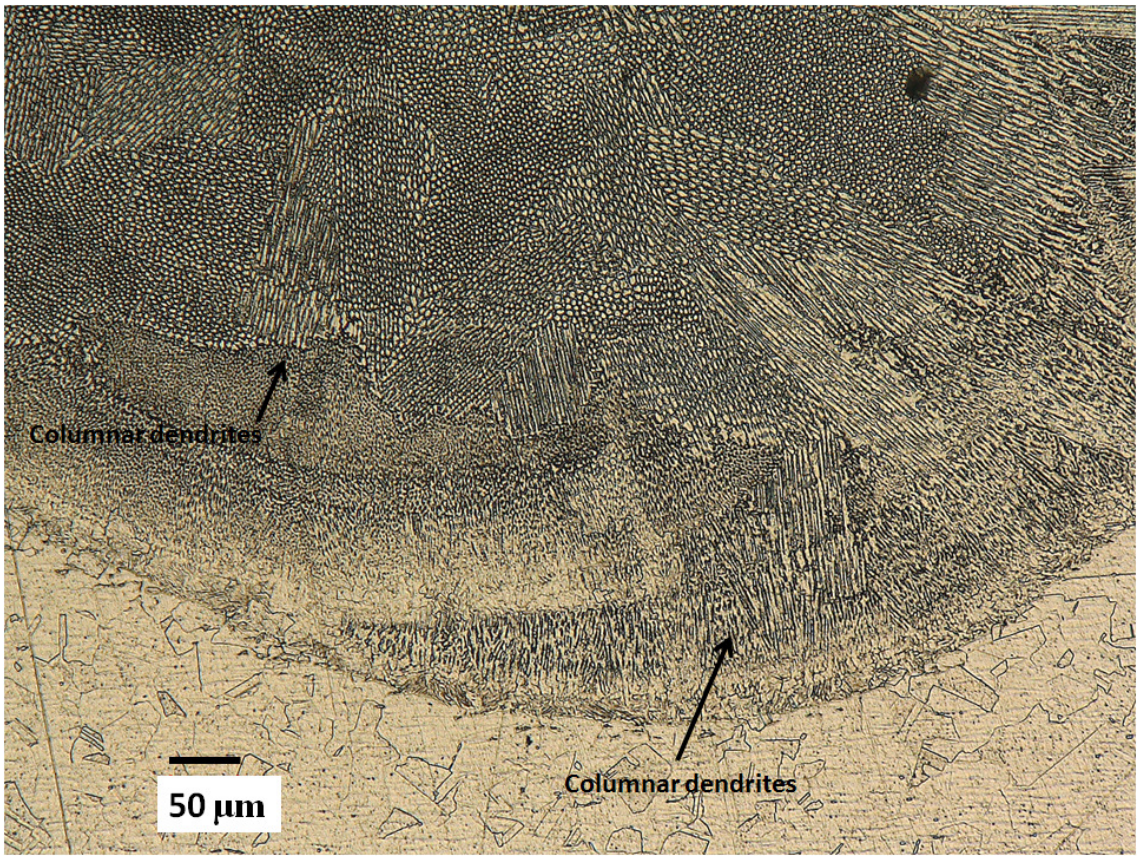

Figure 4.12 Optical micrographs showing the clad layer microstructures developed with the laser cladding process using grade 316L stainless steel as both the powder and the base material, with a laser power of 850 W; a traverse speed of 240 mm.min^{-1}; and a powder feed rate of 6.3g.min^{-1}. Epitaxial columnar microstructure was developed perpendicular to the interface zone and along the clad layer in multiple directions.

Since AISI grade 316L stainless steel was used as both the cladding and base material, the effects of dilution can be ignored. According to the WRC-1992 diagram (Figure 4.7), a predominatly γ-austenite microstructure with a small portion of δ-ferrite would be expected to form. However, the quantity of ferrite present in the clad layer is very small, so the micostructure appears to be fully austenitic in the figure.

No further phase transformations would be expected during cooling, as was discussed above, because the traverse speed that was used in the manufacture of these samples was not high enough to generate cooling rates that would produce such a transformation.

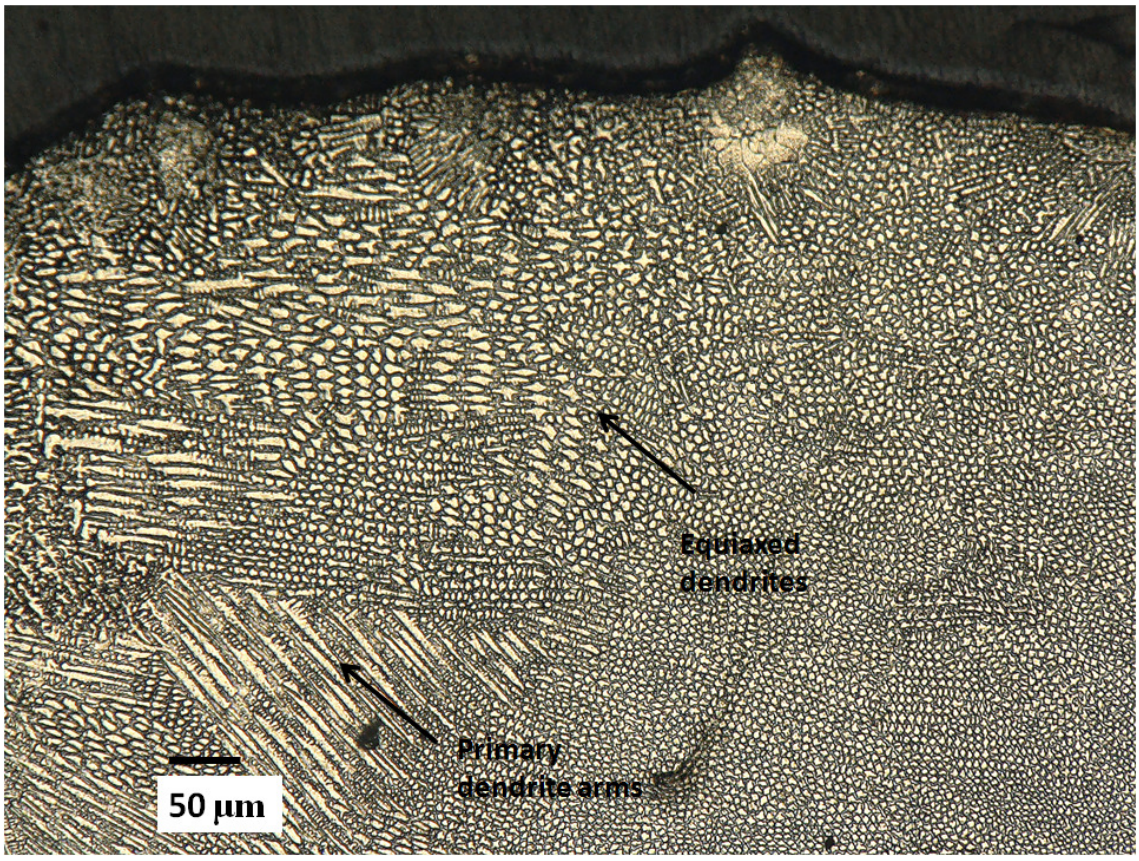

Figure 4.13 Optical micrographs showing the clad layer microstructures developed with the laser cladding process using grade 316L stainless steel as both the powder and the base material, with a laser power of 850 W; a traverse speed of 240 mm.min^{-1}; and a powder feed rate of 6.3g.min^{-1}. Equiaxed dendrites were developed at the top of the cladding. Furthermore, primary dendrites were also observed.

4.3.2.1 Hardness

The hardness values in laser cladding samples for which grade 316L stainless steel was used as the powder, and S275 steel was used as base material, were assessed. The changes have been related to the process parameters that were used for each sample. Hardness measurements were performed following the same procedure explained in Section 4.2.2.

The hardnesses generated as a function of laser power, traverse speed and powder feed rate are presented in Figure 4.14, Figure 4.15 and Figure 4.16, respectively.

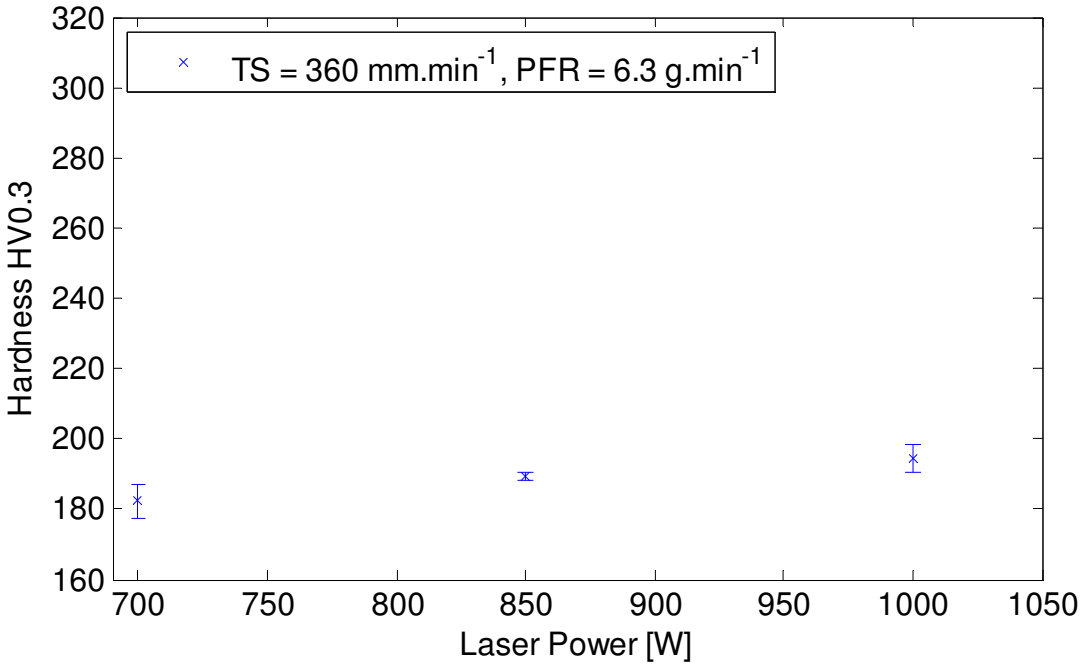

Figure 4.14 Hardnesses developed in laser cladding samples with grade 316L stainless steel as the powder and also as the base material at different laser powers, with a constant traverse speed (360 mm.min^{-1}) and a constant powder feed rate (6.3 g.min^{-1}).

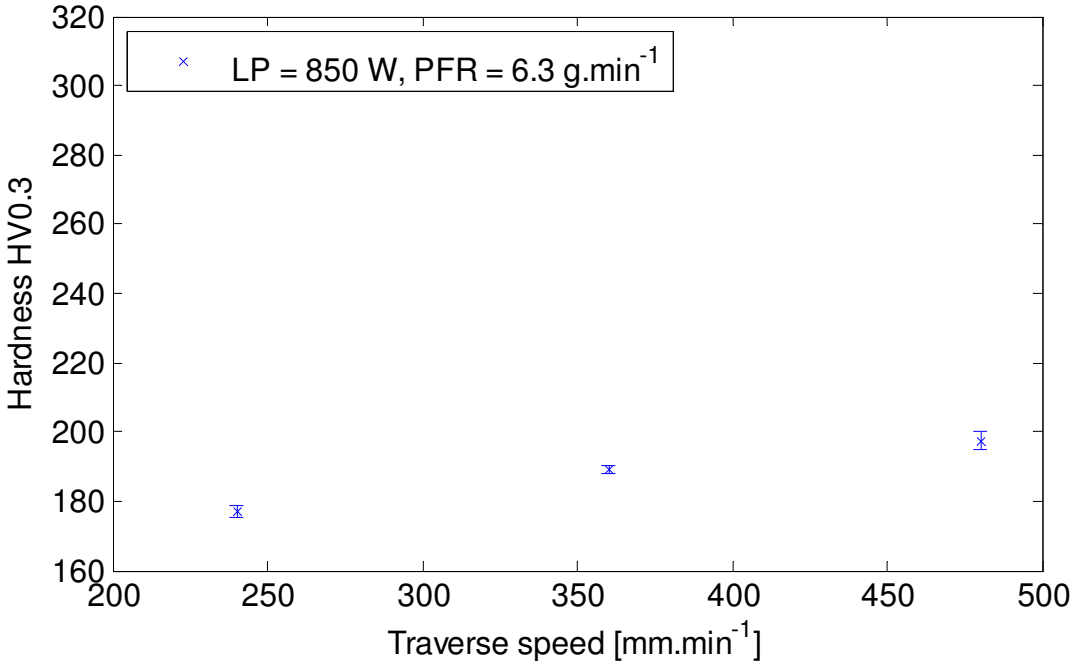

Figure 4.15 Hardnesses developed in laser cladding samples with grade 316L stainless steel as the powder and also as the base material at different traverse speeds, with a constant laser power (850 W) and a constant powder feed rate (6.3g.min^{-1}).

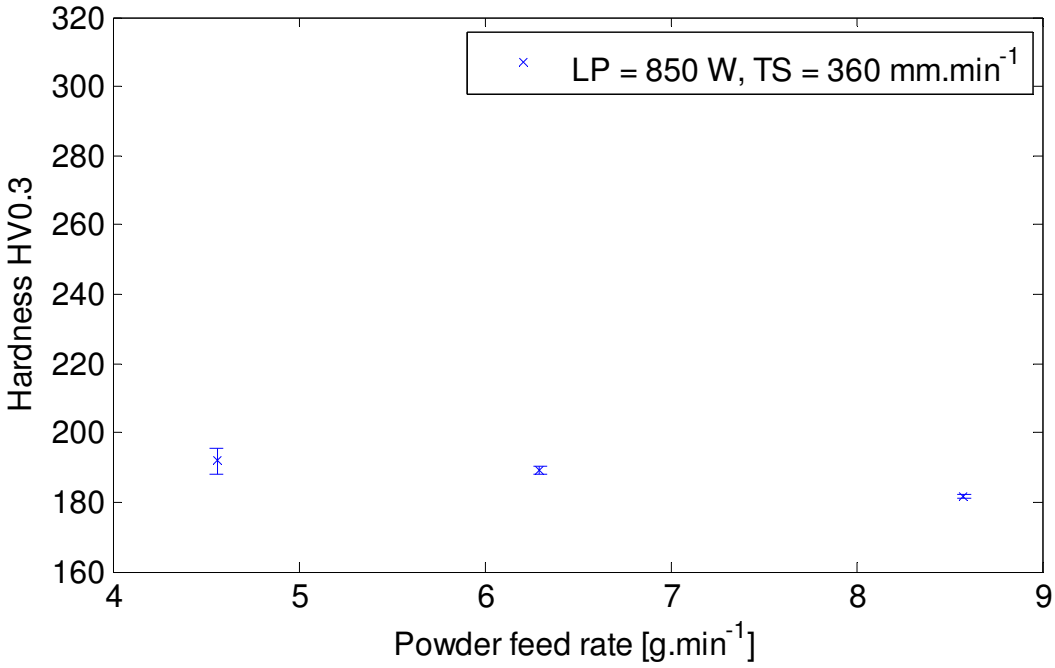

Figure 4.16 Hardnesses developed in laser cladding with grade 316L stainless steel as the powder and also as the base material at different powder feed rates, with a constant laser power (850 W) and a constant traverse speed (360 mm.min^{-1}).

It was noticed that only small variations in hardness occurred with all sets of parameters. These results were to be expected because the effects of dilution can be ignored, owing to the chemical composition of the powder matching that for the base material. This, in turn, means changes of phase in the microstructure would not be expected. Therefore, variations in hardness can be attributed to differences in the microstructures resulting from small variations in the cooling rate. For instance, the highest hardness was produced with the high traverse speed condition, for which fine microstructures were expected because high cooling rates will have manifested. Furthermore, small variations in hardness were developed between each area that was measured. However, the variations in hardness between all the samples were small, in the range between 177 and 192 HV0.3. These values are lower when compared with the hardnesses that arose when S275 steel was used as the base material.

4.4 Discussion

Laser power, the traverse speed and the powder feed rate are the main parameters that determine the cladding profiles, and also that affect the different microstructures and morphologies that develop. The high cooling rates that are produced in laser cladding are directly related to the process parameters, and these cooling rates promote the generation of finer microstructures, such as cellular and columnar dendrites, after solidification. Even though equiaxed dendrites have also been generated in laser cladding, the conditions that are required to form such a microstructure are complex, and the values of the process parameters that were chosen in this study did not produce this type of structure in the majority of the cases.

Process parameters also have a direct effect on the dilution generated in laser cladding. Under the conditions proposed in this study, the lowest powder feed rate produced the highest dilution and this was equalled by the condition using the lowest traverse speed. This is because the powder density is affected by these parameters.

A narrow layer was developed parallel to the fusion boundary in all of the clad overlays where S275 steel was uses as the base material. This was attributed to the migration of some carbon from the heat affected zone to the fusion zone. It was found that an increment of hardness was generated in this region which suggested that martensite could have been formed.

The hardnesses generated in laser cladding can be related to the phase composition and the microstructural morphologies. In this study, the microstructures developed in the different samples were similar, but the effects of dilution in dissimilar materials played an important role in determining the hardness. A high dilution contributed to the generation of austenite and martensite phases in the cladding, as shown in the WRC-1992 constitutional diagram for stainless steels, owing to the inclusion of base material elements, thereby generating high values of hardness. Although, a high dilution leads to a high percentage of the base material elements being incorporated into the clad layer, the possibility of some powder material not melting could also promote an imbalance in the chemical composition of the cladding. In addition, it was difficult to identify martensite in the clad overlays microstructure owing to the fact that martensite does not normally develop in austenitic stainless steels during cooling after solidification.

However, the values of hardness agreed with the phase microstructure estimated with the WRC-1992 diagram.

A coating layer of grade 316L stainless steel was deposited over S275 steel substrates and the hardness that is developed can contribute to enhancing the wear resistance. However, the corrosion resistance could be adversely affected in the samples that showed high dilution. Therefore, it is necessary to clearly define the objectives when establishing the most appropriate conditions for treating the sample.

Chapter 5

Residual stress measurements

5.1 Introduction

The development of residual stresses in laser cladding can affect the performance of the final coating. Tensile and compressive residual stresses can develop due to the constrained expansion of material prior to melting, and constrained shrinkage after solidification. Since laser cladding is used either to restore worn components or to produce coatings with superior mechanical properties in comparison to the base material, dissimilar materials are often used.

In the event where dissimilar materials are used, thermal properties such as the coefficient of thermal expansion, the thermal conductivity and the melting point play an important role in the development of the nature and magnitude of the residual stresses. Furthermore, laser cladding process parameters such as laser power, traverse speed and powder feed rate directly affect the magnitude and nature of residual stresses because different cladding morphologies and phases that are generated with different combinations of process parameters. However, the study and analysis of residual stresses generated in laser cladding is complex due to all the variables that are involved.

It is crucial to have an understanding of the residual stresses generated in laser cladding because these stresses can be a major contributing factor to failures [185]. The most common failures produced by residual stresses are related with the generation of cracks which directly affect the fatigue resistance of the metals. Furthermore, if the materials are exposed to corrosive environments, residual stresses can affect the corrosion resistance, promoting failure modes such as intergranular corrosion or stress corrosion cracking.

Owing to the importance of residual stresses, this chapter describes the methodology that was used in the measurement of residual stresses that are developed during laser cladding with different values for process parameters such as the laser power, traverse

speed and powder feed rate. Two techniques were used in their assessment, the shallow hole drilling technique and the contour method. As mentioned in section 2.10, these techniques have been widely used in the assessment of residual stresses generated by laser cladding.

5.2 Experimental procedures

5.2.1 Sample preparation

In order to quantify the residual stresses that are developed in laser cladding, and the influence of process parameters, laser cladding samples were prepared with the centre-point process parameters and the high-laser-power conditions (Table 3.3). AISI grade 316L stainless steel powder material was deposited onto both S275 steel and AISI grade 316L stainless steel coupons. Given that two or more layers are often deposited in laser cladding in order to achieve a specific cladding thickness and an acceptable level of dilution, the centre-point conditions were also used to prepare samples with two layers of cladding.

As mentioned in Section 3.5, twenty single tracks were deposited with 40% overlap. After completion, the clad surface was gently ground and manually polished in order to get a flat surface. This procedure could modify the original residual stress state. However laser cladding normally is followed by a post-processing operation such as milling or turning in order to achieve the final dimensions. Therefore, it was considered necessary to assess the residual stresses in coupons that were prepared in a way that is representative of industrial practice.

5.2.2 Samples analysis

5.2.2.1 Contour method

As mentioned in Section 2.10.5, the contour method is based on the principle of stress relaxation as applied to a cut surface. Therefore, an appropriate cutting method should

be selected. In this study, the samples were cut using electric discharge machining (EDM), where an electric discharge is generated between a copper wire and the work piece in order to provide the thermal energy to cut the material.

The centre-point sample, for which laser cladding process parameters have been defined in Table 3.3, was selected to be assessed with the contour method. Two samples were prepared, one using S275 steel and the other grade 316L stainless steel as the base material. In each case, two layers of cladding were deposited. Furthermore, the base materials were also assessed prior to cladding in order to know the initial residual stress state.

The uncertainty in the estimated stresses generated with the contour method is directly affected by the cutting process and there are several factors with the potential to affect the uncertainties. For example, in order to produce smooth surfaces after cutting, low speeds and low voltages were used. Therefore, the same cutting conditions were used in all the cladding configurations.

If some discontinuities such as porosity or lack of fusion are produced in the cladding, several problems can arise, such as wire breakage, and then the smoothness of the cut surface can be affected, producing errors in the displacements generated by the stress relief.

Another important aspect to consider before the cutting step is the way in which the sample is clamped, because an inappropriate clamping configuration can generate dissimilar contours on the two opposing cut surfaces. [126]. This normally occurs when only one half of the sample is clamped. Accordingly, special jaws were manufactured in order to provide effective clamping for the samples. Figure 5.1 shows an example of the way in which the samples were held. It can be observed that the samples were held at four different locations in order to avoid any movements in each half of the sample. Any unexpected movement between the parts could introduce anti-symmetric errors.

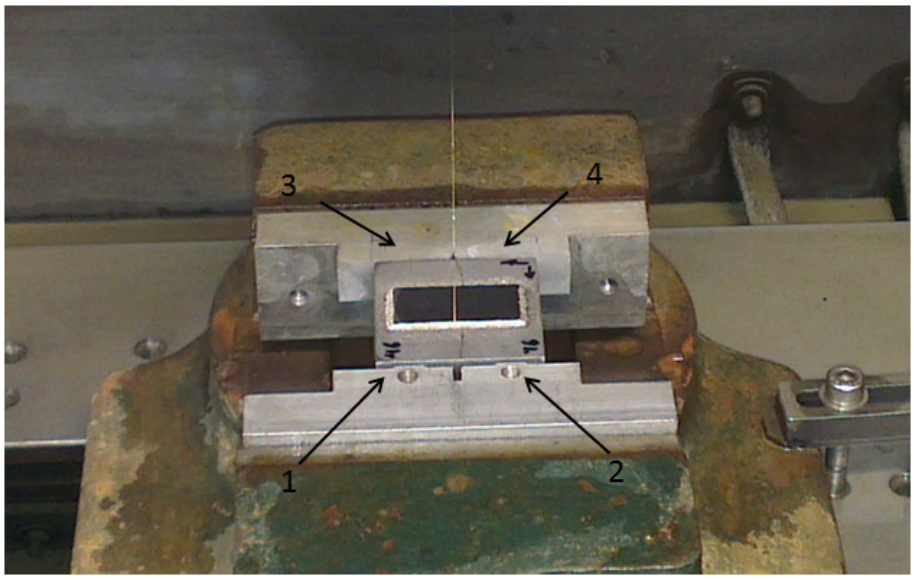

Figure 5.1 Jaws manufactured to grip samples for contour method measurements. The samples were held at four points in order to avoid any movement of either half of the sample being cut

The contour method only measures stresses that act in a direction that is normal to the cut surface, so it is important to identify the component of stress that is of greatest interest. Several studies have been made in order to understand the stress distribution in laser clad test pieces with varying configurations, with common variables including the selected process parameters, the choice of overlay and base materials, whether single layers or multiple layers are used and whether they comprise several overlapping tracks [13, 122, 128, 131].

In general, the results have shown that high tensile stresses have been produced in the cladding direction. On this basis, the centre-point samples were cut on a plane that was orientated transversely to the cladding direction. The cutting was carried out at the mid-length position of the overlay, and perpendicular to the cladding or longitudinal direction. Thus, the residual stresses acting in the longitudinal direction were measured. Figure 5.2 provides a schematic representation of the EDM cutting set-up.

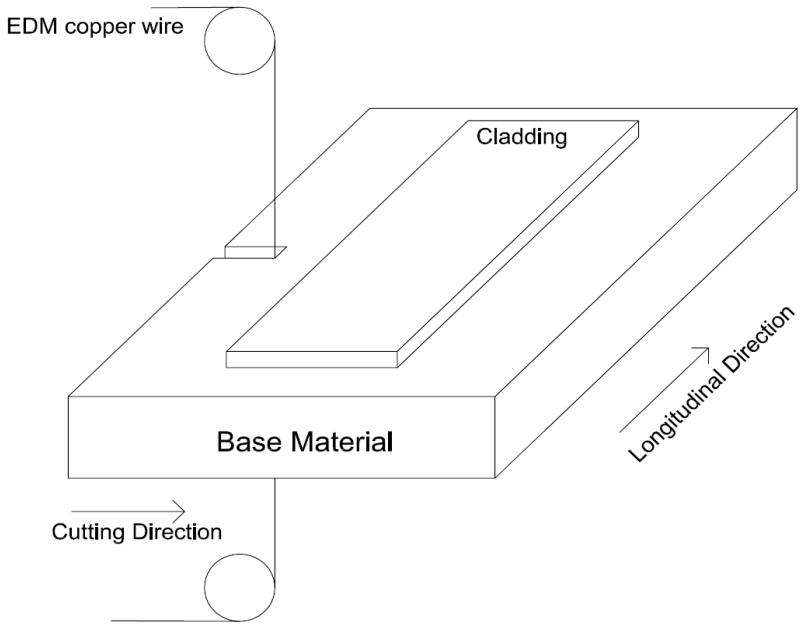

Figure 5.2 EDM cutting direction.

Once a sample had been cut, the displacements that were produced on both halves due to the relaxation of stresses were measured with the help of a Laser scanner (NanoFocus AG model D-46047 Oberhausen), where the measurements were made with a resolution of 30 μm. Figure 5.3 shows the laser scanner that was used in the measurements. The data obtained after laser scanning were processed using Matlab scripts and, with the help of a finite element package, the stresses related to the displacements produced after the cutting can be obtained. In this case, ABAQUS was used in order to calculate the stresses developed.

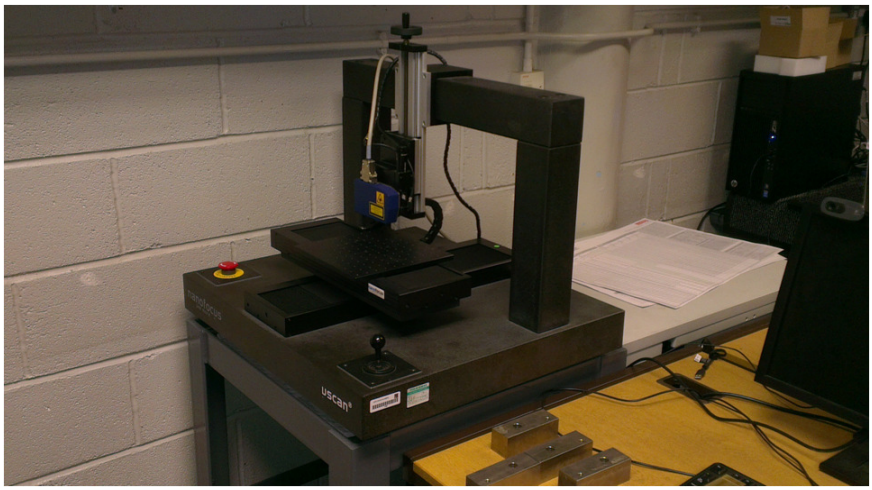

Figure 5.3 NanoFocus laser scanner used to measure the surface displacements for the contour method measurements.

5.2.2.2 Shallow hole drilling technique

The residual stresses generated using the centre-point conditions were assessed with the shallow hole drilling technique, for the samples that comprised a single layer and two deposited layers, respectively. Two such centre point samples were manufactured using an S275 steel substrate, while another two were manufactured using AISI grade 316L stainless steel as the base material. Furthermore, in order to assess the effects of process parameters such as laser power on the generation of residual stresses, the high-laser-power sample (see Table 3.3) was also assessed with each base material. A total of 6 samples were measured. The sample surfaces were also gently ground and manually polished. The shallow hole drilling technique is a standardised test, so these measurements were carried out by an external company according to instructions that were provided by the author.

The gauge position for these measurements was offset longitudinally by 10 mm from the mid-length position of the cladding. It was considered that, in the event of a gauge or drill failure, a replacement gauge could be installed and drilled without significant interference from the previously drilled hole. Furthermore, quasi-stationary conditions were considered to be developed in this region due to stabilised dilution. Figure 5.4 shows the way in which the gauge was installed on one of the laser cladding samples. The gauge type selected for the assessment of residual stresses was a Vishay Precision Group type EA-06-125RE-120 gauge which provided residual stress data to a depth of 2.05 mm.

Orbital drilling was carried out starting with four depth increments 64 μm, followed by four depth increments of 128 μm, followed by eight depth increments of 256 μm, which resulted in a final hole depth of 2.82 mm and provided residual stress data to a depth of 2.05 mm. Some stress uncertainties can be produced due to material properties, the drilling process, strain gauge and strain indicator. Therefore, it has been established a range stress uncertainties in the longitudinal and traverse stresses in depth such as:

- Depth 224 μm; ±84 MPa
- Depth 1024 μm; ±31 MPa
- Depth 2048 μm; ±51 MPa

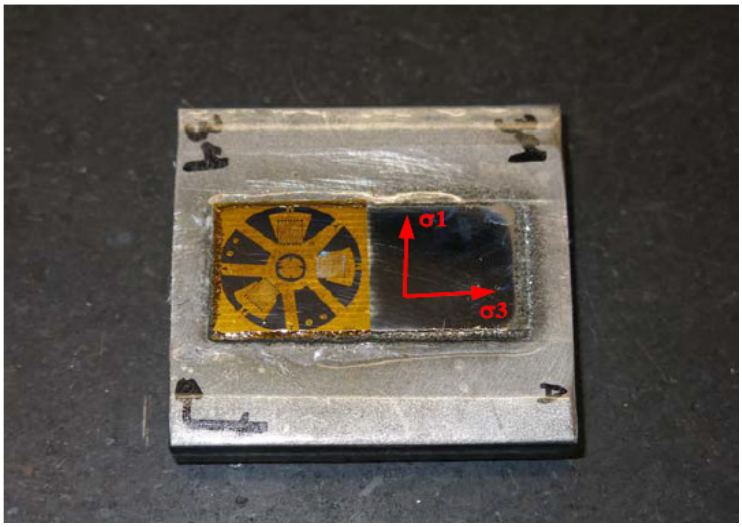

Figure 5.4 A strain gauge rosette installed for residual stress measurements using the shallow hole drilling method. The longitudinal or cladding direction is denoted by σ_3 and the transverse direction is denoted by σ_1

5.3 Results

5.3.1 Contour method

Some uncertainties in the results assessed with the contour method can arise near to the cut edges because of changes in the cut width [126]. It has been suggested that data obtained from near to the cut edges, i.e. within approximately 0.2 up to 2 mm of the edge, should not be considered. On this basis, the results obtained at locations within 1 mm in the top of the cutting have been omitted. It has been decided, however, to show the complete surface in all the samples assessed with the contour method.

As was mentioned in Chapter 3, the original dimensions of the base material coupons were 50 × 50 × 10 mm. However, in order to reduce any contamination and to provide a flat surface for the deposition of the overlays, the base material coupons were milled on one surface, resulting in a final thickness of 9.5 mm. Furthermore, prior to the deposition, the flat surface was sand blasted. These manufacturing operations will have influenced the residual stresses within the base material. Considering the importance of the initial stress state in the assessment of residual stresses, the S275 mild steel and the grade 316L base material coupons were assessed with the contour method, prior to the deposition of any cladding.

Figure 5.5 shows the stresses that were measured in the S275 mild steel substrate. It can be observed that tensile stresses are located near to the top surface and these gradually turn to compressive stresses towards the bottom of the coupon, producing a balanced stress distribution overall.

For comparison, the initial residual stress state of the AISI grade 316L stainless steel coupons is shown in Figure 5.6. It can be observed that tensile stresses are developed near to the top surface and this turn compressive with increasing depth. Compressive stresses are found at the bottom of the coupon; these can be attributed to the cold rolling process.

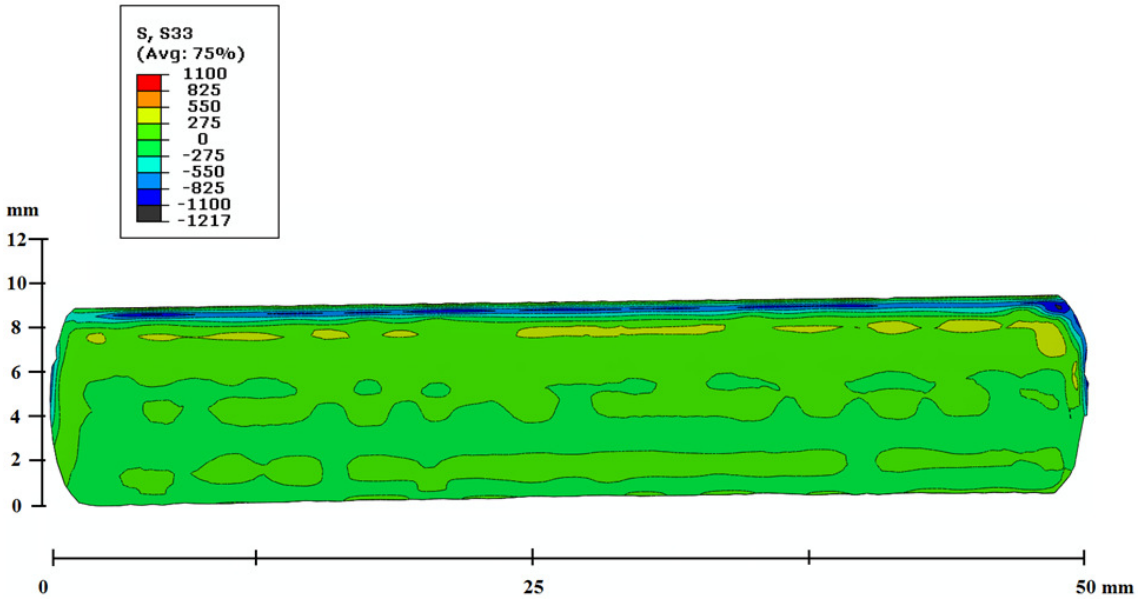

Figure 5.5 Residual stress distributions measured using the contour method in an S275 steel base material coupon. Tensile stresses are observed near to the top surface and these are balanced by compressive stresses towards the bottom of the coupon. Stresses are in MPa.

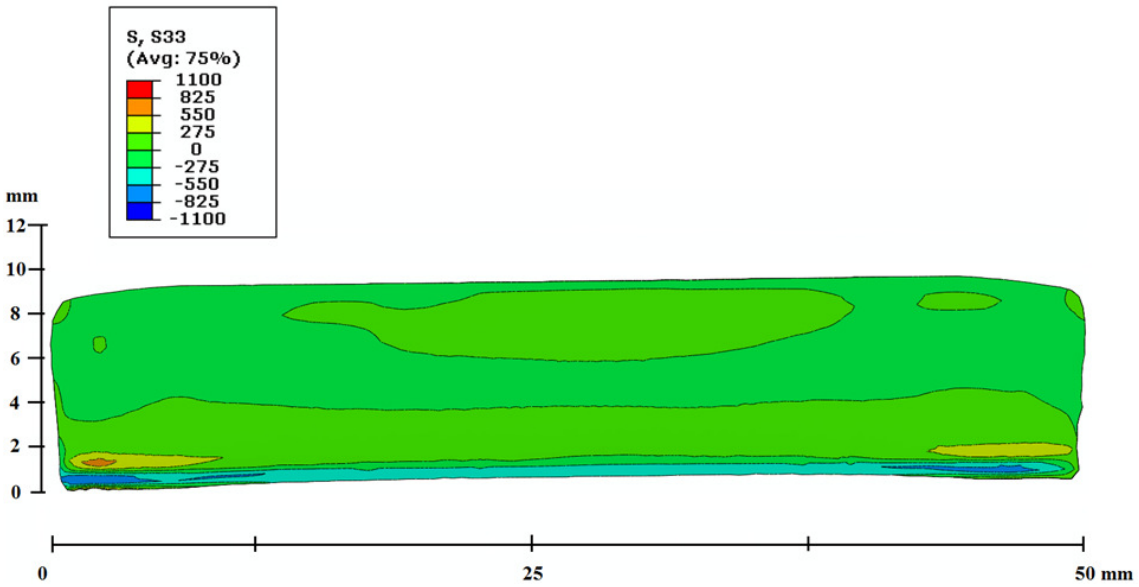

Figure 5.6 Residual stresses measured in AISI grade 316L stainless steel base material using the contour method. Contours show tensile stresses toward the top surface of the coupon and these are balanced by compressive and tensile stresses near to the bottom of the coupon. Stresses are in MPa.

The longitudinal stresses developed in the centre-point sample, with two layers of cladding deposited on the S275 steel base material are shown in Figure 5.7. The cladding thickness was approximately 1.60 mm. The deposition started on the left side. Discarding the residual stresses near to the edges along the top surface in a depth of approximately 1 mm, it can be observed that tensile stresses were generated increasing in magnitude in an area that can be considered close to the HAZ. The residual stresses in the remaining surface did not suffer considerably changes in comparison with the residual stresses developed in the S275 base material (see Figure 5.5).

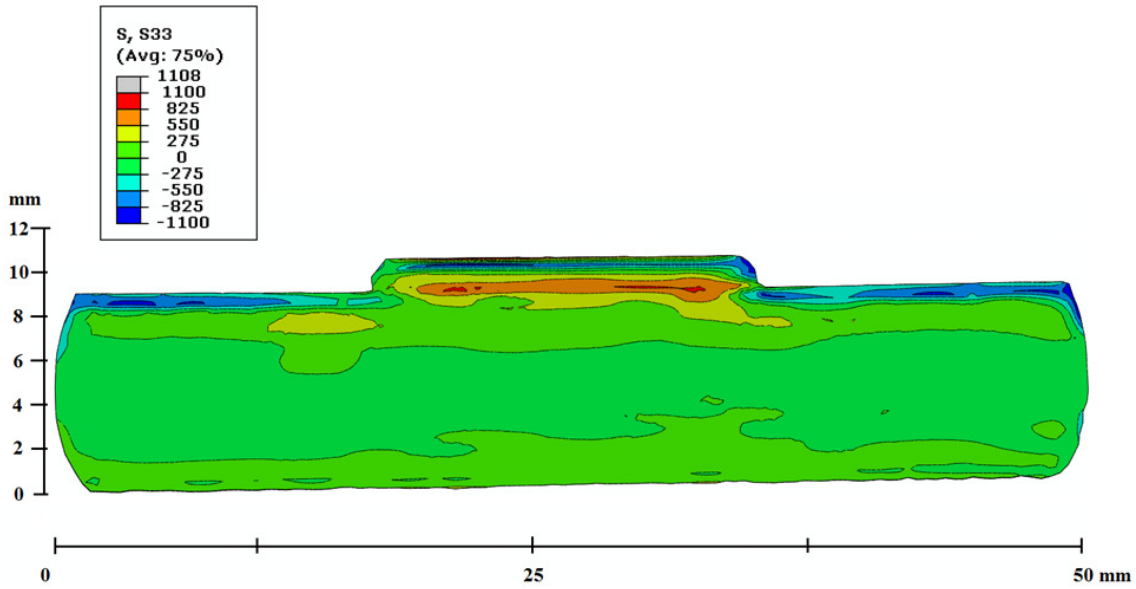

Figure 5.7 Residual stresses measured with the contour method for an S275 steel coupon that has been coated with two layers of cladding. Tensile stresses were developed in the cladding area, showing high magnitudes in an area that can be considered to be close to the HAZ. Stresses are in MPa.

The stresses corresponding to the same (centre-point) deposition conditions, but using an AISI grade 316L stainless steel base material coupon, are presented in Figure 5.8. The cladding thickness was approximately 1.7 mm. The deposition sequence was from left to right. Considering the same criteria used in the sample with S275 steel as the base material, it can be observed that tensile stresses were generated increasing in magnitude in an area that can be considered to be close to the HAZ. No considerable changes were observed in the remaining surface of the sample in comparison with the residual stresses generated in the grade 316L stainless steel base material (see Figure 5.6).

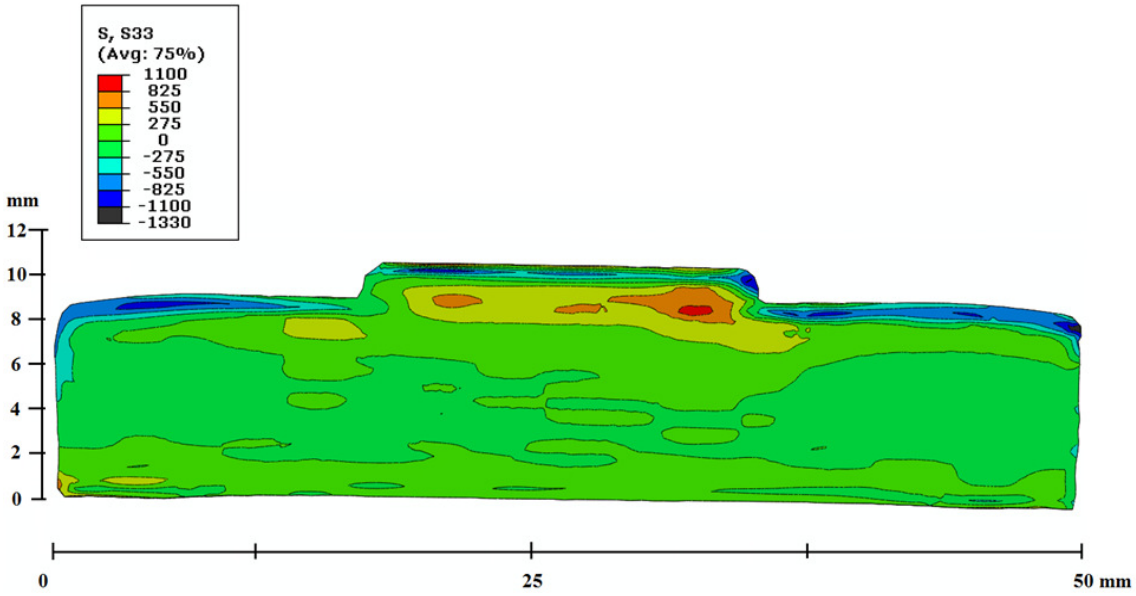

Figure 5.8 Residual stresses measured using the contour method for the AISI 316L stainless steel coupon that was coated with two layers of cladding using the centres point conditions. Tensile stresses were developed in the cladding area, showing high magnitudes in an area that can be considered to be close to the HAZ. Stresses are in MPa.

As it was expected, tensile stresses were generated in the longitudinal direction in the vicinity of the deposited overlay, when using the centre-point conditions. This can be attributed to the constrained expansion and shrinkage of the molten material during the solidification process. Furthermore, compressive residual stresses were generated in the substrate material, which balance the tensile residual stresses in the overlay region. Comparing the residual stresses generated with different base materials, it can be seen that higher tensile stresses were developed in the sample for which mild steel was used as the base material. The higher tensile stresses in the sample with an S275 mild steel coupon can be attributed to the fact that high thermal stresses will have developed owing to the differences in the thermal expansion coefficients for the cladding and the base materials.

5.3.2 Shallow hole drilling technique

The residual stresses generated in the centre-point samples, for both one and two layers of cladding, together with the high-laser-power condition (Table 3.3) were assessed with the shallow hole drilling technique. Measurements were made on the samples with an S275 steel substrate as well as on the samples with AISI grade 316L stainless steel

substrates. As mentioned previously, these measurements were carried out by an external company.

5.3.2.1 Residual stresses developed using S275 steel as the base material

The residual stresses developed in the centre-point sample, for both one and two clad deposits, and in the high laser power sample, using S275 steel as the substrate, are shown in the longitudinal and transverse directions in Figure 5.9 and Figure 5.10 respectively. Tensile stresses were developed in the longitudinal and transversal directions due to thermal expansion and contraction of the molten material that occurred during the solidification-cooling cycle. In all the samples, the first measurement was recorded at a depth of 32 μm beneath the ground surface. From Figure 5.9 and Figure 5.10, the following observations can be addressed:

- The cladding thickness of the centre-point sample with one-layer deposit was approximately 650 μm. A longitudinal stress of 224 MPa was developed at a depth of 570 μm while a transverse stress of 282 MPa was developed at the same depth.
- The cladding thickness of the centre-point sample with two-layer deposits was approximately 1.5 mm. The interface between the second layer and the first layer was approximately at a depth of 1000 μm. Higher tensile stresses in the longitudinal and transverse directions were developed in the second layer rather than the one-layer deposit sample. This may be attributed to the generation of martensite, during the deposition of the first layer (see Figure 4.7). This means that, it would be expected to obtain higher values of hardness in the first clad layer deposit. Assessing the hardness developed in the centre-point sample with two layers of cladding (Figure 5.11), it can be observed that hardness approximately of 200HV0.3 was developed in the first layer, and 180HV0.3 in the second layer. This may validate the assumption that martensite was generated. It has been reported in Ref. [184], that the generation of austenite and martensite tend to decrease the tensile residual stresses, since the thermal contraction is affected by the strains associated with the martensite transformation. Therefore, it was expected to find lower residual stresses in the first layer. On the contrary, austenite and a small quantity of δ-ferrite may have been formed in the second layer at relatively high temperatures, and their formation would not have the same effect reducing the generation of tensile stresses.

- The cladding thickness of the high-laser-power sample was approximately 800 µm. A longitudinal stress of 200 MPa was developed at a depth of 220 µm while a transverse stress of 432 MPa was developed at the same depth. Residual stresses were higher than centre-point sample with one-layer deposit due to high power density was used. Interestingly, residual stresses tended to decrease until a depth of 800 µm. This depth can be considered close to the interface zone. This can be related to the generation of martensite near to the interface zone (Figure 4.5).

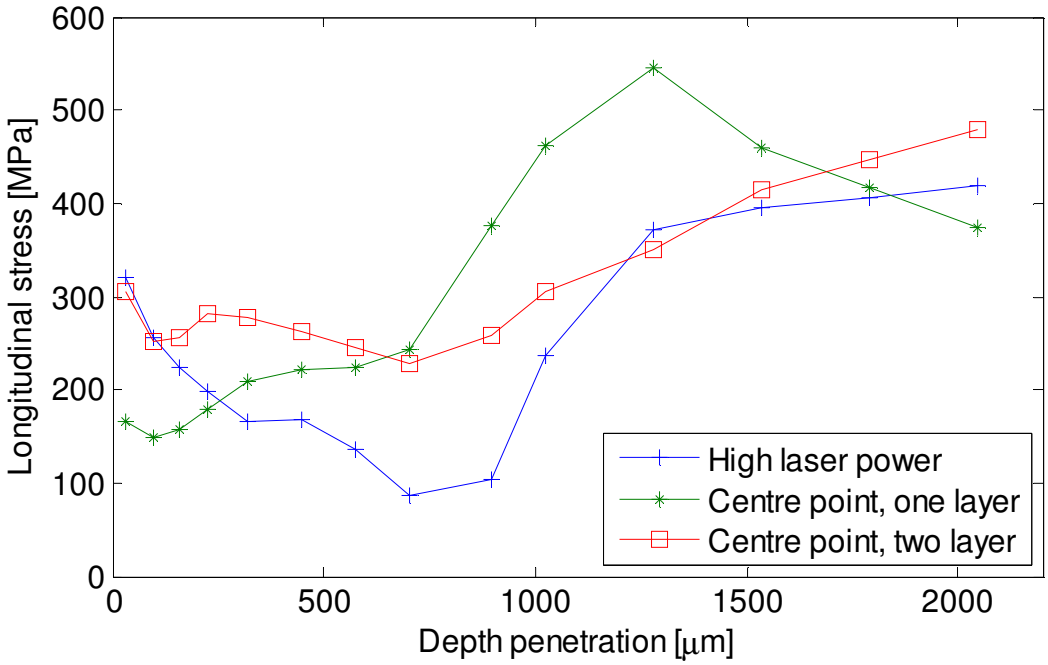

Figure 5.9 Longitudinal stresses measured with shallow hole drilling in the high laser power sample, and centre point samples with one and two layer deposits, with S275 steel base material.

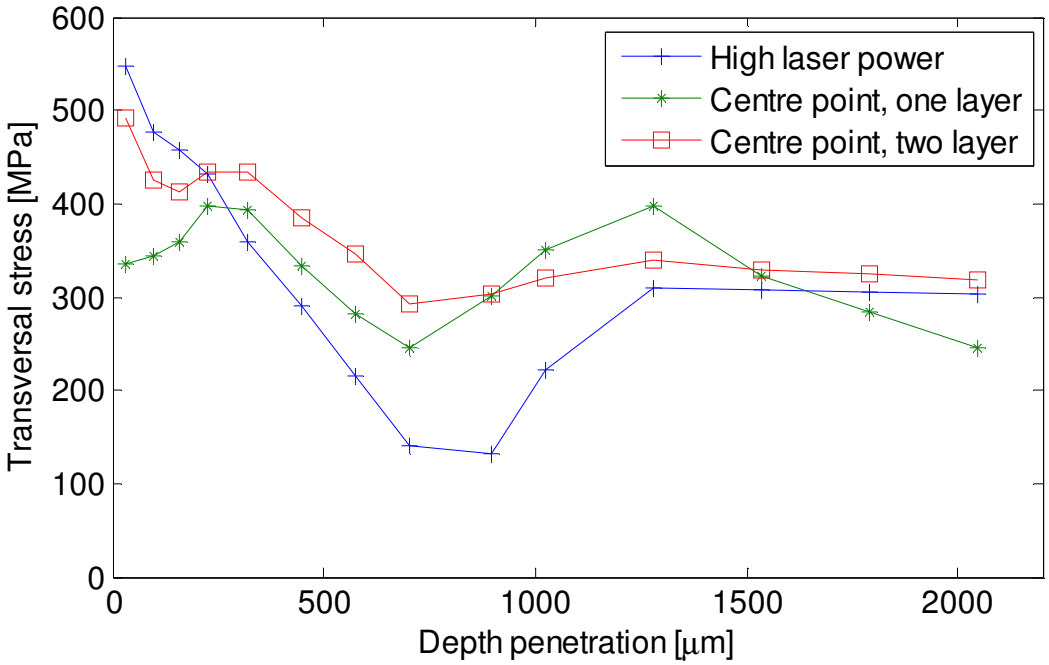

Figure 5.10 Transverse stresses measured with shallow hole drilling in the high laser power sample, and centre point samples with one and two layer deposits, with S275 steel base material.

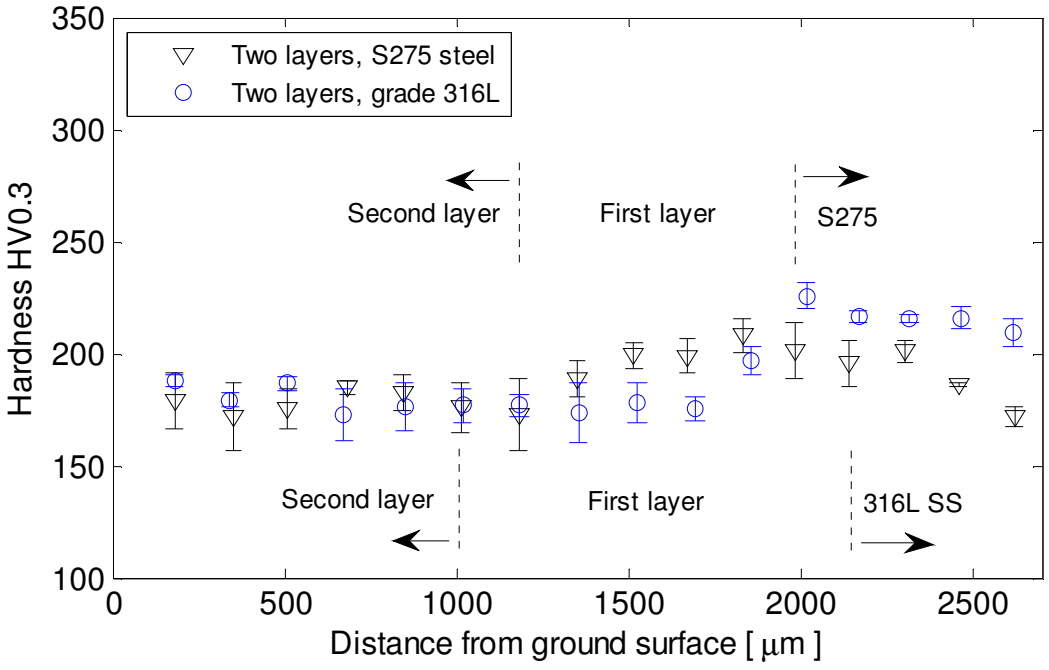

Figure 5.11Hardness measured from the ground surface in the centre-point sample with two-layer overlays for the S275 mild steel and the grade 316L stainless steel substrates. Transition from the second layer to the first layer is highlighted on the plot. The plotted values correspond to an average of three measurements. High values of hardness are developed in the first-layer deposit for the S275 mild steel substrate.

Higher transversal residual stresses were developed in all of the assessed samples. The same behaviour was also observed in Ref. [13].This can be attributed to the way residual stresses evolve during the deposition of several beads. Tensile stresses would be expected during the deposition of a single pass in both longitudinal and transverse directions, with highest magnitude in the longitudinal stresses. However, as subsequent overlapping beads are deposited, the thermal contraction that occurs in the longitudinal direction in the vicinity of the most recent clad pass will act to introduce longitudinal compression at different locations such as previous deposited beads and the substrate. Even though, clad passes might sustain highly tensile longitudinal residual stresses immediately after they are deposited, the deposition of later passes may act to reduce the tensile nature of the longitudinal residual stresses in large parts of the overlay. In contrast, the development of transverse stresses in the last pass to be deposited does not act to reduce the transverse stresses in earlier passes in the same way, so large transverse stresses can be realised in a multi-pass overlay.

It can be seen that tensile residual stresses were generated in laser cladding after solidification in both, longitudinal and transverse directions. Furthermore, the stresses fluctuated because they were subjected to minor changes of the process parameters or cladding configuration such as the deposition of two or more overlays. This can be attributed to natural fluctuation of processing, or minor changes by the operator. This should be considered in the application of laser cladding, owing to any change in the variables that define the process can develop different residual stresses state. That could affect the performance of the clad layers having a detrimental effect, for instance, in the corrosion resistance.

5.3.2.2 Residual stresses developed using AISI grade 316L stainless steel as the base material

Longitudinal and transverse stresses developed in the high-laser-power sample, and using the centre point conditions both with one and two deposited layers, and using AISI 316L stainless steel as the base material are shown in Figure 5.12 and Figure 5.13 respectively. The cladding thickness for the high-laser-power sample was approximately

740 µm, whereas it was 650 µm in the one layer deposition and 1.5 mm for the two layer deposition sample.

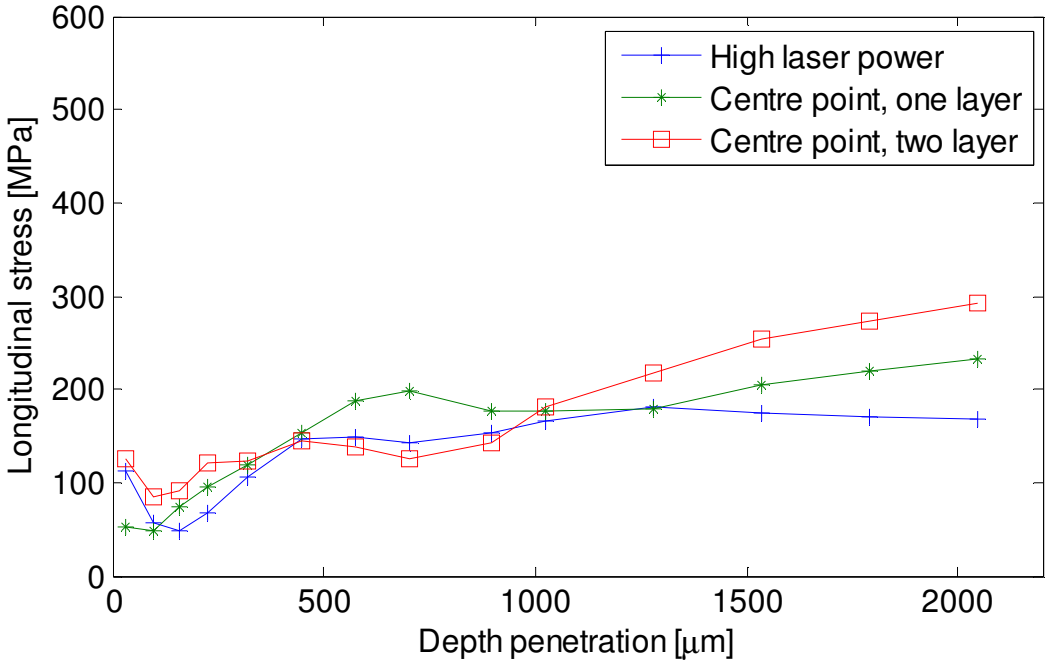

Figure 5.12 Longitudinal stresses measured with shallow hole drilling in the high laser power sample, and centre point samples with one and two layer deposits, with AISI 316L stainless steel base material.

Tensile residual stresses were developed in both directions, with higher stresses in the transverse direction. The residual stresses in each sample were similar. However, the magnitude of the residual stresses was lower than the stresses developed using S275 mild steel as the base material. This can be attributed to the fact that the same material was used as the powder and the base material. That is to say, the potential effect of any differences in the coefficient of thermal expansion on the generation of thermal stresses has been eliminated. Furthermore, unexpected phases are not present owing to the same material being used for cladding.

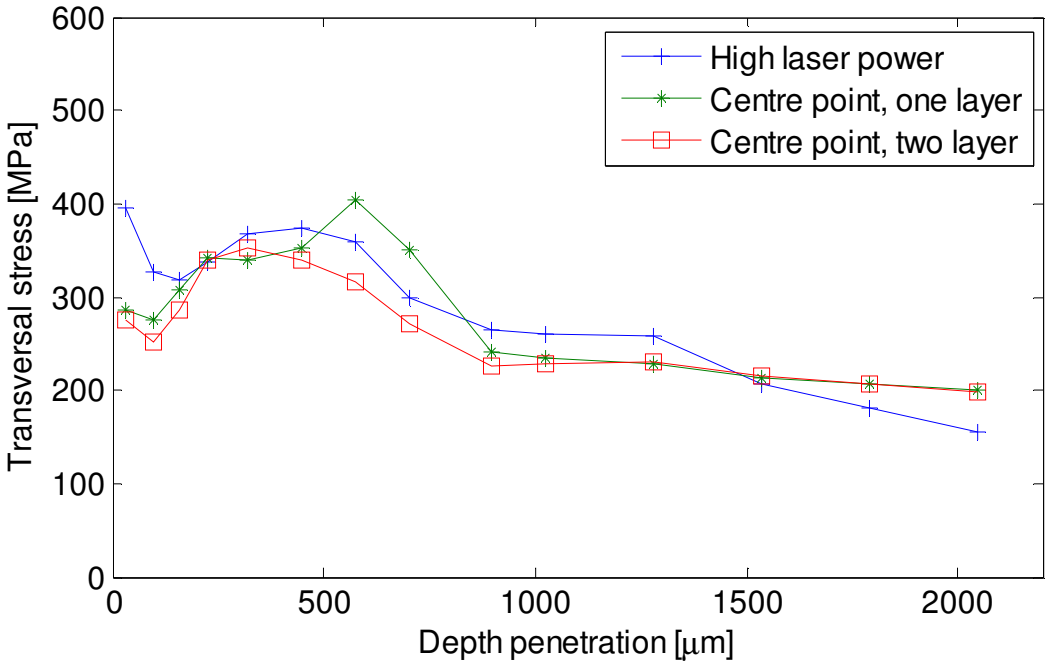

Figure 5.13 Transverse stresses measured with shallow hole drilling in the high laser power sample, and centre point samples with one and two layer deposits, with AISI 316L stainless steel base material.

5.3.3 Comparison between shallow hole drilling and contour method results

Comparing the results obtained from the contour method and the shallow hole drilling technique for the longitudinal stresses, using both S275 steel and AISI grade 316L stainless steel substrates, these showed acceptable results. Figure 5.14 shows the residual stresses assessed with the contour method and the shallow hole drilling technique for the two-layer deposit using grade 316L stainless steel as the base material. The contour method values correspond to the stresses measured from the ground surface towards the base material at three different positions (black lines on the traverse section in Figure 5.14).

The stresses close to the edges of the ground surface (from 0 to 1000 µm), measured with the contour method, were discarded due to high uncertainties with the data. Higher tensile residual stresses, in the order of 550 MPa, were measured with the contour method between 1000 to 2000 µm depths. On the contrary, stresses in the order of 250 MPa, were assessed with the shallow hole drilling at the same depths. Even though, higher residual stresses were measured with the contour method, these tend to be similar

than the shallow hole drilling after 2 mm depth. In this study, however, the contour method enabled the identification of general trends, with less accuracy at the surface. This was in agreement with the shallow hole drilling results. In general, the contour method is more reliable at greater depths.

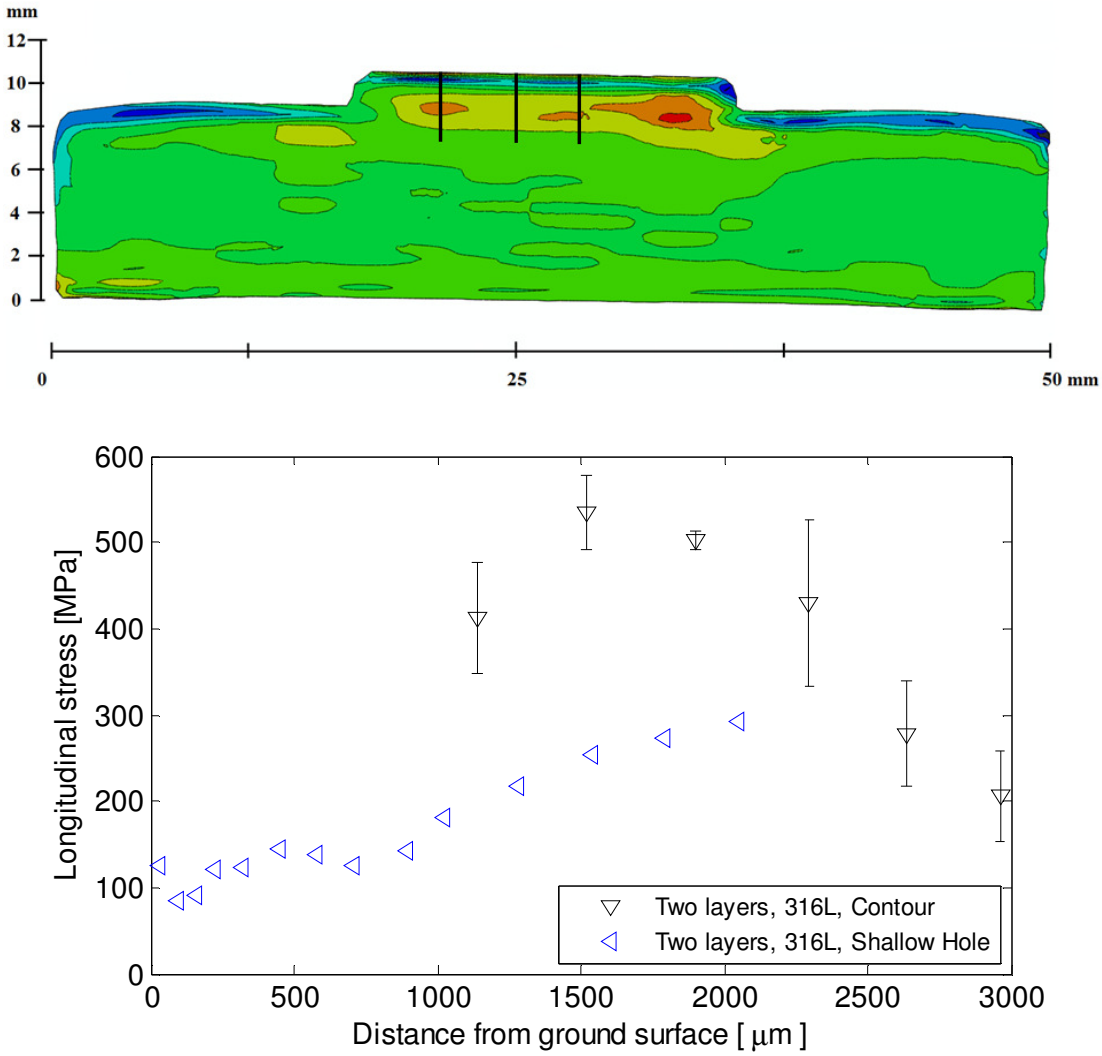

Figure 5.14 Comparison between the residual stresses assessed with the contour method and the shallow hole drilling for the two-layer deposit using grade 316L stainless steel as the base material. The contour method plotted points correspond to an average of three measurements. Higher tensile stresses were assessed with the contour method between 1000 and 2000 µm depths.

5.4 Discussion

Residual stresses are an important aspect to consider in the manufacturing process because they can have either a detrimental or beneficial effect on the performance of metals. In laser cladding, the residual stresses are mainly generated by thermal stresses where constrained expansion and shrinkage of the molten material take place. The magnitude and nature of the residual stresses is defined by some aspects such as temperature gradients, changes in phase, and differences in the coefficients of thermal expansion for the base material and the cladding material. Although different techniques and methods have been developed in order to assess the residual stresses, each technique has its limitations, and the nature of the specimens to be measured can place limitations on the techniques that are available. This fact emphasises the complexity associated with the determination of the residual stresses.

Tensile residual stresses were developed in the laser cladding samples assessed in this study because during and after the solidification process, the molten material begins to shrink but it is constrained from doing so by the surrounding material. These results agree broadly with other studies that have been carried out on the development of residual stresses in laser cladding. In the case where S275 mild steel was used as the substrate material, the thermal expansion coefficient of the substrate (~ 12×10^{-6} °C^{-1})[186] was lower than the corresponding value for the overlay (~ 20×10^{-6} °C^{-1})[99]. This would lead to the overlay undergoing thermal contraction to a greater extent on cooling after welding and, as such, it would lead to higher tensile residual stresses in the overlay. This is indeed what was observed.

The development of different phases in the microstructure tends to affect the magnitude of the residual stresses, especially when two or more layers are deposited. In this study, the generation of martensite in the centre point sample with a two-layer deposit slightly reduced the residual stresses in the first-layer since the strains associated with the formation of the martensite phase can, to some degree, offset the thermal contraction that occurs on cooling after cladding.

Higher stresses were present in the transverse direction. It is difficult to identify the factors that produced higher transverse stresses than longitudinal stresses, but some thought is given to this observation here. The thermal contraction that occurs in the

longitudinal direction in the deposition of a clad bead, may introduce longitudinal compression at different locations, such as previous deposited clad beads and the substrate. This means, the deposition of consecutive clad beads could reduce the tensile residual stresses in large parts of the cladding. From the measurements that have been presented in this work, it would appear that the deposition of overlapping weld passes does not act to reduce the transverse stresses in earlier passes in the same way.

The magnitude of the stresses obtained by the contour method and the shallow hole drilling technique indicates that the yield stress was reached in all of the samples. This is expected for processes such as welding and laser cladding, where plastic stains are developed owing to the steep temperature gradients. This means that some uncertainties in the results for the shallow hole drilling technique and the contour method will arise because the calculation of the stresses is obtained considering only the elastic relaxation of stress. However, Nobre *et al*.[187] has showed that, reliable results can still be obtained with the shallow hole drilling technique even if the material yield strength has been exceed.

Chapter 6

Residual stress mitigation

6.1 Introduction

The performance of metals is considerably affected by the residual stresses developed after manufacturing processes such as arc welding or laser cladding. These residual stresses are normally tensile, which can have a detrimental effect on the fatigue performance, wear resistance, and in some cases on the corrosion resistance when metals are exposed to corrosive environments. Therefore, some post-manufacturing processes have been developed over the years in order to diminish the effect of tensile residual stresses.

Laser shock peening (LSP) is a novel process that has been used in order to mitigate tensile residual stresses, generally by introducing compressive stresses. The effects of introducing compressive stresses can improve the performance of metals, as was discussed in Section 2.7. This means, LSP could be applied to laser clad surfaces in order to enhance the performance of clad materials. Some researchers [163-166] have investigated the effects of LSP on laser clad surfaces, reporting the mitigation of tensile residual stresses and the generation of compressive stresses at the clad surfaces, and the enhancement of fatigue life. Furthermore, increases in the material hardness were also reported. However, good results have just been reported for treating small clad areas with a single or multiple shots and there is no evidence of the benefits of LSP treating large clad areas. Therefore, in this work a large clad area have been laser shock peened and examined. Furthermore, stress corrosion cracking tests were performed in order to assess the effects of laser shock peening in the corrosion resistance of the clad layers. This is discussed in Chapter 7.

Post weld heat treatment (PWHT) has been implemented in order to relieve the residual stresses generated after welding processes. However, owing to the fact that this generally involves exposing metals to high temperatures, special consideration should

be given to the maximum temperature to be used, the exposure time and the cooling rate in order to satisfy the stress relieve. Some studies have been carried out in order to assess the effects of PWHT on materials that have been laser clad, as was mentioned in Section 2.11 [140-142].

Given that tensile residual stresses were developed in the laser cladding samples in the current work, this chapter describes the effects of laser shock peening and post weld heat treatment on the samples manufactured with the centre-point conditions. The methodology followed during the PWHT is explained in detail below. The residual stresses have been assessed using the contour method and the shallow hole drilling technique. As with previous measurements, the shallow hole drilling technique was performed by an external company. In addition, the Vickers hardness and the microstructure developed after LSP have also been assessed.

6.2 Experimental procedure

6.2.1 Sample preparation

In order to assess the effects of applying laser shock peening and post weld heat treatment to laser clad coupons, centre-point samples (Table 3.3) with one layer and two layers of cladding, using both S275 steel and AISI grade 316L stainless steel substrates were prepared. The same conditions and surface preparation procedures as those used in the assessment of residual stresses (Chapter 5) were applied in these experiments.

6.2.2 Sample analysis

6.2.2.1 Laser shock peening

The laser shock peening process was performed by Metal Improvement Company. The samples were treated using confined ablation in order to avoid any considerable damage to the sample surfaces. A power density of 10 $GW.cm^{-2}$, and a pulse length of 18 nanoseconds were used. As explained in Section 2.7, the values for these parameters

will govern the generation of compressive stresses on the treated surfaces. An area of 36 × 15 mm^2 was laser peened; this means that an area close to the cladding edges in both the longitudinal and transverse directions remained unpeened. The residual stresses generated after LSP were assessed using the contour method and the shallow hole drilling technique. The procedures have been explained in detail in Chapter 5.

The microstructures generated after laser shock peening were examined on a transverse section of the cladding following standard metallographic procedures. The samples were electrolytically etched in 10% oxalic acid for a period of 2 minutes with a voltage of 7 V and then rinsed with alcohol and water. Finally, the microstructure was examined using a Keyence VHX-500P optical microscope.

The hardness of the samples was measured using a Buehler Micromet Vickers Hardness Tester following the Standard Test Method for Vickers Hardness of Metallic Materials (ASTM E 92-82). The first indentation was taken at a distance from the edge of the ground surface equal to three times the length of the diagonal of the indentation. In similar way, the hardness was measured in three different positions in the clad layer, corresponding to the positions of the 6^{th}, 10^{th} and 15^{th} cladding tracks to be deposited. These tracks represent an area where the dilution stabilised and it can be considered that quasi-stationary conditions were developed

6.2.2.2 Post weld heat treatment

The post weld heat treatment was carried out in a furnace (model Carbolite CWF 1300). An inert gas, argon, was supplied to the furnace chamber in order to reduce the levels of oxygen contained in the sample environment and to avoid oxidation of the samples surfaces at high temperatures. Since S275 steel and AISI grade 316L stainless steel were used as the base materials for the laser cladding samples, two different soak temperatures were proposed for the post weld heat treatments.

For the S275 steel coupons, the heat treatment temperature was set at 650°C and this temperature was maintained for 30 minutes in order for the temperature to stabilise through the sample thickness, and finally the coupons were slowly cooled in air. The

same procedure was applied to the AISI grade 316L stainless steel coupons, but with a soak temperature of 900°C.

The soak temperatures were selected in order to avoid a phase transformation (S275 steel) or sensitization (316L stainless steel) of the material. In the case of the S275 steel, a phase transformation to austenite would expected to commence at temperatures above 700°C, whereas stainless steels can sensitise due to carbide precipitation if held at temperatures in the range between 425 and 870 °C for long periods of time [99]. This is illustrated in Figure 6.1. It can be seen that sensitization starts to manifest when stainless steels with a carbon concentration of 0.03 wt. % (AISI 316L) are exposed for 9 hours to temperatures in the range between approximately 425 and 680°C.

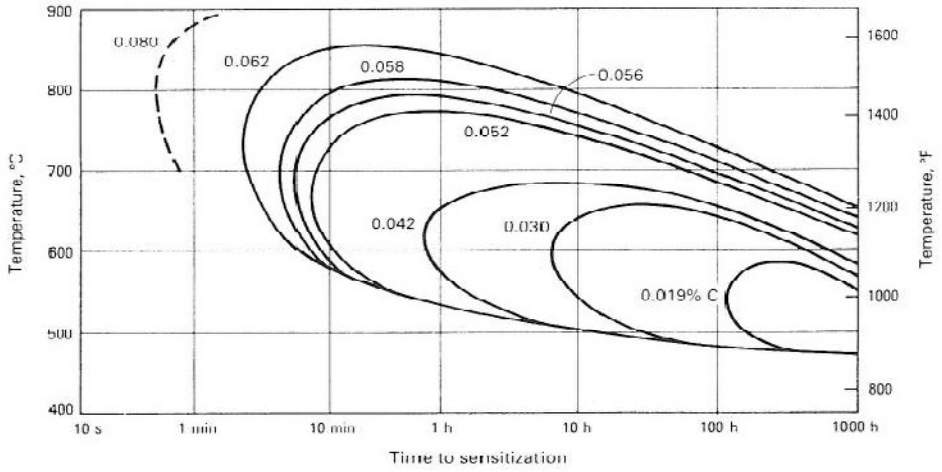

Figure 6.1 Time-temperature-sensitization curves showing the times and temperatures required to develop carbide precipitation in steels with various carbon contents. Sensitization starts to manifest on the right hand side of the curves. [99]

The control of temperature in the post weld heat treatment operation is crucial, therefore the temperature was monitored by type K thermocouples attached near to the clad surface, and the readings were compared with those from a digital thermometer attached to the furnace. The thermocouple arrangement is showed in Figure 6.2.

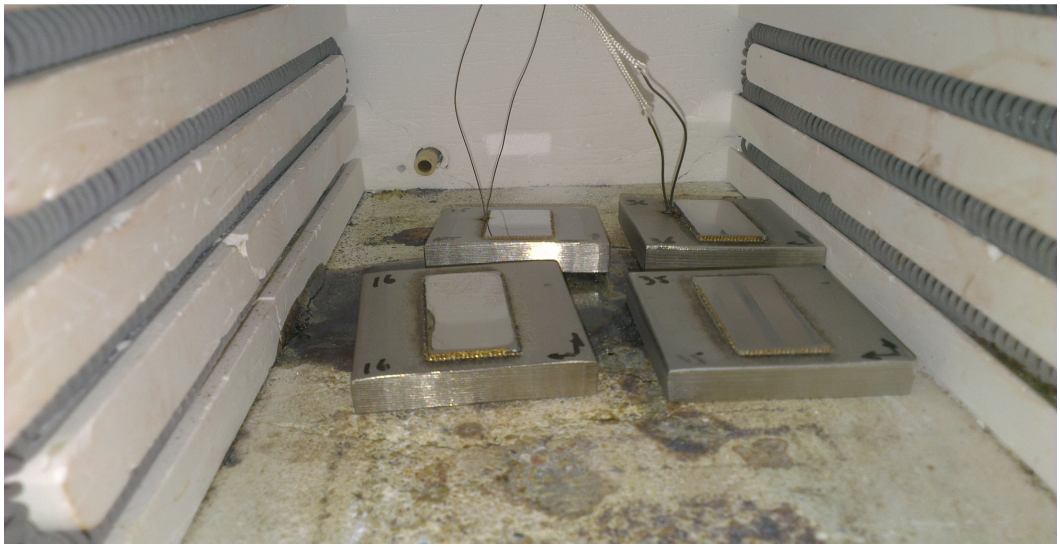

Figure 6.2 Thermocouple arrangement for the post-weld heat treatment of test coupons.

6.3 Results

6.3.1 Laser shock peening

6.3.1.1 Residual stresses

As was mentioned in Chapter 5, the samples were cut transversely in order to assess the longitudinal stresses (refer to Figure 5.2). It has been advised that some uncertainties in the stresses developed near to the cut edges can be generated. Therefore, the results generated in the region close to the ground surface were discarded (approximately 1 mm depth). However, it was decided to show the complete surface in all the samples assessed with the contour method.

The contour method was used to assess the residual stresses developed in the longitudinal direction for the centre-point samples with one layer and two layers of cladding, and using S275 steel as the base material. The results are shown in Figure 6.3 and Figure 6.4 respectively. The thicknesses of the cladding for the one layer and two layer overlays were 700 and 1500 μm respectively.

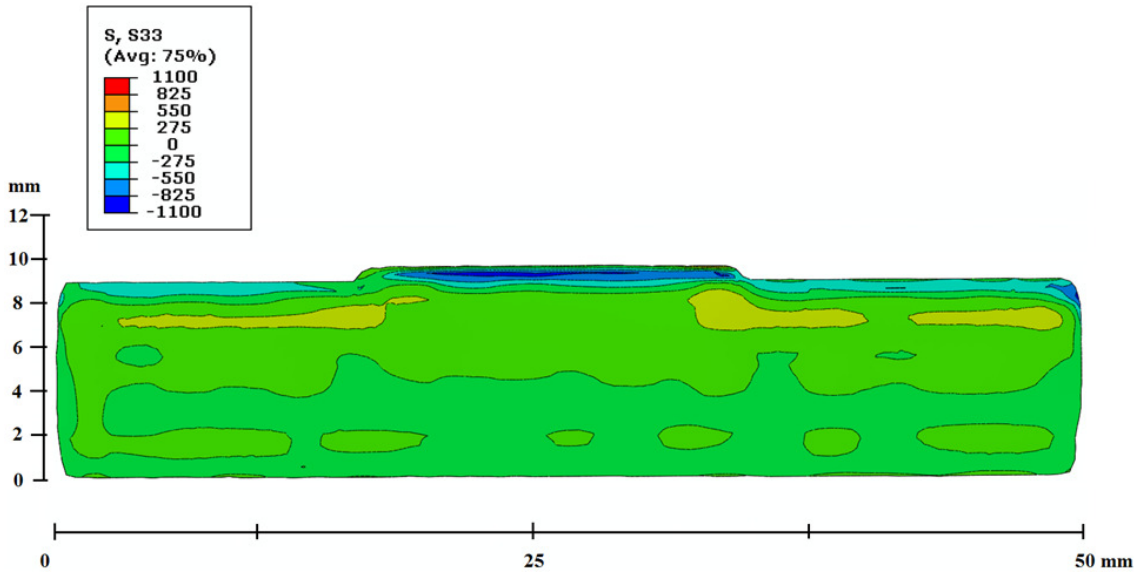

Figure 6.3. Stress map obtained using the contour method for the centre point sample with one layer deposited on to an S275 steel coupon. The transverse section of the cladding is shown at the top of the map and the corresponding base material beneath it. Compressive stresses in the longitudinal direction were developed in the cladding area and these were balanced by tensile stresses in the base material Stresses are in MPa.

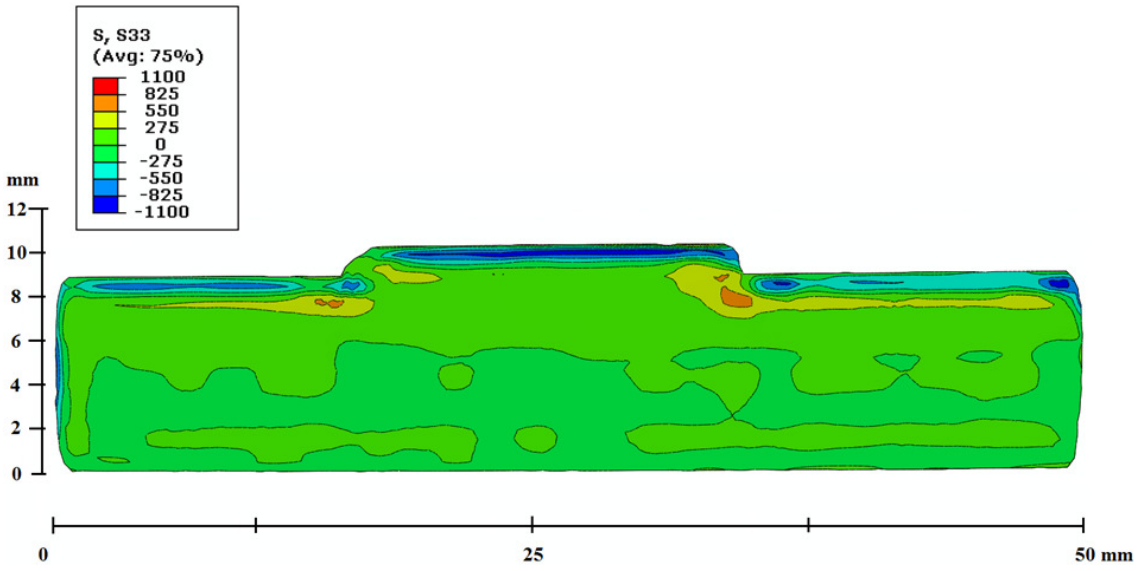

Figure 6.4. Stress map obtained using the contour method for the centre point sample with two layers deposited on to an S275 steel substrate. The transverse section of the cladding is shown at the top and the corresponding base material beneath it. Compressive stresses were developed in the longitudinal direction in the overlay, with tensile stresses toward the bottom of the overly near to the base material. Stresses are in MPa.

It can be observed that compressive stresses were generated in the overlay in both cases by the laser shock peening process, and that tensile stresses were also developed away from the overlay in order to balance the compressive stresses. The conditions for the

LSP were capable of introduce compressive stresses to a depth up to 1000 μm; this means that tensile stresses were found in the cladding region in the two-layer sample. The compressive stresses generated were approximately 300 MPa and 275 MPa for the two layer and one layer deposition samples respectively.

The corresponding residual stresses developed in the longitudinal direction for the samples with one and two layers of cladding when AISI grade 316L stainless steel was used as the base material are shown in Figure 6.5 and Figure 6.6 respectively. The cladding thickness for the one layer sample was approximately 800 μm; whereas it was 1600 μm for the two layers.

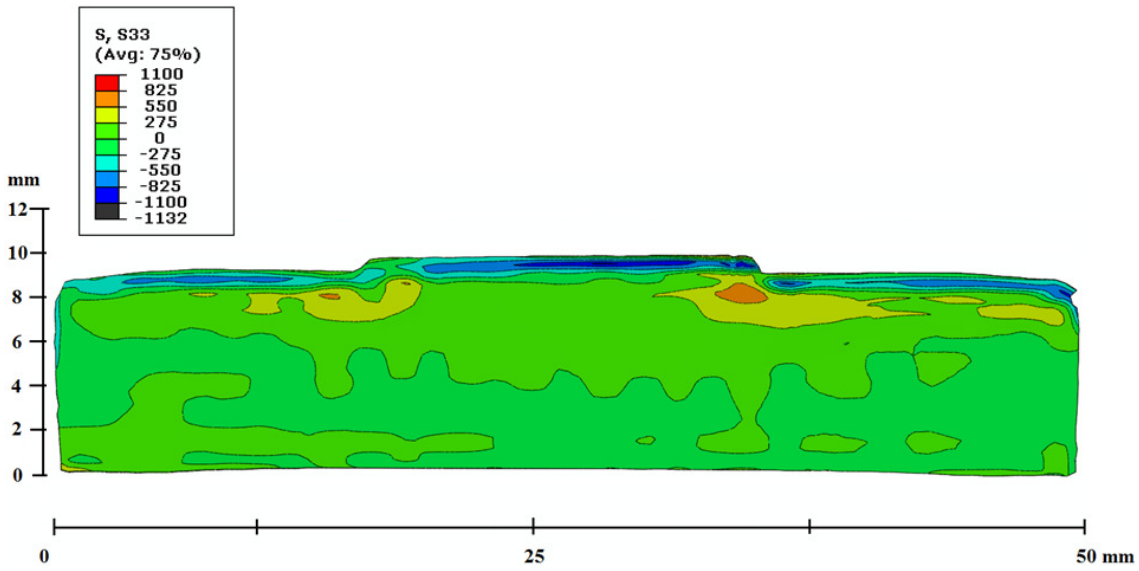

Figure 6.5. Stress map obtained using the contour method for the centre point sample with one layer deposited on to an AISI grade 316L stainless steel substrate. The transverse section of the cladding is shown at the top and the corresponding base material beneath it. Compressive stresses were developed in the longitudinal direction within the overlay to a depth of ~1200 μm, balanced by tensile stresses in the substrate Stresses are in MPa.

It can be seen that compressive stresses were developed through the cladding owing to the effects of laser shock peening. The compressive stress developed in the one layer sample was approximately 300 MPa, while it was 275 MPa in the two layer sample. In the same way, for the two layer sample, a few hundreds of micrometres of the clad layer remained under tensile stress.

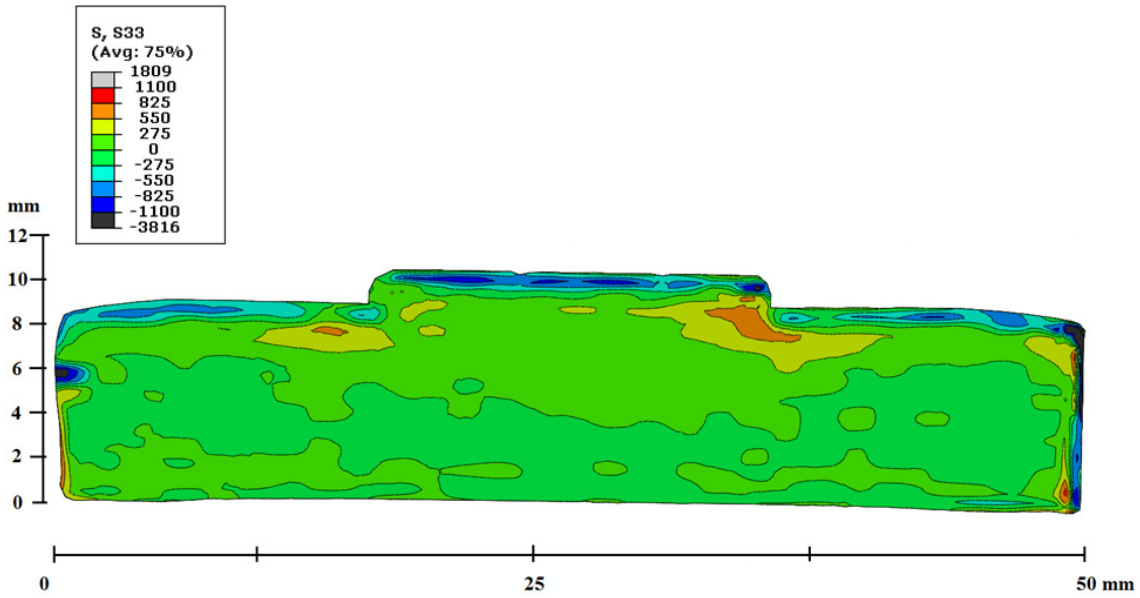

Figure 6.6 Stress map obtained using the contour method for the centre point sample with two layers deposited on to an AISI grade 316L stainless steel substrate. The transverse section of the cladding is shown at the top and the corresponding base material beneath it. Compressive stresses were developed in the longitudinal direction within across the cladding to a depth of ~1200 µm, balanced by tensile stresses at greater depths. Stresses are in MPa.

The contour method is most frequently used in medium and larger parts, for instance with thicknesses of 10 mm or greater. This is partly due to the fact that uncertainties can be generated in small parts, since a greater proportion of the sample is close to the surface, where errors are more likely. Nevertheless, the stress maps obtained in the laser clad samples provide a general idea of the stresses and the way that they are likely to be distributed in the peened samples, in spite of these uncertainties.

The stresses developed in the centre-point samples with one and two layer deposit were also assessed with the shallow hole drilling technique. As mentioned in Chapter 5, some stress uncertainties can be produced due to material properties, the drilling process, strain gauge and strain indicator. Therefore, it has been established a range stress uncertainties in the longitudinal and traverse stresses in depth such as:

- Depth 224 µm; ±84 MPa
- Depth 1024 µm; ±31 MPa
- Depth 2048 µm; ±51 MPa

The longitudinal and transversal stresses generated in the samples with S275 steel as the base material are shown in Figure 6.7 and Figure 6.8 respectively. The cladding thickness for the one layer sample was approximately 700 µm, while it was 1500 µm for the two layer sample.

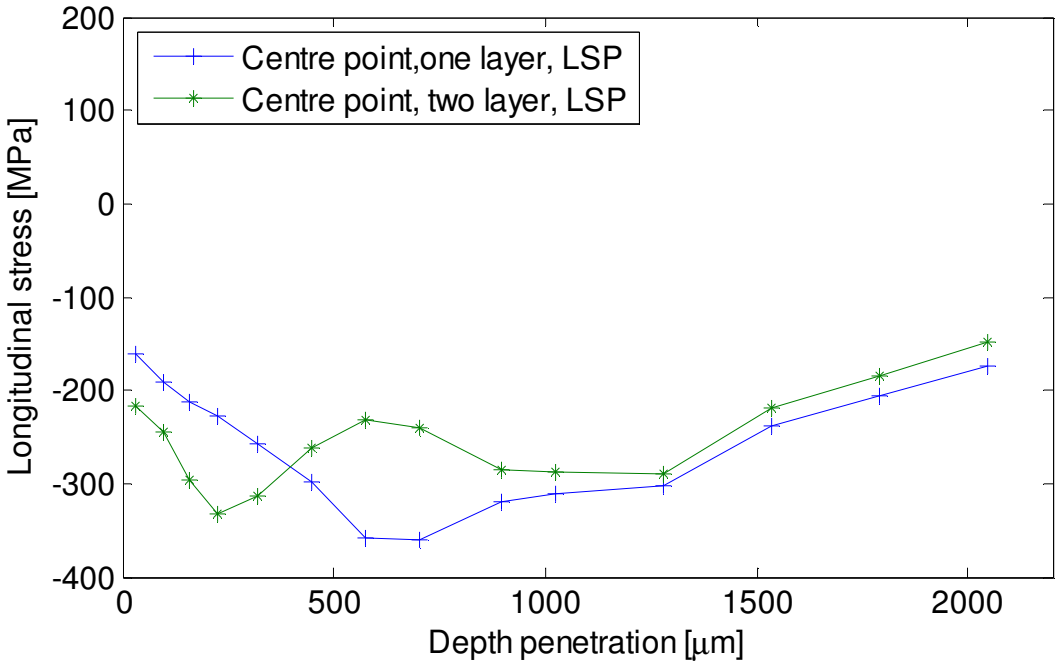

Figure 6.7 Longitudinal residual stresses measured with the shallow hole drilling technique for centre point samples with one layer and two layers deposited on to S275 steel substrates, after treatment with LSP. Similar compressive stresses were developed in both one and two layer overlays, with stresses tending to become more tensile stresses at depths greater than 2000 µm.

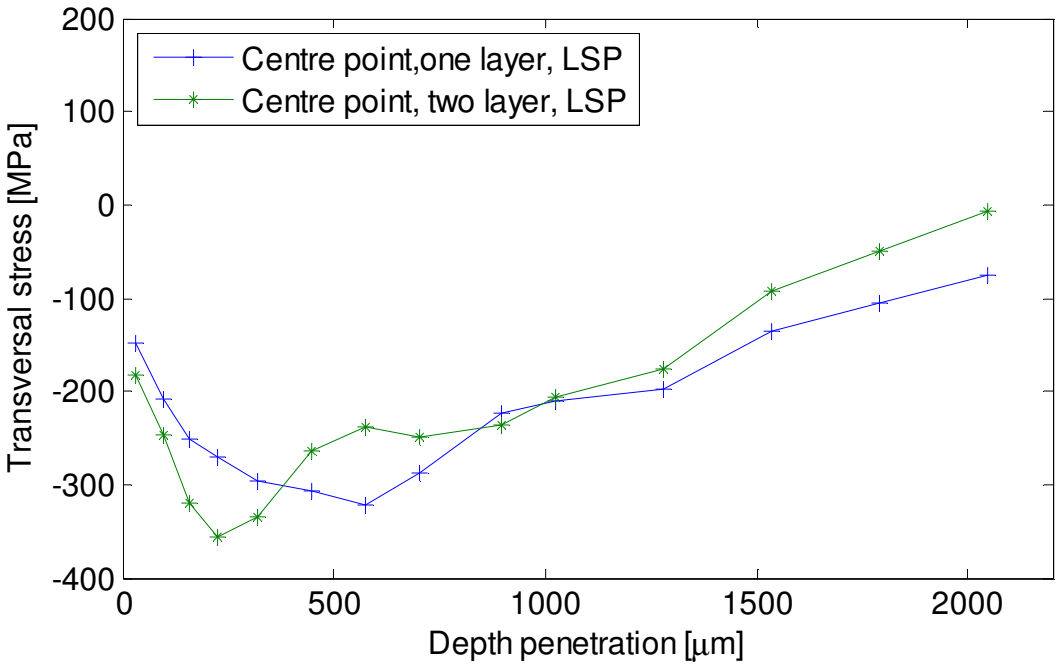

Figure 6.8 Transversal stresses assessed with the shallow hole drilling technique for the centre point samples with one layer and two layers deposited on to S275 steel substrates, after treatment with LSP. Higher compressive stresses were developed for the two layer deposition in the first 400 µm. It can be assumed that the interface between the first and second layer occurred at a depth of 500 µm.

The first stress measurement was recorded at a depth of 32 μm. The longitudinal and transverse stresses were slightly higher for the two layer sample in the first 400 μm in depth, but at greater depths the stresses tended to be similar. Although compressive stresses were developed through the cladding thickness, the magnitude of these stresses tended to decrease moving in to the base material.

The longitudinal and traverse stresses generated in the centre-point sample with an AISI grade 316L stainless steel substrate were also assessed with the shallow hole drilling technique. The longitudinal stresses developed in the centre-point samples with one-layer and two-layer deposit are shown in Figure 6.9. The cladding thickness was approximately 800 μm for the one layer deposit and 1600 μm for the two layer deposit.

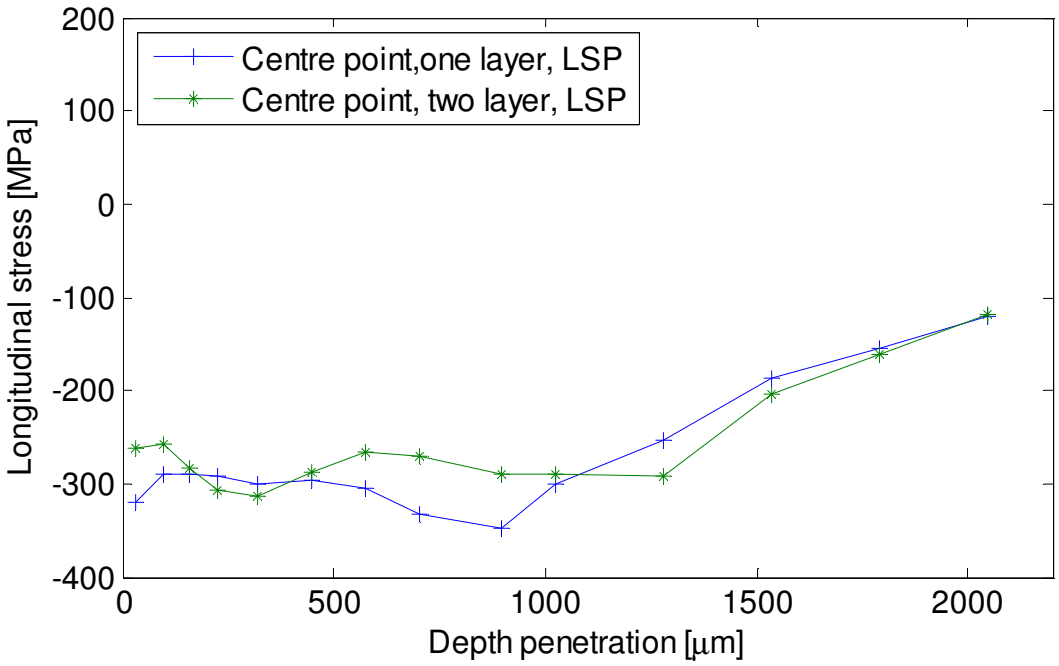

Figure 6.9 Longitudinal residual stresses assessed after LSP with the shallow hole drilling technique. The samples were clad using the centre point conditions, with one layer and two layer deposits respectivively, with AISI grade 316L stainless steel as the substrate.

Compressive stresses were generated in the longitudinal direction. The longitudinal stress remained almost constant to a depth of 800 μm in the one layer deposit and to 1300 μm in the two layer deposit. This distance corresponds approximately with the cladding thickness in each case.

The transverse stresses developed in the centre-point samples with one and two layer deposits are shown in Figure 6.10. It can be observed that similar compressive stresses were developed in traverse direction in both cases and that, below 600 μm depth, the stresses showed a clear trend to become more tensile.

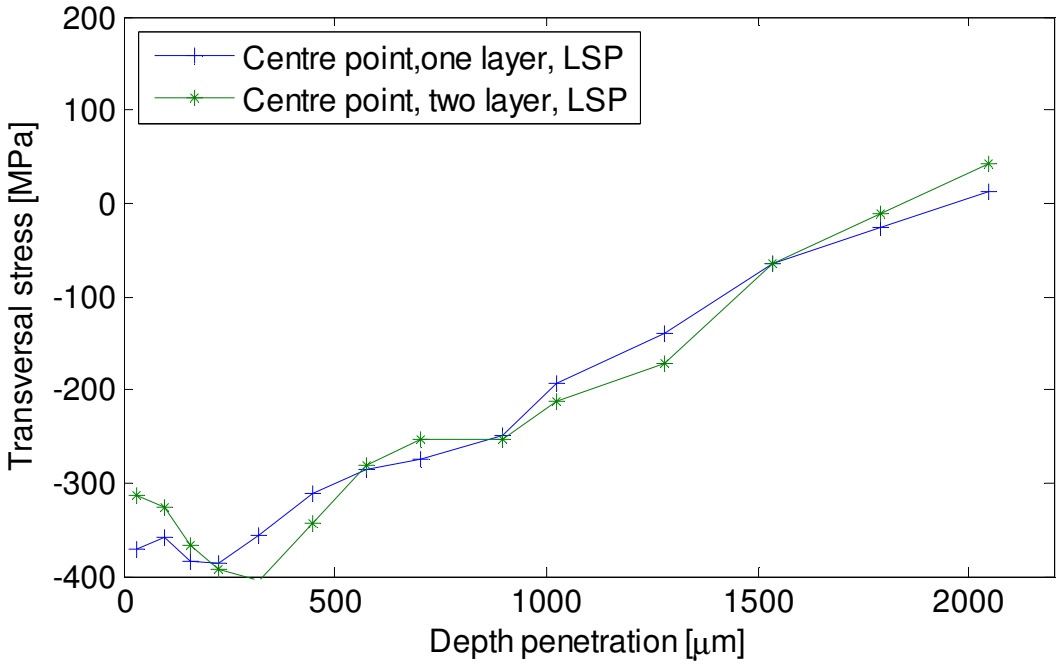

Figure 6.10 Transversal residual stresses assessed after LSP with the shallow hole drilling technique. The samples were clad using the centre point conditions, with one layer and two layer deposits respectively, with AISI grade 316L stainless steel as the substrate.

In general, laser shock peening was able to introduce compressive residual stresses in both directions for the different cladding configurations. This can be attributed to the strain hardening developed on the cladding surfaces due to the laser impacts.

The results obtained with the contour method are not consistent with the results obtained with the shallow hole drilling. Shallow hole drilling assessed compressive stresses in all the cladding configurations until 2 mm depth. However, discarding the stresses generated at 1 mm near to the ground surface, the contour method assessed slightly tensile stresses in the two-layer deposit samples. As mentioned before, some uncertainties can be generated near to the cut edges since plastic deformation is generated due to the cutting process.

6.3.1.2 Microstructure

The microstructure developed by the centre-point sample with two layer clad deposit using AISI 316L stainless steel as base material, before and after laser shock peening is shown in Figure 6.11 and Figure 6.12 respectively. It can be observed that finer microstructures were developed in some areas near to the ground surface and below after laser shock peening. As explained in Section 2.8.4, high dislocations densities can be developed after being treated by LSP. This can be related to an increase in hardness.

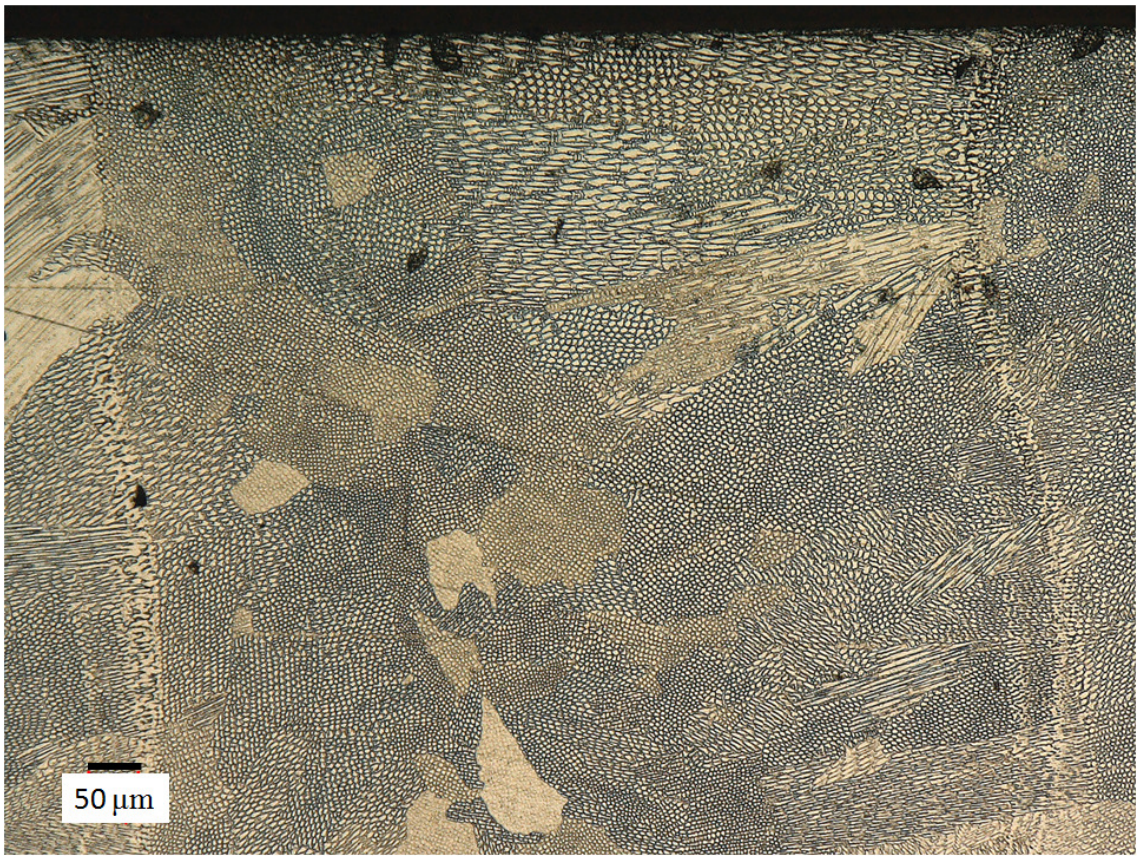

Figure 6.11 Optical micrographs showing the microstructures of the centre-point sample using AISI 316L stainless steel as base material before LSP.

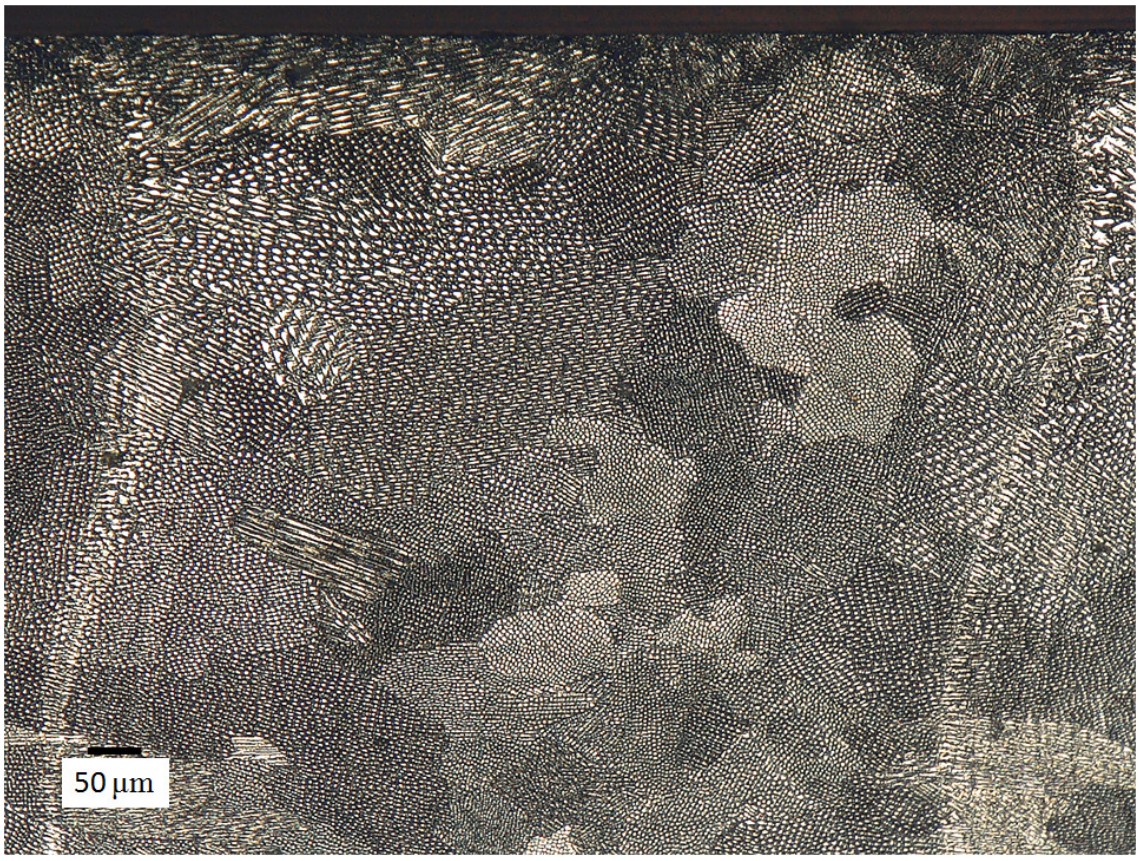

Figure 6.12 Optical micrographs showing the microstructures of the centre-point sample using AISI 316L stainless steel as base material after LSP. Finer microstructures are shown in some areas.

6.3.1.3 Hardness

Several investigations [117, 188] have found that samples treated with laser shock peening have shown an increase in hardness. This has been attributed to the development of high dislocation densities at the metal surfaces, owing to plastic deformation. Therefore, it can be assumed that laser shock peening can be used to enhance the clad layer hardness. The hardnesses developed as a function of depth after laser shock peening on the centre-point samples with one layer and two layer deposits, and with S275 steel as the base material, are shown in Figure 6.13and Figure 6.14, respectively.

From Figure 6.13 it can be seen that an increase in hardness has occurred in the laser shock peened sample. However, variability in the values of hardness was observed through the cladding thickness. This can be attributed to the development of different phases within the cladding because of dilution.

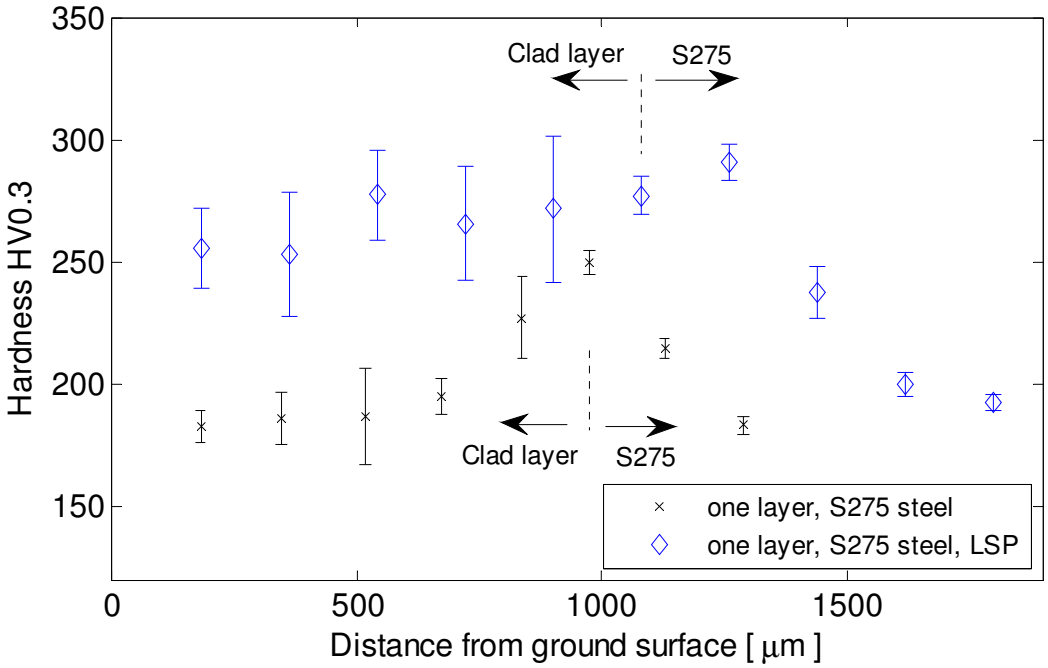

Figure 6.13 Hardness developed as a function of depth from the ground surface for laser clad centre-point samples, with one layer deposits and S275 steel as the base material, before and after laser shock peening. The plotted values correspond to an average of three measurements. An increase in hardness was observed after laser shock peening.

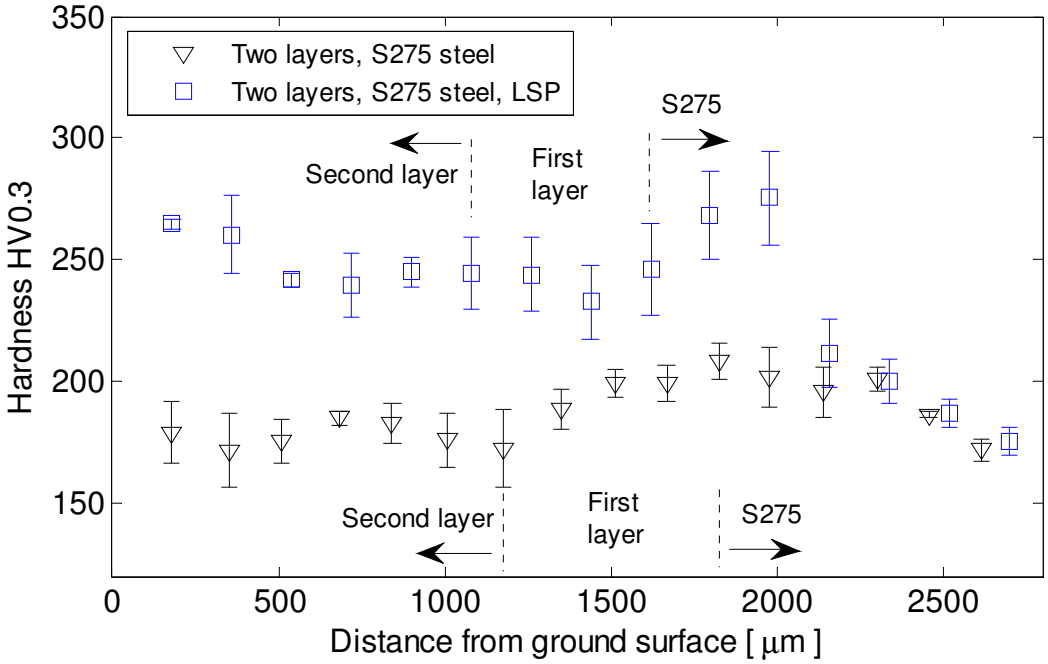

Figure 6.14 Hardness developed as a function of depth from the top surface for laser clad centre point samples with two layer deposits, using S275 steel as the base material, before and after being laser shock peening. The plotted values correspond to an average of three measurements. An increase in hardness is observed after laser shock peening.

From Figure 6.14, the two layer samples showed similar behaviour, with higher hardnesses for the LSP sample. The average Vickers hardness in the one layer samples was 196 in the unpeened condition and 270 for the LSP condition; this is an increase of approximately 30%. For the two layer deposits an increase of 30% was also found, with average Vickers hardnesses of 182 and 244, before and after LSP, respectively.

The hardnesses for the centre-point samples with one and two layer deposits, using AISI grade 316L stainless steel as the base material, are shown in Figure 6.15 and Figure 6.16, respectively. The Vickers hardness developed after laser shock peening in the one layer deposit (Figure 6.15) was higher, with an average value of 243, than before LSP, where the average value was 188. In the case of the two layer samples (Figure 6.16), average Vickers hardnesses of 185 and 234 were measured before and after LSP respectively. It can also be seen that, for both one layer and two layer samples, more uniform hardness was developed through the clad layers. This can be attributed to the same material being used for the powder and the base material, so no unexpected changes of phase or microstructure were likely to occur.

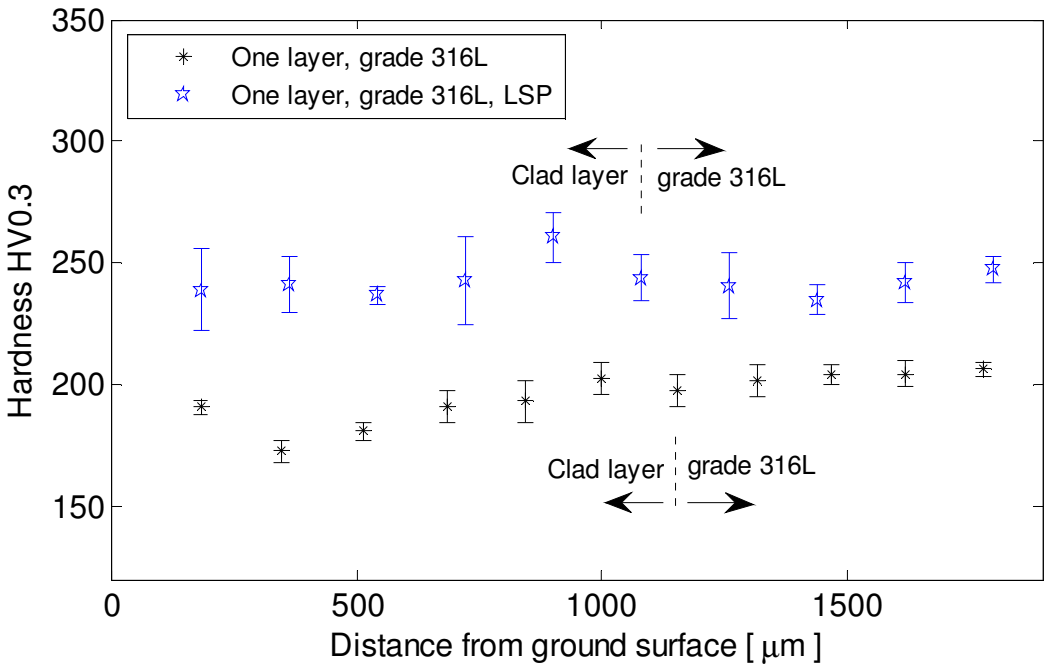

Figure 6.15 Hardness developed as a function of depth from the top surface for laser clad samples with one layer deposit using AISI grade 316L stainless steel as the base material, before and after laser shock peening. The plotted values correspond to an average of three measurements. An increase in hardness occurs in the laser clad sample after laser shock peening.

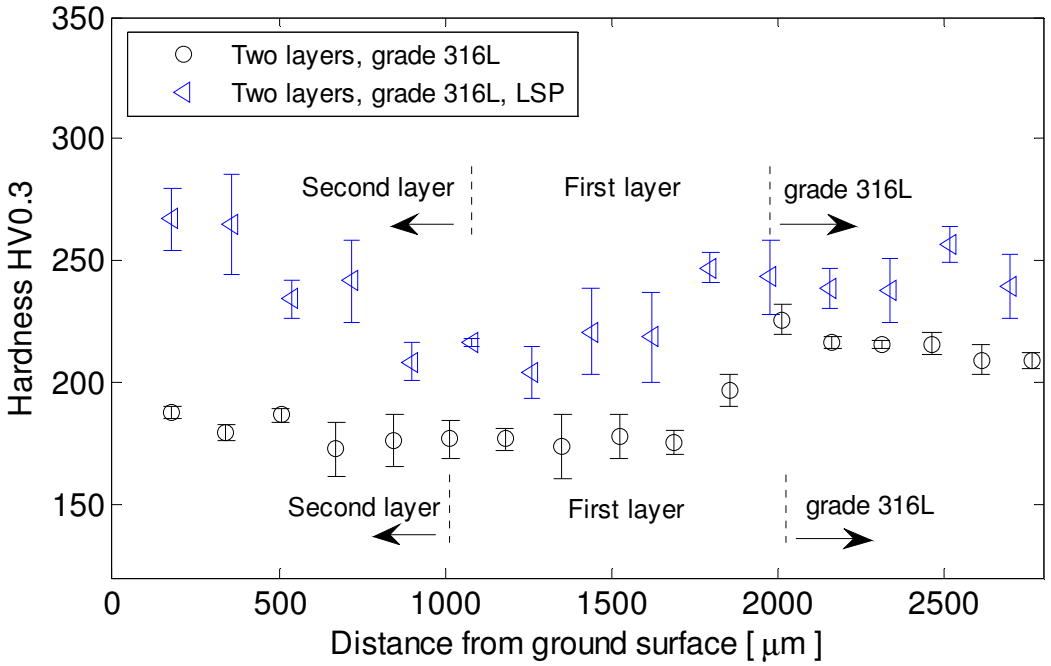

Figure 6.16 Hardness developed as a function of depth from the top surface for laser clad samples with two layer deposit using AISI grade 316L stainless steel as the base material, before and after laser shock peening. The plotted values correspond to an average of three measurements. An increase in hardness occurs in the laser clad sample after laser shock peening.

The hardness results show that laser shock peening can be used to post-process laser clad surfaces in order to improve the cladding hardness, which can contribute to an increase in the wear resistance of metals. Furthermore, the plastic deformation that occurs at the surface due to the laser peening contributes to the refining of the grains in the microstructure [162]. The refinement of microstructure was observed in the entire laser cladding samples after laser shock peening process.

6.3.2 Post weld heat treatment

Post weld heat treatment has been used in order to restore toughness and to relieve residual stresses that are generated after welding and cladding process [142, 144]. It has also been used in order to reduce the hardness of some metals. In this study, the centre-point samples with two layer deposits, using both S275 steel and AISI grade 316L stainless steel as base materials, were post weld heat treated in order to relieve the

tensile stresses generated after laser cladding, and the resulting residual stresses were assessed with the shallow hole drilling technique.

The stresses measured in the longitudinal direction after PWHT for the centre-point samples with two layer deposits on S275 steel and AISI grade 316L stainless steel base materials are shown in Figure 6.17. The stresses measured in the longitudinal direction in the sample with an S275 substrate were tensile, with a slight increase over those measured in the same samples without PWHT (Figure 5.9) across the cladding thickness. In this case, the PWHT produced a detrimental effect, increasing the magnitude of the tensile residual stresses. However, the AISI grade 316L stainless steel sample developed compressive stresses across the cladding thickness in the longitudinal direction. This suggests that the tensile stresses developed in the longitudinal direction before PWHT (Figure 5.12) were mitigated.

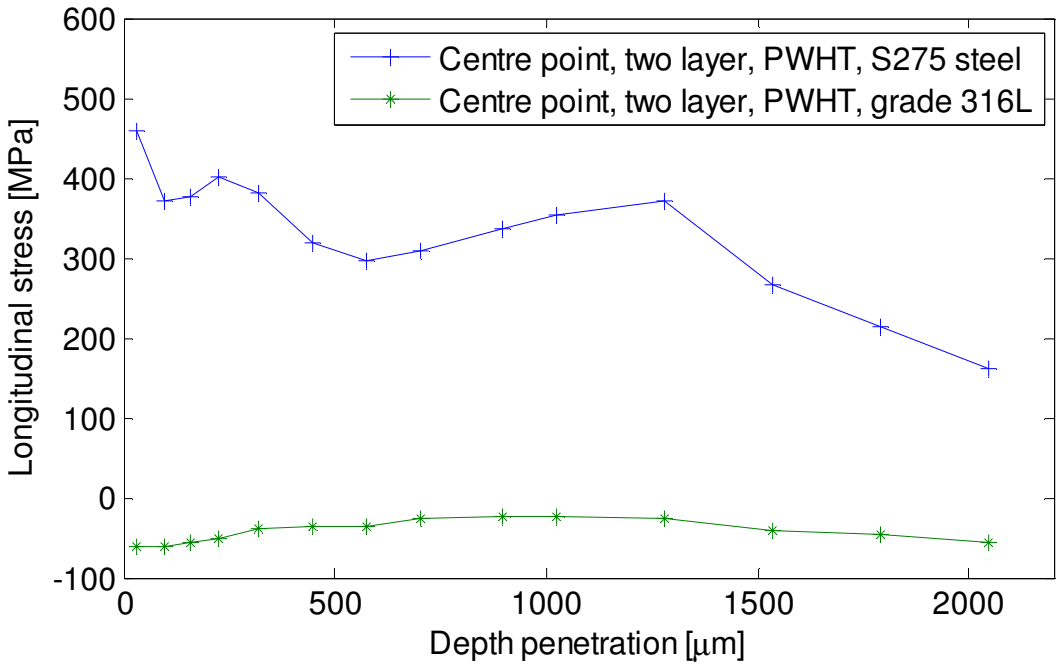

Figure 6.17 Residual stresses measured in the longitudinal direction in the centre-point laser clad samples after post weld heat treatment. The assessment was carried out with the shallow hole drilling technique. The sample with the S275 steel base material was held at 650°C for 30 minutes. The sample with the AISI grade 316L stainless steel base material was held at 900°C for 30 minutes.

The effects of PWHT on the stresses in the transverse direction in the two layer deposit centre point samples are shown in Figure 6.18. It can be seen that tensile stresses are still present in the S275 steel sample. Similar residual stresses were found in the centre-

point two layer deposit before PWHT (Figure 5.10) and after PWHT along the cladding thickness. The results indicate that no substantial changes were produced by the PWHT procedure that was applied to these samples. However, the transverse stresses found in the AISI grade 316L stainless steel samples after PWHT showed that slightly compressive stresses were generated along the cladding. In this case, the tensile stresses developed in the transverse direction in sample (Figure 5.13) were relieved and in fact became slightly compressive instead. This can be attributed to some contraction between the clad layer and the base material in the cooling process.

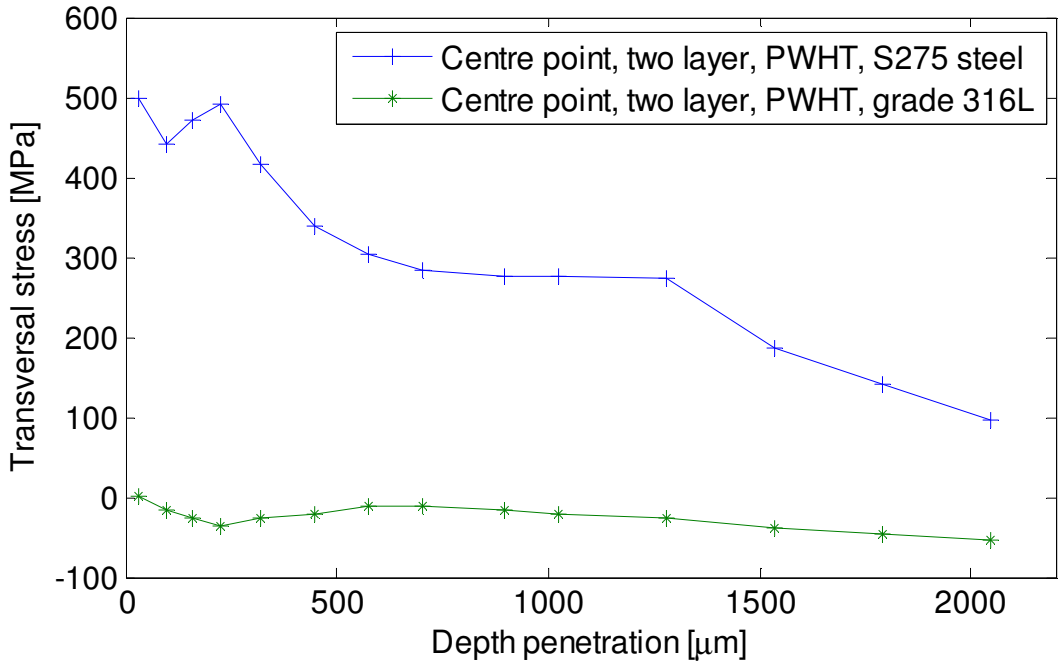

Figure 6.18 Residual stresses measured in the transversal direction in the centre-point laser clad samples after post weld heat treatment. The assessment was carried out with the shallow hole drilling technique. The sample with the S275 steel base material was held at 650°C for 30 minutes. The sample with the AISI grade 316L stainless steel base material was held at 900°C for 30 minutes.

In general, the PWHT procedures applied in this study generated beneficial results for the samples when AISI grade 316L stainless steel was used as base material. In contrast, there were not beneficial changes in the samples when S275 mild steel was used as the base material.

6.4 Discussion

Laser cladding has traditionally been used in order to repair or restore worn metallic components and to produce corrosion resistant coatings. However, the nature of the process develops residual stresses, in general tensile stresses, owing to the constrained expansion and contraction of the heated material, and these tensile stresses can have a detrimental effect on the performance of metals. Therefore, the addition of a second treatment to the laser clad samples in order to mitigate the tensile stresses was studied.

The tensile residual stresses developed in the laser clad samples assessed in this study were satisfactorily mitigated by laser shock peening, because compressive stresses were generated in the clad layers to depths of up to 1000 μm. Compressive stresses can enhance of fatigue resistance of metals because these tend to delay the initiation of cracks on the metal surface.

Furthermore, the hardness of the clad samples was also enhanced because plastic deformation almost certainly took place during LSP. This work hardening effect can contribute to an improvement in the wear resistance. In addition, the use of LSP in the confined ablation mode was beneficial because no damage was generated on the sample surfaces. In general, laser shock peening produced compressive stresses in the laser clad samples regardless of whether S275 steel or AISI grade 316L stainless steel was used as base material.

Post weld heat treatment can also be applied in order to mitigate tensile residual stresses. However, the conditions established in the process, such as soak temperature and exposure time, need to be chosen carefully as they depend heavily on the metals to be treated, and if they are not suitable a detrimental effect can be produced. In the case where AISI grade 316L stainless steel was used both for the overlay and the substrate, PWHT was found to be effective in mitigating residual stresses. However, it was observed that for the samples where S275 steel was used as the base material, the tensile stresses increased slightly in both directions after PWHT. This can be attributed to the differences in the thermal expansion coefficients for the overlay and base material. Although the residual stresses might be relieved at high temperature, the AISI grade 316L stainless steel has a higher thermal expansion coefficient than S275 steel. Therefore, during the cooling down of the material after the soak stage of the PWHT,

the stainless steel tends to contract more than S275 steel, leading to the regeneration of highly tensile residual stresses in the overlay.

Small compressive stresses were generated through the cladding in the transverse and longitudinal directions in the samples with AISI grade 316L stainless steel as the base material. In this case, clad and base materials were similar and the thermal expansion coefficient did not have influence during the solidification process. Therefore, the soak temperature proposed satisfactorily relieved the tensile residual stresses.

Finally, it can be assumed that laser shock peening has some advantages over the post weld heat treatment such as introducing compressive stresses in different materials.

Chapter 7

Corrosion testing

7.1 Introduction

The improvement of the corrosion resistance of metals that are exposed to certain corrosion environments has been the aim of several investigations. Therefore, the development of either metals with higher corrosive resistance or processes capable to enhance the corrosion resistance has been developed. There are various metals alloys with high corrosion resistance, such as Inconel, that has been used in the nuclear industry [155] ,and grade 316L austenitic stainless steels that has been also used in the nuclear industry and gas and oil refineries [112]. However, manufacturing operations can affect the resistance of corrosion of metals promoting the initiation of pits or cracks on the metal surfaces under certain corrosive environments. [189-192]

Laser cladding is a process that has been used in order to develop a corrosion resistant coating layer, and this involves in the deposition of a clad layer with higher corrosion resistance than the base material. This has been achieved because of the versatility of the process that allows using several cladding materials with good resistance to corrosion. However, the variables that controls the process, such as the laser power, the traverse speed and the powder feed rate, have an important relationship with the final corrosion resistance of the clad layer. Stress corrosion cracking can be produced because of the residual stresses developed in the clad layers. Furthermore, when dissimilar materials are used as the cladding and the base material, the dilution generated because of the process parameters can also affect the corrosion resistance.

This chapter describes the corrosion resistance developed in the deposition of grade 316L stainless steel clad layer on S275 steel and grade 316L stainless steel base materials. In order to investigate the corrosion protection afforded by the clad layer developed under different laser cladding process parameters, such as the laser power, the traverse speed and the powder feed rate, the corrosion rate was assessed. In addition

the chemical composition of some samples was examined via Energy Dispersive Spectroscopy (EDS) and related with the corrosion results. Furthermore, stress corrosion cracking was assessed in order to study the effects of the residual stresses developed in the cladding. Finally, stress corrosion cracking was also examined in the samples that were laser shock peened and post weld heat treated.

7.2 Experimental procedures

7.2.1 Sample preparation

Laser cladding samples were prepared with the process parameters established in Table 3.3 with S275 steel and grade 316L stainless steel as the base materials. The cladding procedure has been explained in Chapter 3. In addition, the centre-point sample with two layers deposition was also prepared with both base materials. The entire cladding configuration samples were assessed on one occasion. The cladding surfaces were gently grinded and manually polished in order to produce a flat surface. An area of approximately one centimetre square was considered to be tested. A copper wire was spot welded on the opposite face of the cladding and then protected with a plastic pipe and resin. Finally, the samples were covered with Lacomit peelable varnish excluding the cladding area to be tested.

Various standard practice tests have been developed in order to assess the stress corrosion cracking. The Bent-Beam practice consists in the bending of a metal specimen in order to introduce stresses and then is exposed to an established corrosion environment. This practice is referred as the ASTM G39. Another practice consists in the preparation of samples to tensile test. The samples are subjected to an established constant stress and exposed to certain corrosive environment. This practice is referred as the ASTM G36. The aim of these practices consists in introducing stresses and tested under corrosive environments in order to know whether a failure on the material surface, such as cracks, is generated.

Laser cladding is a process were tensile residual stresses beyond the yield strength are developed (refer to Chapter 5). These can cause the initiation of cracks when exposed to corrosive environments. Therefore, stress corrosion cracking experiments were carried

out in the centre-point samples with one and two layer deposition. S275 steel and grade 316L stainless steel were used as the base material. Additional centre-point sample with one and two layers deposition using both base materials were prepared in order to assess the effect of laser shock peening and post weld heat treatment. The cladding surface was kindly grinded and manually polished in order to produce a flat surface. The PWHT procedure has been explained in Chapter 6. The laser shock peening was carried out by Metal Improvement Company.

7.2.2 Sample analysis

7.2.2.1 Corrosion rate

The corrosion rate of the laser cladding samples was assessed using the linear polarisation resistance method [150]. A three electrode cell arrangement was used. In order to measure the potential, a Saturated Calmonel Electrode (SCE) was used as a reference electrode and a platinum electrode was used as a counter electrode. The samples were immersed in a glass container with 3.5% NaCl solution. A potentiostat was used in order to carry out Potentiodynamic Polarisations Scans in the range of -10 mV to 10 mV and then back vs open circuit polarization with a scan rate of 0.1667 $mV.s^{-1}$. The corrosion rate was calculated by the following expression.

$$\text{Corrosion Rate} = \frac{i_{corr} RMM}{nF\rho} \tag{7.1}$$

where i_{corr} is the corrosion current density (Acm^{-2}), the *RMM* is the atomic weight ($gMol^{-1}$), *n* is the valance , *F* is the Faraday constant ($CMol^{-1}$) and ρ is the density of the material (gcm^{-3}). i_{corr} is obtained by the equation

$$i_{corr} = \frac{B}{R_p} \tag{7.2}$$

where B is the Stern-Geary constant (mV) and R_p is the polarisation resistance (ohmcm^2) obtained by the average gradient of the current vs potential graph. The values used for the calculation of the corrosion rate are showed in Table 7.1.

Table 7.1 Parameters for the corrosion rate calculation

Symbol	Meaning	Value
RMM	Atomic weight	55.84 gMol^{-1}
n	Valance	2
F	Faraday constant	96485 CMol^{-1}
ρ	Material density	8 gcm^{-3}
B	Stern-Geary constant	0.026 V
R_p	Polarisation resistance*	Ohmcm^2

*Polarisation resistance obtained by the average gradient of the current vs potential graph

The chemical composition of the low feed rate sample and the centre point sample with two layer deposition using S275 steel as the base material was examined via Energy Dispersive Spectroscopy in a depth cladding of 300 μm from the top surface.

7.2.2.2 Stress corrosion cracking

The stress corrosion cracking experiments were carried using Magnesium Chloride ($MgCl_2$) as the corrosive species. Four magnesium chloride concentrations were prepared and deposited as droplets on the cladding surfaces. In addition, two more concentrations were prepared with the inclusion of sodium chloride (NaCl). Table 7.2 shows the magnesium chloride equivalence for each concentration.

Table 7.2 Magnesium Chloride concentrations used for SCC tests.

Concentration	$MgCl_2$ (gl^{-1})	$MgCl_2$ deposition density (μgcm^{-2})	NaCl (mgl^{-1})
1	30.188	1000	-
2	15.09	500	-
3	7.54	250	-
4	3.0188	100	-
5	7.54	250	540
6	3.0188	100	210

Each droplet represented a volume of 5 µl of magnesium chloride deposited on the sample surfaces. For simplicity, the laser cladding samples were separated in two sets; one represented the S275 steel the base material and the other grade 316L stainless steel as the base material sample. Each set was protected by a plastic box where two vessels with salty water were included in order to control the humidity. The two plastic boxes where put into an oven in order to generate a 60°C atmosphere. This temperature was considered in order to accelerate the process. The samples were left in the oven for a period of 5 weeks. The magnesium chloride concentrations and the conditions described above have been previously used in Refs. [193-195] for the study of stress corrosion cracking on grade 316L stainless steel.

7.3 Results

7.3.1 Corrosion rate

The corrosion protection afforded by the clad layer was assessed calculating the corrosion rate and expressed in terms of mass loss ($\mu myear^{-1}$). The cladding samples produced with S275 steel and grade 316L stainless steel as the base material were assessed. In addition, the centre-point sample with two layers deposition was also assessed in both cases. In order to calculate the corrosion current density (i_{corr}), the polarisation resistance for each sample was obtained measuring the average gradient of the current vs potential polarisation curve. A schematic illustration of the linear

polarisation curve of the centre-point sample using S275 steel as the base material is showed in Figure 7.1. Two gradients of current density vs potential were calculated; this is when an increase between potential and current started to manifest, and when a decrease of potential and current density is produced.

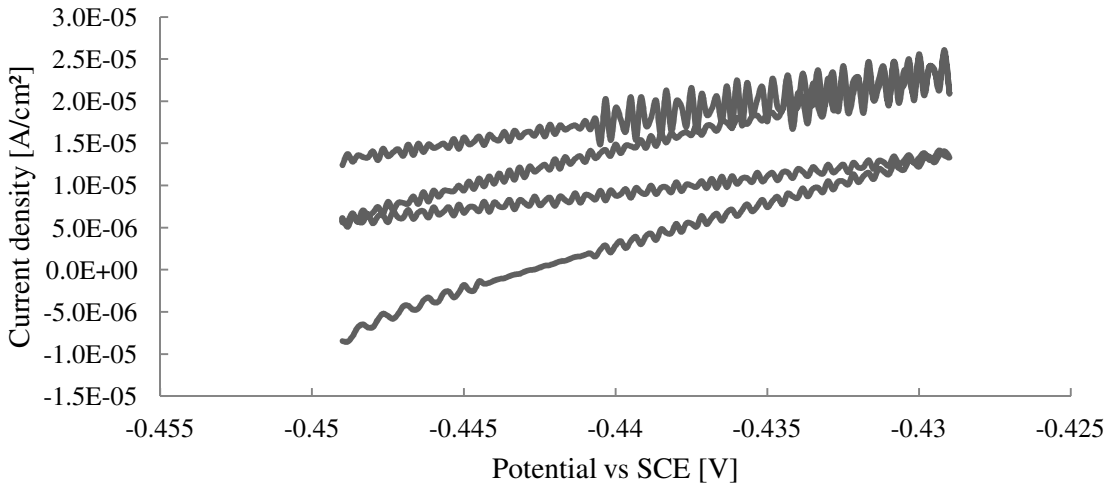

Figure 7.1 Linear polarisation curve of centre point sample using S275 steel as the base material. The gradient of the current and potential was obtained in order to calculate i_{corr} .

Different polarisation resistance values were obtained for each cladding sample. This can be related with the final chemical composition generated after cladding solidification. The corrosion current density and the corrosion rate were calculated with Equation 7.1 and Equation 7.2 respectively. The results obtained are shown in Table 7.3.

Table 7.3 Corrosion rates for cladding samples using S275 steel as the base material.

Sample	Dilution (%)	i_{corr} (Acm^{-2})	Corrosion rate (μmyear^{-1})
Low laser power	17	1.79×10^{-5}	203
Centre point	25	1.77×10^{-5}	201
High laser power	30	3.06×10^{-5}	348
Low speed	10	1.33×10^{-5}	151
High speed	35	1.27×10^{-5}	145
Low feed rate	47	2.98×10^{-5}	339
High feed rate	10	1.86×10^{-5}	211
Centre point (two layers deposition)	5	8.03×10^{-6}	90
S275 steel	-	7.28×10^{-5}	846

In Table 7.3, a trend can be observed in which an increase in dilution leads to an increase in corrosion rate. High dilution samples, such as those with a high laser power or a low feed rate, developed the highest corrosion rates. On the contrary, low dilution samples, such as those with a low speed or a high feed rate, manifested low corrosion rates. These observations can be attributed to the chemical compositions produced at different dilution levels. In the case where a high dilution was developed, more base material elements were mixed to the final clad layer. Curiously, the high-speed sample also resulted in a high dilution, but showed a low corrosion rate. Comparing the corrosion rates of all samples (Figure 7.2), this sample does not appear to fit the general trend. There may therefore be other factors, perhaps in the microstructure, that lead to the corrosion rate for the high speed sample generating an atypical value.

The lowest corrosion rate was developed by the centre-point sample with two layers deposition. This can be related to the fact that the chemical composition of the second layer is less affected by the elements composition of the base material. Based on these results, it can be observed that when two layers are deposited it has a greater influence on the corrosion rate rather than the lowest dilution samples. This means that, corrosion rate was more sensitive to the deposition of clad layers than dilution.

Owing to the highest dilution has been related to the highest corrosion rate on the low feed rate sample, the clad chemical composition was examined. Furthermore, the clad

chemical composition of the centre-point with two layer deposition was also examined. Table 7.4 shows the clad chemical composition of both samples.

Table 7.4 Chemical composition at 300 μm clad depth of low feed rate sample and centre point with two layers deposition sample using S275 steel as the base material. (wt. %)

Element	Low feed rate	Centre point (two layers deposition)
Fe	79.04	64.59
Cr	8.61	15.85
Ni	5.78	10.59
Mn	2.54	2.31
Mo	1.5	3.31
C	0.96	0.7
Si	0.34	0.96
P	0.17	0.35
S	0	0

According to the values showed in Table 7.4, low levels of chromium and nickel are present in the low feed rate sample. This can explain the high corrosion rates developed in this sample. However, the chromium and nickel levels in the centre point sample were close to the level of grade 316L stainless steel.

The polarisation resistance method was also used in order to assess the corrosion rate in all the samples using grade 316L stainless steel as the base material. The corrosion rate results are showed in Table 7.5. It can be seen that the corrosion rate was improved in some laser cladding samples comparing with the base material. However, the samples that showed higher dilution developed lower corrosion rate than the base material. In this case, the base material and the clad material were the same, and the different corrosion rates can be justified by the finer microstructures developed [196].

Table 7.5 Corrosion rates for cladding samples using grade 316L stainless steel as the base material.

Sample	Dilution (%)	i_{corr} (Acm^{-2})	Corrosion rate (μmyear^{-1})
Low laser power	29	3.83×10^{-8}	0.437
Centre point	31	2.69×10^{-7}	3.07
High laser power	34	7.19×10^{-7}	8.2
Low speed	18	4.16×10^{-7}	4.74
High speed	44	9.16×10^{-7}	10.4
Low feed rate	51	3.29×10^{-6}	37.6
High feed rate	19	1.76×10^{-7}	2.01
Centre point (two layers deposition)	12	1.39×10^{-7}	1.59
Grade 316L SS	-	4.65×10^{-7}	5.3

Comparing the corrosion rates developed in the 316L/S275 cladding samples (Table 7.3) and the corrosion rated developed in the both base materials; it can be observed that corrosion rates tend to be affected by dilution. This can be observed in Figure 7.2 where a straight line represents the corrosion rate of grade 316L stainless steel (0 % dilution) and S275 steel (100% dilution).

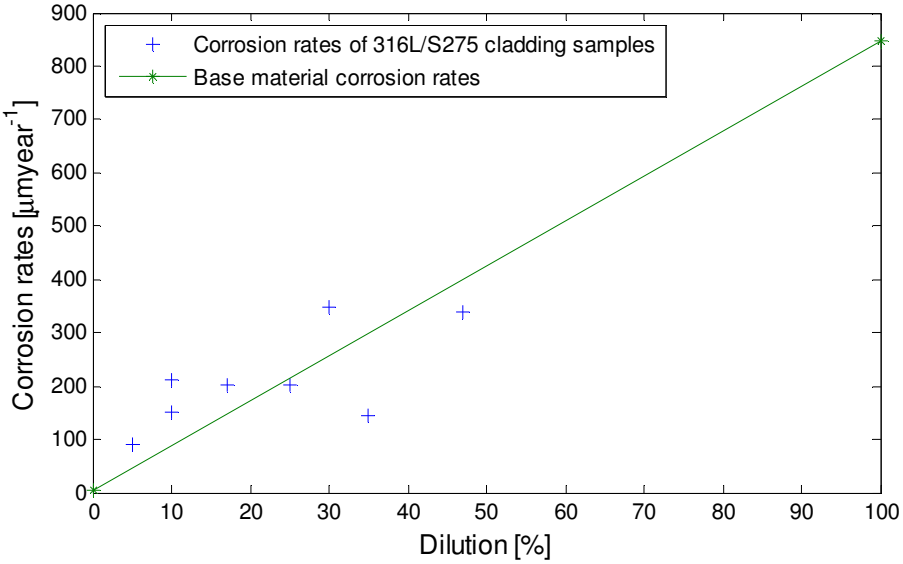

Figure 7.2 Corrosion rates of 316L/S275 cladding samples. The straight line indicates the corrosion rate of the grade 316L stainless steel and S275 steel as the base materials.

7.3.2 Stress corrosion cracking

The centre point-sample with one and two layers deposits using S275 steel as the base material was exposed to $MgCl_2$ in order to investigate whether the residual stresses developed by laser cladding process in a corrosive environment developed stress corrosion cracks. Figure 7.3 shows the centre-point sample with one layer deposition exposed to chloride environment for a period of time of five weeks. It can be observed that pits were developed on the clad surface generating cracks in some cases. From Figure 7.3 (b), it can be observed that the cracks tend to follow the grain boundaries. This could indicate the presence of intergranular corrosion. In all the cases, a few microns of the clad surface were corroded and then the generation of cracks was developed. According to Figure 5.9 and Figure 5.10, the residual stresses in the transversal and longitudinal directions increased in depth. The information about grade 316L stainless steel exposed to stress corrosion cracking tests is limited. However, Ref. [197] examined the effects of grade 316L stainless steel under magnesium chloride in a U-bend test finding that cracks were generated by the influence of tensile stresses and a corrosive environment.

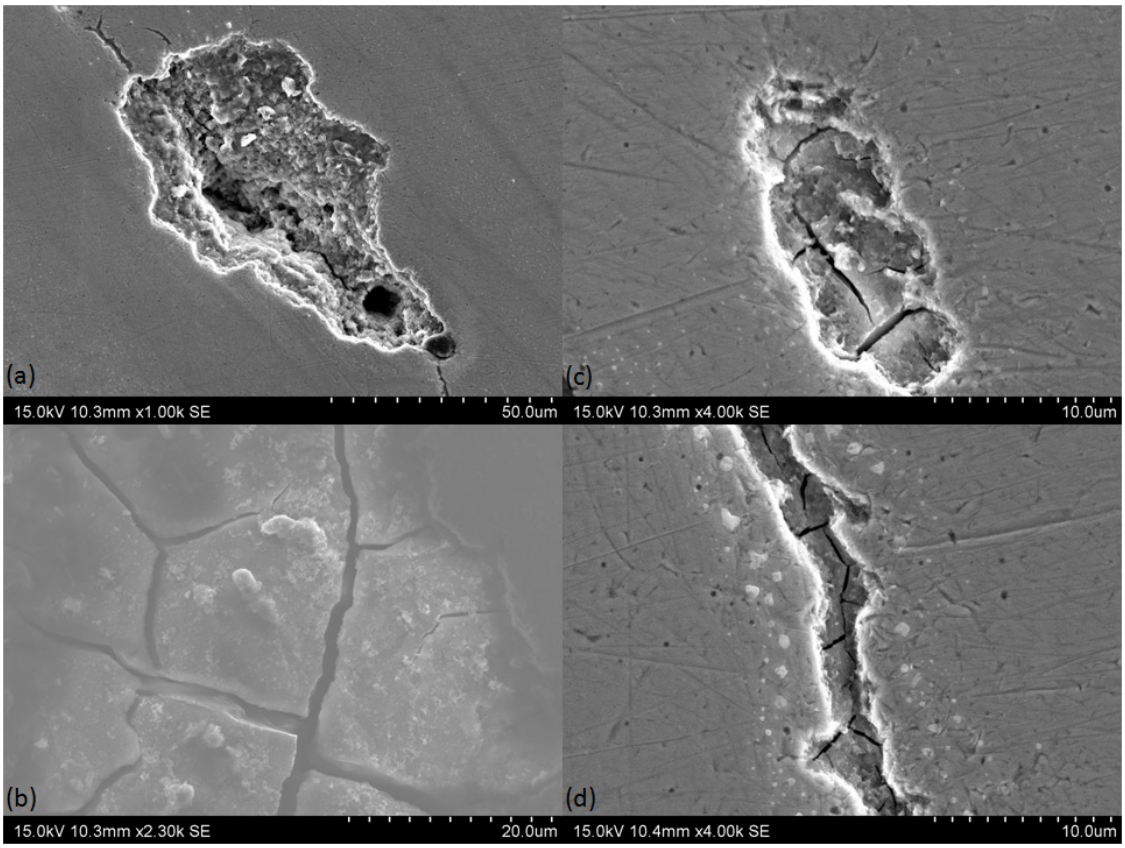

Figure 7.3 SEM micrographs showing the evaluation of the centre-point sample with one layer deposition using S275 steel as the base material exposed to $MgCl_2$ for 5weeks. (a) Pits were observed on the clad surface; (b) the appereace of intregranular corrosion in some of the pits; (c) another pit developed with the presence of cracks; (d) long pit with the presence of cracks with different directions.

In the same way, the centre-point samples that where treated with laser shock peening in order to introduce a compressive layer were exposed to the magnesium chloride. Figure 7.4 shows the effects of the magnesium chloride on the shock peened surfaces of the centre-point sample with one and two layers deposition using S275 steel as the base material. It can be seen that small pits were developed on the clad surface and no cracks were generated. This can be attributed to the fact that compressive stresses were produced by the laser shock peening process. Some investigations have been carried out in order to know if the pitting corrosion is affected by the laser shock penning. It has been reported by Ref. [157-158, 161] that an improvement on the pitting corrosion resistance has been generated on stainless steel after laser shock peening process and it has been related to the generation of compressive stresses and work-hardening on the metal surfaces.

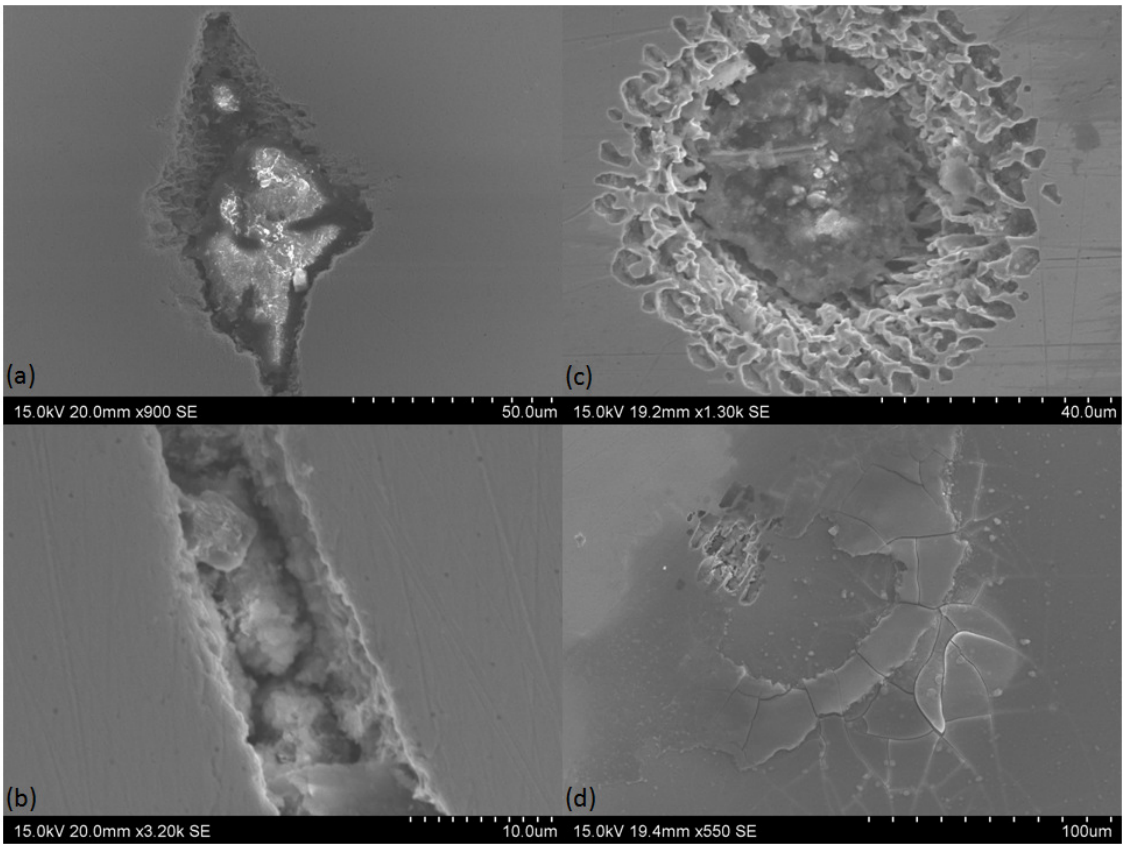

Figure 7.4 SEM micrographs showing the laser shock peen centre-point sample with S275 steel as base material. (a) and (b) Generation of pits without the prescsence of cracks on the laser shock peen centre point sample with one layer deposition. (c) The presence of pits without the generation of cracks on the centre point sample wih two layers deposition. (d) the onset of pits sorrounding with some cracks on the centre point sample with two layers deposition.

The post weld heat treatment laser cladding samples were also exposed to magnesium chloride. Figure 7.5 shows the effect of the magnesium chloride on the post weld heat treatment centre-point sample with two layers deposition using S275 steel as the base material. It can be observe that pits were produced on the surface with the presence of cracks. As mentioned in Section 5, high tensile residual stresses were produced after post weld heat treatment, and this can be the reason that crack were generated after the pitting onset.

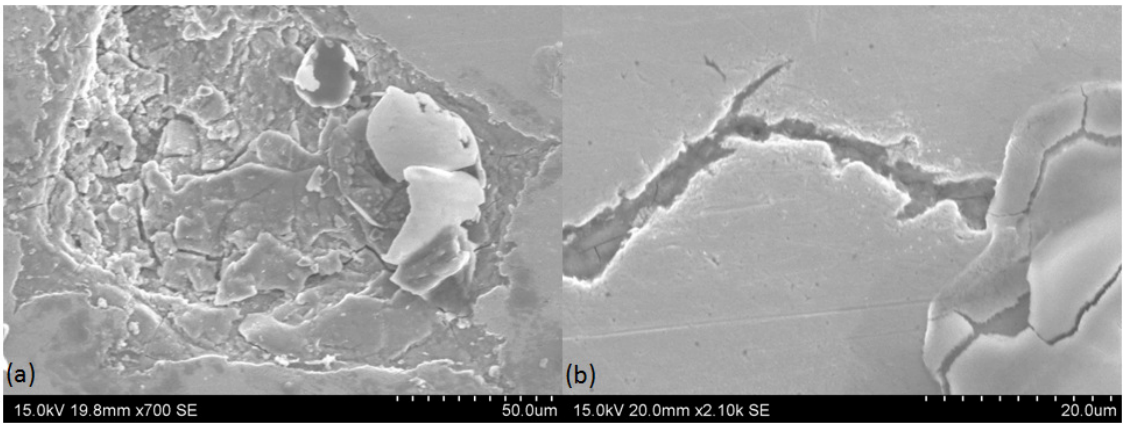

Figure 7.5 SEM micrographs showing the post weld heat treatment centre-point sample with two layer deposition using S275 as the base material exposed to $MgCl_2$. (a) Pit with the presence of cracks; (b) long pit with the presence of cracks.

The centre-point samples using grade 316L stainless steel as the base material were also treated with magnesium chloride. The presence of cracks were also generated in the centre-point sample with one layer deposition using grade 316L stainless steel as the base material (Figure 7.6). This can be attributed to the presence of tensile residual stresses in the transversal and longitudinal direction. This can be observed in Figure 5.12 and Figure 5.13 respectively.

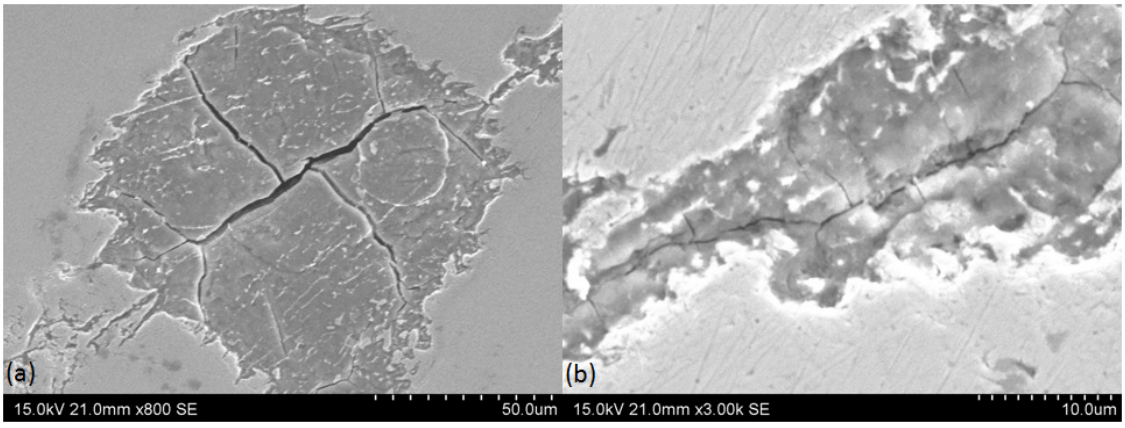

Figure 7.6 SEM micrographs showing the centre-point sample with one layer deposition using grade 316L stainless steel as the base material exposed to $MgCl_2$. (a) and (b) Presence of cracks after some corroded material.

The effects of laser shock peening were also assessed. Figure 7.7 shows the effects of magnesium chloride on the shock peened surface of the centre-point sample with one layer deposition. It can be observed that just general corrosion was produced and no cracks were found. Similar results were observed by the centre-point with one layer

deposition with S275 steel as the base material (Figure 7.4). In this case, compressive residual stresses were also developed after laser shock peening process.

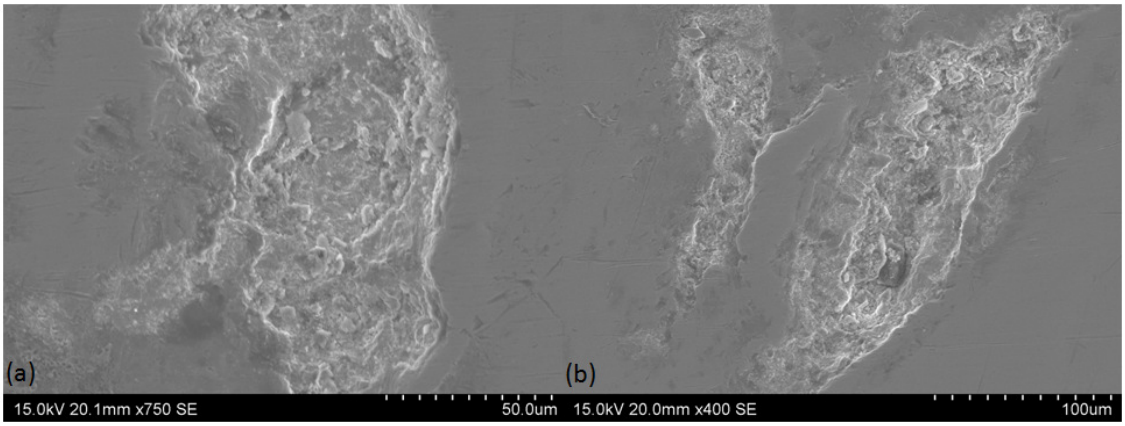

Figure 7.7 SEM micrographs showing the laser shock peen centre-point sample with one layer deposition using grade 316L stainless steel as base material exposed to $MgCl_2$. (a) and (b) general corrosion without the presence of cracks on the clad layer.

Finally, the samples that were post weld heat treatment using grade 316L stainless steel as the base material were also exposed to the magnesium chloride. Figure 7.8 shows an SEM picture of the post weld heat treatment centre point sample with one layer deposition using grade 316L stainless steel as the base material. It can be observed that just general corrosion without the presence of cracks was developed. This can be attributed due to tensile residual stresses were mitigated after post weld heat treatment.

The samples with grade 316L stainless steel used as the base material with two layers deposition showed slightly compressive stresses in the transversal and longitudinal direction. It can be assumed that the post weld heat treatment mitigate the tensile residual stresses on the one layer deposition sample because the same procedure was used. This assumption is considered due to the residual stresses were just measured for the two layer deposition centre point sample.

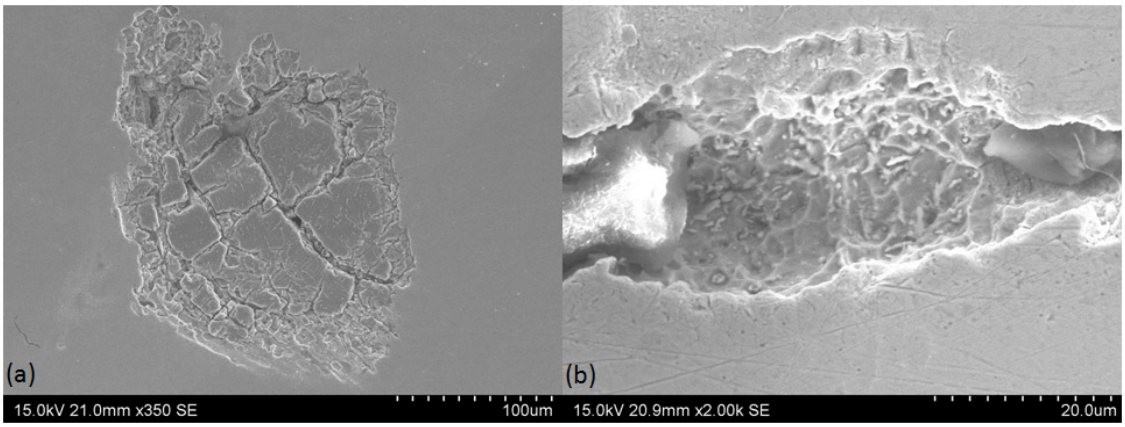

Figure 7.8 SEM micrographs showing the post weld heat treatment centre-point sample with one layer deposition using grade 316L stainless steel as the base material exposed to $MgCl_2$. (a) and (b) general corrosion without the presence of cracks on the layer cladding.

7.4 Discussion

Laser cladding is a process used to improve the corrosion resistance of metals. However, the variables that control the process such as the laser power, the traverse speed and the powder feed rate, have an important influence in the final condition of the clad layer specially when dissimilar materials are used as the clad and base material.

The corrosion rates obtained on the cladding samples where grade 316L stainless steel was used as the clad material and S275 steel as the base material showed the effects of the process parameters. In this case, dilution was an important parameter to consider in the assessing of the corrosion rate due to the inclusion of base material elements to the cladding were crucial for the corrosion resistance of the clad. This was demonstrated by the examination of the clad chemical composition of low feed rate sample where high corrosion rates were developed owing to low wt% of chromium and nickel were found.

The laser cladding samples where grade 316L stainless steel was used as both the clad and base material showed different corrosion rates. Even though, dilution should not considerably affect the final corrosion resistance because of similar materials were used, the different corrosion rates generated can be attributed to the fine microstructures developed in some parameters.

The stress corrosion cracking experiments showed that cracks were developed on the clad surfaces. However, the cracks were developed few microns beneath the surface. According to the stress evaluation, the residual stresses in the transversal and

longitudinal direction started to increase in depth. The same behaviour was observed for both base materials. It was also observed that the cracks tended to follow the grain boundaries; therefore it can be assumed that intergranular corrosion was manifested.

Pits without cracks were found on the clad surfaces that were treated by laser shock peening. This can be attributed to the generation of compressive residual stresses and the work-hardening layer developed after LSP. The same effect was found on the samples where S275 steel and grade 316L stainless steel were used as base materials. On the contrary, general corrosion without the presence of cracks was only found on samples were grade 316L stainless steel was used as the base material after post weld heat treatment.

It can be seen that laser shock peening retarded the initiation of crack in the samples where S275 steel was used as the base material and in the samples where grade 316L was used as the base material. This can be considered an advantage of LSP over post weld heat treatment process.

Further investigation should be developed in the assessment of stress corrosion cracking on laser cladding samples owing to little information can be found. However, the results generated in this study can contribute to the acknowledgement of the development of stress corrosion cracks on laser cladding.

Chapter 8

Conclusions and Suggestions for Future Work

8.1 Conclusions

In the present work the principles of the laser cladding process were investigated, assessing the hardness, the microstructure, the residual stresses and the corrosion resistance as a function of process parameters such as laser power, traverse speed and powder feed rate. AISI grade 316L stainless steel was used as the powder material and it was deposited on to two different substrate materials, S275 steel and AISI grade 316L stainless steel. Furthermore, the clad surfaces of some samples were treated after the deposition process in order to examine the effects of introducing compressive residual stresses on the cladding performance. The laser shock peening process was chosen as one post-cladding treatment process. In addition, some of the clad surfaces were subjected to post weld heat treatment in order to relieve the residual stresses and examine the effects on cladding performance.

The dilution, microstructure and hardness resulting from the laser cladding operation with different process parameters were investigated. The corrosion rate of the clad surfaces was also evaluated by the linear polarisation resistance method and the results were related to the process parameters. Furthermore, the residual stresses and the hardness resulting from the laser cladding process were examined before and after laser shock peening and after post weld heat treatment. Finally, the stress corrosion cracking performance was evaluated on the laser clad samples before and after laser shock peening and after post weld heat treatment.

To the author's knowledge, this is the first detailed study that has attempted to link the deposition parameters that are used in laser cladding operations to both the residual stress distributions and the corrosion performance in stainless steel overlays. Of course, the residual stresses can have a significant impact on the corrosion performance of a material. The conclusions that can be drawn from this investigation are described here:

1. **The Removal of Tensile Stresses through Post-Cladding Treatments Retards the Development of Cracks.** Pits and cracks were generated on the clad surfaces exposed to magnesium chloride. The cracks tended to follow the grain boundaries indicating that intergranular corrosion was occurring. However, the cladding samples treated by laser shock peening only showed pits, without cracking. This would indicate that the compressive stresses generated on the clad surfaces retarded the onset of cracks. Interestingly, the same effect was found on the cladding samples after post weld heat treatment where AISI grade 316L stainless steel was used as the base material. In this case, only corrosion pits were observed on the clad surface without the presence of cracks. This can be attributed to the fact that tensile residual stresses were mitigated by the post weld heat treatment. However, it is likely that the stresses in the laser clad AISI grade 316L coupons were close to zero after PWHT, whereas they were under significant compressive stresses in the case of the samples subjected to LSP. These preliminary results would suggest that, in order to retard cracking, it is sufficient to remove the tensile stresses and it may not be necessary to introduce compressive stresses. However, further work would be required to confirm this. In contrast, when S275 steel was used as the base material, pits and cracks were evident in those samples that underwent post weld heat treatment. However, for these samples, tensile stresses were present after post weld heat treatment.
2. **The number of clad layers deposited has a greater influence on the corrosion rate than the choice of process parameters.** The results generated on the samples for which S275 steel was used as the base material, with all combinations of process parameters, showed that corrosion rates were generally affected by dilution. This can attributed to the fact that significant concentrations of base material elements were dissolved within the clad layer thereby affecting the corrosion resistance of the cladding material. However, the two layer sample generated the lowest corrosion rate even in comparison with the lowest dilution sample. This means that the deposition of two layers had a greater influence on the corrosion rate than dilution. It can therefore be concluded that it is not worth trying to identify low dilution parameters, since the corrosion resistance is more sensitive to the number of layer deposited. Further work would be required to confirm this.
3. **Post weld heat treatment was only effective on cladding samples with matching cladding and base materials.** The residual stresses developed within

the cladding samples where AISI grade 316L stainless steel was used both as the powder and the base material were satisfactorily relieved by post weld heat treatment. However, contrary effects were found in the cladding samples for which S275 steel was used as the base material, due to higher tensile stresses being present after post weld heat treatment. It can be concluded that PWHT is effective for matching stainless steel overlay and substrate materials, but that it might not be effective if the different thermal contraction coefficients in the 316L/S275 lead to tensile stresses in the overlay regenerating as the sample cools after PWHT.

4. **The residual stresses in the overlays were not sensitive to process parameters or the number of layers that were deposited.** The magnitude of the residual stresses developed with the high laser power, centre point and two-layer deposition centre point samples were similar in both the transverse and longitudinal directions. This means that two or more layers can be deposited in order to achieve better corrosion resistance in the clad layer without there being any considerable changes to the residual stresses in the clad layer which may affect, for example, the fatigue resistance of the component.
5. **Residual stresses were higher in the transverse direction than in the longitudinal direction.** It was found that higher residual stresses were generated in the transverse direction than in the longitudinal or welding direction. This means that if cracks are generated these will be most likely to grow parallel to the welding direction. This was observed in the stress corrosion cracking samples whereby the cracks that were generated in the cladding tended to grow parallel to the weld direction.
6. **Laser shock peening was effective at mitigating tensile residual stresses in laser cladding overlays.** The laser shock peening process was capable of mitigating the tensile stresses in the transverse and longitudinal directions, introducing compressive stresses. This could lead to an improvement in the fatigue and wear resistance of the cladding. This would require further investigation.

8.2 Future work

The following areas have been identified as being worthy of further investigation:

- The effects of laser shock peening on the laser cladding samples were only assessed in terms of the effects on stress corrosion cracking. It would certainly be worth investigating the effectiveness of laser shock peening on the fatigue and wear resistance of laser clad surfaces.
- With S275 steel as the base material, the lowest corrosion rates were measured on samples with two layer overlays. It would be worthwhile investigating the performance of overlays comprising three or more layers in order to establish if the corrosion rates continue to decrease, and to observe how the corrosion performance compares with undiluted material.
- Pitting corrosion tests could be carried out on laser-shock-peened cladding samples in order to establish whether the compressive stresses developed by LSP influence the generation of pits.
- Pitting corrosion tests could be carried out on the post weld heat treated samples and the results could be compared with those for laser shock peening in order to establish whether pitting is retarded by the introduction of compressive stresses in particular, or whether it is sufficient to remove the tensile stresses from the overlay.
- Further work on laser-shock-peened cladding samples is necessary to establish whether the work hardening that occurs due to LSP is beneficial or detrimental in terms of the resulting corrosion rates.
- Post weld heat treatment could be carried out on cladding samples using different soak temperatures to establish the temperatures at which such treatments begin to have detrimental effects on the corrosion performance of the overlays.
- Different cladding materials, such as AISI grade 304L stainless steel, could be investigated in order to establish whether the findings arising from this work are transferrable to other alloys.

References

1. Mazumder, W.S.K.G.W.J., *Laser Material Processing*. Fourth edition ed. 2010: Springer London.
2. Dowden, J., *The Theory of Laser Materials Processing. Heat and Mass Transfer in ModernTechnology.* 2009: Dordrecht: Springer Netherlands.
3. Ehsan Toyserkani, A.K., Stephen Corbin, *Laser Cladding*. 2004: CRC PRESS. 280.
4. Mellor, B.G., *Surface coatings for protection against wear*. First Edition ed. 2006, Cambridge: Woodhead Publishing Limited.
5. Elijah Kannatey-Asibu, J., *Principles of Laser Materials Processing*. 2009, New Jersey: Wiley.
6. Sexton, L., S. Lavin, G. Byrne, and A. Kennedy, *Laser cladding of aerospace materials.* Journal of Materials Processing Technology, 2002. **122**(1): p. 63-68.
7. Kathuria, Y.P., *Some aspects of laser surface cladding in the turbine industry.* Surface and Coatings Technology, 2000. **132**(2-3): p. 262-269.
8. Xiong, Z., G.-x. Chen, and X.-y. Zeng, *Effects of process variables on interfacial quality of laser cladding on aeroengine blade material GH4133.* Journal of Materials Processing Technology, 2009. **209**(2): p. 930-936.
9. Navas, C., A. Conde, B.J. Fernández, F. Zubiri, and J. de Damborenea, *Laser coatings to improve wear resistance of mould steel.* Surface and Coatings Technology, 2005. **194**(1): p. 136-142.
10. Comesaña, R., F. Lusquiños, J. del Val, M. López-Álvarez, F. Quintero, A. Riveiro, M. Boutinguiza, A. de Carlos, J.R. Jones, R.G. Hill, and J. Pou, *Three-dimensional bioactive glass implants fabricated by rapid prototyping based on CO2 laser cladding.* Acta Biomaterialia, 2011. **7**(9): p. 3476-3487.
11. Müller, S., H. Pries, K. Dilger, S. Ocylok, A. Weisheit, and I. Kelbassa, *Applying Functionally Graded Materials by Laser Cladding: a cost-effective way to improve the Lifetime of Die-Casting Dies*, in *Glocalized Solutions for Sustainability in Manufacturing*, J. Hesselbach and C. Herrmann, Editors. 2011, Springer Berlin Heidelberg. p. 235-239.
12. Hidouci, A., J.M. Pelletier, F. Ducoin, D. Dezert, and R. El Guerjouma, *Microstructural and mechanical characteristics of laser coatings.* Surface and Coatings Technology, 2000. **123**(1): p. 17-23.
13. de Oliveira, U., V. Ocelík, and J.T.M. De Hosson, *Residual stress analysis in Co-based laser clad layers by laboratory X-rays and synchrotron diffraction techniques.* Surface and Coatings Technology, 2006. **201**(3-4): p. 533-542.
14. Narendra B. Dahotre, S.P.H., *Laser Fabrication and Machining of Materials*. 2008: Springer.
15. Ye, K.D.a.L., *Laser Shock Peening. Performance and process simulation.* First Edition ed. 2006, Cambridge: Woodhead Publishing Limited.
16. L. Zhou, Y.H.L., W.F. He, X.D. Wang, Q.P. Li, *Laser Shock Processing of Ni-Base Superalloy and High Cycle Fatigue Properties.* Materials Science Forum, 2012. **Volumes 697 - 698**: p. 235-238.
17. Aldajah, S.H., *Effect of laser surface modifications tribological performance of 1080 carbon steel.* Journal of Tribology, 2005. **127**(3): p. 596-604.

18. Atwood, C., M. Ensz, D. Greene, M. Griffith, L. Harwell, D. Reckaway, T. Romero, E. Schlienger, and J. Smugeresky, *Laser Engineered Net Shaping (LENS(TM)): A Tool for Direct Fabrication of Metal Parts*. 1998. Medium: ED.
19. Mazumder, J., J. Choi, K. Nagarathnam, J. Koch, and D. Hetzner, *The direct metal deposition of H13 tool steel for 3-D components.* JOM, 1997. **49**(5): p. 55-60.
20. Meiners W, W.K., Poprawe R, *Direct generation of metal parts and tools by selective laser powder remelting (SLPR)*, in *Conference of proceedings, ICALEO, 1998. Section-E: 31–37*. 1998.
21. Paul, C.P., A. Jain, P. Ganesh, J. Negi, and A.K. Nath, *Laser rapid manufacturing of Colmonoy-6 components.* Optics and Lasers in Engineering, 2006. **44**(10): p. 1096-1109.
22. Gnanamuthu, D.S., *Laser Surface Treatment.* Optical Engineering, 1980. **19**(5): p. 195783-195783-.
23. Barnes, S., N. Timms, B. Bryden, and I. Pashby, *High power diode laser cladding.* Journal of Materials Processing Technology, 2003. **138**(1-3): p. 411-416.
24. Santhanakrishnan, S., F. Kong, and R. Kovacevic, *An experimentally based thermo-kinetic hardening model for high power direct diode laser cladding.* Journal of Materials Processing Technology, 2011. **211**(7): p. 1247-1259.
25. Fallah, V., S.F. Corbin, and A. Khajepour, *Solidification behaviour and phase formation during pre-placed laser cladding of Ti45Nb on mild steel.* Surface and Coatings Technology, 2010. **204**(15): p. 2400-2409.
26. Gedda, H., A. Kaplan, and J. Powell, *Melt-solid interactions in laser cladding and laser casting.* Metallurgical and Materials Transactions B: Process Metallurgy and Materials Processing Science, 2005. **36**(5): p. 683-689.
27. Lugscheider, E., H. Bolender, and H. Krappitz, *LASER CLADDING OF PASTE BOUND HARDFACING ALLOYS.* Surface Engineering, 1991. **7**(4): p. 341-344.
28. Kim, J.-D. and Y. Peng, *Plunging method for Nd : YAG laser cladding with wire feeding.* Optics and Lasers in Engineering, 2000. **33**(4): p. 299-309.
29. Vilar, R., *Laser cladding.* Journal of laser applications, 1999. **11**(2): p. 64-79.
30. Mazumder, J., D. Dutta, N. Kikuchi, and A. Ghosh, *Closed loop direct metal deposition: art to part.* Optics and Lasers in Engineering, 2000. **34**(4-6): p. 397-414.
31. Liu, J. and L. Li, *Study on cross-section clad profile in coaxial single-pass cladding with a low-power laser.* Optics & Laser Technology, 2005. **37**(6): p. 478-482.
32. Lin, J. and B.-C. Hwang, *Coaxial laser cladding on an inclined substrate.* Optics & Laser Technology, 1999. **31**(8): p. 571-578.
33. Liu, J. and L. Li, *In-time motion adjustment in laser cladding manufacturing process for improving dimensional accuracy and surface finish of the formed part.* Optics & Laser Technology, 2004. **36**(6): p. 477-483.
34. Lin, J., *Concentration mode of the powder stream in coaxial laser cladding.* Optics & Laser Technology, 1999. **31**(3): p. 251-257.
35. Yang, N., *Concentration model based on movement model of powder flow in coaxial laser cladding.* Optics & Laser Technology, 2009. **41**(1): p. 94-98.
36. Lin, J., *Powder flow and catchment during coaxial laser cladding.* Proceedings of SPIE--the international society for optical engineering, 1997. **3097**: p. 517-528.
37. Lin, J. and W.M. Steen, *Design characteristics and development of a nozzle for coaxial laser cladding.* Journal of laser applications, 1998. **10**(2): p. 55-63.

38. Pinkerton, A.J. and L. Li. *A verified model of the behaviour of the axial powder stream concentration from a coaxial laser cladding nozzle*. in *ICALEO 2002 - 21st International Congress on Applications of Laser and Electro-Optics, Congress Proceedings*. 2002.
39. Pinkerton, A.J. and L. Li, *Modelling Powder Concentration Distribution From a Coaxial Deposition Nozzle for Laser-Based Rapid Tooling.* Journal of Manufacturing Science and Engineering, 2004. **126**(1): p. 33-41.
40. Lin, J., *A simple model of powder catchment in coaxial laser cladding.* Optics & Laser Technology, 1999. **31**(3): p. 233-238.
41. Chryssolouris, G., S. Zannis, K. Tsirbas, and C. Lalas, *An Experimental Investigation of Laser Cladding.* CIRP Annals - Manufacturing Technology, 2002. **51**(1): p. 145-148.
42. Paulo Davim, J., C. Oliveira, and A. Cardoso, *Predicting the geometric form of clad in laser cladding by powder using multiple regression analysis (MRA).* Materials & Design, 2008. **29**(2): p. 554-557.
43. El Cheikh, H., B. Courant, J.Y. Hascoët, and R. Guillén, *Prediction and analytical description of the single laser track geometry in direct laser fabrication from process parameters and energy balance reasoning.* Journal of Materials Processing Technology, 2012. **212**(9): p. 1832-1839.
44. de Oliveira, U., V. Ocelík, and J.T.M. De Hosson, *Analysis of coaxial laser cladding processing conditions.* Surface and Coatings Technology, 2005. **197**(2–3): p. 127-136.
45. Lu, Z.L., D.C. Li, Z.Q. Tong, Q.P. Lu, M.M. Traore, A.F. Zhang, and B.H. Lu, *Investigation into the direct laser forming process of steam turbine blade.* Optics and Lasers in Engineering, 2011. **49**(9–10): p. 1101-1110.
46. El Cheikh, H., B. Courant, S. Branchu, J.-Y. Hascoët, and R. Guillén, *Analysis and prediction of single laser tracks geometrical characteristics in coaxial laser cladding process.* Optics and Lasers in Engineering, 2012. **50**(3): p. 413-422.
47. Awasthi, R., S. Kumar, K. Chandra, B. Vishwanadh, R. Kishore, C.S. Viswanadham, D. Srivastava, and G.K. Dey, *Effect of Specific Energy Input on Microstructure and Mechanical Properties of Nickel-Base Intermetallic Alloy Deposited by Laser Cladding.* Metallurgical and Materials Transactions A, 2012. **43**(12): p. 4688-4702.
48. Pinkerton, A.J. and L. Li, *The significance of deposition point standoff variations in multiple-layer coaxial laser cladding (coaxial cladding standoff effects).* International Journal of Machine Tools and Manufacture, 2004. **44**(6): p. 573-584.
49. Mazumder, J., A. Schifferer, and J. Choi, *Direct materials deposition: designed macro and microstructure.* Materials Research Innovations, 1999. **3**(3): p. 118-131.
50. Kim, J.-D. and Y. Peng, *Melt pool shape and dilution of laser cladding with wire feeding.* Journal of Materials Processing Technology, 2000. **104**(3): p. 284-293.
51. Huang, Y., *Characterization of dilution action in laser-induction hybrid cladding.* Optics & Laser Technology, 2011. **43**(5): p. 965-973.
52. Hofman, J.T., D.F. de Lange, B. Pathiraj, and J. Meijer, *FEM modeling and experimental verification for dilution control in laser cladding.* Journal of Materials Processing Technology, 2011. **211**(2): p. 187-196.
53. Zhang, K., *Influences of processing parameters on dilution ratio of laser cladding layer during laser metal deposition shaping Advanced Materials Research*. Vol. 549. 2012. 785-789.

54. Sun, S., Y. Durandet, and M. Brandt, *Parametric investigation of pulsed Nd: YAG laser cladding of stellite 6 on stainless steel.* Surface and Coatings Technology, 2005. **194**(2–3): p. 225-231.
55. Francis, J.A., B. Bednarz, and J.V. Bee, *Prediction of steady state dilution in multipass hardfacing overlays deposited by self shielded flux cored arc welding.* Science and Technology of Welding & Joining, 2002. **7**(2): p. 95-101.
56. Saqib, S., R.J. Urbanic, and K. Aggarwal, *Analysis of Laser Cladding Bead Morphology for Developing Additive Manufacturing Travel Paths.* Procedia CIRP, 2014. **17**(0): p. 824-829.
57. Francis, J.A., *Predicting steady state dilution in multipass hardfacing overlays - geometric approach.* Science and Technology of Welding & Joining, 2002. **7**(5): p. 331-338.
58. Deam, R.T., B.E. Bednarz, and J.A. Francis, *Welding parameters that control dilution in hardfacing overlays*.
59. Pinkerton, A.J. and L. Li, *An analytical model of energy distribution in laser direct metal deposition.* Proceedings of the Institution of Mechanical Engineers, Part B: Journal of Engineering Manufacture, 2004. **218**(4): p. 363-374.
60. Qi, H., J. Mazumder, and H. Ki, *Numerical simulation of heat transfer and fluid flow in coaxial laser cladding process for direct metal deposition.* Journal of applied physics, 2006. **100**(2): p. -.
61. Sun, S., Y. Durandet, and M. Brandt, *Melt pool temperature and its effect on clad formation in pulsed Nd:yttrium-aluminum-garnet laser cladding of Stellite 6.* Journal of laser applications, 2007. **19**(1): p. 32-40.
62. Messler, R.W., *Principles of Welding Processes, Physics, Chemistry, and Metallurgy*. 2008: Hoboken : Wiley
63. Peyre, P., P. Aubry, R. Fabbro, R. Neveu, and A. Longuet, *Analytical and numerical modelling of the direct metal deposition laser process.* Journal of Physics D: Applied Physics, 2008. **41**(2): p. 025403.
64. Farahmand, P. and R. Kovacevic, *An experimental–numerical investigation of heat distribution and stress field in single- and multi-track laser cladding by a high-power direct diode laser.* Optics & Laser Technology, 2014. **63**(0): p. 154-168.
65. Limmaneevichitr, C. and S. Kou, *Experiments to simulate effect of Marangoni convection on weld pool shape.* Welding Journal (Miami, Fla), 2000. **79**(8): p. 231s-237s.
66. Anthony, T.R. and H.E. Cline, *Surface rippling induced by surface-tension gradients during laser surface melting and alloying.* Journal of applied physics, 1977. **48**(9): p. 3888-3894.
67. Lei, Y.P., H. Murakawa, Y.W. Shi, and X.Y. Li, *Numerical analysis of the competitive influence of Marangoni flow and evaporation on heat surface temperature and molten pool shape in laser surface remelting.* Computational Materials Science, 2001. **21**(3): p. 276-290.
68. David, S.A. and J.M. Vitek, *Correlation between solidification parameters and weld microstructures.* International Materials Reviews, 1989. **34**(1): p. 213-245.
69. Pinkerton, A.J., *16 - Laser direct metal deposition: theory and applications in manufacturing and maintenance*, in *Advances in Laser Materials Processing*, J. Lawrence, et al., Editors. 2010, Woodhead Publishing. p. 461-491.
70. Kobryn, P.A., E.H. Moore, and S.L. Semiatin, *The effect of laser power and traverse speed on microstructure, porosity, and build height in laser-deposited Ti-6Al-4V.* Scripta Materialia, 2000. **43**(4): p. 299-305.

71. Katayama, S., M. Mizutani, and A. Matsunawa. *Development of porosity prevention procedures during laser welding*. 2003.
72. Wang, L. and S. Felicelli, *Process Modeling in Laser Deposition of Multilayer SS410 Steel.* Journal of Manufacturing Science and Engineering, 2007. **129**(6): p. 1028-1034.
73. Sallamand, P. and J.M. Pelletier, *Laser cladding on aluminium-base alloys: microstructural features.* Materials Science and Engineering: A, 1993. **171**(1-2): p. 263-270.
74. Wang, F., H. Mao, D. Zhang, and X. Zhao, *The crack control during laser cladding by adding the stainless steel net in the coating.* Applied Surface Science, 2009. **255**(21): p. 8846-8854.
75. Wang, D.-s., E.-j. Liang, M.-j. Chao, and B. Yuan, *Investigation on the microstructure and cracking susceptibility of laser-clad V2O5 /NiCrBSiC alloy coatings.* Surface and Coatings Technology, 2008. **202**(8): p. 1371-1378.
76. Brückner, F., D. Lepski, and E. Beyer, *Modeling the Influence of Process Parameters and Additional Heat Sources on Residual Stresses in Laser Cladding.* Journal of Thermal Spray Technology, 2007. **16**(3): p. 355-373.
77. Jendrzejewski, R. and G. Sliwinski, *Investigation of temperature and stress fields in laser cladded coatings.* Applied Surface Science, 2007. **254**(4): p. 921-925.
78. Jendrzejewski, R., G. Sliwinski, M. Krawczuk, and W. Ostachowicz, *Temperature and stress during laser cladding of double-layer coatings.* Surface and Coatings Technology, 2006. **201**(6): p. 3328-3334.
79. Fallah, V., M. Alimardani, S.F. Corbin, and A. Khajepour, *Impact of localized surface preheating on the microstructure and crack formation in laser direct deposition of Stellite 1 on AISI 4340 steel.* Applied Surface Science, 2010. **257**(5): p. 1716-1723.
80. Huang, Y. and X. Zeng, *Investigation on cracking behavior of Ni-based coating by laser-induction hybrid cladding.* Applied Surface Science, 2010. **256**(20): p. 5985-5992.
81. Alimardani, M., V. Fallah, A. Khajepour, and E. Toyserkani, *The effect of localized dynamic surface preheating in laser cladding of Stellite 1.* Surface and Coatings Technology, 2010. **204**(23): p. 3911-3919.
82. Zhou, S., X. Zeng, Q. Hu, and Y. Huang, *Analysis of crack behavior for Ni-based WC composite coatings by laser cladding and crack-free realization.* Applied Surface Science, 2008. **255**(5, Part 1): p. 1646-1653.
83. Fabbro, R., Fournier, J., Ballard, P., Devaux, D., Virmont, J., *Physical study of laser-produced plasma in confined geometry.* Journal of Applied Physics 1990. **68 (2)**: p. 775-784
84. Guo, Y.B. and R. Caslaru, *Fabrication and characterization of micro dent arrays produced by laser shock peening on titanium Ti-6Al-4V surfaces.* Journal of Materials Processing Technology, 2011. **211**(4): p. 729-736.
85. H. Nakano, S.M., N. Butani, T. Shibayanagi, M. Tsukamoto, N. and Abe, *Femtosecond Laser Peening of Stainless Steel.* Journal of Laser Micro/Nanoengineering, 2009. **4(1)**: p. 35-38.
86. Sagisaka, Y., M. Kamiya, M. Matsuda, and Y. Ohta, *Thin-sheet-metal bending by laser peen forming with femtosecond laser.* Journal of Materials Processing Technology, 2010. **210**(15): p. 2304-2309.
87. Wu, B., S. Tao, and S. Lei, *Numerical modeling of laser shock peening with femtosecond laser pulses and comparisons to experiments.* Applied Surface Science, 2010. **256**(13): p. 4376-4382.

88. Trdan, U., J.A. Porro, J.L. Ocaña, and J. Grum, *Laser shock peening without absorbent coating (LSPwC) effect on 3D surface topography and mechanical properties of 6082-T651 Al alloy.* Surface and Coatings Technology, 2012. **208**(0): p. 109-116.
89. Sano, Y., M. Obata, T. Kubo, N. Mukai, M. Yoda, K. Masaki, and Y. Ochi, *Retardation of crack initiation and growth in austenitic stainless steels by laser peening without protective coating.* Materials Science and Engineering: A, 2006. **417**(1–2): p. 334-340.
90. Peyre, P. and R. Fabbro, *Laser shock processing: a review of the physics and applications.* Optical and Quantum Electronics, 1995. **27**(12): p. 1213-1229.
91. Berthe, L., R. Fabbro, P. Peyre, L. Tollier, and E. Bartnicki, *Shock waves from a water-confined laser-generated plasma.* Journal of applied physics, 1997. **82**(6): p. 2826-2832.
92. Wu, B. and Y.C. Shin, *A self-closed thermal model for laser shock peening under the water confinement regime configuration and comparisons to experiments.* Journal of applied physics, 2005. **97**(11): p. 113517-11.
93. Berthe, L., Fabbro, R., Peyre, P., Bartnicki, E., *Wavelength dependent of laser shock-wave generation in the water-confinement regime.* Journal of Applied Physics, **1999**. **85 (11)**: p. 7552-7555.
94. Gomez-Rosas, G., C. Rubio-Gonzalez, J.L. Ocaña, C. Molpeceres, J.A. Porro, M. Morales, and F.J. Casillas, *Laser Shock Processing of 6061-T6 Al alloy with 1064 nm and 532 nm wavelengths.* Applied Surface Science, 2010. **256**(20): p. 5828-5831.
95. Hemmati, I., V. Ocelík, and J. De Hosson, *Microstructural characterization of AISI 431 martensitic stainless steel laser-deposited coatings.* Journal of Materials Science, 2011. **46**(10): p. 3405-3414.
96. Kou, S., *Welding metallurgy*. 2nd ed ed. 2003 New Jersey : Wiley.
97. He, X., L. Song, G. Yu, and J. Mazumder, *Solute transport and composition profile during direct metal deposition with coaxial powder injection.* Applied Surface Science, 2011. **258**(2): p. 898-907.
98. Lippold, J.C. and D.J. Kotecki, *Welding Metallurgy and Weldability of Stainless Steels*, John Wiley & Sons.
99. Davis, J.R., A. International, and H. Committee, *Stainless steels*. 1994: Materials Park, Ohio : ASM International p577
100. Altshulin, S., J. Zahavi, A. Rosen, and S. Nadiv, *The interaction between a pulsed laser beam and a steel surface.* Journal of Materials Science, 1990. **25**(4): p. 2259-2263.
101. Chu, J.P., J.M. Rigsbee, G. Banaś, and H.E. Elsayed-Ali, *Laser-shock processing effects on surface microstructure and mechanical properties of low carbon steel.* Materials Science and Engineering: A, 1999. **260**(1-2): p. 260-268.
102. Fairand, B.P., Wilcox, B.A., Gallagher, W.J., Williams, D.N., *Laser shock-induced microstructural and mechanical property changes in 7075 aluminum.* Journal of Applied Physics, 1972. **Journal of Applied Physics**: p. 3893-3895
103. Hong, Z. and Y. Chengye, *Laser shock processing of 2024-T62 aluminum alloy.* Materials Science and Engineering: A, 1998. **257**(2): p. 322-327.
104. Luo, K.Y., J.Z. Lu, Y.K. Zhang, J.Z. Zhou, L.F. Zhang, F.Z. Dai, L. Zhang, J.W. Zhong, and C.Y. Cui, *Effects of laser shock processing on mechanical properties and micro-structure of ANSI 304 austenitic stainless steel.* Materials Science and Engineering: A, 2011. **528**(13-14): p. 4783-4788.
105. Montross, C.S., T. Wei, L. Ye, G. Clark, and Y.-W. Mai, *Laser shock processing and its effects on microstructure and properties of metal alloys: a review.* International Journal of Fatigue, 2002. **24**(10): p. 1021-1036.

106. Ren, X.D., Y.K. Zhang, H.F. Yongzhuo, L. Ruan, D.W. Jiang, T. Zhang, and K.M. Chen, *Effect of laser shock processing on the fatigue crack initiation and propagation of 7050-T7451 aluminum alloy.* Materials Science and Engineering: A, 2011. **528**(6): p. 2899-2903.
107. William D. Callister, J., *Materials science and engineering : an introduction*. 2007: New York : John Wiley.
108. Busby, J.T., M.C. Hash, and G.S. Was, *The relationship between hardness and yield stress in irradiated austenitic and ferritic steels.* Journal of Nuclear Materials, 2005. **336**(2–3): p. 267-278.
109. Liu, M.Y., B. Shi, C. Wang, S.K. Ji, X. Cai, and H.W. Song, *Normal Hall–Petch behavior of mild steel with submicron grains.* Materials letters, 2003. **57**(19): p. 2798-2802.
110. Baufeld, B., O.V.d. Biest, and R. Gault, *Additive manufacturing of Ti–6Al–4V components by shaped metal deposition: Microstructure and mechanical properties.* Materials & Design, 2010. **31, Supplement 1**(0): p. S106-S111.
111. Davim, J.P., *Laser cladding: An experimental study of geometric form and hardness of coating using statistical analysis.* Proceedings of the Institution of Mechanical Engineers. Part B, Journal of engineering manufacture, 2006. **220**(9): p. 1549-1554.
112. Dutta Majumdar, J., A. Pinkerton, Z. Liu, I. Manna, and L. Li, *Mechanical and electrochemical properties of multiple-layer diode laser cladding of 316L stainless steel.* Applied Surface Science, 2005. **247**(1–4): p. 373-377.
113. Anandkumar, R., A. Almeida, and R. Vilar, *Wear behavior of Al-12Si/TiB2 coatings produced by laser cladding.* Surface and Coatings Technology, 2011. **205**(13-14): p. 3824-3832.
114. Syed, W.U.H., A.J. Pinkerton, Z. Liu, and L. Li, *Coincident wire and powder deposition by laser to form compositionally graded material.* Surface and Coatings Technology, 2007. **201**(16–17): p. 7083-7091.
115. Alemohammad, H., S. Esmaeili, and E. Toyserkani, *Deposition of Co–Ti alloy on mild steel substrate using laser cladding.* Materials Science and Engineering: A, 2007. **456**(1–2): p. 156-161.
116. Guo, C., J. Zhou, J. Chen, J. Zhao, Y. Yu, and H. Zhou, *Improvement of the oxidation and wear resistance of pure Ti by laser cladding at elevated temperature.* Surface and Coatings Technology, 2010. **205**(7): p. 2142-2151.
117. Maawad, E., H.G. Brokmeier, L. Wagner, Y. Sano, and C. Genzel, *Investigation on the surface and near-surface characteristics of Ti–2.5Cu after various mechanical surface treatments.* Surface and Coatings Technology, 2011. **205**(12): p. 3644-3650.
118. Peyre, P., R. Fabbro, P. Merrien, and H.P. Lieurade, *Laser shock processing of aluminium alloys. Application to high cycle fatigue behaviour.* Materials Science and Engineering: A, 1996. **210**(1–2): p. 102-113.
119. Nalla, R.K., I. Altenberger, U. Noster, G.Y. Liu, B. Scholtes, and R.O. Ritchie, *On the influence of mechanical surface treatments—deep rolling and laser shock peening—on the fatigue behavior of Ti–6Al–4V at ambient and elevated temperatures.* Materials Science and Engineering: A, 2003. **355**(1–2): p. 216-230.
120. Withers, P.J. and H.K.D.H. Bhadeshia, *Residual stress. Part 2 – Nature and origins.* Materials Science and Technology, 2001. **17**(4): p. 366-375.
121. Withers, P.J. and H.K.D.H. Bhadeshia, *Residual stress. Part 1 – Measurement techniques.* Materials Science and Technology, 2001. **17**(4): p. 355-365.
122. Chen, J.Y., K. Conlon, L. Xue, and R. Rogge, *Experimental study of residual stresses in laser clad AISI P20 tool steel on pre-hardened wrought P20*

substrate. Materials Science and Engineering: A, 2010. **527**(27-28): p. 7265-7273.

123. Plati, A., *Residual stress generation during laser cladding of steel with a particulate metal matrix composite.* Advanced engineering materials, 2006. **8**(7): p. 619-624.
124. Kruusing, A., *Handbook of Liquids-Assisted Laser Processing*. 2008: Elsevier Science.
125. Prime, M.B., *Cross-Sectional Mapping of Residual Stresses by Measuring the Surface Contour After a Cut.* Journal of Engineering Materials and Technology, 2000. **123**(2): p. 162-168.
126. Prime, M. and A. Kastengren, *The Contour Method Cutting Assumption: Error Minimization and Correction*, in *Experimental and Applied Mechanics, Volume 6*, T. Proulx, Editor. 2011, Springer New York. p. 233-250.
127. Pagliaro, P., M.B. Prime, H. Swenson, and B. Zuccarello, *Measuring Multiple Residual-Stress Components using the Contour Method and Multiple Cuts.* Experimental Mechanics, 2010. **50**(2): p. 187-194.
128. Suárez, A., J.M. Amado, M.J. Tobar, A. Yáñez, E. Fraga, and M.J. Peel, *Study of residual stresses generated inside laser cladded plates using FEM and diffraction of synchrotron radiation.* Surface and Coatings Technology, 2010. **204**(12–13): p. 1983-1988.
129. de Oliveira, U., V. Ocelík, and J.T.M. De Hosson, *Microstresses and microstructure in thick cobalt-based laser deposited coatings.* Surface and Coatings Technology, 2007. **201**(14): p. 6363-6371.
130. D'Oliveira, A.S.C.M., P.S.C.P. da Silva, and R.M.C. Vilar, *Microstructural features of consecutive layers of Stellite 6 deposited by laser cladding.* Surface and Coatings Technology, 2002. **153**(2–3): p. 203-209.
131. Moat, R.J., A.J. Pinkerton, L. Li, P.J. Withers, and M. Preuss, *Residual stresses in laser direct metal deposited Waspaloy.* Materials Science and Engineering: A, 2011. **528**(6): p. 2288-2298.
132. Zhu, L.-N., B.-S. Xu, H.-D. Wang, and C.-B. Wang, *Microstructure and nanoindentation measurement of residual stress in Fe-based coating by laser cladding.* Journal of Materials Science, 2012. **47**(5): p. 2122-2126.
133. Gomez-Rosas, G., C. Rubio-Gonzalez, J.L. Ocaña, C. Molpeceres, J.A. Porro, W. Chi-Moreno, and M. Morales, *High level compressive residual stresses produced in aluminum alloys by laser shock processing.* Applied Surface Science, 2005. **252**(4): p. 883-887.
134. Akita, K., *Compressive residual stress evolution process by laser peening Materials Science Forum*. Vol. 490-491. 2005. 370-375.
135. Evans, A.D., A. King, T. Pirling, P. Peyre, and P.J. Withers, *Characterisation of Residual Stresses Generated by Laser Shock Peening by Neutron and Synchrotron Diffraction Engineering Against Fracture*, S. Pantelakis and C. Rodopoulos, Editors. 2009, Springer Netherlands. p. 383-398.
136. Rubio-González, C., C. Felix-Martinez, G. Gomez-Rosas, J.L. Ocaña, M. Morales, and J.A. Porro, *Effect of laser shock processing on fatigue crack growth of duplex stainless steel.* Materials Science and Engineering: A, 2011. **528**(3): p. 914-919.
137. Brockman, R.A., W.R. Braisted, S.E. Olson, R.D. Tenaglia, A.H. Clauer, K. Langer, and M.J. Shepard, *Prediction and characterization of residual stresses from laser shock peening.* International Journal of Fatigue, 2012. **36**(1): p. 96-108.

138. King, A., A. Steuwer, C. Woodward, and P.J. Withers, *Effects of fatigue and fretting on residual stresses introduced by laser shock peening.* Materials Science and Engineering: A, 2006. **435-436**(0): p. 12-18.
139. Ren, X.D., T. Zhang, Y.K. Zhang, D.W. Jiang, H.F. Yongzhuo, H.B. Guan, and X.M. Qian, *Mechanical properties and residual stresses changing on 00Cr12 alloy by nanoseconds laser shock processing at high temperatures.* Materials Science and Engineering: A, 2011. **528**(4-5): p. 1949-1953.
140. Cottam, R., V. Luzin, Q. Liu, E. Mayes, Y.C. Wong, J. Wang, and M. Brandt, *The role of microstructure in the stress relaxation and tempering of laser clad Ti–6Al–4V.* Materials Science and Engineering: A, 2014. **601**(0): p. 65-69.
141. Lambarri, J., J. Leunda, V. García Navas, C. Soriano, and C. Sanz, *Microstructural and tensile characterization of Inconel 718 laser coatings for aeronautic components.* Optics and Lasers in Engineering, 2013. **51**(7): p. 813-821.
142. Li, G.J., J. Li, and X. Luo, *Effects of post-heat treatment on microstructure and properties of laser cladded composite coatings on titanium alloy substrate.* Optics & Laser Technology, 2015. **65**(0): p. 66-75.
143. Liu, H., C. Wang, X. Zhang, Y. Jiang, C. Cai, and S. Tang, *Improving the corrosion resistance and mechanical property of 45 steel surface by laser cladding with Ni60CuMoW alloy powder.* Surface and Coatings Technology, 2013. **228, Supplement 1**(0): p. S296-S300.
144. Sun, S.D., Q. Liu, M. Brandt, V. Luzin, R. Cottam, M. Janardhana, and G. Clark, *Effect of laser clad repair on the fatigue behaviour of ultra-high strength AISI 4340 steel.* Materials Science and Engineering: A, 2014. **606**(0): p. 46-57.
145. Zhang, D.-w., T.C. Lei, J.-g. Zhang, and J.-h. Ouyang, *The effects of heat treatment on microstructure and erosion properties of laser surface-clad Ni-base alloy.* Surface and Coatings Technology, 1999. **115**(2–3): p. 176-183.
146. Schweitzer, P.A., *Fundamentals of corrosion : mechanisms, causes, and preventative methods*. 2010: Boca Raton, FL : CRC Press, Taylor and Francis Group.
147. Basu, A., A.N. Samant, S.P. Harimkar, J.D. Majumdar, I. Manna, and N.B. Dahotre, *Laser surface coating of Fe-Cr-Mo-Y-B-C bulk metallic glass composition on AISI 4140 steel.* Surface and Coatings Technology, 2008. **202**(12): p. 2623-2631.
148. Liu, Z., P.H. Chong, P. Skeldon, P.A. Hilton, J.T. Spencer, and B. Quayle, *Fundamental understanding of the corrosion performance of laser-melted metallic alloys.* Surface and Coatings Technology, 2006. **200**(18-19): p. 5514-5525.
149. Conde, A., R. Colaço, R. Vilar, and J. de Damborenea, *Corrosion behaviour of steels after laser surface melting.* Materials & Design, 2000. **21**(5): p. 441-445.
150. Sedriks, A.J., *Corrosion of stainless Steel*. second edition ed. 1996: John Wiley & Sons.
151. de Damborenea, J., A.J. Vázquez, and B. Fernández, *Laser-clad 316 stainless steel with Ni・Cr powder mixtures.* Materials & Design, 1994. **15**(1): p. 41-44.
152. Li, R., M.G.S. Ferreira, M. Anjos, and R. Vilar, *Localized corrosion performance of laser surface cladded UNS S44700 superferritic stainless steel on mild steel.* Surface and Coatings Technology, 1997. **88**(1-3): p. 96-102.
153. Li, R., M.G.S. Ferreira, M.A. Anjos, and R. Vilar, *Localized corrosion of laser surface cladded UNS S31254 superaustenitic stainless steel on mild steel.* Surface and Coatings Technology, 1997. **88**(1-3): p. 90-95.

154. Mahmood, K., N. Stevens, and A.J. Pinkerton, *Laser surface modification using Inconel 617 machining swarf as coating material.* Journal of Materials Processing Technology, 2012. **212**(6): p. 1271-1280.
155. Baldridge, T., G. Poling, E. Foroozmehr, R. Kovacevic, T. Metz, V. Kadekar, and M.C. Gupta, *Laser cladding of Inconel 690 on Inconel 600 superalloy for corrosion protection in nuclear applications.* Optics and Lasers in Engineering, 2013. **51**(2): p. 180-184.
156. Hazra, M., A.K. Mondal, S. Kumar, C. Blawert, and N.B. Dahotre, *Laser surface cladding of MRI 153M magnesium alloy with (Al+Al2O3).* Surface and Coatings Technology, 2009. **203**(16): p. 2292-2299.
157. Peyre, P., C. Carboni, P. Forget, G. Beranger, C. Lemaitre, and D. Stuart, *Influence of thermal and mechanical surface modifications induced by laser shock processing on the initiation of corrosion pits in 316L stainless steel.* Journal of Materials Science, 2007. **42**(16): p. 6866-6877.
158. Peyre, P., X. Scherpereel, L. Berthe, C. Carboni, R. Fabbro, G. Béranger, and C. Lemaitre, *Surface modifications induced in 316L steel by laser peening and shot-peening. Influence on pitting corrosion resistance.* Materials Science and Engineering: A, 2000. **280**(2): p. 294-302.
159. Rouleau, B., P. Peyre, J. Breuils, H. Pelletier, T. Baudin, and F. Brisset, *Characterization at a local scale of a laser-shock peened aluminum alloy surface.* Applied Surface Science, 2011. **257**(16): p. 7195-7203.
160. Sano, Y., *Enhancement of surface property by low-energy laser peening without protective coating.* Key engineering materials, 2007. **345-346 II**: p. 1589-1592.
161. Lim, H., P. Kim, H. Jeong, and S. Jeong, *Enhancement of abrasion and corrosion resistance of duplex stainless steel by laser shock peening.* Journal of Materials Processing Technology, 2012. **212**(6): p. 1347-1354.
162. Zhang, Y., J. You, J. Lu, C. Cui, Y. Jiang, and X. Ren, *Effects of laser shock processing on stress corrosion cracking susceptibility of AZ31B magnesium alloy.* Surface and Coatings Technology, 2010. **204**(24): p. 3947-3953.
163. Jiang, S., *Mechanism and experiment of surface modification by means of laser cladding combined with laser shot peening 3rd Pacific International Conference on Applications of Lasers and Optics, PICALO 2008 - Conference Proceedings*. 2008. 100-105.
164. Jin Zhon Lu, Y.K.Z., Y.Y. Xu, De Jun Kong, H.B. Yao, Xu Dong Ren, *Experimental Study on Residual Stress of K24 Superalloy in Laser Cladding Zone by Laser Shock Processing.* Key Engineering Materials 2007. **Volumes 353 - 358**: p. 453-456.
165. Wang, C., *Study on the experiment of laser cladding and shock processing TC4 titanium alloy Advanced Materials Research*. Vol. 538-541. 2012. 1823-1827.
166. Wang, C., Z. Lai, Z. An, W. He, and L. Zhou, *Properties improvement of laser cladded TC4 Titanium alloy by laser shock processing.* Jiangsu Daxue Xuebao (Ziran Kexue Ban)/Journal of Jiangsu University (Natural Science Edition), 2013. **34**(3): p. 331-334.
167. Bernstein, D.P.I.M., *Handbook of stainless steels*. 1977: New York ; London etc. : McGraw-Hill 1107p.
168. Elchalakani, M., *CFRP strengthening and rehabilitation of degraded steel welded RHS beams under combined bending and bearing.* Thin-Walled Structures, 2014. **77**(0): p. 86-108.
169. Institution, B.S. *British Standards Online*. 2001; Available from: https://bsol.bsigroup.com/.

170. Ibarra Medina, J.R., *DEVELOPMENT AND APPLICATION OF A CFD MODEL OF LASER METAL DEPOSITION*. 2013, The University of Manchester: Manchester, UK.
171. Pinkerton, A., *An experimental and numerical study of the influence of diode laser beam shape on thin wall direct metal deposition.* Journal of laser applications, 2005. **17**(1): p. 47.
172. Mahmood, K. and A.J. Pinkerton, *Direct laser deposition with different types of 316L steel particle: A comparative study of final part properties.* Proceedings of the Institution of Mechanical Engineers, Part B: Journal of Engineering Manufacture, 2013. **227**(4): p. 520-531.
173. Bramfitt, B.L., *Metallographer's guide : practices and procedures for irons and steels*. 2002: Materials Park, OH : ASM International
174. Mahmood, K., *An investigation into laser deposition of machining chips and characteristics of the final clad*. 2012, The University of Manchester: Manchester, UK. p. 195.
175. Li, H.S., M.X. Li, Y.Z. He, J.H. Yoon, and K. Shin, *Microstructure of cobalt based alloy coatings produced by laser deposit welding.* Science and Technology of Welding & Joining, 2006. **11**(5): p. 567-571.
176. Askeland, D.R., *The science and engineering of materials*. 2003: Pacific Grove, Calif. ; London : Brooks/Cole.
177. Kar, A. and J. Mazumder, *One-dimensional diffusion model for extended solid solution in laser cladding.* Journal of applied physics, 1987. **61**(7): p. 2645-2655.
178. Kar, A. and J. Mazumder, *One-dimensional finite-medium diffusion model for extended solid solution in laser cladding of Hf on nickel.* Acta Metallurgica, 1988. **36**(3): p. 701-712.
179. Fisher, W.K.D.J., *Fundamentals of solidification*. Third edition ed. 1984: Aedermannsdorf : Trans Tech
180. Nelson, T.W., J.C. Lippold, and M.J. Mills, *Nature and evolution of the fusion boundary in ferritic-austenitic dissimilar weld metals, Part 1 - nucleation and growth.* Welding Journal (Miami, Fla), 1999. **78**(10): p. 329-s.
181. Nelson, T.W., J.C. Lippold, and M.J. Mills, *Nature and evolution of the fusion boundary in ferritic-austenitic dissimilar metal welds - Part 2: on-cooling transformations.* Welding Journal (Miami, Fla), 2000. **79**(10): p. 267s-277s.
182. Gittos, M.F. and T.G. Gooch, *The interface below stainless steel and nickel alloy claddings.* Welding Journal, 1992. **71**(12): p. 461s-472s.
183. Kotecki, D.J., *Martensite boundary on the WRC-1992 Diagram - Part 2: The effect of manganese.* Welding Journal (Miami, Fla), 2000. **79**(12): p. 346-s.
184. Francis, J.A., H.K.D.H. Bhadeshia, and P.J. Withers, *Welding residual stresses in ferritic power plant steels.* Materials Science and Technology, 2007. **23**(9): p. 1009-1020.
185. Withers, P.J., *Residual stress and its role in failure.* Reports on Progress in Physics, 2007. **70**(12): p. 2211.
186. Hayward, A. and F. Weare, *Steel detailer's manual*. 1989: Oxford : BSP Professional
187. Nobre, J.P., M. Kornmeier, A.M. Dias, and B. Scholtes, *Use of the hole-drilling method for measuring residual stresses in highly stressed shot-peened surfaces.* Experimental Mechanics. **40**(3): p. 289-297.
188. Gujba, A. and M. Medraj, *Laser Peening Process and Its Impact on Materials Properties in Comparison with Shot Peening and Ultrasonic Impact Peening.* Materials, 2014. **7**(12): p. 7925-7974.

189. Watanabe, A., Y. Wada, K. Ishida, M. Tachibana, N. Shigenaka, N. Kawashima, and M. Aizawa, *Effects of local radiolysis and geometric parameters on intergranular attack caused by crevice corrosion.* Journal of Nuclear Science and Technology, 2014: p. 1-9.
190. Katsuyama, J., Y. Yamaguchi, Y. Li, and K. Onizawa, *Effect of cyclic loading on the relaxation of residual stress in the butt-weld joints of nuclear reactor piping.* Nuclear Engineering and Design, 2014. **278**(0): p. 222-228.
191. You, Y., Z. Zhang, and L. Ma, *Cracking analysis of 316L stainless steel lining plates in alkaline environments.* Engineering Failure Analysis, 2014. **39**(0): p. 34-40.
192. Panda, B., M. Sujata, M. Madan, and S.K. Bhaumik, *Stress corrosion cracking in 316L stainless steel bellows of a pressure safety valve.* Engineering Failure Analysis, 2014. **36**(0): p. 379-389.
193. Cook, A.B., S.B. Lyon, N.P.C. Stevens, M. Gunther, G. McFiggans, R.C. Newman, and D.L. Engelberg, *Assessing the risk of under-deposit chloride-induced stress corrosion cracking in austenitic stainless steel nuclear waste containers.* Corrosion Engineering, Science and Technology, 2014. **49**(6): p. 529-534.
194. Cook, A.B., S.B. Lyon, N.P.C. Stevens, R.C. Newman, M. Gunther, G. McFiggans, and D.L. Engelberg, *Under-Deposit Chloride-Induced Stress Corrosion Cracking in Austenitic Stainless Steels: Aspects Associated with Deposit Type, Size and Composition.* ECS Transactions, 2014. **58**(29): p. 25-39.
195. Cook, A.B., J. Duff, N. Stevens, S. Lyon, A. Sherry, and J. Marrow, *Preliminary Evaluation of Digital Image Correlation for In-situ Observation of Low Temperature Atmospheric-Induced Chloride Stress Corrosion Cracking in Austenitic Stainless Steels.* ECS Transactions, 2010. **25**(37): p. 119-132.
196. Weerasinghe, V.M., W.M. Steen, and D.R.F. West, *LASER DEPOSITED AUSTENITIC STAINLESS STEEL CLAD LAYERS.* Surface Engineering, 1987. **3**(2): p. 147-153.
197. Albores-Silva, O.E., E.A. Charles, and C. Padovani, *Effect of chloride deposition on stress corrosion cracking of 316L stainless steel used for intermediate level radioactive waste containers.* Corrosion Engineering, Science and Technology, 2011. **46**(2): p. 124-128.